DISSERTATIONES
CHIMICAE
UNIVERSITATIS
TARTUENSIS
185

MAREK MOOSTE

Surface and electrochemical characterisation of aryl film and nanocomposite material modified carbon and metal-based electrodes

DISSERTATIONES CHIMICAE UNIVERSITATIS TARTUENSIS
185

DISSERTATIONES CHIMICAE UNIVERSITATIS TARTUENSIS
185

MAREK MOOSTE

Surface and electrochemical characterisation of aryl film and nanocomposite material modified carbon and metal-based electrodes

UNIVERSITY OF TARTU
Press

Institute of Chemistry, Faculty of Science and Technology, University of Tartu, Estonia

The dissertation is accepted for the commencement of the degree of Doctor of Philosophy in Chemistry on 11th June, 2019 by the Council of Institute of Chemistry, University of Tartu.

Supervisors: Assoc. Prof. Kaido Tammeveski
Institute of Chemistry, University of Tartu, Estonia

PhD Elo Kibena-Põldsepp
Institute of Chemistry, University of Tartu, Estonia

Opponent: Prof. Lasse Murtomäki
Department of Chemistry, Aalto University, Finland

Commencement: August 26th, 2019, 10:15
Ravila Street 14a, Tartu (Chemicum), auditorium 1020

ISSN 1406-0299
ISBN 978-9949-03-106-1 (print)
ISBN 978-9949-03-107-8 (pdf)

University of Tartu Press
www.tyk.ee

TABLE OF CONTENTS

1. LIST OF ORIGINAL PUBLICATIONS

This thesis consists of eleven original publications listed below which are referred in the text by Roman numerals I–XI.

I **M. Mooste**, E. Kibena-Põldsepp, B.D. Ossonon, D. Bélanger, K. Tammeveski, Oxygen reduction on graphene sheets functionalised by anthraquinone diazonium compound during electrochemical exfoliation of graphite, *Electrochimica Acta* 267 (2018) 246–254.

II **M. Mooste**, E. Kibena-Põldsepp, L. Matisen, K. Tammeveski, Oxygen reduction on anthraquinone diazonium compound derivatised multi-walled carbon nanotube and graphene based electrodes, *Electroanalysis* 29 (2017) 548–558.

III **M. Mooste**, E. Kibena, J. Kozlova, M. Marandi, L. Matisen, A. Niilisk, V. Sammelselg, K. Tammeveski, Electrografting and morphological studies of chemical vapour deposition grown graphene sheets modified by electroreduction of aryldiazonium salts, *Electrochimica Acta* 161 (2015) 195–204.

IV **M. Mooste**, E. Kibena, A. Sarapuu, U. Mäeorg, G. Maia, K. Tammeveski, Electrocatalysis of oxygen reduction on glassy carbon electrodes modified with anthraquinone moieties, *Journal of Solid State Electrochemistry* 18 (2014) 1725–1733.

V **M. Mooste**, E. Kibena, A. Sarapuu, L. Matisen, K. Tammeveski, Oxygen reduction on thick anthraquinone films electrografted to glassy carbon, *Journal of Electroanalytical Chemistry* 702 (2013) 8–14.

VI **M. Mooste**, E. Kibena-Põldsepp, M. Marandi, L. Matisen, V. Sammelselg, K. Tammeveski, Electrochemical properties of gold and glassy carbon electrodes electrografted with an anthraquinone diazonium compound using the rotating disc electrode method, *RSC Advances* 6 (2016) 40982–40990.

VII **M. Mooste**, E. Kibena, L. Matisen, K. Tammeveski, Blocking properties of nickel electrodes modified with aryldiazonium compounds, *International Journal of Electrochemical Science* 10 (2015) 3803–3819.

VIII **M. Mooste**, E. Kibena-Põldsepp, M. Marandi, L. Matisen, V. Sammelselg, F.I. Podvorica, K. Tammeveski, Surface and electrochemical characterization of aryl films grafted on polycrystalline copper from the diazonium compounds using the rotating disk electrode method, *Journal of Electroanalytical Chemistry* 817 (2018) 89–100.

IX **M. Mooste**, E. Kibena-Põldsepp, L. Matisen, M. Merisalu, M. Kook, V. Kisand, V. Vassiljeva, A. Krumme, V. Sammelselg, K. Tammeveski, Oxygen reduction on catalysts prepared by pyrolysis of electrospun styrene-acrylonitrile copolymer and multi-walled carbon nanotube composite fibres, *Catalysis Letters* 148 (2018) 1815–1826.

X **M. Mooste**, E. Kibena-Põldsepp, V. Vassiljeva, M. Merisalu, M. Kook, A. Treshchalov, V. Kisand, M. Uibu, A. Krumme, V. Sammelselg, K. Tammeveski, Electrocatalysts for oxygen reduction reaction based on

electrospun polyacrylonitrile, styrene-acrylonitrile copolymer and carbon nanotube composite fibres, *Journal of Materials Science* 54 (2019), 11618–11634.

XI T. Canuto de Almeida e Silva, **M. Mooste**, E. Kibena-Põldsepp, L. Matisen, M. Merisalu, M. Kook, V. Sammelselg, K. Tammeveski, M. Wilhelm, K. Rezwan, Polymer-derived Co/Ni–SiOC(N) ceramic electrocatalysts for oxygen reduction reaction in fuel cells, *Catalysis Science & Technology* 9 (2019) 854–866.

Author's contribution:

Paper I: The author has performed all electrochemical measurements, analysed the data and is mainly responsible for writing of the paper.

Paper II: The author has performed all electrochemical measurements, analysed the data and is mainly responsible for writing of the paper.

Paper III: The author has performed all electrochemical measurements and participated in the analysis of the data and in the writing of the paper.

Paper IV: The author has performed all electrochemical measurements and participated in the analysis of the data and in the writing of the paper.

Paper V: The author has performed all electrochemical measurements and participated in the analysis of the data and in the writing of the paper.

Paper VI: The author has performed all electrochemical measurements, analysed the data and is mainly responsible for writing of the paper.

Paper VII: The author has performed all electrochemical measurements, analysed the data and is mainly responsible for writing of the paper.

Paper VIII: The author has performed all electrochemical measurements, analysed the data and is mainly responsible for writing of the paper.

Paper IX: The author has performed all electrochemical measurements, analysed the data and is mainly responsible for writing of the paper.

Paper X: The author has performed all electrochemical measurements, analysed the data and is mainly responsible for writing of the paper.

Paper XI: The author has performed all electrochemical measurements and participated in the analysis of the data and in the writing of the paper.

2. ABBREVIATIONS AND SYMBOLS

A	geometric electrode area
$Ar^{\bullet}$	aryl radical
$Ar–N_2^+$	aryldiazonium cation
ACN	acetonitrile
AFM	atomic force microscopy
AP	aminophenyl
AQ	9,10-anthraquinone
Br-MAQ	2-bromomethyl-anthraquinone
BE	binding energy
c^b_{O2}	concentration of oxygen in the bulk solution
Cl-MAQ	2-chloromethyl-anthraquinone
CNF	carbon nanofibres
CV	cyclic voltammetry
CVD	chemical vapour deposition
Co-N_x	cobalt ion coordinated to nitrogen
D	diffusion coefficient
D_{O2}	diffusion coefficient of oxygen
DCDA	dicyandiamide
DMF	*N,N*-dimethylformamide
E^o	redox potential
$E_{1/2}$	half-wave potential
E_{onset}	onset potential
E_p	peak potential
EG	electrochemically exfoliated graphene sheets
EG-AQ	electrochemically exfoliated and AQ grafted graphene sheets
Φ	percentage of peroxide formation
F	Faraday constant
FC	fuel cell
FRA	Fast Red AL salt
Γ_{AQ}	surface concentration of electrochemically active AQ groups
Γ_{NP}	surface concentration of electrochemically active NP groups
GC	glassy carbon
GR	graphene
I_d	diffusion-limited current
I_D	disc current
I_k	kinetic current
I_{pc}	cathodic peak current
I_R	ring current
I_{rel}	calculated blocking efficiency
k	electrochemical rate constant
K–L	Koutecky-Levich
MAQ	methylanthraquinone

MFC	microbial fuel cell
MWCNTs	multi-walled carbon nanotubes
n	number of electrons
N	collection efficiency
NBD	4-nitrobenzenediazonium tetrafluoroborate
NP	4-nitrophenyl
NPM	nonprecious metal
$O_2^{\bullet-}$	superoxide radical anion
ORR	oxygen reduction reaction
PAN	polyacrylonitrile
PBS	phosphate buffer solution
PDC	polymer-derived ceramics
Q	consumed charge
RDE	rotating disc electrode
RG	redox grafting
RRDE	rotating ring-disc electrode
SAN	styrene-acrylonitrile copolymer
SCE	saturated calomel electrode
SDS	sodium dodecyl sulphate
SEM	scanning electron microscopy
SiOC	silicon oxycarbide
$TBABF_4$	tetrabutylammonium tetrafluoroborate
TBAI	tetrabutylammonium iodide
v	potential sweep rate
ω	electrode rotation rate
XPS	X–ray photoelectron spectroscopy

3. INTRODUCTION

The daily increasing word population and energy consumption drives the demand for utilising more resources and materials. The necessary resources on the planet are limited and also more attention has been drawn to the environmental problems regarding the increasing use of available resources. Corresponding problems can be satisfied to some extent by the more effective use of the resources and the greater deployment of renewable energy devices. These directions are also recognised and supported by the Smart Specialisation approach, which is one of the cornerstones of innovation policy across the European Union and also has supported the research in this PhD thesis.

For the more effective use of the resources, the surface functionalisation can be used to modify the physical and chemical properties of the materials towards the required needs. One option for the surface functionalisation with desired molecules or organic aryl films is to use the aryldiazonium salt reduction method [1]. This method is very versatile allowing the functionalisation of different carbon materials and metals with and without the application of electrical potential [2]. In this way, the cheaper and more available materials can be tailored to meet the properties inherent to more expensive or less common materials. The main applications of aryl film modified materials are in the field of electronics (e.g. sensors, electrodes and energy storage devices [3, 4]).

The aim of the present PhD thesis was to prepare and study the aryl film functionalised electrodes and non-precious metal catalysts. The first part of the thesis is focused on the grafting of different carbon materials with aryl films via reduction of aryldiazonium salt [I–VI]. In the second part of the thesis, the electrochemical derivatisation of metal (Au, Ni, Cu) electrodes is described [VI–VIII]. The prepared aryl films on carbon and metal electrodes are characterised by several physical or chemical methods and electrochemically using the cyclic voltammetry (CV) and rotating disc electrode (RDE) technique. Among the renewable energy applications, fuel cells (FCs) are promising energy conversion devices due to high power density, easy deployment in different areas and also relatively low maintenance costs [5, 6]. Furthermore, considering the environmental needs for water treatment, microbial fuel cells (MFCs) also play an important role in the technology development regarding smart specialisation strategies [7, 8]. In the FCs and MFCs, the oxygen reduction reaction (ORR) at the cathode is very often limiting the performance of the device due to its slow reaction kinetics [9]. To increase the ORR activity, the catalyst material is needed and up to date, the Pt-based catalysts are most often used. The high price and scarcity of the Pt drives the need for cheaper and more available nonprecious metal (NPM) catalyst for ORR [6]. Therefore, the third part of the PhD thesis describes the development of catalysts for ORR from electrospun polymer based multi-walled carbon nanotubes containing carbon nanofibres and the nitrogen and transition metal codoped SiOC based polymer-derived ceramics (PDC) [IX–XI].

4. LITERATURE OVERVIEW

4.1. Oxygen reduction reaction

The ORR is one of the most widely studied electrochemical reactions since it occurs in the energy conversion systems (e.g. fuel cell) [6, 8, 9]. This process has been studied on a large number of different metal and carbon electrode materials. The main factors that affect the ORR process are the electrolyte solution, properties of the catalyst and the potential of the electrode. The ORR is a multielectron process. The elementary stages of the ORR can proceed via different parallel and sequential combinations. In aqueous solution, the ORR can occur via direct 4-electron process straight to water or via 2-electron process that includes the production of the hydrogen peroxide as a final product. In addition, a two-step $2e^-$ pathway, forming hydrogen peroxide as an intermediate product is possible [6]. As in the present PhD thesis, the ORR is mainly studied in alkaline conditions [I, II, IV–VI, IX–XI], the possible pathways in alkaline medium are as follows:

The direct $4e^-$ reduction:

$$O_2 + 2H_2O + 4e^- \rightarrow 4OH^- \quad (1)$$

The $2e^-$ reduction resulting the production of hydrogen peroxide:

$$O_2 + H_2O + 2e^- \rightarrow HO_2^- + OH^- \quad (2)$$

The formed hydrogen peroxide can be further reduced (3) or disproportionate (4)

$$HO_2^- + H_2O + 2e^- \rightarrow 3OH^- \quad (3)$$

$$2HO_2^- \rightarrow 2OH^- + O_2 \quad (4)$$

The $4e^-$ reduction is a slow reaction as the stability of the oxygen-oxygen (O=O) bond is very high and the dissociation energy of this bond is 494 kJ mol^{-1}. Therefore, the $4e^-$ reduction usually occurs on the metal electrodes (e.g. Pt and Ag). On the undoped carbon materials (e.g. GC) the ORR usually proceeds via $2e^-$ pathway. According to the experimental data obtained on different electrodes, a general scheme for the reactions of oxygen and hydrogen peroxide has been proposed for alkaline solution (Scheme 1) [10]. In addition to hydrogen peroxide, the superoxide radical anion ($O_2^{\bullet -}$) or its protonated version ($HO_2^{\bullet}$) can be formed and both of them can also desorb.

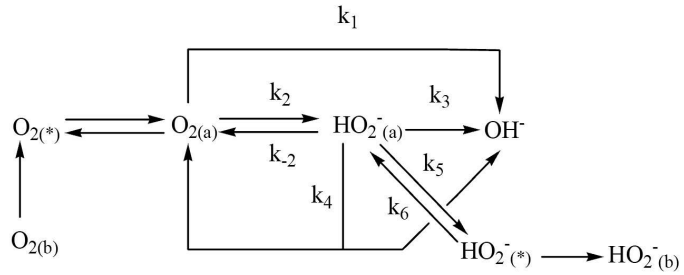

Scheme 1. Simplified scheme for electrocatalytic ORR in alkaline solution, k_i is the reaction rate constant. (b), (*) and (a) denote the O_2 and HO_2^- in the solution, in the surface layer and as the adsorbed form, respectively [10].

The ORR on carbon electrodes, e.g. graphene (GR) [I, II] [11], multi-walled carbon nanotubes (MWCNTs) [II] [12], glassy carbon (GC) [IV–VI] [11, 13, 14] modified with AQ and its derivatives like methylanthraquinone (MAQ) [IV] [15] has drawn a lot of attention because the ORR on quinone-modified electrodes follows an electrochemical-chemical mechanism [14, 16]:

$$Q + e^- \rightarrow Q^{\bullet -} \tag{5}$$

followed by the chemical step

$$Q^{\bullet -} + O_2 \rightarrow O_2^{\bullet -} + Q \tag{6}$$

The superoxide ion can be further reduced to peroxide

$$O_2^{\bullet -} + H_2O + e^- \rightarrow HO_2^- + OH^- \tag{7}$$

or undergo the disproportionation process

$$2O_2^{\bullet -} + H_2O \rightarrow O_2 + HO_2^- + OH^- \tag{8}$$

in which Q is the quinone moiety bound to the surface. The reaction (6) is the rate-determining step and in the presented reaction model the overall reaction rate is determined by the surface concentration of $Q^{\bullet -}$ [14, 16]. As observed from the reactions (7) and (8), the quinone-modified electrodes could be used for the electrochemical synthesis of hydrogen peroxide [17]. This is possible because the reactions (7) and (8) are considered to be fast and they both result in the formation of HO_2^-. The electrochemical-chemical mechanism of O_2 reduction on quinone-modified electrodes, emphasising the extremely high activity of semiquinone radical ions, has been confirmed using CV according to the literature [18]. Therefore, one possible application of the AQ-modified carbon materials described in the present thesis is the environmentally greener

production of hydrogen peroxide compared to the chemical system that is currently most widely used for this application [19–21] .

Two novel carbon nanomaterials, MWCNTs and GR, have been extensively studied due their unique and extraordinary properties [22, 23]. It is well-known that the purified MWCNTs possess good electrocatalytic activity towards the ORR in alkaline solution since the number of electrons (n) transferred per O_2 molecule [24] is usually between 2 and $4e^-$, which refers to the ORR proceeding via mixed 2- and $4e^-$ pathways [25, 26]. Furthermore, Gong et al. have reported monohydroxy-anthraquinone modified MWCNTs to exhibit higher activity towards the ORR than the unfunctionalised MWCNTs [15]. Moreover, Dyke and Tour have published a different method [27] applicable for the covalent modification of MWCNTs with aryl groups by the spontaneous reduction of aryldiazonium salts. Considering the gathered information, the ORR investigation on the purified MWCNTs grafted with AQ moieties using the spontaneous diazonium reduction method would therefore be a very attractive study. In addition, the electrografting of chemical vapour deposition (CVD) grown GR with AQ functionalities was found to increase the electrocatalytic activity of GR towards the ORR [11]. Therefore, the parallel study with commercially available GR would add an extra value to the corresponding investigation [II].

In addition to the nanocarbons such as MWCNTs and GR, the GC electrodes can be also covalently functionalised with AQ [14]. According to the previous studies by our workgroup, the AQ-modified GC electrodes have exhibited high electrocatalytic activity towards the ORR in alkaline medium [13, 14, 28–35]. It should be noted that the electrografting of AQ groups was performed in various conditions to yield the Γ_{AQ} value less than 1 nmol cm^{-2}. Although, there was no information available for the ORR studies on thick AQ films with high Γ_{AQ} values on GC electrodes. Recently, Daasbjerg and co-workers established a redox grafting (RG) procedure for electrografting different electrodes with AQ films with high thickness [36–38]. Therefore, it was of special interest to use RG modification procedure to prepare thick AQ film modified GC electrodes and study their catalytic properties towards the ORR [V]. In addition to the RG method, another new procedure has been proposed to functionalise the GC electrode surface with AQ groups *via* methylene linker (designated as MAQ) [39]. In specific, Jouikov and Simonet [39] reported a successful attachment of AQ moieties to GC using 2-(bromomethyl)anthraquinone to derivatise GC with MAQ groups. This grafting procedure is based on the $1e^-$ reduction of AQ-CH_2-Br to a free radical (AQ-$CH_2^{\bullet}$) and the formed radical bounds to the GC surface giving a strong covalent bond [39]. There was no information available for the ORR activity of MAQ functionalised GC electrodes and therefore, corresponding work was carried out as a part of this PhD thesis. Additionally, for modification also the 2-(chloromethyl)anthraquinone derivate was used to assess the possible influence of the grafting agent towards the ORR [IV].

In addition to the AQ functionalised carbon materials (e.g. MWCNTs, GR and GC), the ORR on aryl-modified metal electrodes (e.g. Au, Cu) is also important aspect to study since they have a potential use in the sensing applica-

tions [4, 40]. The polycrystalline Au itself is relatively active electrode material towards the ORR in alkaline medium and the process proceeds via the mixed 2- and $4e^-$ reduction [41–44]. The aryl films grafted on metal electrodes via reduction of aryldiazonium salts are known to suppress the ORR kinetics and also favour the $2e^-$ reduction pathway on Au [41–43]. In previous studies by our workgroup, the ORR has been investigated on Au electrodes grafted with several aryl films (e.g. nitrophenyl (NP) [43], 4-bromophenyl [41], azobenzene derivatives [42]). Although, there was no information available about the blocking behaviour of thick AQ films on Au electrodes towards the ORR. Therefore, as a part of the present thesis, the ORR was studied on Au electrodes electrografted with AQ films with various thicknesses and Γ_{AQ} values including the films prepared by recently established RG [36–38] procedure [VI].

Another metal electrode that is attractive for ORR studies is polycrystalline Cu. Since Cu is one of the most important materials in the industry and the inhibition of its corrosion is challenging [45–47]. It is well-known that the reduction of oxygen on bare Cu electrodes proceeds predominantly via $4e^-$ pathway in a broad pH range [46, 48–54]. However, no information about the influence of the (thick) aryl films grafted via reduction aryldiazonium salts on polycrystalline Cu electrode towards the ORR was available. Therefore, the corresponding investigations were carried out within this PhD work [VIII].

Non-precious metal (NPM) catalysts are especially attractive to be studied from the fuel cell application point of view [6, 9]. N-doped metal-free carbon-based catalysts are known to catalyse the ORR via $2\times2e^-$ (reactions (2) and (3)) or direct $4e^-$ (reaction (1)) reduction in alkaline medium [55–61]. Moreover, on the transition metal (e.g. Co, Fe) and nitrogen codoped carbon-based catalysts the ORR proceeds via $4e^-$ pathway [61–64]. In case of codoped electrospun and pyrolysed polyacrylonitrile (PAN) based NPM catalysts, the ORR is also known to proceed mainly via $4e^-$ pathway [65–70] and on the materials functionalised with N without incorporated transition metals the reaction is reported to occur by $2\times2e^-$ process [71–74]. The last part of the present PhD thesis is devoted to the ORR studies on nitrogen functionalised NPM catalysts with and without transition metal content. The corresponding ORR studies were carried out for the first time on these specific NPM catalysts with the mission of further possible application as a catalyst at the (microbial) fuel cell cathode [IX–XI].

4.2. Grafting of the electrodes by reduction of aryldiazonium salts

Functionalisation of the electrode surface by the reduction of aryldiazonium salts has been widely investigated since the first report describing this procedure via electrografting by Pinson and co-workers in 1992 [75]. The diazonium chemistry is very versatile method giving the opportunity to attach different modifiers to various carbon-based materials and metals by spontaneous grafting or electrochemical modification [1, 4, 76]. The most relevant feature of this

method is the reduction of aryldiazonium cations ($Ar–N_2^+$). This reduction process produces highly reactive aryl radicals ($Ar^\bullet$), which react with the electrode surface forming a strong covalent C−C bond between the underlying substrate and organic group [2]. Scheme 2 depicts the illustration of the described process as an example with the grafting of AQ groups to the GC electrode [VI].

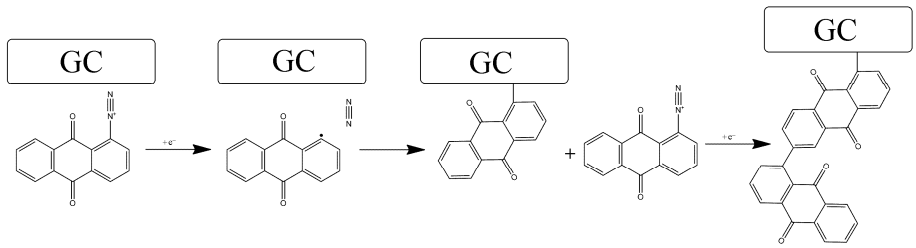

Scheme 2. The illustration of electrografting process of anthraquinone-1-diazonium compound on the GC surface by electrochemical reduction of AQ diazonium salts [VI].

The process is facilitated by the adsorption of the $Ar–N_2^+$ and by the relatively positive reduction potential of $Ar–N_2^+$. In addition, the $Ar^\bullet$ may also react with the already surface-bound modifier molecules forming multilayer films (Scheme 2). One possible opportunity to perform this grafting process is by electrochemical reduction, where the $Ar–N_2^+$ cation is reduced to the $Ar^\bullet$ radical and the N_2 is released [1]. In latter case, the electron for the reduction of $Ar–N_2^+$ is obtained from the electrode under the applied potential. Another option for surface functionalisation via reduction of aryldiazonium salts is by applying non-electrochemical spontaneous derivatisation [77]. This method is widely used on the reducing surfaces employing easily reducible diazonium salts (e.g. 4-nitrobenzenediazonium tetrafluoroborate (NBD) and Fast Red AL (FRA)) [77, 78]. Spontaneous grafting is a relatively simpler method as there is no need to apply the electric potential to the electrode. In the present thesis, the spontaneous modification was employed for grafting the AQ groups on the MWCNT and GR surfaces according to the procedure presented by Dyke and Tour [II].

Recently, the spontaneous functionalisation with surface modifiers has been incorporated into the preparation procedure of the GR via electrochemical exfoliation [79]. In specific, a relatively convenient one-pot synthesis method has been developed in which the production of GR as well as *in situ* modification of GR sheets are carried out simultaneously in one electrolyte solution [79]. Using the established one-pot synthesis method, GR or GR-like materials (e.g. graphene oxide) have been modified for example with nitrogen [79–83], sulphur [84] and AQ moieties [85]. In the latter study by Ossonon and Bélanger [85], the functionalisation of GR sheets with AQ during electrochemical exfoliation of graphite was performed using spontaneous reduction of aryldiazonium salts [85]. Although, there was no information about the ORR on GR modified with

AQ diazonium salt using the above-described one-pot synthesis. Therefore, the corresponding study was carried out as a part of this PhD thesis [I].

In general, the electrochemical reduction of aryldiazonium salts for surface functionalisation has been performed by CV in a narrow potential range or in potentiostatic conditions by holding the electrode at a certain potential. In case of the potentiostatic modification, the potential is chosen to be the peak potential or more negative than the one of $Ar–N_2^+$ reduction peak on the corresponding CV curve [1]. If using the CV method, the potential is cycled over the potential range where only the reduction peak of $Ar–N_2^+$ is observed and on the subsequent cycles the decrease in the current values refers to the blocking of the electrode surface by the aryl film [14, 86]. The latter modification procedure is referred to as "normal" electrografting in the present PhD thesis. Using the "normal" electrografting method [38], thicker modifier films and more efficient control over the film growth can be achieved compared to the spontaneous modification [87]. Although, the thickness of the aryl film on the electrode does not exceed usually 10 nm using the "normal" electrografting because of the restricted electron transfer between the electrode and $Ar\text{-}N_2^+$ [36–38]. However, thicker aryl films could be beneficial for blocking the electrode surface and in the development of sensors and supercapacitors [36, 37].

Some years ago, the research on the formation of thick aryl films on electrode surfaces via diazonium electroreduction was further developed. In more specific, Daasbjerg's group proposed a new method called RG based on the diazonium chemistry and cyclic voltammetry (CV) to form thick aryl layers on various electrode materials. Already, a systematic investigations about the formation of thick organic layers on different electrodes (e.g. GC, Au and stainless steel) [36–38] and in addition, GR-based materials [11] via RG of aryldiazonium salts had been carried out. In case of RG method, the electron transfer in the film does not become restricted and the RG enables the film growth up to 900 nm for example in case of Au electrode modified with NP groups [36]. To prepare organic films of high thickness via diazonium chemistry, the main contributing factors are as follows: the aryldiazonium salt should contain redox active functionality (e.g. quinone, nitro group) in order to maintain the charge propagation in the growing film; the sweeping of potential is essential during the electrografting process to avoid the clogging of the physisorbed species in the electrolyte channels in the film; a higher sweep rate than 500 mV s^{-1} is preferred and last but not least, the switching potential during RG must be chosen so that the electrode is cycled over the redox potential of the redox active moiety [36–38]. In the RG method, the film growth of thick organic layers is accomplished by reducing the electroactive functional group (e.g. AQ, NP) of an aryl-modifier to an anion radical (e.g. $AQ^{\bullet-}$, $NP^{\bullet-}$) under more negative potential which should promote the growth of an aryl layer. In the present PhD thesis the RG method was used for the first time for the functionalisation of Ni electrodes and CVD-grown GR on Ni substrates with NP films of high thickness [III, VII]. In addition, it was of special interest to expand the RG method by combining the RDE method with the RG for possibly

even thicker aryl film formation. Therefore, in the present work, the RG and RDE combined method was employed for preparing the thick AQ films on Au and GC electrodes [VI] and thick AQ and NP films on the Cu electrodes [VIII].

The composition and the layer thickness of the multilayer aryl films can be determined by various surface characterisation methods (e.g. atomic force microscopy (AFM) and X–ray photoelectron spectroscopy (XPS)). In addition, the electroactive moieties (e.g. AQ, NP) containing aryl films can be characterised by measuring the surface concentration of these aryl groups (Γ_{AQ} and Γ_{NP} values) [56]. For the surface-confined quinone groups, the determination of the surface concentration can be easily performed by the charge integration under the redox peaks appearing on the CV curve [59]. According to the study by Ernst et al. [60] the surface coverage for closely-packed monolayer of anthraquinonyl groups is 3.45×10^{-10} mol cm^{-2}.

The potential applications for the different aryl film modified electrodes prepared in this PhD thesis could be as follows: carbon materials derivatised with AQ groups can be employed in the preparation of (bio)sensors [4, 40, 88] and energy storage devices [3, 89]. Also, quinone-modified graphene materials have been investigated for battery and electrochemical capacitor applications [89, 90]. In case of metal electrodes (e.g. Ni and Cu), the aryl films obtained by the reduction of aryldiazonium salts have also been proposed to be suitable for the protection against corrosion [47, 76].

4.3. Nonprecious metal catalysts for the ORR

The electrochemical reduction of oxygen is the key reaction that takes place at the cathode of the fuel cell [6, 9]. Because of the sluggish kinetics of the ORR, intensive research has been performed to design cathode catalysts applicable in the fuel cell [6]. The fuel cell cathode catalyst should support either direct 4-electron (reaction (1)) or 2×2 electron (reactions (2) and (3), respectively) ORR process with minimal peroxide production [6]. In this case, the production of highly reactive HO_2^-, which could degrade the fuel cell components, is avoided and the maximum energy efficiency of the fuel cell is achieved [9]. At the moment, Pt-based materials are the best known catalysts for the fuel cell cathode as Pt supports a 4-electron reduction pathway and the E_{onset} of the ORR on Pt electrode is rather high. The carbon-supported Pt (Pt/C) is the most widely used state-of-the-art catalyst material due to its high activity towards the ORR in acidic and alkaline conditions [91]. Although, the limited availability, high cost and long-term stability issues of Pt influence the commercial viability of low-temperature fuel cells, which operate generally with Pt-based electrocatalysts [9]. Therefore, the efficient, cost-effective and durable cathode NPM catalyst with similar performance to Pt that is also practically applicable in the fuel cell is required. Possible alternative NPM catalysts for addressing the issues of Pt-based materials, can be divided into transition metal-containing and/or heteroatom-doped carbon materials [9].

The diversity and low cost of carbon nanomaterials make them attractive for the application as ORR catalyst [6, 92]. Therefore, several high area nanocarbon materials (e.g. MWCNTs and GR) have already been investigated as NPM ORR catalysts at the fuel cell cathode [6, 9, 92]. MWCNTs are usually preferred, mainly because of their excellent chemical stability, mechanical strength, high aspect ratio and good electrical conductivity [93, 94]. Despite the high surface area of the carbon-based materials, usually the electrocatalytic activity of pristine carbon nanomaterials towards the ORR is insufficient for fuel cell applications [9, 95]. Therefore, N-doping is a typical approach to enhance the electrocatalytic activity of various nanocarbons towards the ORR [92, 96–98]. The covalent attachment of N atoms affects the charge distribution in the graphitic carbon material, which in turn increases the basic nature and electrocatalytic activity of the N-doped nanocarbon materials towards the ORR [92, 96]. As one option for the preparation of N-doped carbon materials is the pyrolysis of carbon-based material along with the N-containing precursor [99–101]. For the introduction of the nitrogen species into the material, several N-sources have been used, e.g. (poly)aniline [102, 103], NH_3 [68, 73, 74, 104–106], and dicyandiamide (DCDA) [107]. At least five different nitrogen species have been reported on the surface of the N-doped carbon nanomaterials [92, 99–101, 108, 109]. According to the literature, the remarkable contribution to the electrocatalytic activity towards the ORR has been observed even for N content as low as 0.5 at% [110]. Several years ago, the novel composite fibre material consisting of styrene-acrylonitrile copolymer (SAN, Scheme 3) and MWCNTs prepared by electrospinning was introduced by Krumme`s workgroup [111]. Because SAN contains nitrogen, it was an appealing idea of using SAN as a N source for the functionalisation of MWCNTs with N-moieties in order to prepare NPM catalyst. Corresponding study was carried out as a part of this thesis [IX].

In recent years, one-dimensional CNFs have drawn a lot of attention and have been widely studied for the preparation of NPM catalysts [62, 112]. The CNFs are attractive because of their interesting properties e.g. high surface area, high length/diameter ratio, specific porosities and multiple functionalities [112]. For the CNF preparation, the electrospinning technique with further pyrolysis of the material in inert atmosphere can be employed. Electrospinning is considered a simple, low cost, and versatile method for producing nanofibres from different materials [62, 112]. To enhance the CNF properties for fuel cell application, the functionalisation with metals or nitrogen [65, 113–116] can also be used.

The optimisation of pyrolysis temperature is very important for obtaining the CNF based NPM catalyst with optimal performance [66, 68, 74, 102, 104, 113, 117–120]. According to the several reports, the electrospun PAN (Scheme 3) based N-doped NPM catalysts have shown high catalytic activity towards the ORR [67, 73, 74, 102, 104]. Similarly to SAN, PAN polymer also contains nitrogen. Therefore, the ORR performance of the NPM catalyst prepared from three component composite material of MWCNTs, SAN and PAN (SAN/PAN/CNT) was studied herein.

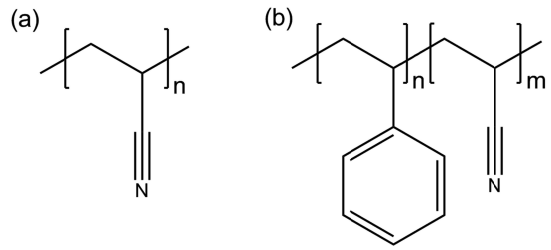

Scheme 3. Repeating units in the structure of (a) polyacrylonitrile (PAN) and (b) styrene-acrylonitrile copolymer (SAN) [X].

A few papers can be found from the literature about the preparation of materials similar to SAN/PAN/CNT. In more specific, Lee et al. have prepared CNFs by pyrolysis of the electrospun PAN and SAN [121] and Zhou et al. have carbonised SAN, PAN and single-walled carbon nanotube composite films. The latter films were prepared by casting on a glass substrate instead of using the electrospinning technique [122]. These described composite materials were tested for the supercapacitor and Li-ion battery applications and there was no information about their performance as ORR catalysts [121, 122]. Therefore, it was very attractive to study the CNFs prepared from electrospun SAN/PAN/CNT composite fibres as NPM catalysts for ORR [X].

From the NPM catalysts based on transition metal-containing and nitrogen-doped carbon materials, the ones functionalised with nitrogen and Co via high-temperature pyrolysis in an inert atmosphere [9, 92] have exhibited improved ORR performance. The increase in the ORR activity due to co-doping with Co and N via carbonisation has been found to be effective on different carbon materials such as carbon nanotubes [123–127], CNFs [64, 68, 128–130], GR [131, 132], carbon aerogels [133–135], carbon spheres [136], carbon nanocomposites [107, 137–139], porous carbon [140–144], carbon dots [145] and carbon black [146]. As one possible reagent, DCDA has been employed as a nitrogen precursor for the modification of the carbon material with nitrogen moieties during carbonisation [56, 107, 124, 126, 127, 132, 134, 142, 144, 146–148].

Low corrosion resistance of carbon materials is one of the major concerns regarding their application as NPM catalyst [5, 149, 150]. To overcome this, silicon oxycarbide (SiOC) is an interesting class of PDCs since their properties can be modified by varying the preceramic polymers and carbonisation conditions. SiOC based ceramics possess high chemical and thermal stability and allow the adjustment of surface properties. The good stability of SiOC is a result of the amorphous structure made of SiO_2/C nanodomains [151, 152]. Since there was no prior information about the use of SiOC based PDC materials as NPM catalyst for the ORR, the corresponding investigation was carried out [XI].

5. AIMS OF THE STUDY

The main purpose of the present PhD thesis was to prepare and characterise the aryl film functionalised electrodes and NPM catalysts. For this reason, the results and discussion section of this PhD thesis is divided into three main chapters and the aims are:

1. to prepare and study the aryl film grafted carbon nanomaterial (EG, GR, CVD-grown GR, MWCNTs) coated and M(AQ) film functionalised GC electrodes. In addition, to apply the RG and RDE combined method for the first time to prepare thick AQ films via reduction of aryldiazonium salts on the GC electrodes [I–VI].
2. to characterise the thick aryl film derivatised Au and Cu electrodes prepared via reduction of aryldiazonium salts for the first time using RG and RDE combined method. Additionally, to functionalise the Ni electrode with NP film using the RG method for the first time [VI–VIII].
3. to prepare the NPM catalysts from the materials that have not been studied before as ORR catalysts [IX–XI].

6. EXPERIMENTAL

6.1. Electrode preparation before modification

The electrodes with geometric area (A) of 0.196 cm^2 were prepared by mounting the discs into Teflon® holders. The discs were prepared from the rods (diameter 5 mm) of GC (GC-20SS, Tokai Carbon, Japan) [I, II, VI, V,VI, IX–XI], Au (99.99%, Alfa Aesar) [VI], Ni (99.995%, Alfa Aesar) [VII] and Cu (99.999%, Puratronic®, Alfa Aesar) [VIII]. The electrodes were polished with silicon carbide grinding paper (P4000) and alumina slurries (1.0 and 0.3 μm, Buehler). After polishing the GC electrodes were sonicated (Bransonic 3510, Branson) in Milli-Q water (Millipore, Inc.), 2-propanol (99.8%, Honeywell Riedel-de Haën) and acetonitrile (ACN, Sigma–Aldrich) for 5 min in each solvent [I, II, IV-VI, IX-XI]. The Au electrodes were additionally polished with 0.05 μm alumina slurry (Buehler) and treated by sonication only in Milli-Q water. After sonication the Au electrodes were cycled between −0.3 and 1.5 V vs SCE (v = 100 mV s^{-1}) in Ar-saturated (99.999%, AGA) 0.5 M H_2SO_4 (96% Suprapur®, Merck) for surface cleaning of Au [VI]. Ni electrodes were cleaned by ultrasonication in Milli-Q water after polishing [VII]. Polycrystalline Cu electrodes were sonicated in Milli-Q water and ACN for removing polishing residue. Prior to electrografting or electrochemical measurements, the Cu electrodes were immersed into CH_3COOH (99.8%, puriss p.a., Sigma–Aldrich) for 30 s [47, 153, 154] and rinsed with Milli-Q water [VIII].

Graphene was prepared by CVD method onto 25 μm thick Ni foil similarly as described earlier [155]. The graphene was used without transferring it to another substrate and therefore it is designated as Ni/Gra electrode [III].

6.1.1. Grafting with AQ during electrochemical exfoliation

AQ-modified graphene (designated as EG-AQ) was synthesised during the electrochemical exfoliation of graphite according to the published procedure [85]. In brief, the EG-AQ-1 was prepared by dispersing 2-aminoanthraquinone (223 mg) in ACN (70 mL) via sonication for 30 min. Then, the suspension was stirred for 12 h at 50 °C [156]. The mixture was cooled down to room temperature and the anthraquinone-2-diazonium cations were generated *in situ* by adding 0.22 mL of tert-butylnitrite (1 equiv. compared to the quinone). After 30 min, another 0.22 mL of tert-butylnitrite was added and the mixture was stirred for 30 min. This solution was added to 130 mL of 0.15 M H_2SO_4 for obtaining the 200 mL anthraquinone diazonium cations solution (5 mM, N_2^+-AQ). The EG-AQ-2 was prepared similarly as EG-AQ-1, but using the 16 mM N_2^+-AQ solution. For comparison purposes, EG without AQ was also prepared.

1 mg of the corresponding nanomaterial (EG, EG-AQ-1, and EG-AQ-2) was dispersed by ultrasonication in 1 mL of *N,N*-dimethylformamide (DMF, Sigma–Aldrich) or 2-propanol that contained 0.05% anion exchange ionomer (OH^-

ionomer, 5 wt%, AS-04, Tokuyama Corp., Japan). Then, 20 μL of the catalyst ink was pipetted onto the GC electrode surface to obtain 0.1 mg cm^{-2} catalyst loading. The solvent from the ink was evaporated in the oven at 60 °C for 20 min. The electrodes were carefully rinsed with Milli-Q water prior to electrochemical measurements and are designated as GC/ followed by the carbon material (e.g. EG, EG-AQ-1 and EG-AQ-2). The additional marking of I is used if the catalyst ink suspension was prepared in 2-propanol containing 0.05% OH^- ionomer [I].

6.1.2. Spontaneous grafting of MWCNTs and graphene with AQ

The procedure for spontaneous grafting was taken from the literature [27]. Specifically, 4 mg of GR (Strem Chemicals, Inc., 06-0235 Graphene nanoplatelets aggregates) containing 1% of sodium dodecyl sulphate (SDS, Sigma–Aldrich) was dispersed in 4 mL of Milli-Q water by sonication. Then to obtain the 59 mM solution of anthraquinone-1-diazonium compound 0.256 g of FRA (Sigma–Aldrich) was added. The spontaneous grafting was carried out by placing the beaker with the solution on the magnetic stirrer for 1 h. Afterwards, the obtained material was filtered 4 times with Milli-Q water and 2 times with ACN. The AQ-modified GR was dried in an oven at 60 °C and is designated as $GR/AQ(W)_S$.

For comparison purposes, the spontaneous grafting was also carried out in 4 mL of ACN instead of SDS containing Milli-Q water. Other conditions of the grafting procedure were the same and the obtained material is designated as GR/AQ_S. In addition, the purified [25] MWCNTs (Nano-Lab, Inc., Brighton, MA, USA) were also grafted in the ACN solution according to the same procedure and the obtained material is designated as $MWCNT/AQ_S$.

For preparing the catalyst ink, 1 mg of the corresponding nanomaterial (GR, MWCNTs, $GR/AQ(W)_S$, GR/AQ_S or $MWCNT/AQ_S$) was dispersed in 1 mL of ACN by sonication. Then 20 μL of the ink was drop casted on the GC electrode followed by ACN evaporation in air resulting in 0.1 mg cm^{-2} catalyst loading on the GC surface. For comparison, some of the electrodes were also coated with OH^- ionomer. In specific, 4 μL of 0.05% OH^- ionomer in 2-propanol was drop-casted onto the electrode to obtain 8 μg cm^{-2} OH^- ionomer loading. The prepared electrodes are designated as GC/ followed by the carbon nanomaterial and /I only in case of OH^- ionomer coating [II].

6.1.3. Electrochemical grafting

6.1.3.1. Carbon nanomaterial coated GC electrodes

The bare GC or unmodified nanomaterial coated GC electrodes (GC/MWCNT or GC/GR) were used for electrografting by the reduction of aryldiazonium salts. The grafting was carried out in Ar-saturated ACN containing 10 mM FRA and 0.1 M $TBABF_4$ as a supporting electrolyte. For electrografting the potential

of the electrode was cycled three times from 0.7 to −0.3 V vs SCE at 50 mV s^{-1}. After the potential cycling the electrode was held at −0.3 V vs SCE for 5 min. The prepared electrodes were then cleaned for 30 min in ACN on the magnetic stirrer. The electrografted electrodes are designated as GC/AQ_E, GC/GR/AQ_E, GC/MWCNT/AQ_E and with additional /I in case of OH^- ionomer coating [II].

6.1.3.2. CVD-grown graphene and Ni electrodes

The electrochemical measurements and electrografting with Ni/Gra electrodes were performed using a special designed three-electrode cell with bare or aryl-modified Ni/Gra as a working electrode (A = 0.64 cm^2) [III]. NBD (97%, Aldrich) was used in order to electrograft the Ni/Gra substrates or Ni electrodes with NP groups. For the clarification, NP-film modified Ni/Gra and Ni electrodes are designated as Ni/Gra/NP and Ni/NP, respectively. Surface modification of Ni/Gra electrodes was performed in Ar-saturated ACN (HPLC grade, Sigma-Aldrich) containing 1 mM of the NBD and 0.1 M $TBABF_4$ as a base electrolyte using repetitive potential cycling. For the Ni electrodes, the 3 mM NBD concentration was used in the electrografting solution. Pt-foil served as a counter electrode and SCE was used as a reference electrode. In some cases, additional holding at a fixed potential was used. After electrochemical grafting, the NP-film modified Ni/Gra electrodes were carefully rinsed with ACN in order to remove most of the adsorbed species [III, VII].

For the “normal” electrografting of Ni electrodes, 10 CV cycles between 0.3 and –0.4 V were used. After potential cycling, the electrode was held at –0.4 V for 10 min. The Ni electrodes were also modified by RG in order to obtain thicker NP films on Ni surface. For that purpose, 10 CV cycles between 0.3 and –1.8 V were carried out. The Ni electrodes modified via “normal” electrografting and RG are designated as Ni/NP1 and Ni/NP2, respectively. In all cases, the potential cycling was performed at 100 mV s^{-1} and after surface grafting the aryl-modified Ni electrodes were sonicated in ACN for 5 min [VII].

6.1.3.3. GC electrodes

In the article [IV], the surface of GC electrodes was covalently modified with 9,10-anthraquinone groups via methylene linker. The electrografting procedure was carried out in the mixture of propylene carbonate and ethylene carbonate 50/50 (v:v) containing 5 mM 2-bromomethyl-anthraquinone (Br-MAQ) or 2-chloromethyl-anthraquinone (Cl-MAQ) and 0.1 M tetrabutylammonium iodide (TBAI) as a supporting electrolyte. All these chemicals were obtained from Sigma-Aldrich and used as received. The GC electrodes electrografted using Br-MAQ or Cl-MAQ are designated as GC/(Br-)MAQ and GC/(Cl-)MAQ, respectively. Different modification procedures were used which are given in Table 1. After electrografting, the electrodes were sonicated in ACN for 5 min to remove the physically adsorbed species [IV].

Table 1. The electrografting conditions for modification of GC electrode surface with MAQ compounds (2-bromomethyl-anthraquinone ((Br-)MAQ) or 2-chloromethyl-anthraquinone ((Cl-)MAQ)). The electrografting solution: 5 mM Br-MAQ or Cl-MAQ in ethylene carbonate-propylene carbonate mixture (50:50, v:v) containing 0.1 M TBAI as supporting electrolyte [IV].

Electrode designation	Modification conditions
GC/(Br-)MAQ[1]	10 cycles between 0 and –0.4 V at 100 mV s^{-1}
GC/(Br-)MAQ[2]	10 cycles between 0 and –0.5 V at 100 mV s^{-1}
GC/(Br-)MAQ[3] GC/(Cl-)MAQ[a]	10 cycles between 0 and –0.6 V at 100 mV s^{-1}
GC/(Br-)MAQ[4] GC/(Cl-)MAQ[b]	10 cycles between 0 and –0.7 V at 100 mV s^{-1}
GC/(Br-)MAQ[5] GC/(Cl-)MAQ[c]	10 cycles between 0 and –0.8 V at 100 mV s^{-1}
GC/(Cl-)MAQ[d]	10 cycles between 0 and –0.9 V at 100 mV s^{-1}
GC/(Br-)MAQ[6]	GC electrode was held at –0.4 V for 10 min
GC/(Br-)MAQ[7]	GC electrode was held at –0.5 V for 10 min
GC/(Br-)MAQ[8] GC/(Cl-)MAQ[e]	GC electrode was held at –0.6 V for 10 min
GC/(Br-)MAQ[9] GC/(Cl-)MAQ[f]	GC electrode was held at –0.7 V for 10 min
GC/(Br-)MAQ[10] GC/(Cl-)MAQ[g]	GC electrode was held at –0.8 V for 10 min
GC/(Cl-)MAQ[h]	GC electrode was held at –0.9 V for 10 min

In the papers [V-VI], the covalent attachment of AQ groups was performed by the electrochemical reduction of the corresponding diazonium salt. The initial modification procedure was taken from the literature [36–38]. The electrografting was carried out by CV using a scan rate of 100 mV s^{-1} in ACN solution containing diazonium salt (FRA) and 0.1 M $TBABF_4$ as supporting electrolyte. Two different concentrations of diazonium salt (2 and 10 mM) and various number of potential cycles were used in order to obtain electrodes with different Γ_{AQ} values. The designations of the electrografted electrodes together with the specific modification conditions are presented in Table 2. If the electrografting was carried out in the ACN solution containing 10 mM Fast Red AL salt the additional marking of $^{\bullet}$ is used in the designation of the electrode. In addition, to study the electrografting of GC electrode with AQ groups in hydrodynamic conditions, the combination of CV and rotating disc electrode (RDE) method was applied [VI]. The RDE experiments were carried out using the EDI101 rotator and a CTV101 speed control unit (Radiometer, Copenhagen). The used rotation rates and specific modification procedures are given in Table 2. After electrografting, the AQ-modified GC electrodes were sonicated in ACN for 5 min for surface cleaning [V, VI].

Table 2. The modification procedures of GC electrodes with anthraquinone groups. Modification conditions: 2 mM or 10 mM Fast Red AL salt in acetonitrile containing 0.1 M $TBABF_4$ as a supporting electrolyte (v = 100 mV s^{-1}). If the 10 mM Fast Red AL salt solution was used for electrografting, the additional marking of $^{\bullet}$ is used [IV, V].

Electrode designation	Modification conditions
GC/AQ-1CV GC/AQ-1CV$^{\bullet}$	1 cycle between 0.6 and −1.45 V, ω = 0 rpm
GC/AQ-2CV$^{\bullet}$	2 cycles between 0.6 and −1.45 V, ω = 0 rpm
GC/AQ-3CV GC/AQ-3CV$^{\bullet}$	3 cycles between 0.6 and −1.45 V, ω = 0 rpm
GC/AQ-5CV$^{\bullet}$	5 cycles between 0.6 and −1.45 V, ω = 0 rpm
GC/AQ-10CV GC/AQ-10CV$^{\bullet}$	10 cycles between 0.6 and −1.45 V, ω = 0 rpm
GC/AQ-1.1	10 cycles between 0.6 and −1.1 V, ω = 1000 rpm
GC/AQ-1.3	10 cycles between 0.6 and −1.3 V, ω = 1000 rpm
GC/AQ-200	10 cycles between 0.6 and −1.2 V, ω = 200 rpm
GC/AQ-500	10 cycles between 0.6 and −1.2 V, ω = 500 rpm
GC/AQ-1	1 cycle between 0.6 and −1.2 V, ω = 1000 rpm
GC/AQ-2	2 cycles between 0.6 and −1.2 V, ω = 1000 rpm
GC/AQ-3	3 cycles between 0.6 and −1.2 V, ω = 1000 rpm
GC/AQ-6	6 cycles between 0.6 and −1.2 V, ω = 1000 rpm
GC/AQ-10	10 cycles between 0.6 and −1.2 V, ω = 1000 rpm
GC/AQ-10*	10 cycles between 0.6 and −1.2 V, ω = 0 rpm

6.1.3.4. Au and Cu electrodes

The functionalisation of Au electrode with AQ groups was carried out in Ar-saturated ACN containing 2 mM FRA and 0.1 M $TBABF_4$ as a supporting electrolyte. The electrografting of polycrystalline Cu electrodes with AQ or NP groups was performed in ACN solution containing 3 mM FRA or NBD, respectively and 0.1 M $TBABF_4$ as a supporting electrolyte. For electrografting, CV or the combination of CV and RDE method was used. To achieve variable surface concentrations of AQ or NP groups on Au or Cu electrodes, several modification procedures were applied (Table 3). The designations for the aryl film functionalised Cu or Au electrodes by specific modification procedure are also given in Table 3. After electrografting, the electrodes were sonicated in ACN for 5 min to remove the physically adsorbed material [VI, VIII].

Table 3. Different procedures applied for the electrografting of Au and Cu electrodes using (a) Fast Red AL (FRA) or (b) 4-nitrobenzenediazonium tetrafluoroborate (NBD). Modification conditions: Ar-saturated ACN solution containing 2 or 3 mM of the corresponding diazonium salt in case of Au and Cu electrodes, respectively, and 0.1 M $TBABF_4$, v = 100 mV s^{-1} [VI, VIII].

Electrode designation	Modification conditions
Au/AQ-0.4	(a) 10 cycles between 0.5 and −0.4 V, ω = 0 rpm
Au/AQ-200	(a) 10 cycles between 0.5 and −1.2 V, ω = 200 rpm
Au/AQ-500	(a) 10 cycles between 0.5 and −1.2 V, ω = 500 rpm
Au/AQ-1	(a) 1 cycle between 0.5 and −1.2 V, ω = 1000 rpm
Au/AQ-2	(a) 2 cycles between 0.5 and −1.2 V, ω = 1000 rpm
Au/AQ-3	(a) 3 cycles between 0.5 and −1.2 V, ω = 1000 rpm
Au/AQ-6	(a) 6 cycles between 0.5 and −1.2 V, ω = 1000 rpm
Au/AQ-8	(a) 8 cycles between 0.5 and −1.2 V, ω = 1000 rpm
Au/AQ-10	(a) 10 cycles between 0.5 and −1.2 V, ω = 1000 rpm
Au/AQ-10*	(a) 10 cycles between 0.5 and −1.2 V, ω = 0 rpm
Cu-AQ-CV-0.7	(a) 10 cycles between –0.35 and –0.7 V, ω = 0 rpm + 300 s hold at constant potential –0.7 V
Cu-NP-CV-0.7	(b) 10 cycles between –0.35 and –0.7 V, ω = 0 rpm + 300 s hold at constant potential –0.7 V
Cu-AQ-CV-1.2	(a) 10 cycles between –0.35 and –1.2 V, ω = 0 rpm
Cu-NP-CV-1.2	(b) 10 cycles between –0.35 and –1.2 V, ω = 0 rpm
Cu-AQ-RDE-1.2	(a) 10 cycles between –0.35 and –1.2 V, ω = 1000 rpm
Cu-NP-RDE-1.2	(b) 10 cycles between –0.35 and –1.2 V, ω = 1000 rpm
Cu-AQ-CV-1.5	(a) 10 cycles between –0.35 and –1.5 V, ω = 0 rpm
Cu-NP-CV-1.5	(b) 10 cycles between –0.35 and –1.5 V, ω = 0 rpm
Cu-AQ-RDE-1.5	(a) 10 cycles between –0.35 and –1.5 V, ω = 1000 rpm
Cu-NP-RDE-1.5	(b) 10 cycles between –0.35 and –1.5 V, ω = 1000 rpm

6.1.4. Preparation of SAN-MWCNTs and SAN/PAN/CNT composite fibre based catalyst materials

Four electrospun nanofibre materials with different composition were prepared [IX, X]. The fibres consisted of PAN (M_W = 150,000, Sigma-Aldrich), SAN (Polimeri Europa SRL) and MWCNTs (90% purity, diameter of 9.5 nm and length of 1.5 μm, NANOCYL™ NC7000) and were used as received without further purification. The designation and composition of these materials is presented in Table 4. The specific conditions for the preparation of the materials by electrospinning can be found in the original articles [IX, X]. For the catalyst material preparation, the fibre materials were pyrolysed in the quartz tube furnace (MTF 12/38/400, Carbolite) under N_2 atmosphere using heating rate of 10 °C min^{-1} to a specific temperature (700, 800, 900, 1000, 1100 or 1200 °C) and kept at that temperature for 2 h. The designation of the prepared materials is based on the precursor material (Table 4) followed by the used pyrolysis temperature. For comparison purposes, additional materials were also prepared

applying the stabilisation at 250 °C in air [67, 102, 106, 122, 157] prior to pyrolysis in inert atmosphere in case of SAN/PAN, SAN/PAN/CNT and PAN/CNT materials. Corresponding materials have the additional marking of 250/ in the designation before the pyrolysis temperature.

Table 4. Designation and the content of fibre precursor materials (wt%) in the precursor mixture for the electrospinning solutions and in the electrospun fibres prepared in the present work [IX, X].

Designation	Composition of fibre material
SAN-MWCNT	99% SAN, 1% MWCNTs
SAN/PAN	25% SAN, 75% PAN
SAN/PAN/CNT	25% SAN, 72.5% PAN, 2.5% MWCNTs
PAN/CNT	97.5% PAN, 2.5% MWCNTs

For the catalyst ink preparation in case of SAN-MWCNT based materials, 1 mg of the pyrolysed material was dispersed in 1 mL of 2-propanol followed by sonication (2 h). To study the influence of OH^- ionomer, the catalyst inks were also prepared in 2-propanol containing 0.05% OH^- ionomer. The catalyst materials prepared with OH^- ionomer containing ink are designated with additional /I. The catalyst ink with pristine MWCNTs was prepared in DMF. For the catalyst ink preparation of SAN/PAN, SAN/PAN/CNT and PAN/CNT based materials, 8 mg of the pyrolysed material together with 10 µL of Nafion® solution (5 wt%, Aldrich) was dispersed in 2 mL of 2-propanol followed by sonication for 1.5 h.

As an underlying substrate, the GC electrode was used as described in Section 6.1. The catalyst ink of SAN-MWCNT based materials was pipetted onto the GC electrode surface yielding a catalyst loading of 0.1 mg cm^{-2}. Pristine MWCNTs dispersed in DMF and coated on GC were dried in oven at 60 °C for 20 min. The catalyst ink of SAN/PAN, SAN/PAN/CNT and PAN/CNT based materials was pipetted (5×2 µL) onto the GC electrode resulting in catalyst loading of 0.2 mg cm^{-2}. After coating, the electrodes were rinsed with Milli-Q water. The prepared electrodes are designated as GC/ followed by specific catalyst material [IX, X].

6.1.5. Preparation of PDC catalyst materials

The SiOC based PDC materials were synthesised according to the previously reported procedure for the preparation of conductive porous materials and hybrid materials containing metallic nanoparticles [158, 159]. The chemicals and precursor materials used for the preparation of PDC catalyst materials with and without the transition metal (Ni or Co) were silicon resin poly(methyl silsesquioxane) (MK, Wacker Chemie AG), poly(methyl phenyl silsesquioxane)

(H44, Wacker Chemie AG), graphite (KS75, IMERYL Graphite & Carbon), molybdenum disilicide ($MoSi_2$, abcr GmbH), azodicarboxamide (Azo, Sigma-Aldrich), nickel chloride ($NiCl_2$, Alfa Aesar), cobalt chloride ($CoCl_2$, Alfa Aesar), xylene (Sigma-Aldrich), imidazole (Imi, Alfa Aesar). The specific procedures for the preparation of the materials can be found in the article [XI]. The synthesised samples are designated as PDC, PDC-Ni, and PDC-Co.

For the nitrogen doping of PDC, PDC-Ni and PDC-Co materials a previously published procedure was used [56]. As the nitrogen source, DCDA was added with a weight ratio of 1:20 (PDC:DCDA, PDC-Ni:DCDA or PDC-Co:DCDA). PVP was employed as a surface-active agent, in an amount of 1/10 of the PDC, PDC-Ni or PDC-Co material. The mixed reagents were transferred to a beaker containing 2-propanol and sonicated for 2 h to obtain a homogeneous mixture. After sonication, the 2-propanol was evaporated at 60 °C. The obtained material was pyrolysed in N_2 atmosphere at 800 °C for 2 h using a heating rate of 10 °C min^{-1}. After pyrolysis, the furnace was slowly cooled to room temperature. The N-doped materials are designated as: PDC-N, PDC-Ni-N, PDC-Co-N.

As an underlying substrate, the GC electrode was used as described in Section 6.1. For coating the GC electrode with the corresponding catalyst material, 2 mg of the nanomaterial was dispersed in 1 mL of 2-propanol followed by sonication for 1 h. Thereafter, 10×2 µL of the catalyst ink was pipetted onto the polished GC surface. The solvent evaporated in air, yielding a 0.2 mg cm^{-2} catalyst loading. Prior to electrochemical measurements, the electrodes were rinsed with Milli-Q water. For clarification, the catalyst-coated GC electrodes are designated as underlying material GC/ followed by the catalyst material. For the comparison, also the Pt/C catalyst coated GC electrode was prepared with the commercial 20 wt% Pt catalyst supported on Vulcan carbon XC-72 (E-TEK, Inc., Framingham, MA, USA). The Pt/C catalyst was dispersed in 2-propanol and the GC electrode was coated with Pt/C ink yielding the Pt loading of 40 µg cm^{-2} [XI].

6.2. Physical characterisation

Raman spectroscopy measurements were carried out with a micro-Raman system (UHTS300) using excitation from an Ar ion laser beam (532 nm) at 2 mW power level in order to avoid the decomposition of organic functional groups. For performing the thermogravimetric analysis a thermogravimetric analyser (TA Instruments TGA (Q500)/Discovery MS) was employed. Into the Pt pan a 2 mg sample was placed and heated (5 °C min^{-1}) from 30 to 800 °C under flowing He atmosphere [I].

The XPS characterisation of the materials was carried out using the 11×11 mm GC plates coated with nanomaterial without the binder (e.g. OH^- ionomer or Nafion®) [II, IX-XI], AQ-modified redox grafted GC plate (Table 2) [V], bare Ni, Ni/Gra and aryl-modified Ni/Gra samples (Section 6.1.3.2) [III], NP film

modified Ni plates (Section 6.1.3.2) [VII], AQ film modified Au discs (A = 0.196 cm^2, Section 6.1.3.4) [VI], bare and AQ or NP modified Cu (99.999%, extra pure) plates (Section 6.1.3.4) [VIII]. The XPS analyses were performed with SCIENTA SES-100 spectrometer with a 300 W unmonochromated Mg K_α X-ray source (incident energy 1253.6 eV) [II, V–XI] or with a 400 W unmonochromated Al Kα X-ray source (incident energy 1486.6 eV) [III, XI], electron take-off angle 90° and pass energy was 200 eV. The pressure inside the analysis chamber was less than 10^{-9} Torr. Step sizes of 0.5 eV and 0.1 eV were used for survey and high-resolution scan, respectively [II, III, V–XI].

In case of composite material coated GC electrodes the determination of doped N species was carried out [IX-XI]. The N1s XPS peak was deconvoluted to 5 components [109]: (i) pyridinic-N, (ii) amines, (iii) pyrrolic-N, (iv) graphitic-N and (v) pyridine-N-oxides. The specific values and procedure for the deconvolution is given in the Experimental section of the articles [IX–XI]. All peaks were assumed to be 70% Gaussian and 30% Lorentzian. A blend of 50% Shirley and 50% linear background was used except in case of the N1s XPS spectra for PDC materials [IX, X]. A linear background was used for PDC-Co, but for all other PDC materials, Shirley background was used [XI]. The software CasaXPS (2.3.18) was used for peak fitting [IX-XI].

AFM experiments were carried out with a multimode AFM Autoprobe CP II (Veeco). The images were recorded in non-contact mode using UL20 (PSI) [III, VI], NSG 01 (NT-MDT) [III, VI] or HA-HR (NT-MDT) [VIII] series cantilevers under ambient conditions. The Gwyddion free software (Czech Metrology Institute) ver. 2.34 [III], ver. 2.42 [VI] or ver. 2.44 [VIII] was employed for image processing. In case of using stationary Au electrode during the modification procedure, the Au film on a mica substrate was used and after electrografting, the substrate was carefully rinsed with ACN [VI]. All images were processed by the first-order flattening for background slope removal, and if necessary, the contrast and brightness were adjusted. For measuring the aryl film thickness, AFM was used in contact mode to scratch off the modifier layer. The scanning continued until a typical image of a clean electrode surface was obtained. Thereafter the height difference was measured in non-contact mode [III, VI, VIII].

For SEM experiments, GC discs were coated with catalyst ink [XI] without OH^- ionomer [IX] or Nafion® [X]. The surface morphology and the transition metal content of the catalyst materials was studied with high-resolution scanning electron microscope (HR-SEM) Helios NanoLab 600 (FEI Company) equipped with an energy-dispersive X–ray (EDX) spectrometer analyser INCA Energy 350 (Oxford Instruments) [IX-XI].

6.3. Electrochemical characterisation

The electrochemical measurements were carried out in Ar-saturated or O_2-saturated (99.999%, AGA) 0.1 M KOH (p.a. quality, Merck). The ferricyanide reduction measurements on bare and aryl film modified GC and Au electrodes were carried out in Ar-saturated 0.1 M K_2SO_4 (p.a. quality, Merck) solution containing 1 mM potassium hexacyanoferrate(III) ($K_3Fe(CN)_6$, Aldrich) [VI]. In case of bare and aryl film modified Ni and Cu electrodes, the ferricyanide reduction was performed in Ar-saturated 0.1 M KOH solution containing 1 mM $K_3Fe(CN)_6$ [VII, VIII]. In two papers, for the determination of the amount of redox active groups within the aryl film on GC, Au and Cu electrodes cyclic voltammograms were recorded in Ar-saturated anhydrous ACN containing 0.1 M vacuum dried $TBABF_4$ [VI, VIII]. The reduction of O_2 on bare and aryl film modified polycrystalline Cu electrodes and PDC based catalyst materials was studied in O_2-saturated 0.1 M phosphate buffer solution (PBS, pH = 7) containing 0.1 M $NaClO_4$ (pro analysi, Merck). The background was recorded in Ar-saturated solution. The PBS was prepared from Na_2HPO_4 (puriss p.a., Fluka) and KH_2PO_4 (pro analysi, Merck) [VIII, XI]. All the presented RDE voltammetry curves are baseline-corrected [I–XI].

For electrochemical characterisation CV and RDE methods were used. The potential was applied to the working electrode with an Autolab potentiostat/ galvanostat PGSTAT30 or PGSTAT128N (Eco Chemie B.V., The Netherlands). For controlling the experiments General Purpose Electrochemical System or Nova 2.1 software was used. The SCE served as the reference electrode and all the potentials presented in this PhD thesis are referred to this electrode. A Pt-foil or Pt-wire was employed as a counter electrode. During the measurements continuous flow of corresponding gas was passed through the electrochemical cell at room temperature (23±1 °C) [I-XI].

For the rotating ring-disc electrode (RRDE) measurements, an interchangeable E6 series RRDE tip of GC (A = 0.196 cm^2) disc-Pt ring [IV] or fixed tip GC disc (A = 0.164 cm^2) and Pt ring electrode [IX] (Pine Research, Grove City, PA, USA) and a Pine Research Instrumentation AFMSRX rotator and MSRX speed controller were used. The collection efficiency (N) was 0.25 [IV] or 0.22 [IX] as determined by the reduction of hexacyanoferrate(III) [160]. The Pt ring electrode was activated prior to recording each scan by applying three potential cycles between –1.0 and 0.7 V at 0.1 V s^{-1} to improve reliability in the determination of peroxide. The potential of the Pt ring electrode was kept under potentiostatic control at 0.55 V vs SCE for peroxide detection [IV, IX].

7. RESULTS AND DISCUSSION

7.1. Aryl films on carbon electrodes

In the first part of the thesis the aryl film modified carbon electrodes are described. The first section of this part concerns the electrochemical grafting of MWCNTs [II], graphene [II, III] and GC electrodes [II, IV–VI] with aryl groups. The second section covers the physical characterisation of the aryl film modified carbon electrodes by Raman spectroscopy [I], thermogravimetry [I], XPS [II, III, V] and AFM [III]. In the third section, the electrochemical characterisation of the aryl-modified carbon electrodes is presented. The surface concentration of the electroactive species on the electrodes is determined [I-VI], the surface blocking towards the ferricyanide probe is studied [III, VI] and the ORR on the prepared electrodes is investigated [I, II, IV, V]. It should be noted that the article [VI] is the first report describing the use of RDE and redox grafting (RG) combined method for grafting aryl films onto the GC electrode via diazonium reduction method.

7.1.1. Electrografting of graphene and MWCNTs with AQ groups

The first CV curve recorded during electrografting of GC, GC/MWCNT and GC/GR electrodes via reduction of aryldiazonium salts in the solution containing 10 mM FRA is depicted in Fig. 1. In case of GC electrode the reduction wave of anthraquinone-1-diazonium compound is observed at *ca* 0.33 V vs SCE [14, 161]. On the GC/MWCNT and GC/GR electrodes the reduction wave appears at a more positive potential (*ca* 0.48 V and 0.53 V, respectively). Similar shift in peak potential has been observed in case of graphene oxide coated GC electrode by Zhou et al. [162] and the exact reason for this is unknown.

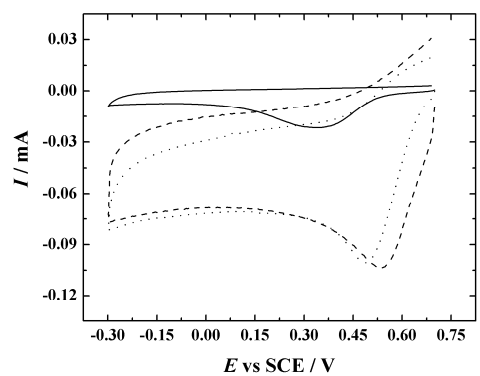

Fig. 1. First cyclic voltammogram of: GC (solid line), GC/MWCNT (dotted line), GC/GR (dashed line) electrodes recorded in Ar-saturated ACN containing 10 mM Fast Red AL and 0.1 M $TBABF_4$ (v = 50 mV s^{-1}) [II].

Although, the electrografted materials (GC, MWCNT and GR) consist mainly of sp^2 carbon [163] we suggest that the observed shift is due to the electronic effects of nanomaterial. In addition to the shift in the potential of the reduction peak, the overall higher reduction current is observed for nanomaterial coated GC electrodes. This can be explained by the higher electroactive surface area of MWCNT and GR compared to the GC [15]. On the subsequent grafting cycles (data not shown) the well-known decrease in reduction current was observed due to the surface blocking by the AQ film grafted via reduction of aryldiazonium salts [14, 164].

7.1.2. Electrografting of CVD-grown graphene with NP films

Ni/Gra electrodes were grafted with NP groups by electrochemical reduction of the corresponding diazonium salt (NBD) using "normal" electrografting or RG method. For "normal" electrografting to obtain Ni/Gra/NP1 and Ni/Gra/NP2 electrodes, a narrow potential range from 0.6 to –0.5 V (v = 100 mV s^{-1}) using one and 10 potential cycles (Fig. 2a) was applied, respectively. After 10 potential cycles, the Ni/Gra/NP2 was additionally held at –0.2 V for 10 min in order to increase the thickness of the aryl layer. As observed in Fig. 2a, a reduction wave of 4-nitrobenzenediazonium cation at *ca* 0.38 V on the first cycle was registered which completely disappears on the consecutive cycles indicating the progressive blocking of the electrode surface with a NP film [165]. Therefore, we may assume that the Ni/Gra electrode becomes covered by NP layers.

The RG method was used in order to prepare thick NP film covered Ni/Gra electrode (Ni/Gra/NP3). In detail, the electrografting (Fig. 2b) was performed in a wider potential range (from 0.6 to -1.4 V) using higher scan rate (v = 1 V s^{-1}).

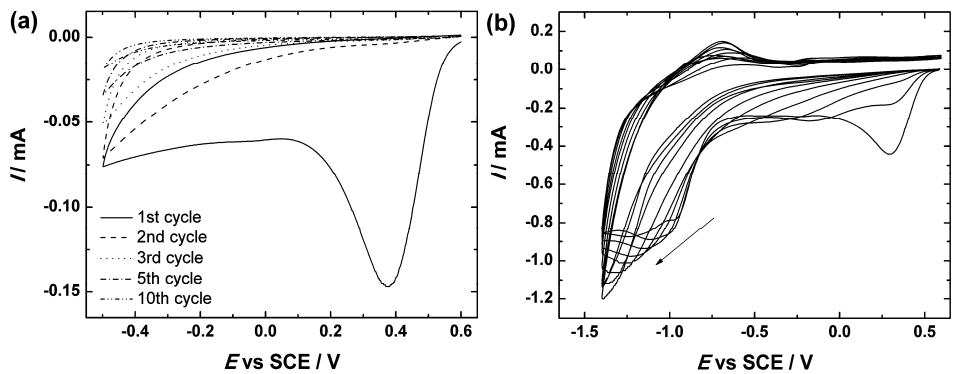

Fig. 2. Electrografting of 4-nitrophenyl groups on Ni/Gra electrodes in Ar-saturated ACN containing 1 mM 4-nitrobenzenediazonium tetrafluoroborate and 0.1 M TBABF4 as a base electrolyte using: **(a)** switching potential –0.5 V and ν = 100 mV s^{-1}; **(b)** switching potential –1.4 V and ν = 1 V s^{-1}. In Fig. (a), the 1st, 2nd, 3rd, 5th and 10th potential cycles are shown and in Fig. **(b)**, the arrow shows the direction for increasing number of potential cycles applied during the redox grafting [III].

The reduction peak of 4-nitrobenzenediazonium cation was registered at a more negative potential ($E_p \approx 0.25$ V) in case of RG method compared to the "normal" electrografting ($E_p \approx 0.38$ V), which is most likely caused by the higher sweep rate. As in case of "normal" electrografting, the reduction peak diminished after 10 consecutive potential cycles. In addition, the second redox wave with an additional cathodic pre-peak was recorded at more negative potentials (at *ca* –1 V) which might correspond to the formation of the NP radical anions [36]. During subsequent potential cycling, the second redox wave shifted to a more negative potential and the increase in the current values of the redox wave was observed (Fig. 2b). Based on the studies by Daasbjerg's workgroup [36–38] this could refer to the increase of the redox active groups attached to the electrode surface [III].

7.1.3. Electrografting of GC electrodes with anthraquinone

7.1.3.1. Electrografting of MAQ groups onto the GC

The surface of the GC electrode was electrografted with AQ groups via methylene linker in the mixture of propylene carbonate and ethylene carbonate containing 5 mM Br-MAQ or Cl-MAQ and 0.1 M TBAI as a supporting electrolyte. The procedure for surface modification was obtained from literature [39]. Firstly, the CV curve of the GC electrode was registered in a wider potential range (Fig. 3a) to confirm the results obtained by Jouikov and Simonet [39]. In the present work, a broader peak at *ca* –0.7 V in case of Br-MAQ was recorded (Fig. 3a). Jouikov et al. [39] reported the appearance of two peaks in the same potential region where the free radical formation and its further reduction occurs. Although, when the experiment in the present work was made with Cl-MAQ (Fig. 3a), two peaks were registered (at *ca* –0.55 and –0.8 V) which might correspond to the formation of the free radical and its further reduction as reported in the literature [39]. In case of both AQ compounds (Br-MAQ and Cl-MAQ), two redox waves at more negative potentials were recorded (Fig. 3a). According to several studies about the redox behaviour of AQ and its derivatives [166–168], these redox waves could correspond to the formation of radical anion ($AQ^{\bullet -}$) and dianion (AQ^{2-}), respectively.

In Figs. 3b and c, the CV curves of a GC electrode modification in the solutions of 5 mM Br-MAQ and Cl-MAQ are shown, respectively. In both cases, the peak currents decreased during the subsequent cycles, which could indicate the partial blocking of the electrode surface due to the formation of MAQ layer. Similar electrochemical grafting behaviour has been observed in case of the diazonium reduction method (Fig. 2a) [14, 29] [II, III]. In both methods, a radical is formed in the first step, which should then react with the GC electrode surface in the following step. However, as presented in Fig. 3b, the reduction peak at *ca* –0.7 V did not disappear eventually. In addition, as can be seen in Fig. 3c, the peak at *ca* –0.55 V shifted towards more negative potentials and

disappeared during the 10 consecutive potential cycles. At the same time, the second peak (at *ca* –0.8 V) did not diminish even after 10 potential cycles. According to these observations, this grafting procedure may not yield in a complete blocking of the GC electrode surface with MAQ groups.

For comparison with the modification via potential cycling, the GC electrode was also electrografted with MAQ groups by holding the electrode at a fixed potential for 10 min (Table 1). The peak current values on the CV curve of the MAQ-modified GC electrode recorded after the electrografting procedure (data not shown) were almost 10 times lower than after cycling the electrode for 10 times in the corresponding modification solution. These observations indicate that in case of holding at a fixed potential the surface blocking of the GC surface by MAQ groups could be more complete than in case of electrografting via potential cycling [IV].

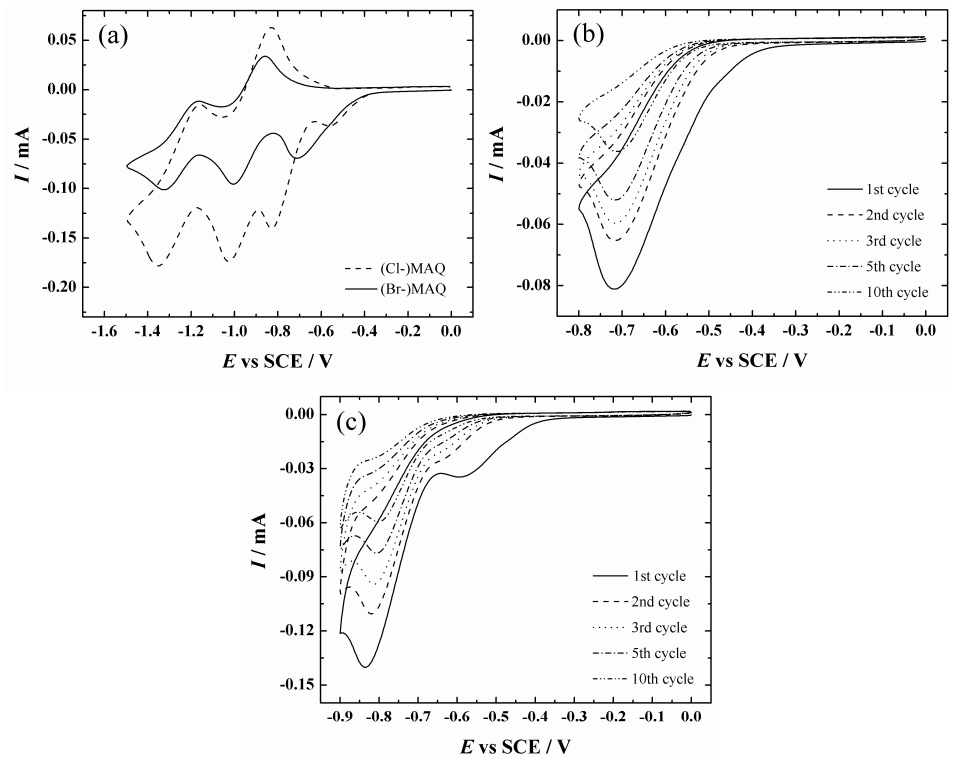

Fig. 3. Cyclic voltammograms of GC electrodes recorded in Ar-saturated solution of propylene carbonate and ethylene carbonate containing 5 mM **(a)** 2-bromomethyl-anthraquinone ((Br-)MAQ) or 2-chloromethyl-anthraquinone ((Cl-)MAQ), **(b)** (Br-)MAQ, **(c)** (Cl-)MAQ) and 0.1 M TBAI as a supporting electrolyte (ν = 100 mV s^{-1}) [IV].

7.1.3.2. Electrografting via reduction of aryldiazonium salts

The cyclic voltammograms presenting the RG of AQ groups on GC electrode by the electrochemical reduction of Fast Red AL salt in the potential range from 0.6 V to –1.45 V are shown in Figs. 4a and b. The RG behaviour is in good agreement with the results obtained by Daasbjerg's workgroup [36, 37]. The difference between RG conditions in Figs. 4a and b was the diazonium salt concentration of 2 and 10 mM, respectively. In both cases, the first cycle showed the reduction wave of AQ diazonium cations at *ca* 0.4 V, which disappeared during subsequent cycles as was also observed in case of Ni/Gra electrode during RG with NP groups (Fig. 2b). In Figs. 4a and b, a redox wave appeared at more negative potentials with the peak potential separation (ΔE_p) and redox potential (E^o) values of *ca* 0.166 V and –0.89 V, respectively. According to the literature [168], this redox wave could correspond to the one-electron reduction of AQ to $AQ^{\bullet-}$. Similarly to the study by Bousquet et al. [37] the increase in the intensity of the redox wave during the following cycles was observed (Figs. 4a, b). This could be due to a steady increase in the number of AQ groups attached to the electrode surface [37]. During potential cycling, a pre-wave at around −0.6 V appeared and the peak was still present up to 10th cycle. It is believed that this peak might originate from the so-called total catalysis situation, where the diazonium salt is consumed in diffusion layer due to the fast mediated (by carbonyl groups within the AQ film) electron transfer from electrode surface to the aryldiazonium salt [37]. It can be noted that the peak currents between the pre-wave around −0.6 V and redox wave at *ca* −0.89 V are different. We propose that the increase in the reduction current of the redox wave at −0.89 V compared to the pre-wave around −0.6 V could be caused by the response of AQ groups, which become electroactive within the already surface bound film. In Fig. 4c, the CV cycles of RG in narrower potential range are presented for comparison as this potential range was also applied for electrografting using RG and RDE combined method as shown next.

For functionalisation of the GC electrodes with AQ by RG and RDE combined method, the rotation rate was applied to the electrode during electrografting. In Figs. 4d, e and f, the *I-E* curves obtained using ω of 200, 500 and 1000 rpm are presented, respectively. In hydrodynamic conditions, the pre-peak at *ca* –0.6 V slightly shifted to more negative potentials compared with the electrochemical behaviour of the electrodes when only CV was used for grafting (Figs. 4a–c). The shift in the pre-peak is presumably attributed to the application of the rotation rate. In addition, in case of the RG and RDE combined method, the current plateau was formed from *ca* −1.0 to −1.2 V (Figs. 4d–f), which may correspond to the reduction of AQ to $AQ^{\bullet-}$, whereas the minor oxidation wave at *ca* −0.85 V may refer to the oxidation of electroactive $AQ^{\bullet-}$ groups back to the AQ in the surface bound aryl film [168]. According to the Levich equation [24] the plateau current is not solely diffusion limited and we propose that the inhibition of mass-transfer occurs by the steric restriction of already surface bound aryl film. In addition, the increase in the reduction

plateau currents up to the 9th, 4th and 3rd *I-E* curves applying 200, 500 or 1000 rpm, respectively, was registered which, similarly to the results obtained by RG method (Fig. 4c), may refer to the increase of electroactive AQ groups in the surface bound aryl film. However, after 9th, 4th and 3rd RDE voltammetry curve, the current signal started to decrease, which is inherent to the electrochemical behaviour of "normal" electrografting.

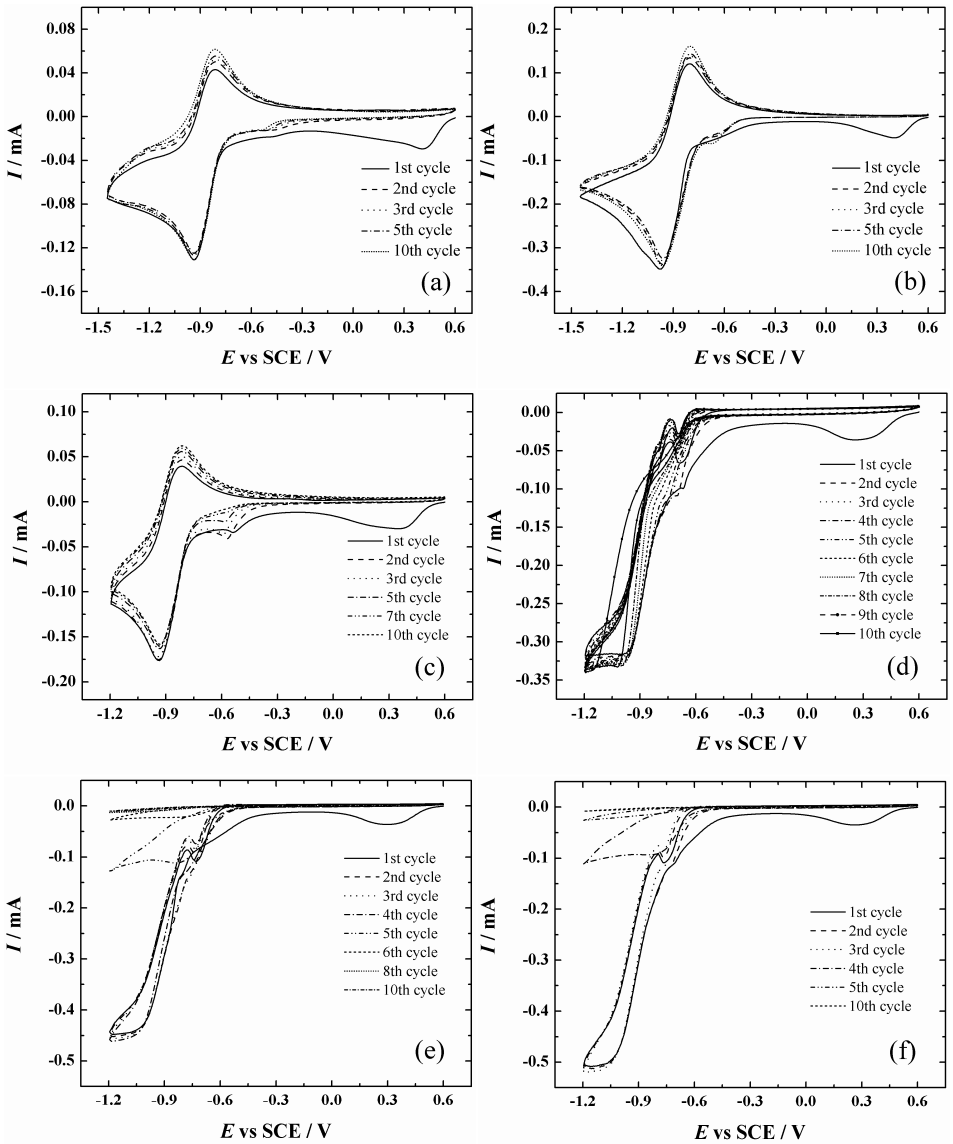

Fig. 4. Redox grafting of anthraquinone on a GC electrode using **(a, c-f)** 2 mM and **(b)** 10 mM Fast Red AL salt in Ar-saturated ACN containing 0.1 M $TBABF_4$ as a base electrolyte by: **(a-c)** cyclic voltammetry (v = 100 mV s^{-1}), **(d-f)** combination of CV and the RDE method (v = 100 mV s^{-1}, ω = **(d)** 200 rpm ; **(e)** 500 rpm; **(f)** 1000 rpm) [V, VI].

The decrease is considered due to the gradual blocking of the electrode surface by the aryl film as explained in Section 7.1.2. In addition, one can notice that the RDE voltammetry curves of GC electrodes recorded at 200, 500 and 1000 rpm (Figs. 4d-f) are different from each other for the plateau currents: the lower the rotation rate, the lower the currents. Simultaneously, the decrease of the current starts later when a lower rotation rate is used. This observation could be explained by the slower mass transfer to the electrode surface at 200 and 500 rpm compared to the 1000 rpm. The electrografting conditions were also varied to optimise the AQ film formation on the GC electrodes (Table 2) [V, VI].

7.1.4. Physical characterisation of aryl-modified carbon electrodes

7.1.4.1. Physical characterisation of the EG-AQ materials

For the determination of the presence of organic groups and the evaluation of AQ loading on the different EG materials the thermogravimetric analysis was carried out (Fig. 5a). The progressive weight loss between 450 and 800 °C in case of EG corresponds to the departure of the oxygen-containing groups from graphene surface. In case of EG-AQ-1 and EG-AQ-2, the sharper weight loss is observed from *ca* 300–400 °C compared to the EG. This is most likely caused by the decomposition of covalently attached organic functional groups [85, 169, 170]. The weight loss of EG at 400 °C is 3.5 and 7% lower compared to the weight loss of EG-AQ-1 and EG-AQ-2, respectively. These differences in weight losses could correspond to the AQ loading on the EG-AQ materials [171, 172] [I].

Raman spectroscopy was used to study the structural defects caused by the covalent attachement of AQ groups onto EG during grafting. The Raman spectra for AQ-modified and pristine EG are presented in Figs. 5b-d. In case of all studied materials, three peaks corresponding to D, G and 2D bands are observed. The D band is related to the amorphous or disordered carbon in the graphitic materials, the G band corresponds to the graphitic carbon (sp^2 carbon) and the 2D band is associated with the two-phonon double resonance Raman process [173–175]. For the quantification of the defects in the graphitic materials the intensity ratio of the D and G bands (I_D/I_G) can be used [173, 176, 177]. In case of EG (Fig. 5b), the I_D/I_G ratio is 0.1 referring to the high quality graphene with low amount of defects [85]. The AQ-modified EG materials possess the I_D/I_G ratio of 0.8 and 0.85 (Figs. 5c-d). The higher I_D/I_G ratio compared to the unmodified EG is explained by the covalent bond between the EG and AQ groups, which converted some C atoms in the graphene from sp^2 to sp^3 hybridisation. This in turn gave rise to the intensity of D band and also results in a higher I_D/I_G ratio [169, 173, 178]. It can be concluded that the increase in the concentration of AQ-N_2^+ in the exfoliation solution from 5 to 16 mM only slightly affects the I_D/I_G ratio.

Due to the functionalisation with AQ, the G peak has shifted positively for 15 and 27 cm^{-1} in case of EG-AQ-1 and EG-AQ-2 samples, respectively. The reason behind this shift could be the presence of isolated sp^2-C which are separated by the AQ groups in the carbon structure [179]. In addition, the positive shift in 2D band and the appearance of D' peak (Fig. 5d) refers to the disorder created in the basal plane of the graphene by grafting with AQ groups [180, 181]. The surface morphology of these materials has also been thoroughly characterised in the previous paper by Ossonon and Bélanger [22]. In the latter work, the AQ-modified EG materials were found to be single layer or bilayer graphene and the graphene structure was not damaged due to the grafting with AQ groups [22] [I].

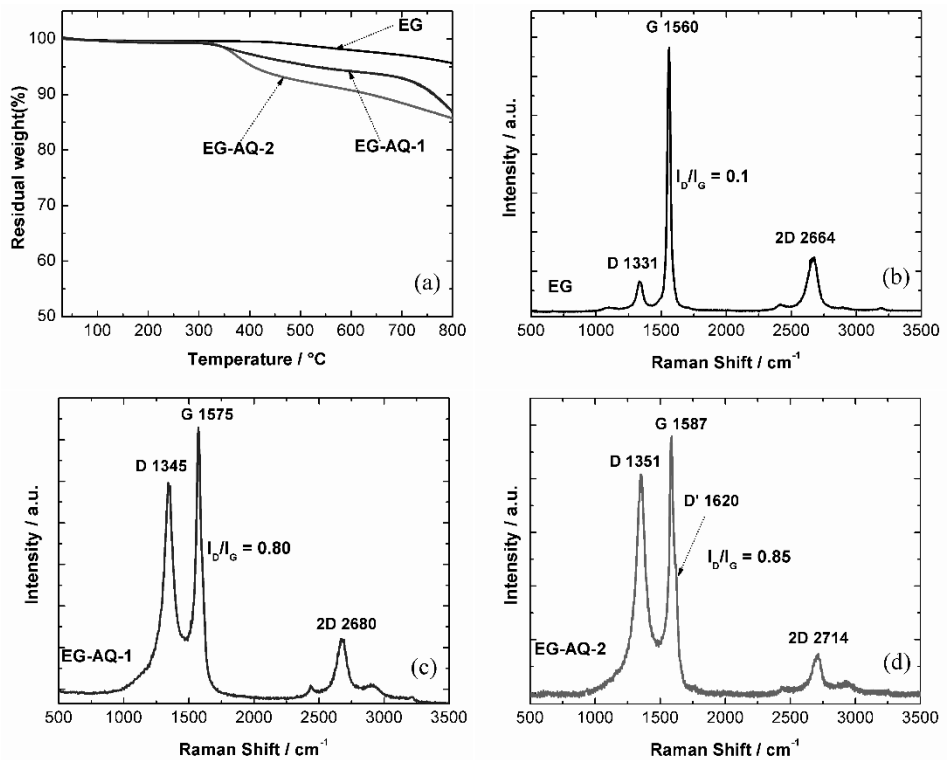

Fig. 5. (a) Thermogravimetric analysis curves of EG, EG-AQ-1 and EG-AQ-2 samples under He atmosphere, Raman spectra of **(b)** EG, **(c)** EG-AQ-1 and **(d)** EG-AQ-2 [I].

7.1.4.2. XPS analysis of the AQ modified nanocarbons

The elemental composition of different carbon nanomaterial coated electrodes was studied by XPS analysis. In Figs. 6a and b the XPS survey spectra of MWCNTs and GR coated electrodes are presented, respectively. The C1s XPS peak at *ca* 284.5 eV corresponds to the graphitic sp^2-carbon [182]. The O1s XPS peak at *ca* 532–533 eV (the insets to Figs. 6a and b) is inherent to these nanomaterials due to the native oxygen-containing groups on the material surface (e.g carboxyl and carbonyl) [163]. The oxygen content was determined to be 6.5 and 2.7 at% for GC/MWCNT and GC/GR electrodes, respectively.

The XPS spectra of GC/MWCNT/AQ_S and GC/GR/AQ_S electrodes (Figs. 6c and d) are very similar to the ones of unmodified nanomaterial (Figs. 6a and b) except the oxygen content was higher: 7.5 and 6 at% in case of spontaneously AQ-modified MWCNT and GR coated electrodes, respectively. The higher oxygen content compared to the unmodified nanomaterials can be explained by greater amount of C=O groups due to the grafted AQ moieties on the surface of nanomaterials [182].

The absence of N1s photoelectron peak indicates that the azo linkages (−N=N− [183]) are not formed within the AQ film during the spontaneous grafting of anthraquinone-1-diazonium compound, which is usually seen in case of electrografted materials [183–186]. The electrochemically AQ-grafted nanomaterial coated GC electrodes were also characterised by XPS (Figs. 6e and f). The oxygen content was determined to be 8 at% in case of both electrodes (GC/MWCNT/AQ_E and GC/GR/AQ_E) indicating the higher amount of electrografted AQ moieties compared to the spontaneously grafted nanomaterials (Figs. 6c and d). Also, the N1s photoelectron peak was registered at *ca* 400 eV for the electrografted catalyst coated electrodes (the insets to Figs. 6e and f). This peak has also been observed in case of GC electrodes electrografted using the FRA [V] and refers to the formation of multilayer AQ film containing –N=N– linkages [183]. The nitrogen content in the present work was calculated to be 3 at% in both cases [II].

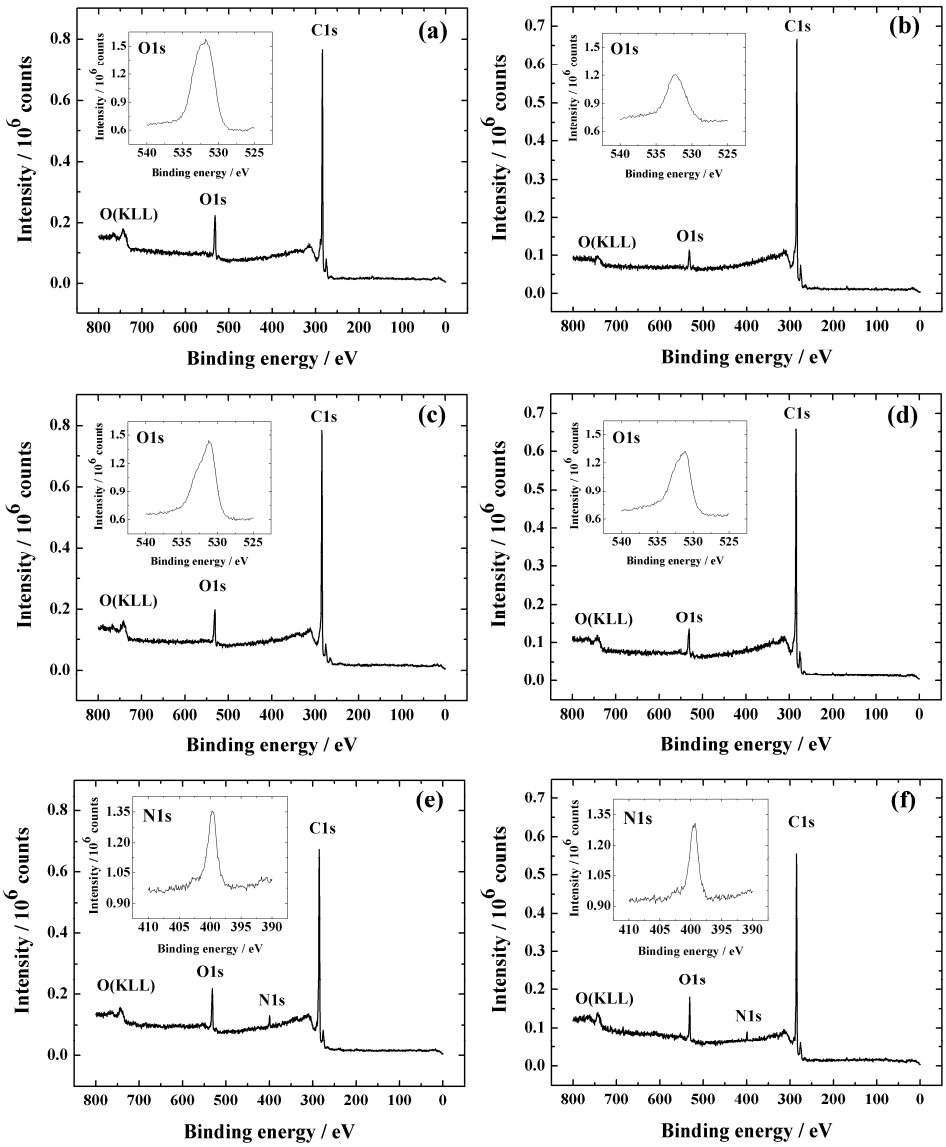

Fig. 6. XPS survey spectra of: **(a)** GC/MWCNT, **(b)** GC/GR, **(c)** GC/MWCNT/AQ_S, **(d)** GC/GR/AQ_S, **(e)** GC/MWCNT/AQ_E, **(f)** GC/GR/AQ_E electrodes. Spontaneous **(c, d)** or electrochemical **(e, f)** grafting of Fast Red AL salt was employed. The insets present high-resolution XPS spectra in the O1s or N1s region [II].

7.1.4.3. XPS and AFM characterisation of the nitrophenyl film modified CVD-grown graphene electrodes

The XPS survey spectra of Ni foil before and after the synthesis of graphene by CVD are presented in Figs. 7a and b, respectively. In case of Ni foil, the characteristic photoelectron peaks of Ni are registered as expected. While in case of Ni/Gra only the C1s photoelectron peak at 284 eV corresponding to the sp^2 carbon was observed. The absence of characteristic Ni photoelectron peaks in case of Ni/Gra (Fig. 7b) indicates the successful formation of graphene onto Ni foil by CVD. It is worth to note that the graphene on Ni foil is high quality multilayer graphene (less than 10 graphene layers) with rather no defects as was confirmed in our workgroup's earlier study [155].

In order to confirm the successful electrografting of Ni/Gra electrodes with NP films, the XPS analyses were also carried out with the electrografted electrodes (Figs. 7c, e and f). All NP film covered Ni/Gra electrodes showed photoelectron peaks of carbon (C1s), nitrogen (N1s) and oxygen (O1s). The O1s peak may be due to the adsorption of oxygen on the surface. The high-resolution spectra in the N1s region of Ni/Gra/NP1 and Ni/Gra/NP2 were very similar (insets to Figs. 7c and e). Obtained data is consistent with the work by Pembroke et al. [187], where the CVD-grown graphene transferred onto Si/SiO_2 substrate was grafted using NBD. The photoelectron peak in the N1s region at a higher binding energy (*ca* 406 eV) is evidently attributed to the nitro groups. While, the peak at lower binding energy (*ca* 400 eV) might be due to the azo linkages [185] within the multilayer NP film on Ni/Gra electrodes or may arise from the reduction of nitro groups under the X-ray beam [188, 189]. The photoelectron peak at 400 eV in N1s region is higher in case of Ni/Gra/NP3 compared to the Ni/Gra/NP1 and Ni/Gra/NP2 electrodes. This could be due to the greater overall amount of azo linkages in the thicker redox grafted NP film for Ni/Gra/NP3 electrode.

Furthermore, it was of special interest to see if it is possible to reduce the NP groups within the film on Ni/Gra electrode to aminophenyl (AP) groups in Ar-saturated 0.1 M KOH solution. For this reason, the XPS spectra after the potential cycling in Ar-saturated 0.1 M KOH were also recorded (Fig. 7d). In case of Ni/Gra electrode grafted with only one potential cycle in "normal" electrografting conditions (Ni/Gra/NP1), the XPS spectra of the electrode showed that the NP groups were mainly reduced to AP groups.

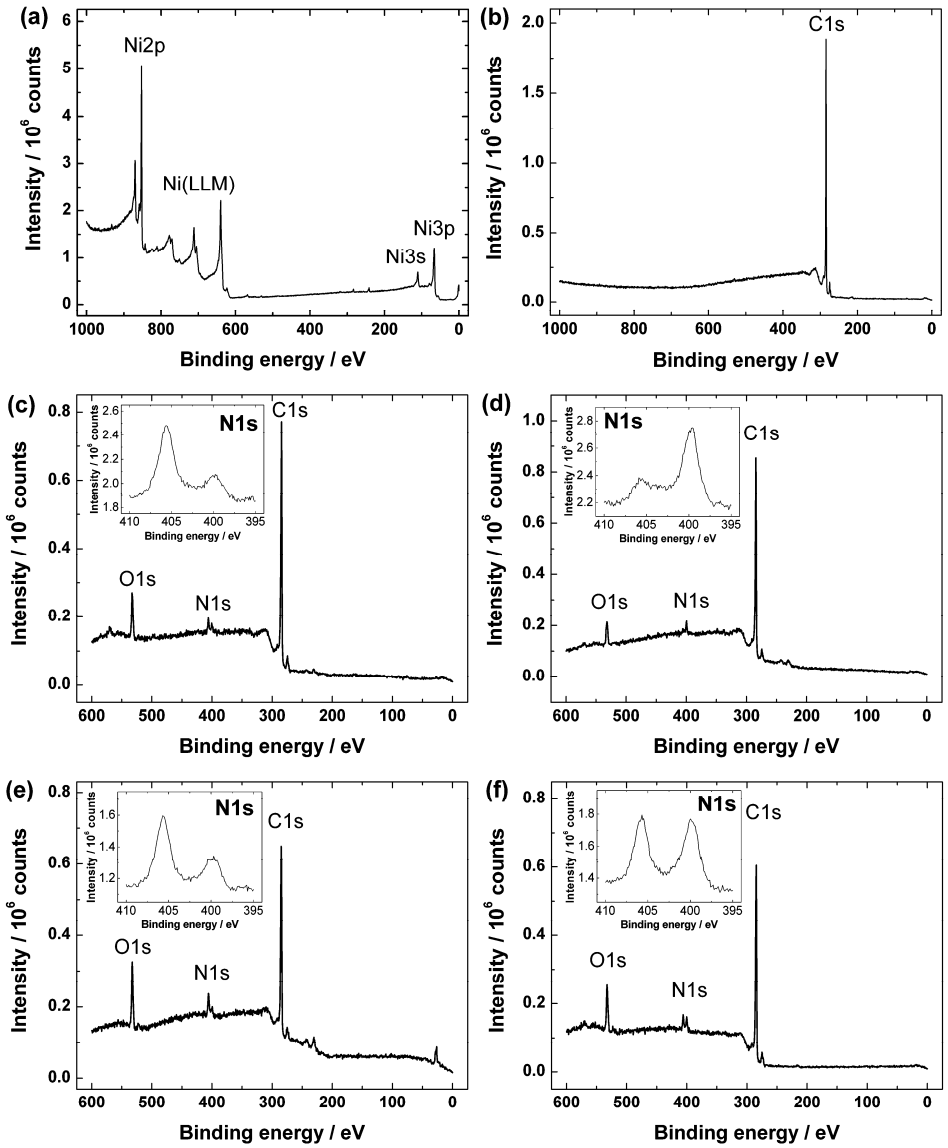

Fig. 7. XPS survey spectra of: **(a)** Ni foil, **(b)** Ni/Gra, **(c)** Ni/Gra/NP1, **(d)** reduced Ni/Gra/NP1, **(e)** Ni/Gra/NP2, **(f)** Ni/Gra/NP3 electrodes. The insets present high-resolution XPS spectra of N1s region [III].

In more specific, the peak at 406 eV was smaller in case of reduced Ni/Gra/NP1 electrode (Fig. 7d) compared with as-prepared Ni/Gra/NP1 electrode (Fig. 7c), meanwhile the peak at 400 eV has increased for reduced Ni/Gra/NP1 compared to the as-prepared Ni/Gra/NP1 electrode. Although, the XPS spectra obtained for Ni/Gra/NP2 and Ni/Gra/NP3 electrodes revealed also two peaks at *ca* 400 and 406 eV (data not shown), the peak at 406 eV remained almost the same

after reduction indicating that the NP film was most likely too thick in order to reduce the NP groups to AP groups.

The AFM images of Ni/Gra/NP1, Ni/Gra/NP2 and Ni/Gra/NP3 electrodes are presented in Fig. 8a, b and c, respectively. In case of Ni/Gra/NP1 and Ni/Gra/NP2 electrodes, the characteristic folds and wrinkles of the underlying Ni/Gra [155] material were still visible. In contrast, the Ni/Gra became fully covered with granular structure and the typical pattern of the underlying material was rarely visible if the RG method was used for grafting the Ni/Gra with NP groups (Ni/Gra/NP3, Fig. 8c). In addition, the thickness of NP film was determined to be about 5, 20 and 30 nm, in case of Ni/Gra/NP1, Ni/Gra/NP2 and Ni/Gra/NP3 electrodes, respectively. Considering the calculated thickness for the NP monolayer (0.68 nm [185]) the findings in the current study indicate that multilayers have been formed on Ni/Gra substrates, which has been also confirmed by the XPS results. In addition to the formation of multilayers through the azo linkages (see the XPS results), the multilayer film may also form due to the electrografting at already surface bound NP groups [165] [III].

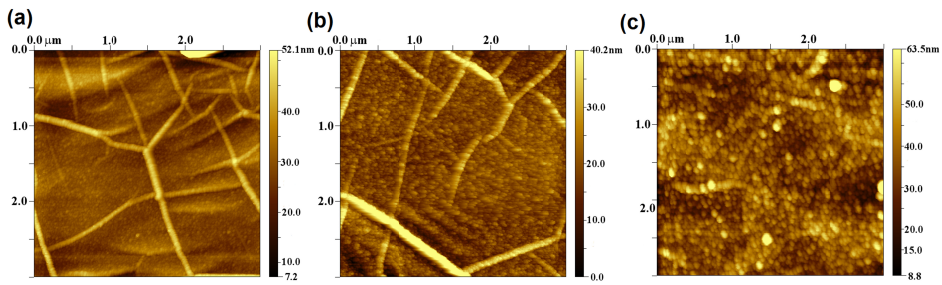

Fig. 8. AFM images (3×3 µm^2) of: **(a)** Ni/Gra/NP1, **(b)** Ni/Gra/NP2 and **(c)** Ni/Gra/NP3 electrodes [III].

7.1.4.4. XPS analysis of the AQ modified GC electrodes

The XPS analyses of differently redox-grafted AQ films on GC plates (Table 2) were carried out to characterise the elemental composition of the prepared aryl films. Since the XPS data obtained with different samples were rather similar, only the XPS survey spectrum of the AQ-modified GC electrode electrografted with one potential cycle (GC/AQ-1CV) is shown in Fig. 9. Three XPS peaks of C1s, N1s and O1s can be seen from the survey spectrum, which refers to the presence of these elements in the AQ film on the GC surface. The C1s peak may originate from the substrate (GC) and from the aromatic groups of the AQ film and the peak of O1s is related to the carbonyl groups of AQ and surface oxides. The XPS peak in the N1s region centred at 400 eV (the inset to Fig. 9) is probably due to the azo linkages (-N=N-) [183] confirming the presence of multilayers on the electrode surface as in case of AQ modified carbon nanomaterials (Section 7.1.4.2). In all samples (Table 2), the N content was

3.5±0.5 at%. This nitrogen content is in good agreement with a report by Bousquet et al. [37] in which AQ films on Au substrate were analysed by XPS [V].

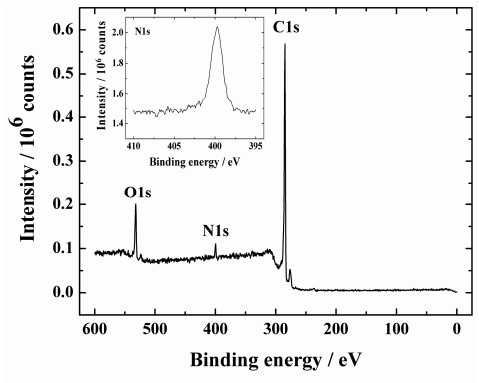

Fig. 9. XPS survey spectrum of a GC/AQ-1CV electrode modified by one potential cycle in acetonitrile solution containing 2 mM Fast Red AL salt and 0.1 M $TBABF_4$ as a base electrolyte. The inset shows the high-resolution spectrum in the N1s region [V].

7.1.5. Electrochemical characterisation of aryl film modified carbon electrodes

7.1.5.1. Surface concentration of AQ groups on the nanomaterial coated GC electrodes

In Fig. 10 the CV curves of bare and different AQ-functionalised or nanomaterial coated GC electrodes recorded in Ar-saturated 0.1 M KOH are presented. The electrode was cycled until a reproducible CV curve was obtained. From the CV data, the peak-to-peak separation (ΔE_p), the redox potential (E^o) of AQ and the surface concentration of electrochemically active AQ groups (Γ_{AQ}) are presented in Table 5. For calculating the Γ_{AQ} values the following equation was used [24]:

$$\Gamma = Q/nFA \tag{9}$$

where A is the geometric area of the GC electrode (A = 0.196 cm^2), F is Faraday constant (96485 C mol^{-1}), n is the number of electrons transferred (n = 2) and Q is the consumed charge (C). Note that the amount of AQ attached to carbon nanomaterials is calculated per geometric surface area of the GC electrode.

As can be seen from the CV curves (Fig. 10), the increase in capacitive baseline current is observed in case of unmodified EG, GR or MWCNT coated electrodes compared to the bare GC. This indicates that the electron transfer occurs between the high surface area nanomaterial and the underlying GC electrode. In Fig. 10a, the lower capacitive current is observed for the GC/EG

compared to the GC/EG-AQ-1 and GC/EG-AQ-2 electrodes despite the equal loading of the material on the electrode. This is not in line with a previous report dealing with the EG-AQ materials [85]. We propose that this might be due to the aggregation of the graphene sheets leading to a decrease of the electrochemically active surface area and the double layer capacitance of the EG when coated on a GC electrode. In Fig. 10a, the well-defined AQ redox wave has developed only in case of GC/EG-AQ-2 electrode and the Γ_{AQ} value was calculated to be 1.37 nmol cm^{-2} (Table 5). A magnitude lower value of Γ_{AQ} has been reported by Lalaoui et al. who studied covalently functionalised reduced graphene oxide obtained by *in situ* formation and reduction of anthraquinone-2-diazonium compound on the GC electrode [190]. This difference could be due to the various nanomaterials and the concentration of catalyst in the ink used for the electrode coating.

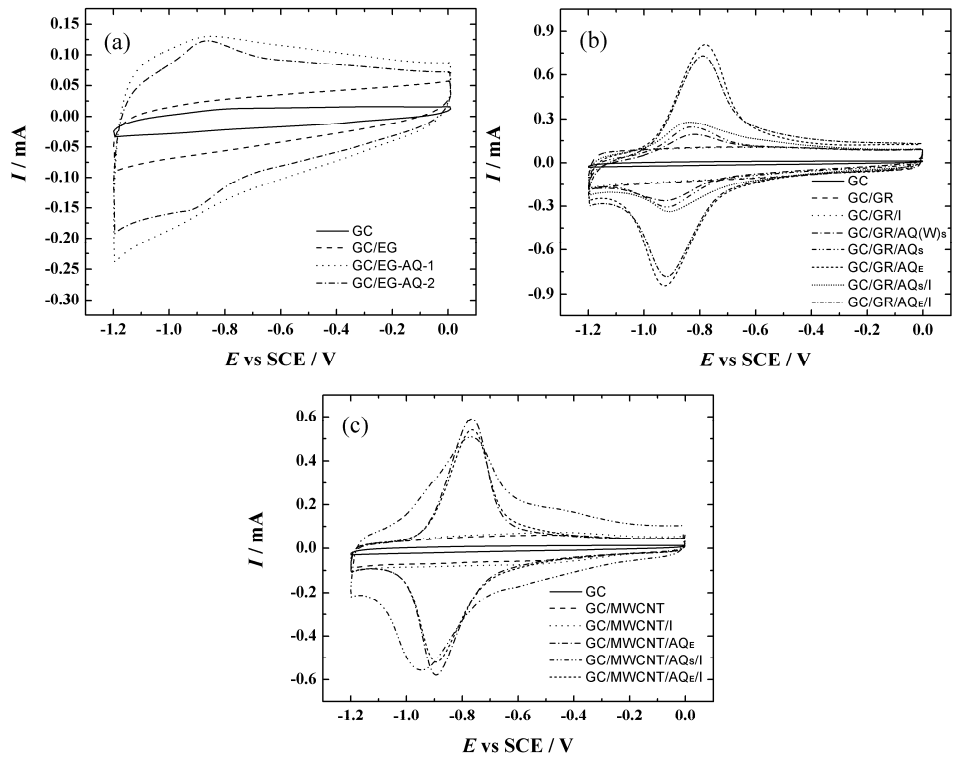

Fig. 10. Cyclic voltammograms of bare and different nanomaterial coated GC electrodes recorded in Ar-saturated 0.1 M KOH (ν = 100 mV s^{-1}) [I, II].

If the GR was modified with AQ groups in ACN or Milli-Q water by spontaneous modification, the calculated Γ_{AQ} and measured E^{o} values were quite similar (Table 5, Fig. 10b) suggesting that the 1 h spontaneous grafting process

on graphene in aqueous solution or ACN gives a similar outcome. The Γ_{AQ} value of GC/GR/AQ_S is *ca* 10 times higher than in case of GC/EG-AQ-2 electrode (Table 5). This can be explained by *ca* 12 times difference in specific surface areas of these graphene materials (60 m^2 g^{-1} [85] vs 750 m^2 g^{-1} [95]). The CV curve of GC/MWCNT/AQ_S/I electrode (Fig. 10c) is somewhat different from the others. Within the quite high baseline current, the second pair of redox peaks at higher potentials is registered. The appearance of double AQ peaks has been previously observed on GC electrodes coated with covalently AQ-modified carbon nanotubes and may occur because of the adsorption of AQ molecules on the carbon nanotube surface of different energy [191].

The electrochemically grafted AQ-derivatised GR or MWCNT coated GC electrodes showed quite comparable CV curves (Figs. 10b and c) and Γ_{AQ} values (*ca* 35 and 25 nmol cm^{-2}, respectively). Zhou et al. has used similar modification conditions for functionalisation of graphene oxide coated GC electrode and reported remarkably lower Γ_{AQ} value [162]. As a difference, the electrode was cycled in 0.1 M PBS prior to the electrografting in latter work. The reported Γ_{AQ} value (*ca* 1 nmol cm^{-2} [162]) is more similar to the one of GC/AQ_E and GC/EG-AQ-2 electrodes (Table 5). In addition, the OH^- ionomer coating has no remarkable influence on the shape of the CV curves of the electrodes (Figs. 10b and c). Although, the Γ_{AQ} values are slightly lower in case of OH^- ionomer coating (Table 5).

Table 5. Surface concentration of anthraquinone groups (Γ_{AQ}), peak-to-peak separation (ΔE_p) and redox potential (E^o) of electroactive anthraquinone moieties recorded in Ar-saturated 0.1 M KOH using a scan rate of 100 mV s^{-1} [I, II].

Electrode designation	Γ_{AQ} [nmol cm^{-2}]	ΔE_p [V]	E^o [V]
GC/EG-AQ-2	1.37	-	−0.88
GC/AQ_E	1.18	0.047	−0.856
GC/GR/$AQ(W)_S$	11.1	0.101	−0.872
GC/GR/AQ_S	12.4	0.084	−0.874
GC/GR/AQ_S/I	12.0	0.079	−0.871
GC/GR/AQ_E	35.1	0.136	−0.852
GC/GR/AQ_E/I	32.3	0.149	−0.852
GC/MWCNT/AQ_S/I	28.5	0.177	−0.854
GC/MWCNT/AQ_E	26.2	0.131	−0.830
GC/MWCNT/AQ_E/I	25.5	0.135	−0.830

7.1.5.2. Surface concentration of NP groups on the NP-modified CVD-grown graphene

For studying the surface concentration of the electroactive NP groups (Γ_{NP}) on the NP film modified Ni/Gra electrodes prepared by different electrografting conditions (Section 7.1.2), the CV curves were recorded in Ar-saturated 0.1 M KOH. The Γ_{NP} values were calculated according to the same equation (9) as was

used for calculating the Γ_{AQ} values (Section 7.1.5.1). In Fig. 11, typical stable CV responses of NP-modified Ni/Gra electrodes with different surface coverages are shown. Interestingly, the Γ_{NP} values did not vary significantly: 2.3×10^{-10}, 2.9×10^{-10} and 2.9×10^{-10} mol cm^{-2} in case of Ni/Gra/NP1, Ni/Gra/NP2 and Ni/Gra/NP3 electrodes, respectively. The reason behind this could be that some NP groups are not electroactive due to the steric hindrance in the compact NP film and therefore, the real Γ_{NP} value cannot be measured from the CV curves [36, 192][III].

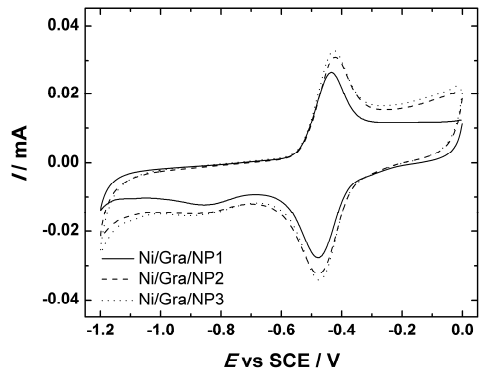

Fig. 11. Cyclic voltammograms of NP-modified Ni/Gra electrodes recorded in Ar-saturated 0.1 M KOH (ν = 100 mV s^{-1}) [III].

7.1.5.3. Surface concentration of MAQ and AQ groups on the electrografted GC electrodes

The presence of MAQ or AQ groups at the GC electrode surface was confirmed by CV in Ar-saturated 0.1 M KOH [IV, V] or ACN containing 0.1 M $TBABF_4$ [VI]. Typical quasi-reversible redox peaks of surface-confined AQ or MAQ groups were observed in case of all electrografted electrodes (Fig. 12). The surface concentration of MAQ groups (Γ_{MAQ}) or Γ_{AQ} were calculated according to the equation (9) from Section 7.1.5.1 for CV data obtained in Ar-saturated 0.1 M KOH. The obtained values are given in Table 6.

Figs. 12a and b only display cyclic voltammograms obtained with differently modified GC/(Br)-MAQ electrodes because the CV results obtained for GC/(Br-)MAQ and GC/(Cl-)MAQ electrodes were rather similar. Surprisingly, no clear dependence between the modification procedure and the value of Γ_{MAQ} was observed. In general, higher Γ_{MAQ} values were obtained by holding the electrode at fixed potentials for 10 min compared to the electrografting by the potential cycling method (Tables 1 and 6). Additionally, GC/(Cl-)MAQ electrodes showed higher Γ_{MAQ} values compared to their GC/(Br-)MAQ counterparts. According to the reported surface coverage for a closely-packed monolayer of anthraquinonyl groups (3.45×10^{-10} mol cm^{-2} [193]), all MAQ-modified

electrodes have the surface concentration less than a monolayer (Table 6). Compared to the GC electrode modified with AQ via reduction of aryldiazonium salts in the ACN solution containing 10 mM FRA, *ca* 5–10 times higher surface concentration of electroactive AQ moieties on the electrode was determined (1.18 nmol cm^{-2}, GC/AQ_E, Table 5). These observations indicate that the reduction of aryldiazonium salts method is more efficient for preparing the aryl films with higher amount of electroactive AQ moieties [IV].

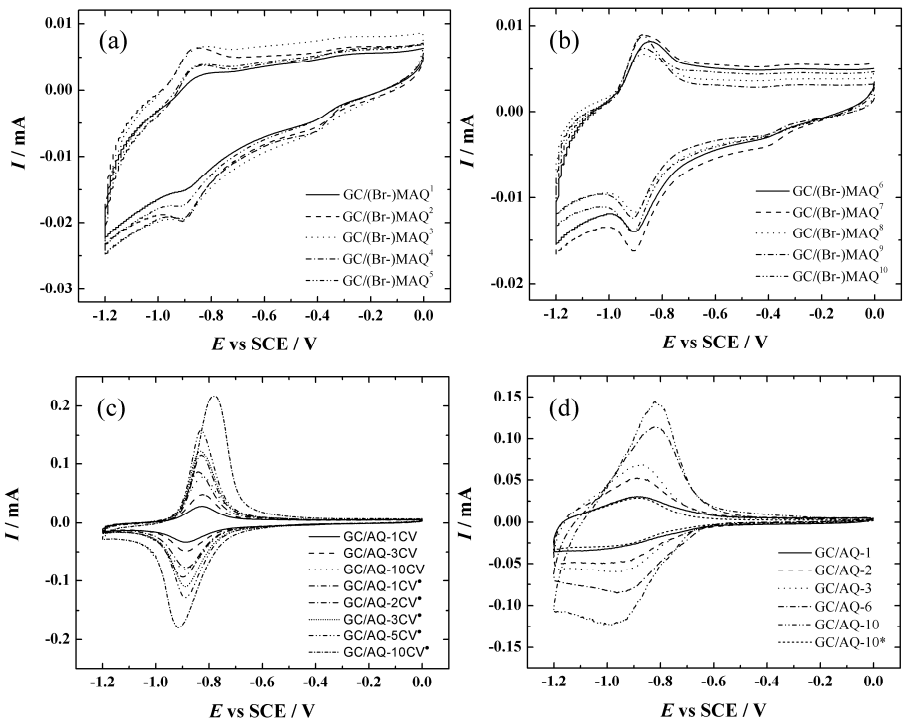

Fig. 12. Cyclic voltammograms of AQ-modified GC electrodes recorded in Ar-saturated **(a-c)** 0.1 M KOH or **(d)** ACN containing 0.1 M $TBABF_4$ using ν of 100 mV s^{-1}. The electrografting of GC electrode with AQ groups was carried out using: **(a-c)** cyclic voltammetry [IV, V] and **(d)** cyclic voltammetry and the RDE combined method [VI].

In Fig 12c, the cyclic voltammograms of GC electrodes redox-grafted via reduction of aryldiazonium salts in 2 or 10 mM FRA solution are presented. The corresponding Γ_{AQ} values are given in Table 6. If we compare the "normal" electrografting with the RG method, then in 10 mM FRA solution with one RG cycle already *ca* 2.5 times higher Γ_{AQ} value is obtained (3 nmol cm^{-2}, GC/AQ-1CV$^{\bullet}$, Table 6) compared to the electrode functionalised in the narrow potential range by "normal" electrografting (1.18 nmol cm^{-2}, GC/AQ_E, Table 5). For comparison with the data obtained with the RG method, Bousquet et al. used similar potential range (from 0.55 to −1.5 V vs SCE), 2 mM (pre-synthesised)

AQ diazonium salt concentration and 10 potential cycles for surface modification of Au electrode [37]. In the latter work, the scan rate was 10 times higher and the surface coverage was investigated in ACN solution containing 0.1 M $TBABF_4$. The Γ_{AQ} value of 10.3 nmol cm^{-2} was determined, which is higher than the ones obtained in the present study most likely due to the higher v used [37]. Herein, if the electrodes were redox grafted in 10 mM diazonium salt solution higher Γ_{AQ} values up to 6.2 nmol cm^{-2} (GC/AQ-10CV$^{\bullet}$, Table 6) were obtained. This indicates that the concentration of AQ diazonium salt in the electrografting solution is an important parameter among the grafting conditions. These Γ_{AQ} values were significantly higher compared to the ones reported in the papers on O_2 reduction studies by our workgroup [13, 14, 28–31, 33–35, 194, 195] prior to this work [V].

Table 6. Surface concentration of anthraquinone (Γ_{AQ}) or methylanthraquinone (Γ_{MAQ}) groups on GC electrode recorded in Ar-saturated 0.1 M KOH using ν of 100 mV s^{-1}. The electrografting conditions of AQ and MAQ modified GC electrodes are given in Table 1 and 2, respectively. The additional marking of ^{ACN} is used if the Γ_{AQ} value was determined from the CV curve recorded in ACN containing 0.1 M $TBABF_4$ [IV–VI].

Electrode designation	$\Gamma_{MAQ} \times 10^{10}$ [mol cm^{-2}]	Electrode designation	Γ_{AQ} [nmol cm^{-2}]
GC/(Br-)MAQ[1]	0.5	GC/AQ-1CV$^{\bullet}$	3.0
GC/(Br-)MAQ[2]	1.4	GC/AQ-2CV$^{\bullet}$	3.7
GC/(Br-)MAQ[3]	1.1	GC/AQ-3CV$^{\bullet}$	4.0
GC/(Br-)MAQ[4]	1.4	GC/AQ-5CV$^{\bullet}$	5.0
GC/(Br-)MAQ[5]	1.2	GC/AQ-10CV$^{\bullet}$	6.2
GC/(Br-)MAQ[6]	1.4	GC/AQ-1CV	1.0
GC/(Br-)MAQ[7]	1.9	GC/AQ-3CV	1.7
GC/(Br-)MAQ[8]	1.6	GC/AQ-10CV	2.8
GC/(Br-)MAQ[9]	1.9	GC/AQ-1.1	11^{ACN}
GC/(Br-)MAQ[10]	2.0	GC/AQ-1.3	10^{ACN}
GC/(Cl-)MAQ[a]	2.2	GC/AQ-200	13^{ACN}
GC/(Cl-)MAQ[b]	2.2	GC/AQ-500	12^{ACN}
GC/(Cl-)MAQ[c]	1.8	GC/AQ-1	5.2^{ACN}
GC/(Cl-)MAQ[d]	2.4	GC/AQ-2	8.6^{ACN}
GC/(Cl-)MAQ[e]	2.0	GC/AQ-3	11^{ACN}
GC/(Cl-)MAQ[f]	2.0	GC/AQ-6	16^{ACN}
GC/(Cl-)MAQ[g]	2.1	GC/AQ-10	18^{ACN}
GC/(Cl-)MAQ[h]	2.4	GC/AQ-10*	4.9^{ACN}

The Γ_{AQ} values of the GC electrodes functionalised with AQ using the RG and RDE combined method were determined from the CV curves obtained in ACN containing 0.1 M $TBABF_4$ (Fig. 12d). The stabilised cyclic voltammogram was already achieved after 5th potential cycle irrespective of whether the ultrasonic

treatment (5 min in ACN) or only rinsing the electrodes after modification process with ACN was used. This was observed only when the RDE method was combined in the modification process suggesting that ultrasonic treatment is not needed when RDE is employed during electrografting. The Γ_{AQ} values (Table 6) were calculated using the equation (9) given in Section 7.1.5.1 with one modification for number of electrons involved (n = 1). If the RDE method was applied during the modification process, the calculated Γ_{AQ} values significantly increased compared to the electrodes prepared in the stationary mode. In specific, the highest Γ_{AQ} value of 18 nmol cm^{-2} was determined (GC/AQ-10, Table 6) when RG with the combination of CV and RDE (ω = 1000 rpm) was applied for the electrode modification. According to our knowledge, this value is the highest reported for AQ-modified GC electrodes. In addition, there is a possibility that some of the AQ moieties in the aryl film are inactive because of the restricted access by counter ions and steric hindrance in the film. In this case, the calculated Γ_{AQ} values in this study may correspond only to the electroactive AQ units in the aryl film and therefore, the real AQ surface coverage could be even higher. For comparison, the RG without the RDE was performed (GC/AQ-10*, Table 2) and the Γ_{AQ} value of 4.9 nmol cm^{-2} (Table 6) was determined. Similar Γ_{AQ} value is obtained in case of RG and RDE combined method already with one grafting cycle (5.2 nmol cm^{-2}, GC/AQ-1, Table 6). Also, it is worth noting that with the increasing number of potential cycles the value of Γ_{AQ} became higher (Fig. 12d, Table 6). This is in accordance with the reports by other workgroups [37, 196, 197] [VI].

7.1.5.4. Electrochemical response of thick AQ film modified GC electrodes towards the ferri/ferrocyanide redox probe

Several studies about ferricyanide reduction on aryl-modified GC electrodes have been carried out according to the literature [11, 38, 198]. Although, for the preparation of aryl-modified electrodes, usually “normal” electrografting or redox grafting by CV has been applied. In Fig. 13, the ferricyanide response on thick AQ film-modified GC electrodes, where the combination of RG and RDE combined method was used for electrografting was reported for the first time.

The response of the $Fe(CN)_6^{3-/4-}$ redox probe is strongly suppressed in case of all electrografted electrodes except for the GC/AQ-1 electrode. This kind of CV behaviour indicates that the AQ film is compact enough to restrict the access of ferricyanide anions to the active sites of GC. The CV curve of GC/AQ-1 shows a small redox wave of $Fe(CN)_6^{3-/4-}$ redox probe compared to other AQ grafted GC electrodes. This may indicate the presence of pinholes in the AQ film if the GC electrode is modified only by one grafting cycle using the RG and RDE combined method ACN containing 2 mM FRA [VI].

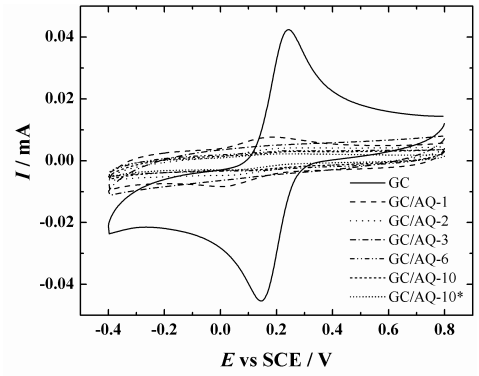

Fig. 13. Cyclic voltammograms of bare and different AQ-modified GC electrodes recorded in Ar-saturated 0.1 M K_2SO_4 containing 1 mM $K_3Fe(CN)_6$ (v = 100 mV s^{-1}). The electrografting of GC electrode with AQ groups was carried out using the combination of cyclic voltammetry and the RDE method [VI].

7.1.6. ORR studies on aryl film modified GC electrodes

7.1.6.1. ORR on AQ-modified nanomaterial coated GC electrodes

In Fig. 14, the RDE polarisation curves for ORR on bare and different nanomaterial coated GC electrodes in 0.1 M KOH (ω = 1900 rpm, v = 20 mV s^{-1}) are presented. The E_{onset} values and O_2 reduction current at −1.2 V ($I_{-1.2\ V}$) derived from these RDE polarisation curves are shown in Table 7. From the RDE voltammetry data we can see that all the nanomaterial coated electrodes are more electrocatalytically active towards the ORR than bare GC in terms of the E_{onset} and O_2 reduction current values. In case of the EG-based catalyst coated electrodes (Fig. 14a), the RDE voltammetry curves for AQ-modified and unmodified materials are very similar. Although, a partial blocking of active O_2 reduction sites on catalyst materials (i.e. native quinone-like groups [199]) is observed at *ca* −0.5 V (GC/EG vs GC/EG-AQ-1 and GC/EG-AQ-2) most likely due to the modification with AQ analogously to that reported on AQ-modified GC electrodes [29]. The commercially available graphene coated GC electrode (GC/GR, Fig. 14c) is more active towards the ORR than the EG coated GC electrode (GC/EG, Fig. 14a, Table 7). This can be explained by 12 times difference in specific surface areas (Section 7.1.5.1). Both, spontaneously and electrochemically AQ-grafted GR-coated GC electrodes (GC/GR/AQ_S, GC/GR/$AQ(W)_S$, GC/GR/AQ_E) have no advantage for ORR performance compared to the GC/GR electrode (Fig. 14c, Table 7) analogously as in case of unmodified and AQ-modified EG-based catalyst materials.

The RDE voltammetry curve of GC/MWCNT compared to bare GC electrode (Fig. 14d, Table 7) shows a similar rise in electrocatalytic activity as in case of GC/GR electrode. This indicates that the electrochemical behaviour of these two specific carbon nanomaterials towards the ORR is quite similar. It

is proposed that the strong electrocatalytic effect could be caused by oxygen-containing functionalities (e.g. quinone groups) on the surface of MWCNTs [15, 26]. When AQ moieties are electrografted onto GC/GR or GC/MWCNT electrode, the E_{onset} is more negative than in case of spontaneously AQ-derivatised GR- or MWCNT-coated electrodes (e.g. GC/GR/AQ_S/I vs GC/GR/AQ_E/I and GC/MWCNT/AQ_E/I vs GC/MWCNT/AQ_S/I). Hence, a possible explanation: during electrografting some of the active O_2 reduction sites of GR or MWCNTs become covalently modified or sterically hindered by AQ moieties resulting in a lower ORR activity.

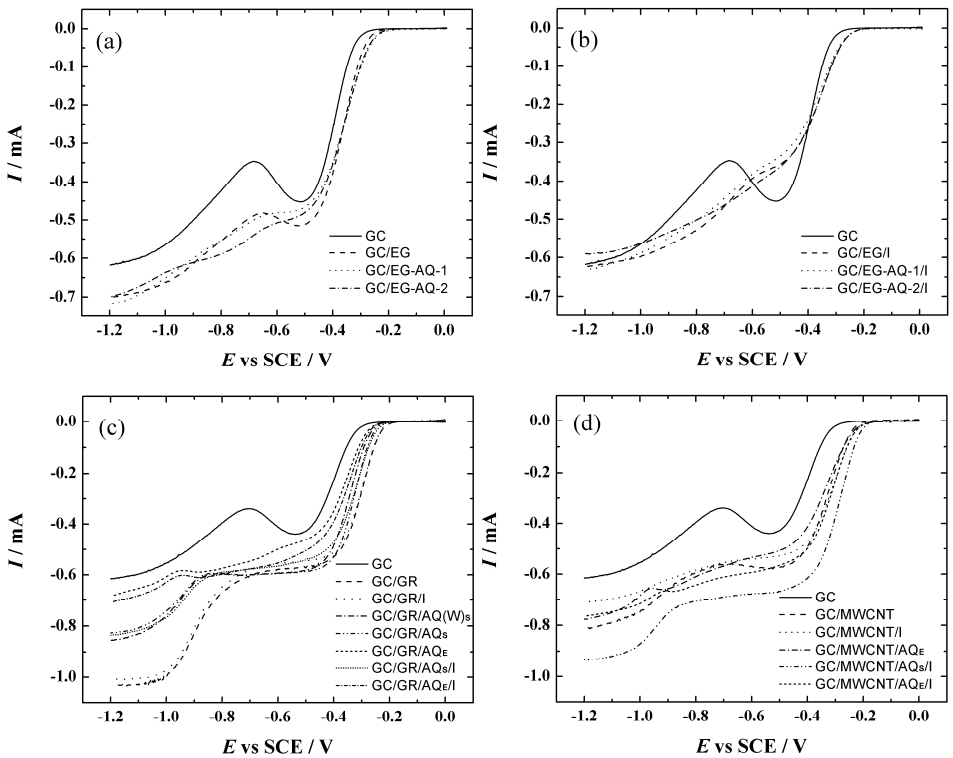

Fig. 14. RDE voltammetry curves for O_2 reduction on bare and different nanomaterial coated GC electrodes recorded in O_2-saturated 0.1 M KOH (ω = 1900 rpm, v = 20 mV s^{-1}) [I, II].

If the OH^- ionomer was used as a catalyst binder on the electrode, the oxygen reduction current was often lower compared to the electrodes without OH^- ionomer (Fig. 14, Table 7). Similar inhibiting effect has been also observed in our previous study with different graphene-based carbon materials [95]. This is an important result regarding the role of OH^- ionomer used for the preparation of cathode catalyst layers for anion-exchange membrane fuel cells or as a binder

of the composite materials used for ORR studies. This inhibiting effect is most likely due to the blocking of the ORR active sites by OH^- ionomer.

The spontaneously modified MWCNTs and OH^- ionomer coated GC electrode (GC/MWCNT/AQ_S/I) showed the lowest E_{onset} and highest O_2 reduction current among all the prepared electrodes (Fig. 14, Table 7). This is an expected result because Gong et al. have reported monohydroxy-anthraquinone modified MWCNTs coated GC electrodes to be also more electrocatalytically active for ORR than unmodified MWCNTs [15]. Although, in the latter study, the MWCNTs were not purified, the binder used was Nafion® and for surface grafting the diazonium reduction process was not used [15]. Gong et al. proposed that the electrocatalytic effect of the catalysts can be explained by the high surface area and low charge transfer resistance provided by MWCNTs and the AQ moieties on the MWCNT surface keep excess electroactive sites, which results in more favourable electron-transfer kinetics for ORR on the modified electrode [15]. In addition, the enhancement in electrocatalytic activity towards the ORR due to the AQ functionalisation has also been observed for different AQ derivatives and carbon materials [11, 200–203].

Table 7. The ORR onset potential (E_{onset}) and O_2 reduction current at −1.2 V ($I_{-1.2\ V}$) for bare GC and different nanomaterial coated GC electrodes obtained from the RDE polarisation curves recorded in O_2-saturated 0.1 M KOH solution (ω = 1900 rpm, v = 20 mV s^{-1}). All the potentials are given with respect to the SCE [I, II].

Electrode designation	E_{onset} [V]	$I_{-1.2\ V}$ [mA]	Electrode designation	E_{onset} [V]	$I_{-1.2\ V}$ [mA]
GC	−0.30	−0.61			
GC/EG	−0.26	−0.70	GC/EG/I	−0.26	−0.62
GC/EG-AQ-1	−0.24	−0.72	GC/EG-AQ-1/I	−0.26	−0.63
GC/EG-AQ-2	−0.25	−0.70	GC/EG-AQ-2/I	−0.26	−0.59
GC/GR	−0.22	−1.03	GC/GR/I	−0.22	−1.01
GC/MWCNT	−0.23	−0.81	GC/MWCNT/I	−0.21	−0.71
GC/GR/AQ_S	−0.24	−0.83	GC/GR/AQ_S/I	−0.23	−0.83
GC/GR/AQ_E	−0.26	−0.68	GC/GR/AQ_E/I	−0.26	−0.71
GC/MWCNT/AQ_E	−0.21	−0.78	GC/MWCNT/AQ_E/I	−0.21	−0.76
GC/GR/AQ(W)$_S$	−0.25	−0.86	GC/MWCNT/AQ_S/I	−0.19	−0.93

To calculate the number of electrons transferred (n) per O_2 molecule from the RDE data, the K-L equation was employed [24]:

$$\frac{1}{I} = \frac{1}{I_k} + \frac{1}{I_d} = -\frac{1}{nFAkc^b_{O_2}} - \frac{1}{0.62nFAD^{2/3}_{O_2}\nu^{-1/6}c^b_{O_2}\omega^{1/2}} \tag{10}$$

where I is the measured current at a specific potential, I_k and I_d are the kinetic and diffusion-limited currents, respectively, k is the electrochemical rate constant for O_2 reduction, F is the Faraday constant, A is the geometric area of GC electrode, ω is the rotation rate, c^b_{O2} is the concentration of oxygen in the bulk (1.2×10^{-6} mol cm^{-3} [204]), D_{O2} is the diffusion coefficient of oxygen (1.9×10^{-5} cm^2 s^{-1} [204]) and v is the kinematic viscosity of the solution (0.01 cm^2 s^{-1} [205]). The value of n was between 2 and 4 (Fig. 15) in case of all MWCNT- and GR-based material coated electrodes in the studied potential range and these n values indicate the partial further reduction of peroxide to water on the nanomaterial.

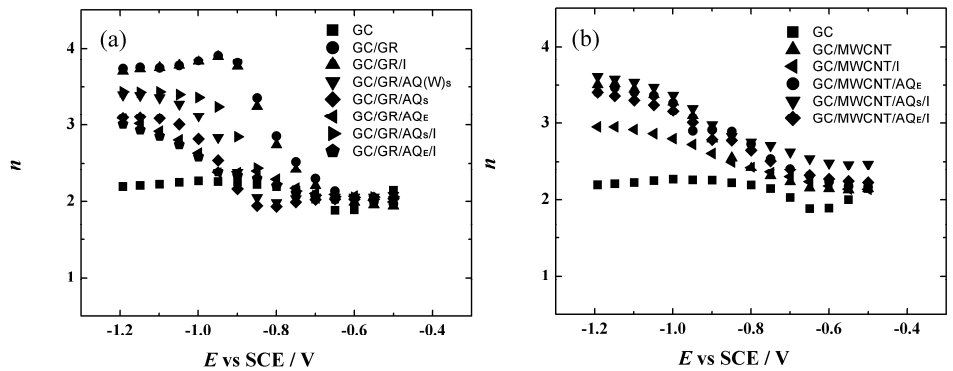

Fig. 15. The number of electrons transferred per O_2 molecule as a function of potential on bare GC and GC coated with unmodified and AQ-modified **(a)** graphene and **(b)** MWCNTs [II].

In Fig. 16a, the RDE polarisation curves for O_2 reduction on the most active GC/MWCNT/AQ_S/I electrode at different rotation rates and in Fig. 16b the K-L plots derived from the RDE data are presented. At lower overpotentials, the reduction of O_2 is under the mixed kinetic-diffusion control and at more negative potentials (*ca* –1.1 and –1.2 V) the extrapolated K-L lines yield intercept close to zero at the y-axis indicating the diffusion-limited O_2 reduction.

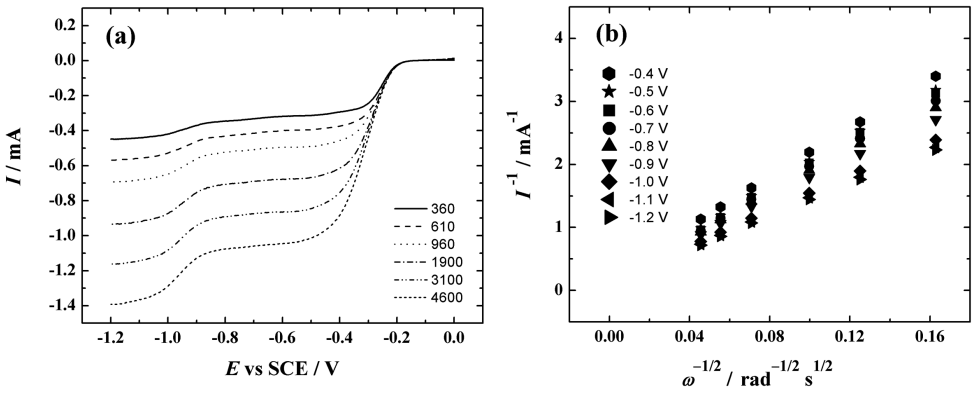

Fig. 16. (a) RDE voltammetry curves for oxygen reduction on a GC/MWCNT/AQ_S/I electrode in O_2-saturated 0.1 M KOH (ω = 360–4600 rpm, v = 20 mV s^{-1}), **(b)** K-L plots for O_2 reduction in 0.1 M KOH derived from the RDE data shown in Fig. **a** [II].

In addition, the stability of the GC/EG-AQ-1, GC/EG-AQ-2, GC/GR/AQ_S and GC/GR/AQ_S/I electrodes was studied in O_2-saturated 0.1 M KOH solution by applying 1000 potential cycles (Fig. 17). The procedure for the stability test was taken from our previous work [206]. For GC/EG-AQ-2, GC/GR/AQ_S and GC/GR/AQ_S/I electrodes, the Γ_{AQ} value was determined after every 100 or 200 cycles (insets to Figs. 17b–d). In case of GC/EG-AQ-1 and GC/EG-AQ-2 electrodes, the E_{onset} did not noticeably change and the decrease in O_2 reduction current at –1.2 V was *ca* 6% after 1000 cycles. The decline in the O_2 reduction current is comparable with the data published previously by our workgroup [59, 206]. The Γ_{AQ} value of the GC/EG-AQ-2 electrode has decreased by 13%. The GC/GR/AQ_S electrode (Fig. 17c) had well reproducible O_2 reduction current during 1000 cycles but in the end of the stability test the Γ_{AQ} value diminished down to 31% of the initial AQ coverage. The Γ_{AQ} value on the electrode with OH^- ionomer coating GC/GR/AQ_S/I (Fig. 17d) was 66% of the initial value (over 2 times higher) at the end of the stability test. Although, the O_2 reduction current decreased noticeably compared to the GC/GR/AQ_S electrode. According to the obtained results, the OH^- ionomer should be used when the aryl groups (e.g. AQ moieties) are needed for the catalyst preparation. If the nanomaterial (e.g. GR) itself is the electrocatalyst for ORR in alkaline solution then the use of OH^- ionomer coating should be avoided for better stability [I, II].

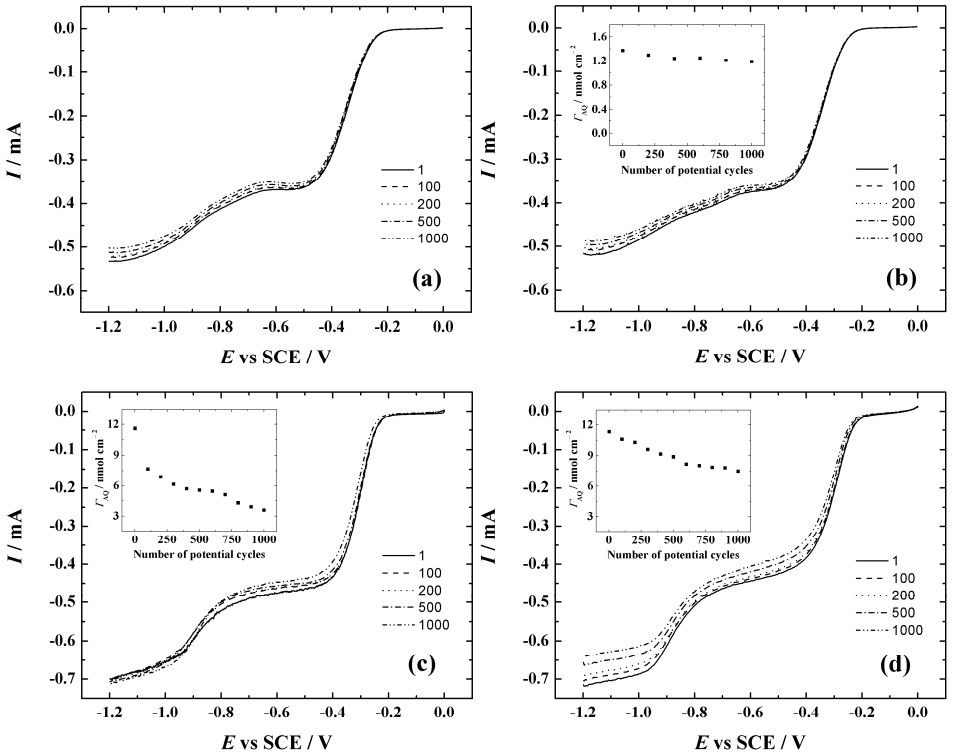

Fig. 17. RDE voltammetry curves for O_2 reduction on: **(a)** GC/EG-AQ-1, **(b)** GC/EG-AQ-2, **(c)** GC/GR/AQ_S and **(d)** GC/GR/AQ_S/I electrodes in O_2-saturated 0.1 M KOH (ω = 960 rpm, v = 20 mV s^{-1}) recorded after 1st, 100th, 200th, 500th and 1000th potential cycle. The insets to (**b-d)** show the dependence of Γ_{AQ} on the number of potential cycles [I, II].

7.1.6.2. ORR on MAQ or AQ-modified GC electrodes

The ORR on MAQ- and AQ-modified GC electrodes was studied using the RDE method. In Figs. 18a-d, the RDE voltammetry curves for different GC/(Br-)MAQ and GC/(Cl-)MAQ electrodes at 1900 rpm and 20 mV s^{-1} are presented. The results for both MAQ derivatives and differently modified GC/MAQ electrodes were rather similar.

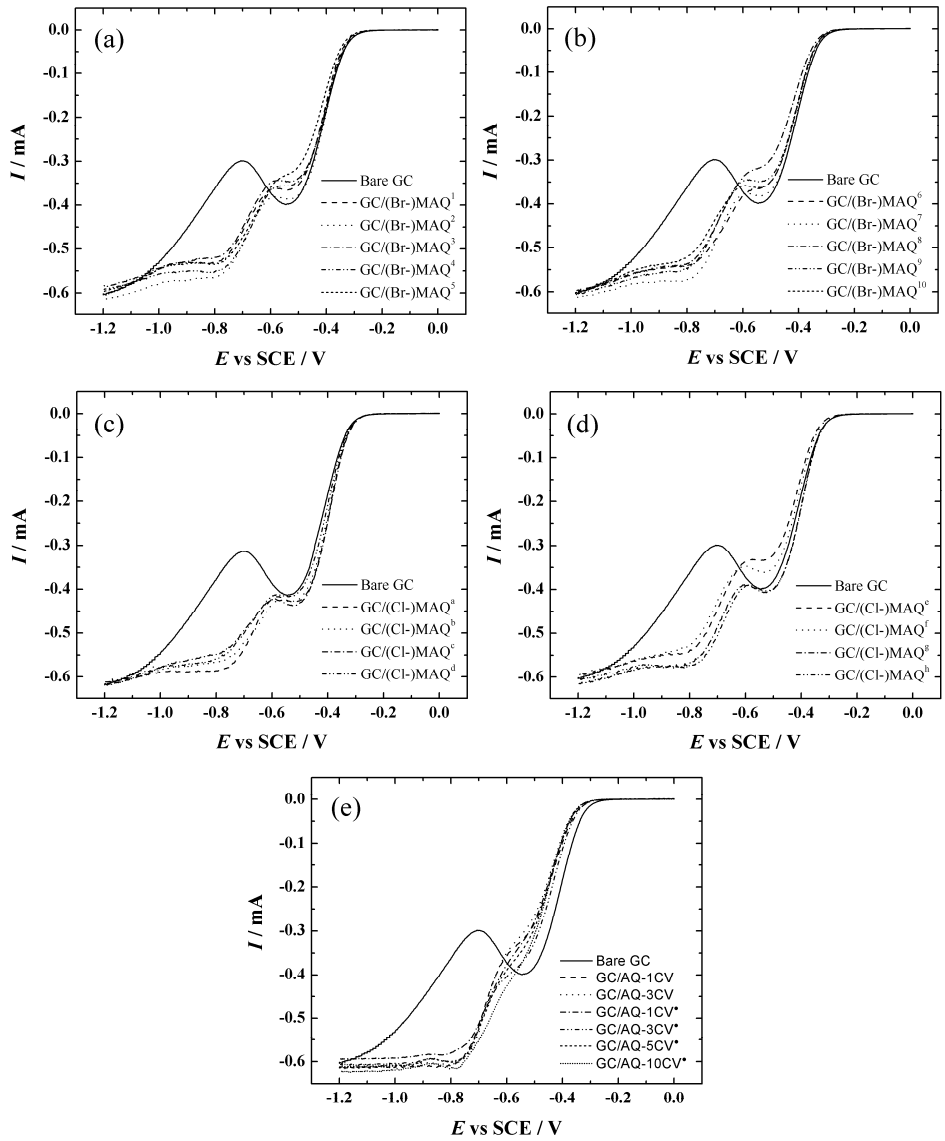

Fig. 18. Comparison of RDE voltammetry curves for oxygen reduction on bare GC and **(a, b)** GC/(Br-)MAQ, **(c, d)** GC/(Cl-)MAQ, **(e)** GC/AQ electrodes in O_2-saturated 0.1 M KOH (ω = 1900 rpm, ν = 20 mV s^{-1}) [IV, V].

In case of all MAQ-modified GC electrodes the O_2 reduction current commenced at *ca* –0.3 V. In addition, the pre-wave of O_2 reduction on bare GC (at *ca* –0.5 V) was rather suppressed on GC/(Br-)MAQ electrodes compared to GC/(Cl-)MAQ electrodes with some exceptions. This could indicate that in some cases the native GC surface sites might be partially blocked by MAQ groups depending on the used electrografting conditions (Figs. 18a-d, Table 1).

On the other hand, the O_2 reduction current increased at more negative potentials for all the MAQ-grafted GC electrodes and this is due to the electrocatalytic activity of the surface-bound MAQ groups. The RDE polarisation curves of O_2 reduction recorded for GC electrodes electrografted with AQ (Table 2) by RG method via reduction of aryldiazonium salts are shown in Fig. 18e. Compared to the MAQ-modified GC electrodes (Figs. 18a-d), the E_{onset} is slightly more negative in case of GC/AQ electrodes. This could be due to the more intense inhibition of O_2 reduction by the thick AQ films in the potential range from –0.3 V > E > –0.6 V compared to the less than a monolayer MAQ films. The difference in the film thickness was confirmed by the fact that the Γ_{AQ} values were 10 times higher compared to the ones of Γ_{MAQ} (Section 7.1.5.3, Table 6). At higher negative potentials (E < –0.7 V) the O_2 reduction current sharply increases similarly as in case of MAQ-grafted electrodes. Although, the stable O_2 reduction current is obtained at lower overpotentials in case of GC/AQ electrodes, which again refers to the higher amount of electrocatalytically active groups in the aryl film compared to the MAQ-modified electrodes. For both, MAQ- and AQ-grafted electrodes, one can consider that the covalently attached AQ groups play a dual role in the process of O_2 reduction: at lower overpotentials the reduction of O_2 is slightly suppressed by surface-bound AQ and at more negative potentials these groups catalyse the ORR process. These observations are in good agreement with previous investigations by our workgroup [13, 14, 28–35, 194, 195, 207].

In Figs. 19a and b, the RDE polarisation curves for O_2 reduction recorded in 0.1 M KOH with the electrodes having highest Γ_{MAQ} and Γ_{AQ} values, GC/(Cl-)MAQ^h and GC/AQ-10CV$^\bullet$, respectively, are presented. These electrodes were chosen because one purpose of the present work was to study the electrocatalytic activity of the thickest prepared aryl films towards the ORR. As seen in Figs. 19a and b, the increase in the electrode rotation rate leads to an increasing O_2 reduction current. The K-L plots (Figs. 19c and d) derived from the RDE data presented in Figs. 19a and b, respectively, showed good linearity and parallelism from which we may conclude that the ORR is under the mixed kinetic-diffusion control at lower overpotentials (E > –0.8 V) in case of both electrodes. From E < –0.8 V, the extrapolated K-L lines yield intercept close to the origin, which indicates fast charge transfer at the surface of AQ-modified GC electrodes. The value of n was almost independent of potential and was close to two (insets to Figs 19c and d) indicating the production of peroxide. These results are in good agreement with the proposed reaction scheme (Section 4.1, reactions 5–8).

The RRDE experiments were performed in order to ascertain the formation of hydrogen peroxide during the electroreduction of O_2 on the MAQ-modified electrode. In Fig. 20, the RRDE results for GC/(Br-)MAQ^4 electrode at a single rotation rate (ω = 960 rpm) are presented. The percentage of peroxide formation (Φ) was calculated from the following equation:

$$\Phi = \frac{200 I_R / N}{I_D + I_R / N} \tag{11}$$

where I_D and I_R are the disc and ring currents, respectively and N is the collection efficiency. The theoretical value of Φ should be 100% if the ORR follows entirely a two-electron pathway. In present study it was found that the peroxide formation was 95% (Fig. 20c).

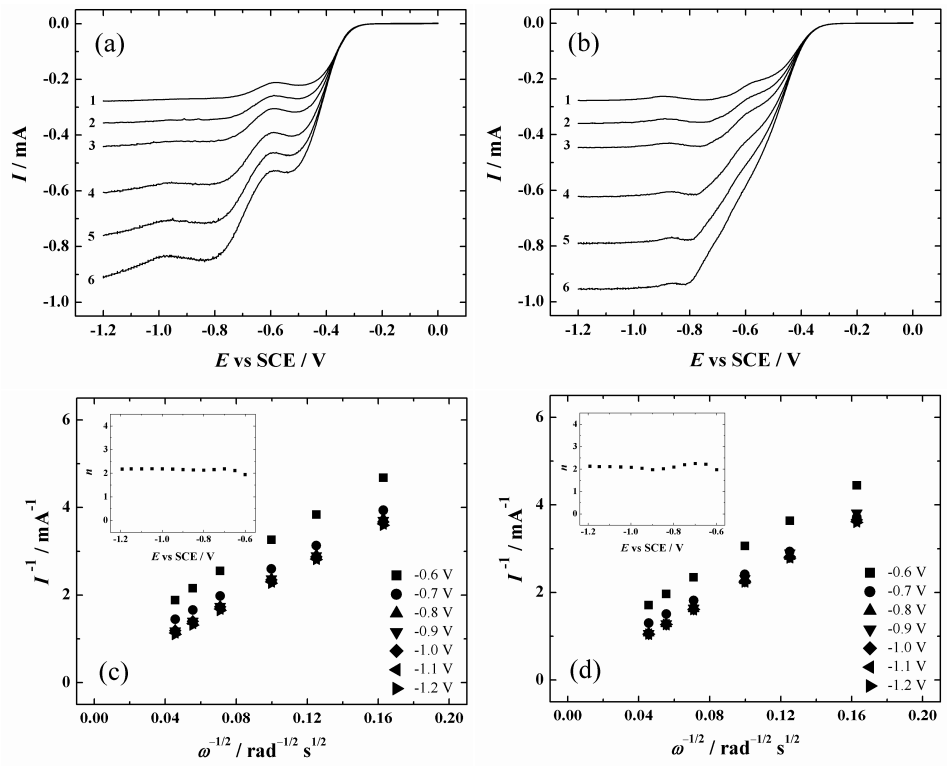

Fig. 19. RDE measurements at different rotation rates: (1) 360, (2) 610, (3) 960, (4) 1900, (5) 3100 and (6) 4600 rpm in O_2-saturated 0.1 M KOH (v = 20 mV s^{-1}) for **(a)** GC/(Cl-)MAQ^h and **(b)** GC/AQ-10CV$^\bullet$ electrodes. **(c)** and **(d)** show the K-L plots at various potentials for oxygen reduction on GC/(Cl-)MAQ^h and GC/AQ-10CV$^\bullet$ electrodes, respectively. The insets to **(c)** and **(d)** present the potential dependence of n [IV, V].

The slightly lower values for the detected peroxide (95%) compared with the theoretical value (100%) could be because of the non-quantitative peroxide detection on the Pt-ring electrode [IV, V].

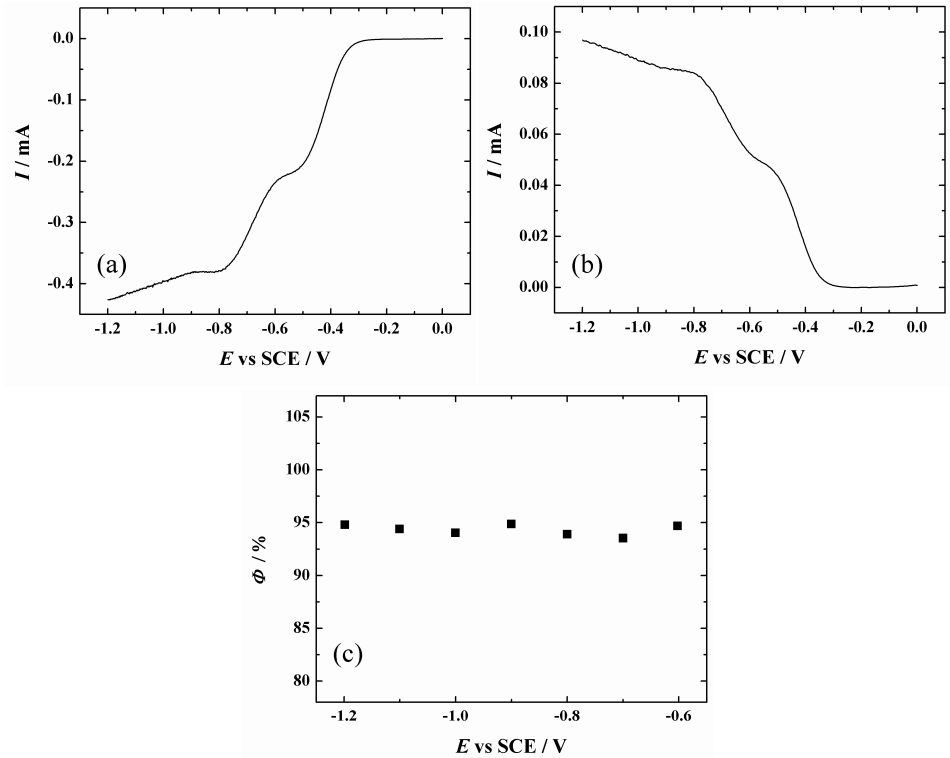

Fig. 20. (a) Disc and **(b)** ring currents for O_2 reduction on a GC/(Br-)MAQ[4] electrode in O_2-saturated 0.1 M KOH (ω = 960 rpm, v = 20 mV s^{-1}). **(c)** Dependence of the yield of peroxide formation (Φ) on potential for a GC/(Br-)MAQ[4] electrode [IV].

7.2. Aryl films on metal electrodes

The second part of the thesis is focused on the aryl film modified metal electrodes. The first section of this part concerns the electrochemical grafting of Ni [VII], Au [VI] and Cu electrodes [VIII] with different aryl films. There was no prior information about the RG of Ni and Cu electrodes. Also, the same applies to the functionalisation of Cu and Au via RG and RDE combined method. The second section covers the physical characterisation of the aryl-modified metal electrodes by XPS [VI-VIII] and AFM [VI, VIII]. In the third section, the electrochemical characterisation of the aryl film modified metal electrodes is presented. The surface concentration of the electroactive species on the electrodes was determined in ACN solution [VI, VIII], the surface blocking towards the ferricyanide probe [VI-VII] and the ORR [VI, VIII] was studied. The article [VIII] is the first known report describing the ferricyanide reduction on bare and aryl film modified polycrystalline Cu electrodes as well as presenting the ORR studies on Cu electrodes modified with AQ and NP films by reduction of aryldiazonium salts.

7.2.1. Electrografting of Ni with nitrophenyl groups

Fig. 21 presents the CV curves recorded during electrografting of Ni electrodes in 3 mM NBD solution. If the "normal" electrografting was used (Ni/NP1, Fig. 21a), a clear cathodic reduction peak of 4-nitrobenzenediazonium cation was observed during the first potential cycle. The CV peak disappears on subsequent cycles referring to the blocking of the Ni surface with the NP layer. This electrochemical behaviour is in accordance with the "normal" electrografting applied to Ni/Gra electrode (Fig. 2a). As a difference, the value of peak potential (E_p) for the reduction of aryldiazonium cation on the Ni electrode is 0.11 V (Fig. 21a) compared to the 0.38 V for Ni/Gra (Fig. 2a). This can be explained by different substrate materials (Ni vs Ni/Gra) and concentration of diazonium salt in the electrografting solution (1 vs 3 mM). In the literature, several studies report the electrografting of Ni electrodes with NP groups by the reduction of aryldiazonium salts using shorter potential range in "normal" electrografting conditions. If the results obtained in the present study are compared to the literature, the electrochemical behaviour and the value of E_p are in accordance with the data reported by other workgroups [86, 189, 208].

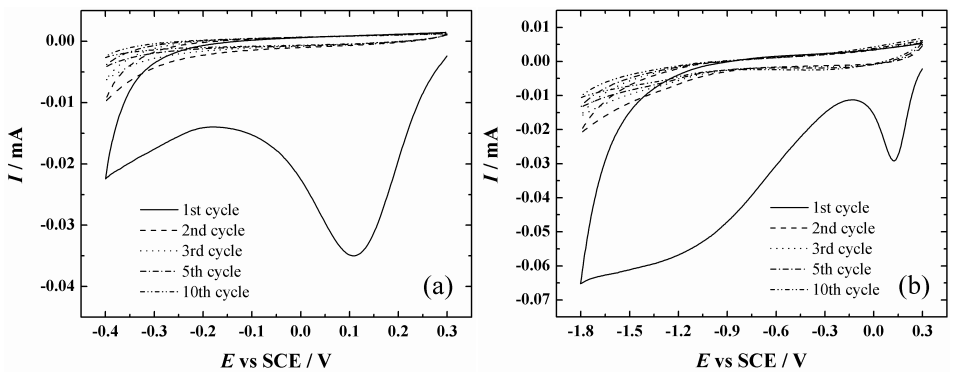

Fig. 21. Functionalisation of Ni electrodes by **(a)** "normal" electrografting or **(b)** redox grafting in Ar-saturated ACN solution containing 3 mM 4-nitrobenzenediazonium tetrafluoroborate and 0.1 M $TBABF_4$ as a base electrolyte (v = 100 mV s^{-1}) [VII].

Herein, the modification of Ni electrodes with thicker NP films by RG was reported for the first time. Prior to this work, several papers had been published by Daasbjerg's and our workgroup about RG of various conducting materials with different thick aryl films (e.g. GC [VI], Au [VI], stainless steel, highly oriented pyrolytic graphite and CVD-grown GR [III] [11, 36–38]. Generally, the CV curves recorded during the RG in a wider potential range have shown that the reduction peak of the aryldiazonium cation diminishes with the following potential cycles and the redox wave at more negative potentials grows during subsequent potential cycling [III, VI] [11, 36–38]. In the present work, a

somewhat different electrochemical behaviour during RG of Ni substrate with NP groups using potential range from 0.3 to –1.8 V was observed (Ni/NP2, Fig. 21b). As shown in Fig. 21b, the second reduction peak appears at *ca* –1.0 V which could refer to the reduction of NP to its radical anion and which is in accordance with earlier reports [III] [36]. Surprisingly, a reproducible redox wave did not appear during potential cycling (Fig. 21b) as observed in case of RG of Ni/Gra with NP groups (Fig. 2b). The disappearance of the reduction peak(s) during subsequent potential cycling observed herein (Fig. 21b) is rather similar to the electrochemical behaviour registered during "normal" electrografting (Fig. 21a), but different from the RG data reported for other electrode materials (Ni/Gra and GC) [III, VI] [11, 36–38]. The electrochemical behaviour observed herein could indicate to the gradual blocking of the aryl film during electrografting process. To our knowledge, for comparison there is no information available for the RG of Ni electrodes except for the data presented in this work (Fig. 21b) [VII].

7.2.2. Electrografting of Au with anthraquinone groups

The electrografting of Au electrodes with AQ groups was carried out in Ar-saturated ACN containing 2 mM FRA by RG (Fig. 22a) and by the RG and RDE combined method (Figs. 22b–d). The *I-E* curves recorded on a stationary Au electrode were quite similar to the ones obtained within GC electrode (Fig. 4c). Although, one difference can be observed on the first CV curve at positive potential values. In more specific, two reduction peaks (at *ca* 0.32 V and 0.15 V) were registered, while on the GC electrode rather single aryldiazonium cation reduction peak was observed (Fig. 4a–c). As a remark, it is worth to note that the disappearance of the reduction peak(s) during potential cycling is rather inherent to the "normal" electrografting process [37, 38, 209]. In the present case, the appearance of these peaks on the first CV cycle and diminishing of the peaks during following potential cycling can be explained by the slower scan rate used (v = 0.1 V s^{-1}). Lee et al. [210] have shown that using lower v, two reduction peaks appeared, but if the v was increased (e.g. 0.5 V s^{-1}), only a single reduction peak was observed. In addition, an intense and distinctive reduction peak was recorded throughout 10 potential cycles by RG at high scan rate (v = 1 V s^{-1}) [37], but considerably diminished when lower v of 0.4 V s^{-1} was applied for electrografting [38].

Interestingly, if the RG was combined with the RDE method for the electrografting in hydrodynamic conditions (ω = 200; 500; 1000 rpm, Figs. 22b–d), only a single reduction wave of diazonium cation appeared at *ca* 0.28 V in the first grafting cycle. This behaviour is very similar to the one observed for GC electrodes together with the disappearance of the peak during the subsequent potential cycling (Figs. 4d–f). In addition, the overall electrochemical behaviour is very similar among the GC and Au electrodes if the RG or the RG and RDE combined method was employed for electrografting (Figs. 4c–f vs 22a–d).

Therefore, the discussion in Section 7.1.3.2 for Figs. 4c–f also applies for Figs. 22a–d. Moreover, the electrografting conditions were also varied to optimise the AQ film formation on the Au electrode (Table 3) [VI].

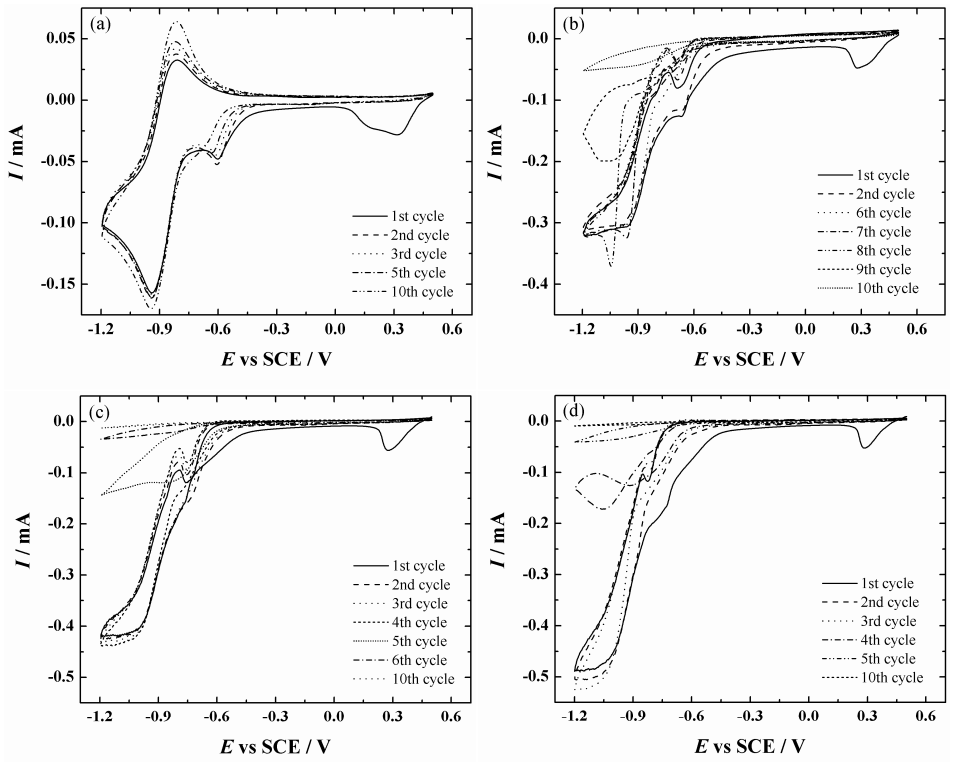

Fig. 22. Redox grafting of AQ groups on Au electrode using 2 mM Fast Red AL salt in Ar-saturated ACN containing 0.1 M $TBABF_4$ as a base electrolyte by: **(a)** cyclic voltammetry (v = 100 mV s^{-1}), **(b–d)** combination of CV and the RDE method (v = 100 mV s^{-1}, ω = **(b)** 200 rpm ; **(c)** 500 rpm; **(d)** 1000 rpm). In all Figs, up to 10 potential cycles are shown [VI].

7.2.3. Electrografting of Cu with AQ and NP groups

Previously, the electrografting of Ni using NBD [VII] and Au using FRA [VI] was investigated. Therefore, for the surface modification of Cu both diazonium salts (FRA and NBD) were employed [VIII]. Firstly, CV cycle between –0.35 to –2.0 V was registered in ACN containing 3 mM corresponding diazonium salt (NBD or FRA) and 0.1 M $TBABF_4$. If the FRA was used, two redox waves were recorded with the E^o values of –0.88 and –1.52 V (Fig. 23a). The redox wave at –0.88 V and –1.52 V corresponds to the $AQ/AQ^{\bullet-}$ redox couple and $AQ^{\bullet-}/AQ^{2-}$ redox couple, respectively [168]; both waves are known to appear if the potential of the Cu electrode is cycled in ACN solution containing AQ

molecules [86]. In contrast, only a single redox wave with E^o of –1.19 V was observed in NBD containing electrografting solution (Fig. 23b), which has been seen earlier [86] and corresponding to the NP/NP$^{\bullet-}$ redox couple [36]. The well-known reduction peak of aryldiazonium cation (Section 4.2) is not observed on the first CV cycle as it appears at a higher potential value compared to the open circuit potential of Cu (*ca* –0.25 to –0.30 V in the present solutions) at which Cu would be oxidised and dissolved [86, 211].

The RG of polycrystalline Cu electrodes with AQ or NP groups was performed by applying 10 CV cycles between –0.35 and –1.5 V (or –1.2 V) at 100 mV s^{-1} (Table 3). Since the grafting behaviour was similar in both potential ranges, only the CV curves recorded in wider potential range are presented (Figs. 23c and d). In Fig. 23c, repetitive CV curves from *ca* 5th potential cycle were recorded with relatively stable currents of the AQ/AQ$^{\bullet-}$ redox wave. The electrochemical behaviour is somewhat different from the one observed for GC and Au electrodes, where the continuous increase in the current values of the AQ/AQ$^{\bullet-}$ redox wave was recorded up to 10th electrografting cycle (Figs. 4c and 22a) [V, VI]. An explanation for this could be a difference in the conditions for film formation due to the different electrode materials. In Fig. 23d, continuous decrease in the current values of the NP/NP$^{\bullet-}$ redox wave are observed during potential cycling compared to the AQ/AQ$^{\bullet-}$ redox wave (Fig. 23c). This could refer to the saturation or blocking of the aryl film with NP species during the electrografting process similarly as in case of RG of Ni electrodes with NP moieties (Fig. 21b) [VII]. As a difference, the redox wave did not appear during RG of Ni electrode (Fig. 21b).

For the surface functionalisation using the combined RG and RDE method, the optimised rotation rate (ω = 1000 rpm) was applied according to the previous study with GC and Au electrodes [VI]. If the ω of 1000 rpm was employed during the RG of Cu electrode using FRA (Fig. 23e), the recorded *I-E* curves were remarkably different from the ones of the stationary electrode (Fig. 23c) and also from the *I-E* curves obtained with Au and GC electrodes (Figs. 4f and 22d). In the first cycle, the reduction wave at *ca* –0.71 V most likely corresponds to the reduction of AQ to AQ$^{\bullet-}$ and during subsequent potential cycling, the current steadily decreases. At the 10th potential cycle, a relatively stable AQ/AQ$^{\bullet-}$ redox wave was recorded with E^o value of –0.90 V. This refers to a similar electrochemical behaviour on the surface-bound thick AQ film as in case of the stationary electrode (E^o = –0.88 V for Cu-AQ-CV-1.5, Fig. 23c).

Different electrochemical behaviour during grafting was observed if the RDE and RG combined method was employed for functionalisation of Cu using NBD (Fig. 23f) compared to the FRA (Fig. 23e) in three key aspects: (i) the overall shape of the *I-E* curve changed, (ii) the peak current was six times higher for Cu-NP-RDE-1.5 and (iii) the cathodic current was higher during the reverse scan up to –1.0 V. We propose that these phenomena could be due to the additional effect that contributes the RDE response in the potential range where RG occurs. The higher cathodic current for the reverse scan refers to the

formation or the existence of more easily reduced species than in case of the forward scan.

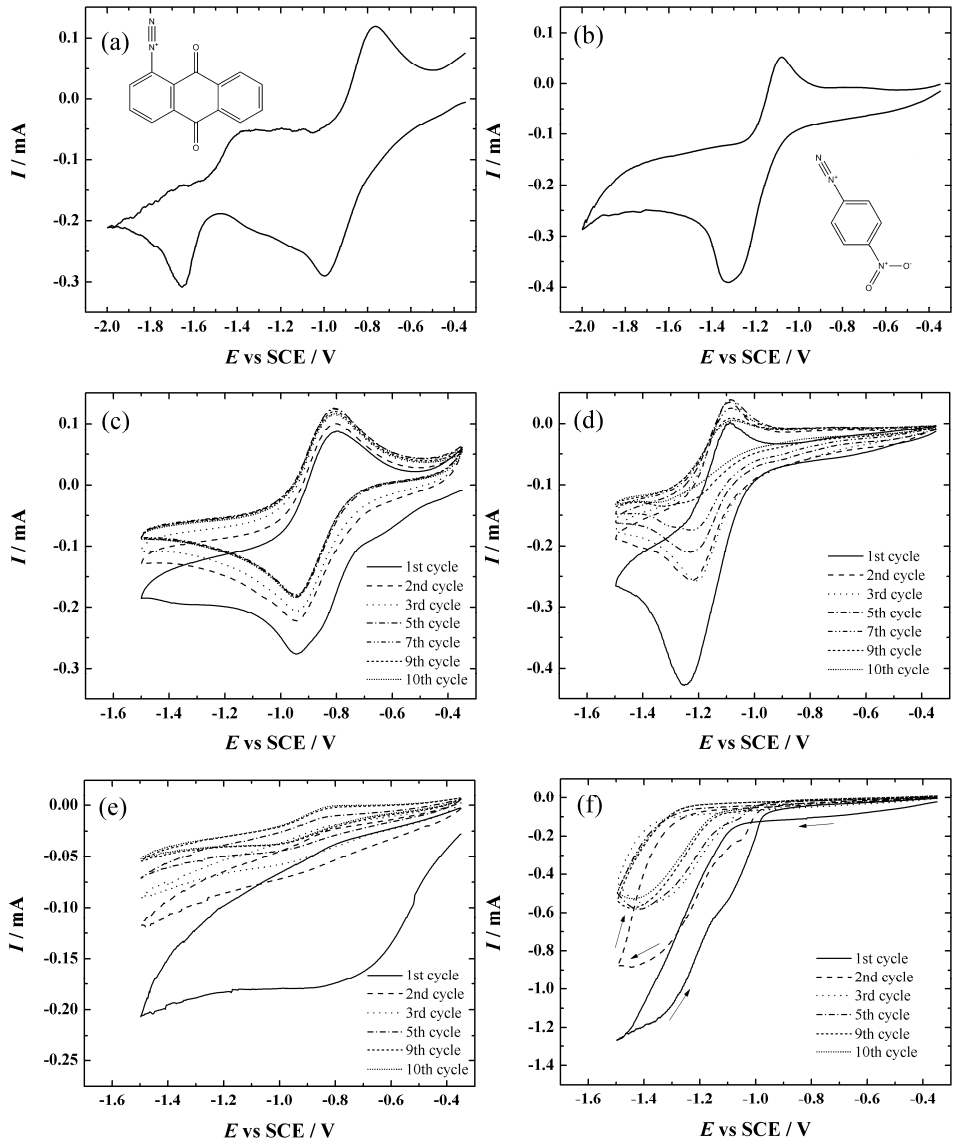

Fig. 23. Electrochemical grafting of: **(a, c, e)** AQ and **(b, d, f)** NP groups on Cu electrode in Ar-saturated ACN containing 3 mM **(a, c, e)** Fast Red AL or **(b, d, f)** 4-nitrobenzenediazonium tetrafluoroborate and 0.1 M $TBABF_4$ as a base electrolyte. (v = 100 mV s^{-1}, **(e, f)** ω = 1000 rpm). Modification conditions: **(c)** Cu-AQ-CV-1.5; **(d)** Cu-NP-CV-1.5; **(e)** Cu-AQ-RDE-1.5; **(f)** Cu-NP-RDE-1.5 (Table 3). Chemical structures of diazonium derivatives are also depicted: **(a)** anthraquinone-1-diazonium and **(b)** 4-nitrobenzenediazonium [VIII].

The species that could be reduced in the corresponding potential region (from –1.2 to –1.5 V) are $–NO_2$ groups, but the cathodic current may also increase by the diazonium groups that are reduced during the contact with the already grafted NP groups. In this situation one may consider that the film is inconsistent and the current could pass through the pinholes (Section 7.2.4.2). In the present case, the grafted film could not be an insulator because of the redox active moieties ($-NO_2$ groups). According to the study by De Feyter's group [212], the attack of the NP radicals on the groups within the aryl film is very fast [213], because these already grafted groups act like ultramicroelectrodes surrounded by a hemispherical diffusion layer [214]. During the following potential cycling, current decreases up to 10th CV cycle but is not completely suppressed. This refers to the partial blocking of the electroactive reduction centres. The redox wave as observed in case of Cu-AQ-RDE-1.5 (Fig. 23e) did not form during subsequent potential cycling indicating that the electrografting behaviour is different between these two diazonium salts (FRA and NBD) in hydrodynamic conditions. This could be explained by the different redox potential for the anion radical formation (E^o (AQ/AQ$^{\bullet-}$) = –0.88 V vs E^o (NP/NP$^{\bullet-}$) = –1.19 V, Figs. 23a and b, respectively) and the size of the modifier molecule (AQ vs NP). In case of both diazonium salts (FRA and NBD), during electrografting via RG and RDE combined method (Figs. 23e and f) the overall decrease in current values during potential cycling is similar to the behaviour observed for GC and Au electrodes using FRA (Figs. 4f and 22d) [VI].

For comparison with the literature, the RDE method has been previously employed for promoting the derivatisation of Cu electrodes with self-assembled monolayers [215]. These monolayers were derived from 3-*N,N*-dimethylaminodithiocarbamoyl-1-propane sulfonic acid in aqueous solution using a ω of 50 rpm for a specified time (2–240 min) [215]. In contrast, the present work reported the electrochemical grafting of aryldiazonium salts with the combination of RDE technique on Cu electrodes for the first time.

For comparison purposes, the Cu electrodes were also grafted via the "normal" electrografting conditions (Cu-NP-CV-0.7 and Cu-AQ-CV-0.7, Table 3). The expected behaviour of surface blocking due to the aryl film formation was observed during the electrochemical functionalisation (data not shown) [VIII].

7.2.4. Physical characterisation of aryl-modified metal electrodes

7.2.4.1. XPS analysis of the aryl-modified Ni and Au electrodes

For AQ and NP-modified Au and Ni electrodes, the XPS analysis revealed that the electrografting with both diazonium compounds (AQ and NP) was in evidence since all the XPS survey spectra showed photoelectron peaks (e.g. N1, C1s, O1s) characteristic to the diazonium salt used (Fig. 24).

The presence of NP film on the electrografted Ni substrate was confirmed by the $–NO_2$ group located at 406 eV in the high-resolution N1s XPS spectra as shown in the insets to Figs. 24a and b. In addition, the peak at 400 eV was also present (insets to Figs. 24a and b) that could be attributed to the amine groups which can be formed when the $–NO_2$ groups are reduced under the X-ray beam during the XPS measurements [77, 208]. These results are in compliance with the earlier studies reporting the XPS data of NP grafted Ni electrodes [189, 208]. In addition, the peak at 400 eV could show the presence of azo linkages within the multilayer aryl film on the Ni surface [47] similarly as in case of AQ derivatised nanomaterial coated GC electrodes [II], NP modified CVD-grown GR [III] and GC electrodes redox grafted with AQ [V] (Sections 7.1.4.2–7.1.4.4).

The XPS survey spectrum of both modified Ni electrodes showed a decrease in the characteristic Ni photoelectron peaks (e.g. Ni2p, Ni(LLM), Ni3s, Ni3p) in comparison with the corresponding peaks in the XPS spectrum of bare Ni (data not shown). Although, after the electrografting these peaks were more or less visible (Figs. 24a and b). This could indicate that the aryl film is partially incomplete or thinner on Ni surface and this is in accordance with the literature [77, 208]. If the XPS spectra of Ni/NP1 (Fig. 24a) and Ni/NP2 (Fig. 24b) are compared, the peaks inherent to Ni (Ni2p, Ni(LLM), Ni3s) were missing in case of Ni/NP2. Only a very small peak of Ni3p was registered when the RG was employed for the electrografting of Ni electrodes (Fig. 24b). From this we can assume that the NP film becomes thicker if the potential of the electrode is cycled to a more negative value. This is supported by the electrochemical measurements carried out with the $Fe(CN)_6^{3-/4-}$ redox probe (Section 7.2.5.2). In addition, Combellas *et al*. [216] have shown that the stronger the decrease of the signal of an underlying substrate material of aryl film modified electrode in the XPS spectra, the thicker is the grafted aryl film [VII].

The XPS survey spectra of Au electrodes modified by "normal" electrografting with 10 CV cycles and by RG with one potential cycle at ω = 1000 rpm are shown in Figs. 24c and d (Au/AQ-0.4 and Au/AQ-1, Table 3), respectively. The insets to Figs. 24c and d present the high resolution spectrum in the Au4f region (e.g. $Au4f_{7/2}$ and $Au4f_{5/2}$ peaks at 84 and 88 eV, respectively) [217]. The XPS peaks of O1s at *ca* 531.5 eV and C1s at *ca* 285–288 eV probably correspond to the carbonyl groups and the aromatic rings in the AQ film [37] as also registered for GC electrodes grafted with AQ (Fig. 9, Section 7.1.4.4) [V]. In Fig. 24d, the lower peaks characteristic to bare Au compared to the ones of Fig. 24c indicate the AQ film on Au electrode surface being thicker in case of Au/AQ-1 than for Au/AQ-0.4 electrode as less Au photoelectrons were registered [37, 217–219]. The XPS survey spectrum of Au/AQ-10 electrode (data not shown) was very similar to the one of Au/AQ-1 electrode (Fig. 24d). In case of Au/AQ-10, the intensity of the Au photoelectron peaks was even smaller but still detectable. This tendency has also been observed by Bousquet et al. [37]: the signal of the Au XPS peaks decreased together with the increase in the aryl film thickness, but even in case of a 50 nm thick aryl film, the XPS

peaks of Au were still detected. The appearance of Au peaks in case of thick AQ films (e.g. Au/AQ-1 and Au/AQ-10) could refer to the pores or pinholes within the AQ film or the AQ film is uneven and the areas of bare Au surface are visible [37, 41].

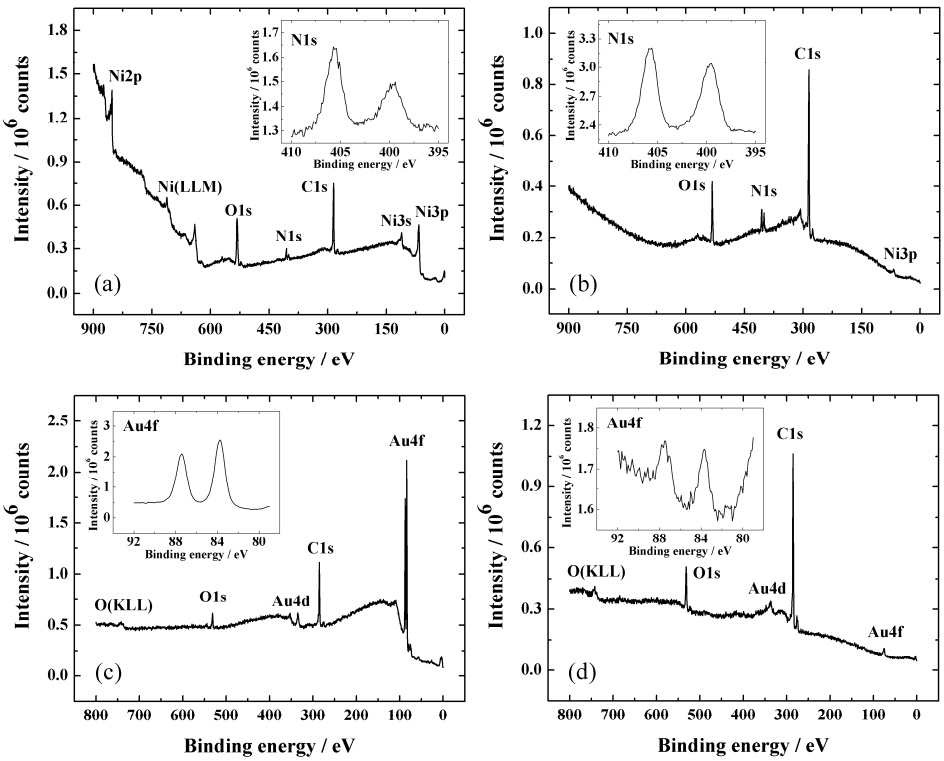

Fig. 24. XPS survey spectra of **(a)** Ni/NP1; **(b)** Ni/NP2; **(c)** Au/AQ-0.4 and **(d)** Au/AQ-1 electrodes (Table 3). The insets show the high-resolution XPS spectrum of **(a, b)** N1s and **(c, d)** Au4f region for aryl-modified Ni and Au electrodes, respectively [VI, VII].

Surprisingly, the N1s peak was hardly noticeable (Figs. 24c and d) compared to the GC electrodes electrografted with thick AQ films (Fig. 9) [V]. Although, the N1s photoelectron peak has been registered in case of Au electrodes functionalised with different aryl groups via diazonium reduction [37, 43, 186, 217]. The N1s peak at *ca* 400 eV may conform to the atmospheric N_2 [189] or originate from the supporting electrolyte together with a small peak of fluorine (at *ca* 685 eV) in the XPS survey spectra of Au/AQ-1 and Au/AQ-10 electrodes. This may indicate that some of the supporting electrolyte could be confined into the AQ film [37]. In addition, there might be a chance that the N1s peak could be attributed to the presence of azo linkages within the grafted multilayer AQ film [37] as observed in case of AQ modified GC (Section 7.1.4.4 [V]) [VI].

7.2.4.2. XPS analysis of the aryl film modified Cu electrodes

In Fig. 25a, the XPS spectrum of polished and CH_3COOH treated (Section 6.1) Cu plate is shown; Figs. 25b-e correspond to the Cu plates electrografted with AQ or NP aryl films (Table 3). In the XPS spectrum of polished Cu (Fig. 25a), photoelectron peaks inherent to Cu and also the XPS peaks of O1s and C1s regions were observed. The broad O1s peak (inset to Fig. 25a) probably corresponds to the Cu_2O [47, 153, 220–222] and to the O-C bond [221]. The latter could be explained by the formation of copper complexes with acetate ions or adsorption of atmospheric CO_2 onto the Cu surface.

The strong suppression of Cu(LMM) peaks [153] and decreased Cu2p ($Cu2p_{3/2}$ at *ca* 932 eV, $Cu2p_{1/2}$ at *ca* 952 eV) photoelectron peaks was observed after grafting the Cu plates with aryl films (Figs. 25b-e). This indicates the presence of the aryl film on the Cu electrode [154, 189, 223]. If the Cu plate was functionalised with AQ groups using FRA by RG method (Cu-AQ-CV-1.5, Fig. 25b), the O1s peak (inset to Fig. 25b) was registered at 531.5 eV. The O1s peak at this BE value is inherent to the oxygen in the AQ [224]. In the C1s region two peaks at *ca* 285 and 288 eV were observed, which correspond to carbon in phenyl ring and C=O groups, respectively, originating from the AQ molecule [VI]. The O1s and C1s photoelectron peaks at similar BE values were also observed in case of AQ modified Au electrodes (Section 7.2.4.1). In addition, the absence of the distinguishable N1s peak from the spectrum indicates that the presence of azo linkages (–N=N–) is unlikely within the AQ film on the Cu if the RG method was used similarly as observed in case of Au (Fig. 24d) [VI]. In contrast, the corresponding N1s peak has been observed for the films on Cu obtained by "normal" electrografting of 4-trifluoromethylbenzenediazonium ions [154] and spontaneous functionalisation with benzene diazonium (BD) salt [47]. The XPS spectrum of Cu-AQ-CV-0.7 (Table 3) prepared by "normal" electrografting was very similar to the one of Cu-AQ-CV-1.5 (Fig. 25b) and therefore it is not shown.

In case of NBD, the XPS survey spectra of three different electrodes are presented in Figs. 25c–e. In all cases, the O1s peak at 532.4 eV and C1s peak at *ca* 284.6 eV were registered. The first peak is characteristic to oxygen in $–NO_2$ group and second peak to the carbon of aromatic ring as reported for NP films grafted by different methods on the Cu surface in ACN using NBD [86, 153].

The insets to Figs. 25c–e shows the high-resolution spectra in the N1s region with the XPS peaks at *ca.* 400 eV (–N=N– [47] and $–NH_2$ [86]) and at *ca.* 406 eV ($–NO_2$ [86]). For all the N1s spectra, the ratio (R) of baseline subtracted peak areas was calculated using the equation: $R \approx A_{400}/A_{406}$ [154]. For the electrode prepared by "normal" electrografting (Cu-NP-CV-0.7, Table 3), the $R \approx 0.31$ was obtained (inset to Fig. 25c). This peak ratio is very similar to the ones from the literature obtained in case of spontaneous grafting [153] and "normal" electrografting [86]. The 400 eV peak could be attributed to the azo linkages as it has been registered with spontaneously grafted films on Cu using BD or NBD in the same conditions [47]. Additionally, the presence of azo

linkages in polyphenylene films on Cu have also been supported by time-of-flight secondary ion mass spectrometry experiments and infrared spectroscopy [184]. Although, the azo linkages bonded to the Cu surface atoms are quite unlikely [184]. The chemical reduction of $–NO_2$ to $–NH_2$ under the X-ray beam should also be taken into consideration [47, 86, 153, 189]. If the RG was used for grafting the Cu plate with NP film (Cu-AQ-CV-1.2, Fig. 25d), then higher $R \approx 1.13$ was obtained (inset to Fig. 25d). This could indicate the reduction of $–NO_2$ groups to $–NH_2$ during RG.

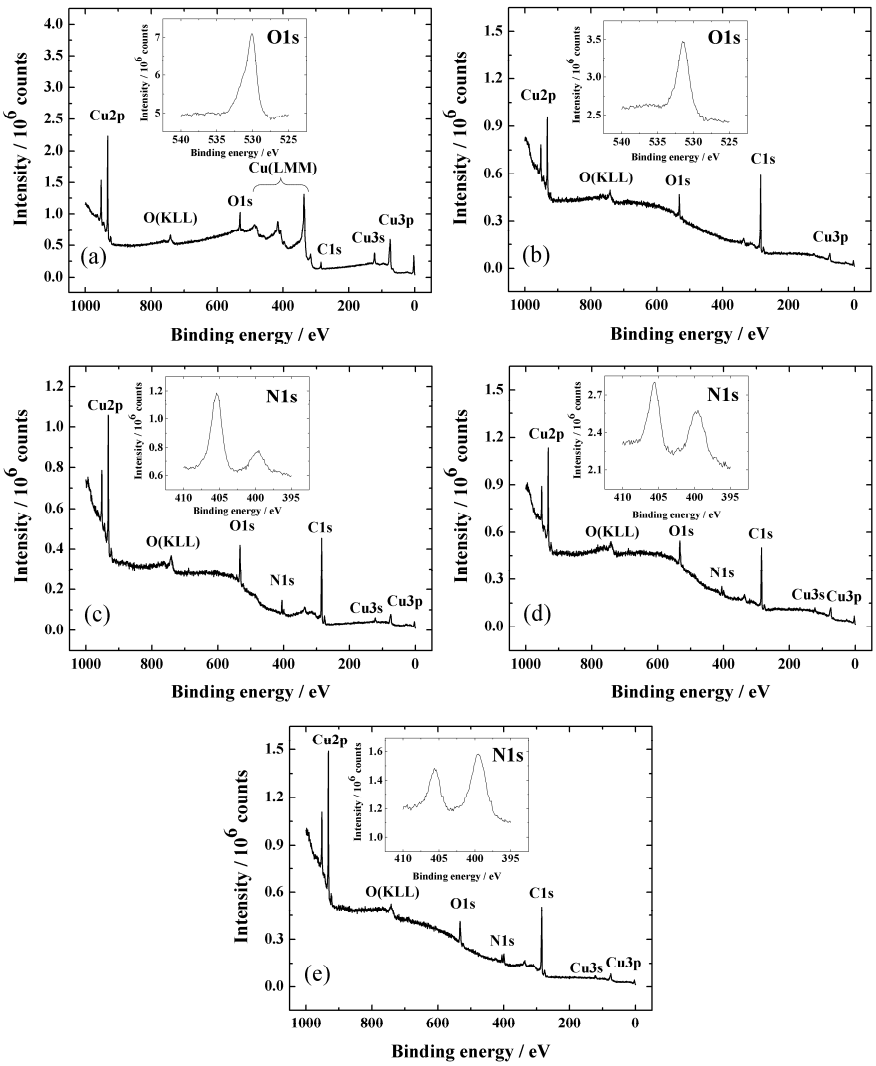

Fig. 25. XPS survey spectra of **(a)** polished and CH_3COOH-treated Cu plate; **(b)** Cu-AQ-CV-1.5; **(c)** Cu-NP-CV-0.7, **(d)** Cu-NP-CV-1.2 and **(e)** Cu-NP-CV-1.5 electrodes (Table 3). The insets show the XPS spectrum of **(a, b)** O1s and **(c-e)** N1s region for aryl-modified Cu electrodes [VIII].

As an evidence to the reduction process, the $R \approx 1.89$ was obtained (inset to Fig. 25e) if the switching potential during RG was adjusted to a more negative value of –1.5 V (Cu-AQ-CV-1.5, Table 3). According to these results, the adjustment of the potential in electrografting/RG procedure allows us to vary the type of nitrogen moieties ($–NO_2$ or $–NH_2$) in the NP film. As the NP film thickness on the Cu-NP-CV-0.7 and Cu-NP-CV-1.5 electrodes was equal (Section 7.2.4.3), the probability of higher amount of azo linkages in the redox grafted films compared to the film obtained via "normal" electrografting is unlikely. In addition, the electrochemical reduction of $–NO_2$ to $–NH_2$ in the NP film on the GC electrode has been also previously reported [225].

The appearance of the azo linkages in the NP film (Figs. 25c-e) compared to the AQ film (Fig. 25b) could be explained by the different properties of the modifier molecule (AQ vs NP). In addition, the AQ and NP films must contain pinholes or pores because the photoelectron peaks of the Cu were detected despite the thickness of the grafted films of 19 to 47 nm (Section 7.2.4.3) if the analysis depth of the XPS method is considered (*ca* 10 nm) [37, 220, 226]. Similar results were obtained for the redox grafted AQ films on the Au electrode (Fig. 24d) [VI].

For comparing the aryl films obtained with RG or RDE and RG combined method, the XPS spectra of Cu-AQ-RDE-1.5 and Cu-NP-RDE-1.5 electrodes was registered in the Cu2p region. The strong suppression of the Cu2p peaks was observed for the electrodes compared to the Cu-AQ-CV-1.5 and Cu-NP-CV-1.5 probably due to the thicker aryl films prepared by RDE and RG combined method [VIII].

7.2.4.3. AFM characterisation of the aryl-modified Au and Cu electrodes

The AFM study of AQ and NP film modified Au and Cu electrodes was performed to obtain additional information about the electrochemical grafting of AQ and NP diazonium cations and the thickness of the AQ and NP layers. Firstly, the AFM image of Au film on a mica substrate functionalised with 10 CV cycles using "normal" electrografting method (Au/AQ-0.4, Table 3) is presented in Fig. 26a. The granular structure inherent to AQ film was observed similarly as in earlier work by our workgroup, where also "normal" electrografting was used for grafting Au film on mica substrate with AQ moieties [209]. In the present study, the thickness of the aryl film of Au/AQ-0.4 electrode was found to be 6 nm. The AFM image of Au electrode modified with one or 10 CV cycles by the RG and RDE combined method using ω of 1000 rpm are presented in Figs. 26b (Au/AQ-1) and c (Au/AQ-10), respectively. The AQ film thickness in case of Au/AQ-1 electrode was found to be around 15–20 nm. Although, in the latter case the surface of mechanically polished Au electrode was still visible. For Au/AQ-10 electrode (Figs. 26c), the underlying mechanically polished Au surface was not as clearly seen. This

difference shows that thicker AQ film has been obtained in case of Au/AQ-10 electrode. Furthermore, the presence of pinholes within the AQ film was observed in case of both electrodes prepared by the combination of RG and RDE method, which could explain the presence of Au photoelectron peaks in the XPS survey spectra (Fig. 24d) [VI].

In Figs. 27a and b, the AFM images of Cu-CV-NP-0.7 and Cu-CV-NP-1.5 electrodes are presented, respectively. In case of both electrodes, the inherent granular structure of the NP film [III] [189] was observed and the film thickness of *ca* 27–28 nm was measured. Very similar value (30 nm) was obtained when the Ni/GRA was functionalised with NP film by RG in similar conditions (except the v of 1 V s^{-1} was used, Ni/Gra/NP3, Section 7.1.4.3). According to the results obtained for Cu electrodes herein, we can conclude that RG seems not to be advantageous for obtaining the NP film with higher thickness compared to the "normal" electrografting. Although, if the RDE and RG combined method was used for the electrografting (Cu-NP-RDE-1.5, Fig. 27c), the thickest film of the present work was obtained (47 nm). In addition, the underlying Cu surface was not as clearly seen as in case of the Cu-CV-NP-1.5 electrode (Fig. 27b). These results indicate that the incorporation of RDE into the electrografting procedure is highly effective for increasing the thickness of the NP film on Cu.

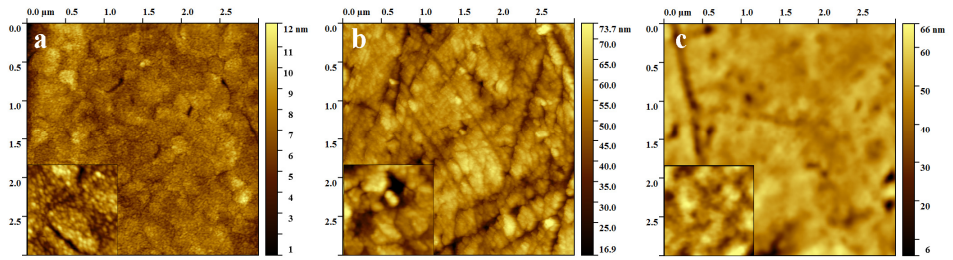

Fig. 26. AFM images (scan area 3×3 μm^2) of: **(a)** Au/AQ-0.4; **(b)** Au/AQ-1 and **(c)** Au/AQ-10 electrode (Table 3). Insets present the AFM images of the respective electrodes with higher magnification (scan area 0.5×0.5 μm^2) [VI].

The AFM images of AQ films prepared via: "normal" electrografting (Cu-AQ-CV-0.7), RG (Cu-AQ-CV-1.5), RG and RDE combined method (Cu-AQ-RDE-1.5) with the film thickness of 19, 26 and 37 nm, respectively, are shown in Figs. 27d–f. The granular structure characteristic to AQ film, which has been observed on Au (Fig. 26a) [37, 209] and CVD-grown graphene [11] was not seen; but clear dependence between the modification procedure and the film thickness was in evidence. Similar thickness to the 26 nm AQ film as in case of Cu-AQ-CV-1.5 has been reported for the redox grafted AQ film (24.5±4.2 nm) on the stainless steel by Ceccato et al. [36]. The thickness of the redox grafted AQ film seems to depend on the substrate material; e.g. on the CVD-grown

graphene, if monolayer graphene on Cu or multilayer graphene on Ni substrate, the four times difference in the film thickness has been found [11]. On Au substrates, if similar conditions to Cu-AQ-CV-1.5 (Table 3) were used for RG (except the $v \geq 0.5$ V s^{-1}) usually *ca* 60±10 nm thick AQ films have been prepared [36–38]. Considering the latter information, it is possible that the film in case of Cu-AQ-RDE-1.5 (37 nm) is thinner than the film on the Au/AQ-10 electrode (Fig. 26c). The visual comparison of AFM images supports this as the underlying Au surface is not as clearly seen as in case of Cu (Figs. 26c vs 27f). Also, *ca* two times difference in the Γ_{AQ} value was measured for Au/AQ-10 supporting the thicker film in the latter case (Section 7.2.5.1). For the formation of thinner films on Cu compared to the Au electrode, the more negative initial potential (–0.35 V for Cu and 0.5 V for Au (Table 3)) during electrografting process can be proposed. Specifically, the charging and discharging of the already grafted film, which is essential for the continuous film growth [36] could be less effective for Cu with shorter electrografting potential range and this could limit the film thickness [VI, VIII].

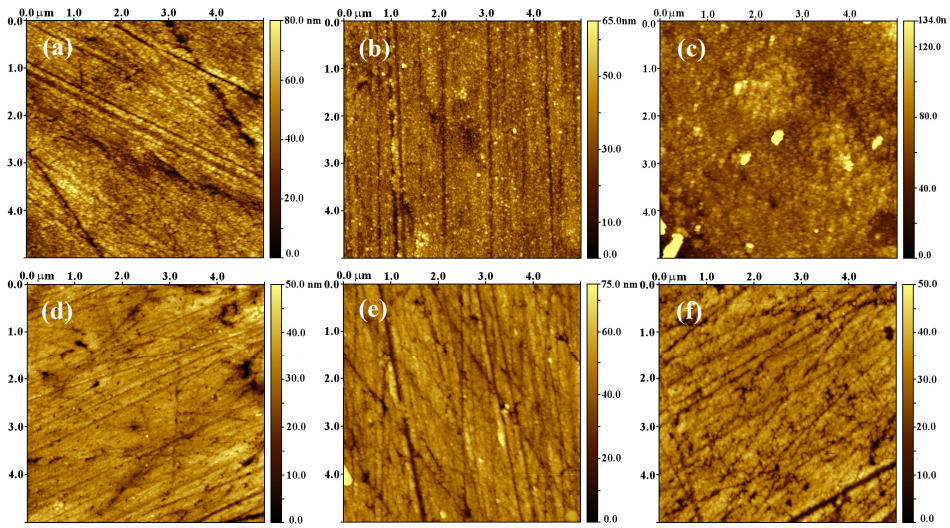

Fig. 27. AFM images (scan area 5×5 μm^2) of: **(a)** Cu-NP-CV-0.7; **(b)** Cu-NP-CV-1.5; **(c)** Cu-NP-RDE-1.5; **(d)** Cu-AQ-CV-0.7; **(e)** Cu-AQ-CV-1.5; **(f)** Cu-AQ-RDE-1.5 electrodes [VIII].

7.2.5. Electrochemical characterisation of aryl film modified metal electrodes

7.2.5.1. Surface concentration of AQ and NP groups on Au and Cu electrodes

The Γ_{AQ} and Γ_{NP} values determined from the CV curves recorded in Ar-saturated ACN containing 0.1 M $TBABF_4$ (Fig. 28) in case of AQ or NP film modified Au and Cu electrodes are presented in Table 8. For the calculation of Γ_{AQ} and Γ_{NP} values equation (9) from Section 7.1.5.1 was used with a modification for the number of electrons involved (n = 1). In case of the Au/AQ electrodes (Fig. 28a), the stabilised CV curve was already achieved after 5th potential cycle irrespective of the ultrasonic treatment similarly as in case of GC/AQ electrodes (Fig. 12d, Section 7.1.5.3). Also, when the RDE method was applied during the modification process, the calculated Γ_{AQ} values drastically increased compared to the electrodes prepared by the stationary mode similarly as in case of GC/AQ electrodes (Fig. 12d, Table 6). The dependence between the calculated Γ_{AQ} value and number of CV cycles used during redox grafting with the combination of CV and RDE (ω = 1000 rpm) method is shown in the inset to Fig. 28a. The highest Γ_{AQ} value was found to be Γ_{AQ} = 21 nmol cm^{-2} (Au/AQ-10, Table 8) when 10 CV cycles were applied during electrografting similarly as in case of GC/AQ electrodes (Table 6). Also, the calculated Γ_{AQ} values on Au/AQ electrodes could correspond only to the electroactive AQ units in the aryl film resulting in the underestimation of real Γ_{AQ} values as in case of GC/AQ electrodes [VI].

The Γ_{AQ} values on the AQ-modified Cu electrodes were determined from the CV curves (Fig. 28b) recorded in the potential range from –0.35 to –1.3 V vs SCE. Similarly, the stable cyclic voltammogram was obtained usually on *ca* 5th cycle as in case of the Au/AQ electrodes. Surprisingly, the Γ_{AQ} value of the film prepared by "normal" electrografting (Cu-AQ-CV-0.7) is *ca* 87% of the Γ_{AQ} value of the films prepared via RG (Cu-AQ-CV-1.2, Cu-AQ-CV-1.5, Table 8). For comparison, in case of Au/AQ electrodes a considerably larger (*ca* 3-fold) difference was obtained in the Γ_{AQ} values of the correspondingly electrografted electrodes (Table 8). If the experimentally determined thickness constant for redox grafted AQ film (on Au) from the literature is considered (0.2 nmol cm^{-2} nm^{-1}) [37], the Γ_{AQ} value difference should be higher according to the 7 nm thicker film in case of Cu-AQ-CV-1.5 compared to the Cu-AQ-CV-0.7 (Section 7.2.4.3) electrode. As an explanation, some of the AQ molecules could be electrochemically non-responsive due to the compactness of the redox grafted film and the internal hindrance within the film [11, 37]. If the RG and RDE combined method was employed for the electrografting (Cu-AQ-RDE-1.2, Cu-AQ-RDE-1.5), the calculated Γ_{AQ} values were *ca* 3-times higher than the ones prepared via RG. Similar tendency was observed also in case of GC/AQ and Au/AQ electrodes (Tables 6 and 8). In turn, the 3-times increase in the Γ_{AQ} value obtained by incorporation of the RDE method is unexpectedly high if the

thickness difference of only 11 nm is considered (Section 7.2.4.3). As a proposed explanation, the electrolyte flow in hydrodynamic conditions could favour the functionalities within the grafted AQ layers to remain accessible for electron transfer in the growing film. In case of the electrode functionalised in the stationary conditions, the AQ film could get more clogged up during grafting.

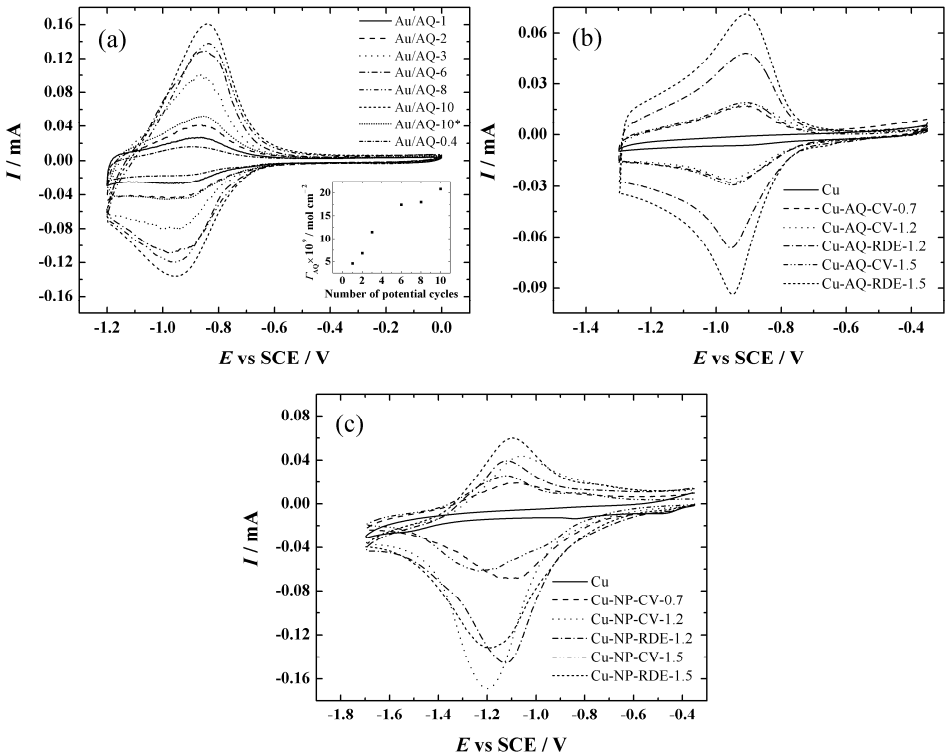

Fig. 28. Cyclic voltammograms of: **(a)** Au/AQ, **(b)** Cu-AQ and **(c)** Cu-NP electrodes registered in Ar-saturated ACN containing 0.1 M $TBABF_4$ (v = 100 mV s^{-1}). In **(b)** and **(c)**, the CV curve of polished and CH_3COOH-treated Cu electrode is also presented for comparison. The inset to 28a presents the dependence between the AQ surface concentration (Γ_{AQ}, Table 8) and the number of potential cycles used during the electrografting of the Au electrode. Modification conditions of the electrodes are presented in Table 3 [VI, VIII].

The determination of Γ_{NP} values from CV curves in ACN is more complicated compared to the redox wave of AQ with stable peak currents (Fig. 28b), because during subsequent potential cycles, the redox peak currents usually continue to decline, which could indicate the decomposition of the NP film [227]. Therefore, in Table 8 the Γ_{NP} values determined from the reduction peak of the first CV cycle recorded on NP grafted Cu electrodes (Fig. 28c) are

presented. This method was taken from the literature [220]. As a remark, no substantial contribution to $–NO_2$ reduction peak by Cu oxides is observed according to the CV curve of bare Cu (Fig. 28c). The maximum of the reduction peak of NP groups appears between –1.1 and –1.2 V (Fig. 28c), which corresponds to the potential range reported for NP film modified Cu electrodes in several studies [86, 153, 189, 220]. Interestingly, NP films with very similar Γ_{NP} values (Table 8) and thicknesses (Section 7.2.4.3) were obtained by "normal" electrografting (Cu-NP-CV-0.7) and RG using a wider potential range (Cu-NP-CV-1.5). While, the XPS results (Figs. 25c and e) revealed the significantly higher amount of electrochemically non-responsive reduced $–NO_2$ moieties and the ferricyanide and O_2 reduction studies showed more effective surface blocking in case of Cu-NP-CV-1.5 compared to the Cu-NP-CV-0.7 electrode (Sections 7.2.5.3 and 7.2.5.4). According to these results, the redox grafted NP film seems to be more dense and compact than the NP film obtained by "normal" electrografting.

For the three remaining electrografted electrodes (Cu-NP-CV-1.2, Cu-NP-RDE-1.2, and Cu-NP-RDE-1.5) *ca* 2-times higher Γ_{NP} value of *ca* 25 nmol cm^{-2} was calculated (Table 8). The reason behind these similar Γ_{NP} values may be caused by the various amount of $–NO_2$ groups electrochemically reduced to $–NH_2$ moieties during electrografting (Section 7.2.4.2) depending on the grafting conditions or a higher number of non-electroactive $–NO_2$ groups within the NP film. Interestingly, the obtained Γ_{NP} value is very similar to the one from the literature (25±1 nmol cm^{-2}) reported for NP film spontaneously grafted onto Cu electrodes in ACN containing 10 mM NBD by Chamoulaud and Bélanger [153]. The presence of electrochemically non-responsive $–NO_2$ moieties due to the hindrance within the NP films has to be also considered similarly as in case of the AQ films [228]. The remarkable difference between the magnitudes of the Γ_{AQ} and Γ_{NP} values for the films prepared in similar conditions with different diazonium salts (FRA or NBD) could be explained by the multilayer film structures [37, 47, 86, 213, 228, 229], different unit volume of NP or AQ film components and due to the different intermolecular bonding.

The Γ_{AQ} values of 12 and 21 nmol cm^{-2} for Cu-AQ-RDE-1.5 and Au/AQ-10, respectively, are the highest known amount of electroactive AQ groups reported for the AQ films on corresponding electrodes grafted using the reduction of aryldiazonium salts method [VI, VIII].

Table 8. The calculated surface concentrations of anthraquinone (Γ_{AQ}) and nitrophenyl (Γ_{NP}) groups on Au and Cu electrodes. Γ_{AQ} values are calculated from the average area of reduction and oxidation peaks in Fig. 28a and b. Γ_{NP} values are calculated from the area of reduction peak in Fig. 28c [220]. Modification conditions of the electrodes are presented in Table 3 [VI, VIII].

Electrode designation	Γ_{AQ} [nmol cm^{-2}]	Electrode designation	Γ_{AQ} or Γ_{NP} [nmol cm^{-2}]
Au/AQ-0.4	2.6	Cu-AQ-CV-0.7	3.1
Au/AQ-200	18	Cu-AQ-CV-1.2	3.5
Au/AQ-500	16	Cu-AQ-RDE-1.2	8.6
Au/AQ-1	4.6	Cu-AQ-CV-1.5	3.6
Au/AQ-2	6.8	Cu-AQ-RDE-1.5	12
Au/AQ-3	12	Cu-NP-CV-0.7	12.2
Au/AQ-6	17	Cu-NP-CV-1.2	25.7
Au/AQ-8	18	Cu-NP-RDE-1.2	23.9
Au/AQ-10	21	Cu-NP-CV-1.5	12.6
Au/AQ-10*	8.0	Cu-NP-RDE-1.5	24.4

7.2.5.2. Blocking properties of the aryl film modified Ni and Au electrodes towards the $Fe(CN)_6^{3-/4-}$ probe

For studying the blocking effect of NP films on Ni electrodes towards the ferri/ferrocyanide redox probe, the bare Ni electrode was first characterised. The RDE voltammetry curves of bare Ni were registered using rotation rates from 360 to 4600 rpm in 0.1 M KOH containing 1 mM $K_3Fe(CN)_6$ (Fig. 29a). All *I-E* curves in Fig. 29a show a well-formed diffusion-limited current plateau and a clear dependence on the ω. This is in accordance with the data published by our workgroup [208]. As observed in Fig. 29b, the reduction current is rather equivalent to the theoretical one calculated using the Levich equation [24]:

$$I_d = 0.62nFAC^{\circ}D^{2/3}\nu^{-1/6}\omega^{1/2} \quad (12)$$

where I_d stands for the diffusion-limited current, n is the number of electrons involved ($n = 1$), F is the Faraday constant, A is the geometric electrode area, C° is the concentration of $Fe(CN)_6^{3-}$ in the bulk (1×10^{-6} mol cm^{-3}), D is the diffusion coefficient of $Fe(CN)_6^{3-}$ (7.63×10^{-6} cm^2 s^{-1} [230]), ν is the kinematic viscosity of the solution (0.01 cm^2 s^{-1} [205]) and ω is the electrode rotation rate.

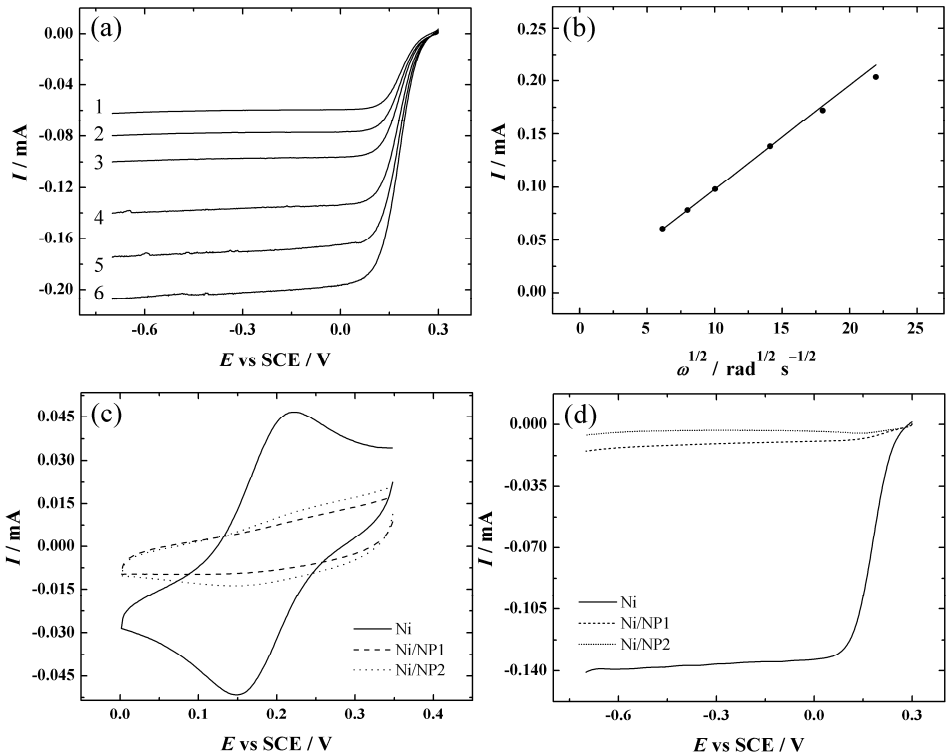

Fig. 29. (a) RDE voltammetry curves of ferricyanide reduction on a bare Ni electrode (v = 20 mV s^{-1}, (1) 360, (2) 610, (3) 960, (4) 1900, (5) 3100 and (6) 4600 rpm), **(c)** cyclic voltammograms (v = 100 mV s^{-1}) and **(d)** comparative RDE voltammetry curves (v = 20 mV s^{-1}, ω = 1900 rpm) for bare and NP modified Ni electrodes registered in Ar-saturated 0.1 M KOH containing 1 mM $K_3Fe(CN)_6$. **(b)** Levich plots of ferricyanide reduction on bare Ni electrode at –0.5 V. The solid and dotted curves correspond to the theoretical and experimental Levich plot, respectively [VII].

In Fig. 29d, the comparative RDE voltammetry curves are in accordance with the data obtained by CV (Fig. 29c). Although, the current of RDE polarisation curves were strongly inhibited on both, Ni/NP1 and Ni/NP2 electrodes, a small difference can be observed between these two (Fig. 29d). In more specific, after modification of Ni electrode with NP groups via "normal" electrografting the ferricyanide reduction current decreased by 92% (Ni/NP1), meanwhile functionalisation of Ni with NP moieties by RG results in the almost totally suppressed current (98%) (Fig. 29d). Furthermore, the efficient blocking behaviour observed with Ni/NP2 electrode towards the ferri/ferrocyanide redox probe is in accordance with the obtained XPS data (Section 7.2.4.1), where the characteristic Ni peaks (Ni2p, Ni(LLM) and Ni3s) in the XPS spectra were suppressed referring to the formation of thick and compact NP layer on Ni surface by RG. The results obtained here are important for the practical

application of NP film modified Ni electrodes in various fields. For example, thick compact NP layers can be used as protective barriers or may be further used for the development of (bio)sensors [VII].

In the literature, several studies have been reported for ferricyanide reduction on aryl-modified Au electrodes [40, 43, 185, 219, 231]. Herein, the ferricyanide response on thick AQ film modified Au electrode prepared by RG and RDE combined method is reported for the first time. In Fig. 30, the CV curves of bare Au and different Au/AQ electrodes recorded in Ar-saturated 0.1 M K_2SO_4 solution containing 1 mM $K_3Fe(CN)_6$ are shown.

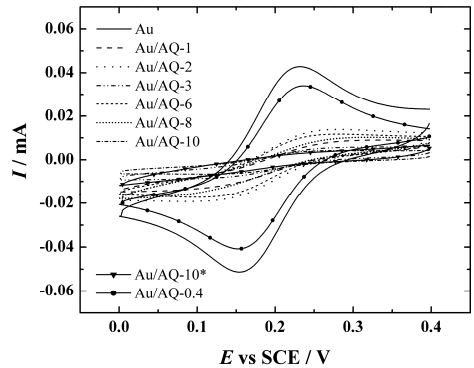

Fig. 30. Cyclic voltammograms of bare and different AQ-modified Au electrodes recorded in Ar-saturated 0.1 M K_2SO_4 containing 1 mM $K_3Fe(CN)_6$ (v = 100 mV s^{-1}). The electrografting conditions of the Au electrodes are presented in Table 3 [VI].

Surprisingly, a redox wave of $Fe(CN)_6^{3-/4-}$ is clearly observable in case of the Au/AQ-0.4 electrode prepared via "normal" electrografting. This indicates the film being porous enough so that the $Fe(CN)_6^{3-}$ anions can access the surface sites of Au. If the RG was used for the Au surface functionalisation with AQ moieties (Au/AQ-10*, Fig. 30), the response of the ferri/ferrocyanide redox probe was strongly suppressed, which is in accordance with the literature [38]. This electrochemical behaviour indicates that the AQ film is sufficiently compact to restrict the access of $Fe(CN)_6^{3-}$ anions to the active sites of the Au electrode. If the RDE method was combined into the electrografting procedure and a lower number of potential cycles ($\leq$ 8) was used, the response of the ferri/ferrocyanide redox probe was less suppressed in comparison with the Au/AQ-10* electrode (Fig. 30). In addition, there seems to be no clear dependence between the blocking intensity and the number of modification cycles. Although, if 10 potential cycles during the grafting via RG and RDE combined method was used, the signal of the $Fe(CN)_6^{3-}$ probe was more suppressed than in case of the Au/AQ-10* electrode [VI].

7.2.5.3. Blocking properties of the aryl film modified Cu electrodes towards the $Fe(CN)_6^{3-/4-}$ probe

Prior to this work, no information could be found describing the ferricyanide reduction on bare and aryl-film modified polycrystalline Cu electrodes. Similarly to the previous $Fe(CN)_6^{3-}$ reduction study on Ni electrodes (Section 7.2.5.2 [VII]), the RDE polarisation curves on polycrystalline Cu electrodes were recorded at different ω values in Ar-saturated 0.1 M KOH solution containing 1 mM $K_3Fe(CN)_6$ (Fig. 31a). The reduction current values were in accordance with the *I-E* curves obtained in case of bare un-oxidized Ni electrodes (Fig. 29a [VII]) [208]. The compliance was additionally confirmed by comparing the experimental reduction current values recorded at –0.15 V (Fig. 31a) with theoretical diffusion-limited currents calculated by equation (12) (Fig. 31b). The obtained results indicated that the reduction of ferricyanide is not noticeably affected by the oxidized surface state (Cu^{2+}) of the poly-crystalline Cu electrode and most likely could be used for studying the blocking behaviour of the aryl films on Cu electrodes.

In Fig. 31c, the CV curves registered on AQ modified Cu electrodes in 0.1 M KOH solution containing 1 mM $K_3Fe(CN)_6$ are presented. For comparing the extent of inhibition, the corresponding values of AQ functionalised electrodes obtained from the CV curves shown in Fig. 31c are given in Table 9 in which ΔE_p presents the peak-to-peak separation, I_{pc} is the cathodic peak current value at maximum and I_{rel} is the blocking efficiency calculated according to the equation (13) taken from the literature [232]:

$$I_{rel}(\%) = \frac{I_{pc}\ \text{with the film}}{I_{pc}\text{for bare Cu}} \times 100 \qquad (13)$$

As can be seen from Fig. 31e, the most effective blocking behaviour towards the $Fe(CN)_6^{3-/4-}$ redox probe is registered in case of Cu electrodes electrografted via RG and RDE combined method (Cu-AQ-RDE-1.2 and Cu-AQ-RDE-1.5). The comparative diffusion-limited reduction current values (I_{DL}) at –0.15 V is given in Table 9. These results indicate that the most dense and impenetrable AQ film towards the $Fe(CN)_6^{3-}$ ion is obtained if the RG and RDE combined method was used for the electrografting. Similar observations were seen also in case of Au/AQ electrodes (Fig. 30 [VI]). The film structure obtained in case of Cu-AQ-RDE-1.2 exhibits slightly stronger blocking intensity than the one of Cu-AQ-RDE-1.5 electrode (Table 9, Figs. 31c and e).

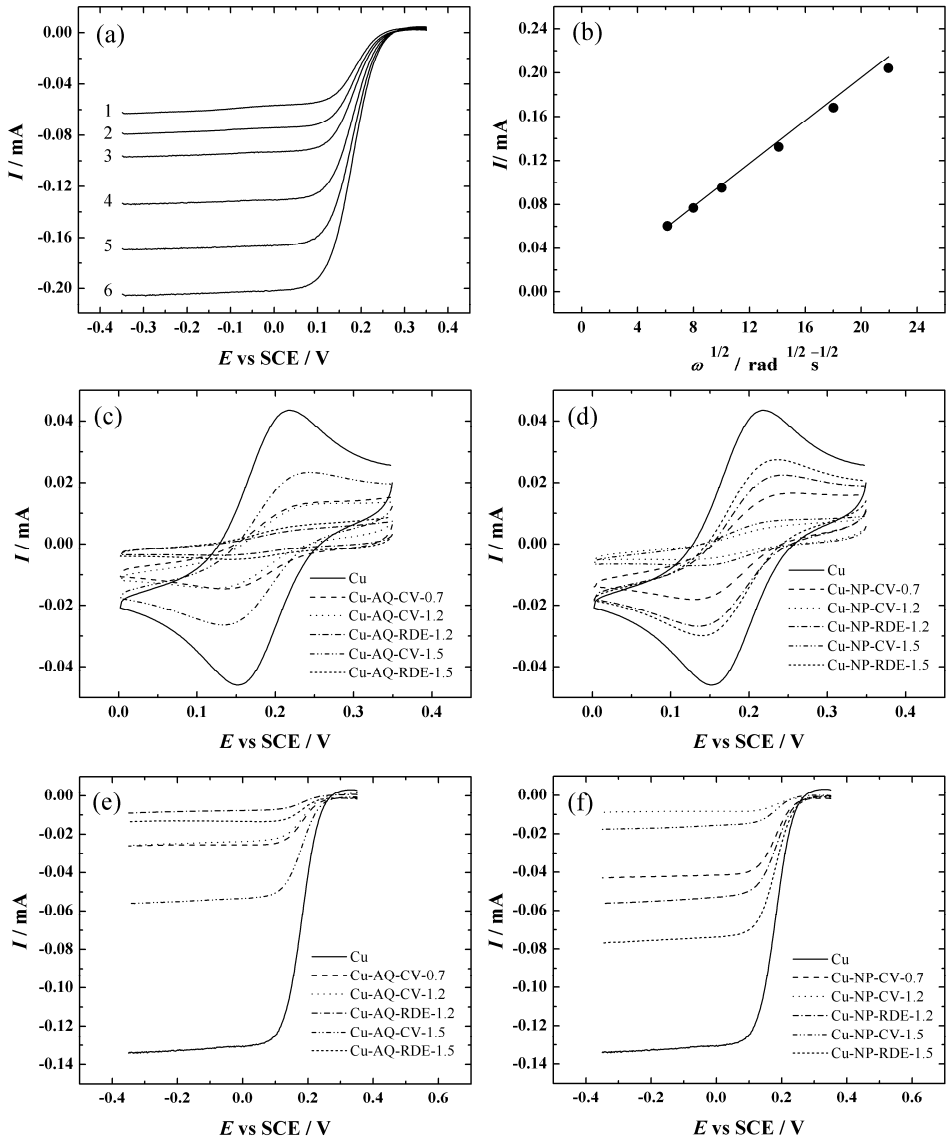

Fig. 31. (a) RDE voltammetry curves of ferricyanide reduction on bare Cu electrode (ω = (1) 360, (2) 610, (3) 960, (4) 1900, (5) 3100, (6) 4600, v = 20 mV s^{-1}), **(c, d)** CV curves (v = 100 mV s^{-1}), **(e, f)** RDE voltammetry curves (v = 20 mV s^{-1}, ω = 1900 rpm) for **(c-f)** bare and different **(c, e)** AQ, **(d, f)** NP-modified polycrystalline Cu electrodes recorded in Ar-saturated 0.1 M KOH containing 1 mM $K_3Fe(CN)_6$. Modification conditions of the electrodes are presented in Table 3. **(b)** Levich plots of ferricyanide reduction on bare Cu electrode at –0.15 V, the solid and dotted curves correspond to the theoretical and experimental reduction current values, respectively [VIII].

Table 9. Different parameters (I_{pc}, I_{rel}, ΔE_p) determined from the CV curves for bare, AQ (Fig. 31c) and NP (Fig. 31d) modified Cu electrodes; comparison of current values (I_{DL}) of ferricyanide reduction at –0.15 V for respective electrodes obtained by the RDE method (Figs. 31e and f). Test solution: Ar-saturated 0.1 M KOH containing 1 mM $K_3Fe(CN)_6$. For RDE: ω = 1900 rpm, v = 20 mV s^{-1}, for CV: v = 100 mV s^{-1}. I_{rel2} (%) is calculated using equation (13) where I_{pc} values are substituted with respective I_{DL} values [VIII].

Electrode designation	I_{pc} [µA]	I_{rel} [%]	ΔE_p [mV]	I_{DL} [µA]	I_{rel2} [%]
Cu	46	-	67	132	-
Cu-AQ-CV-0.7	15	32	-	26	19
Cu-NP-CV-0.7	18	39	125	42	32
Cu-AQ-CV-1.2	14	31	-	25	19
Cu-NP-CV-1.2	5.3	12	-	8.5	6.4
Cu-AQ-RDE-1.2	3.7	8.1	-	8.1	6.1
Cu-NP-RDE-1.2	27	58	108	55	41
Cu-AQ-CV-1.5	26	58	111	55	41
Cu-NP-CV-1.5	7.1	16	-	17	13
Cu-AQ-RDE-1.5	5.1	11	-	13	10
Cu-NP-RDE-1.5	30	65	98	75	57

The CV and RDE voltammetry curves of ferricyanide reduction for NP-modified Cu electrodes are presented in Figs. 31d and f, respectively. In addition, the calculated parameters are listed in Table 9. One can observe that the tendency of surface blocking intensity is different from the AQ-modified electrodes. In specific, the NP films obtained using the RG and RDE combined method (Cu-NP-RDE-1.2 and Cu-NP-RDE-1.5) show significantly lower blocking ability compared to the films (Cu-NP-CV-1.2 and Cu-NP-CV-1.5) prepared by RG. For comparison, the Cu-NP-RDE-1.5 and Cu-NP-RDE-1.2 electrodes were also studied without the 5 min sonication in ACN after electrografting. These electrodes showed the blocking behaviour towards the $Fe(CN)_6^{3-/4-}$ redox probe with a similar intensity as Cu-NP-CV-1.2 and Cu-AQ-RDE-1.2 electrodes (Fig. 31). Although, without the sonication the absence of physisorbed species in these films cannot be verified [87]. We propose that, the NP films prepared by RG and RDE combined method are more fragile compared to the redox grafted ones and therefore do not withstand the sonication with equal durability. According to the gathered results, the redox grafted NP films should be preferred for durability and surface blocking purposes compared to the NP films prepared via RG and RDE combined method (Figs. 31d and f, Table 9).

To our knowledge, this was the first report on the relatively strong suppression of ferricyanide reduction on aryl film modified Cu electrodes electrografted via reduction of aryldiazonium salts (i.e. Cu-NP-CV-1.2 and Cu-AQ-RDE-1.2). In addition, the blocking efficiency towards the ferricyanide reduction of the

AQ and NP films was found to decrease if the aryl film modified Cu electrode was potential cycled in ACN solution in order to determine the Γ_{NP} and Γ_{AQ} values by CV (Fig. 28b and c). Therefore, the surface blocking studies towards the ferri/ferricyanide redox probe should be carried out before performing the CV experiments in ACN solution [VIII].

7.2.5.4. Blocking properties of the aryl film modified Au and Cu electrodes towards the ORR

In Fig. 32a, the RDE voltammetry curves of bare polycrystalline Au and Au/AQ electrodes (Table 3) in O_2-saturated 0.1 M KOH solution are presented for studying the influence of AQ films with different Γ_{AQ} values (Table 8) towards the ORR. As observed in Fig. 32a, the bare polycrystalline Au is relatively active ORR electrocatalyst in alkaline media compared to the AQ film grafted Au electrodes. This is also in agreement with the literature [41–43, 233–235].

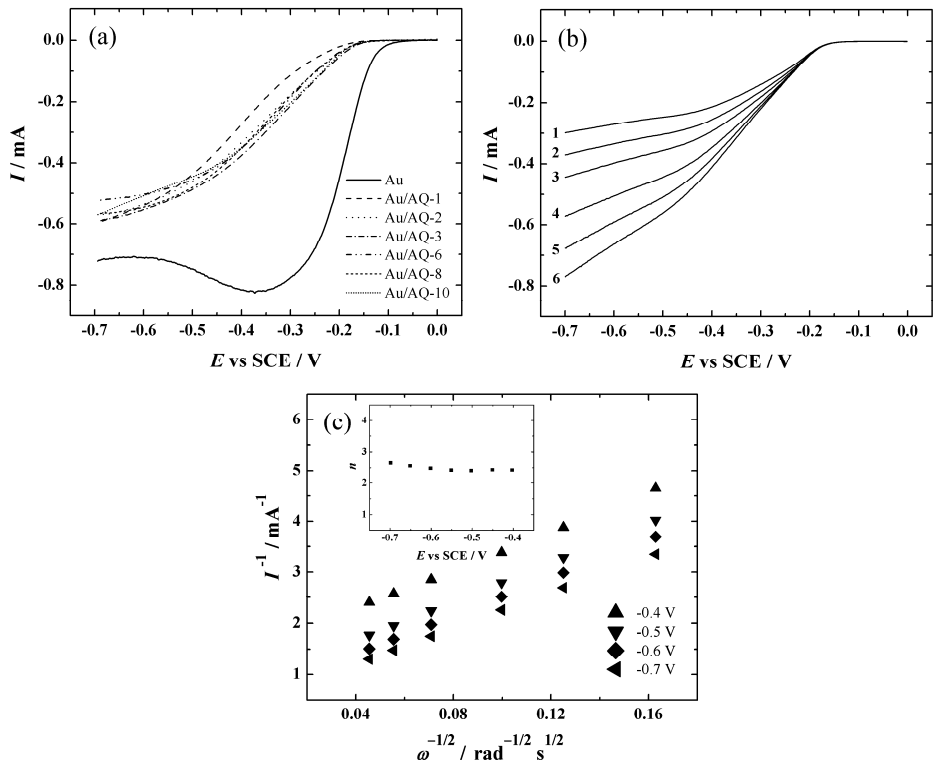

Fig. 32. (a) Comparative RDE voltammetry curves for ORR on bare Au and Au/AQ electrodes (ω = 1900 rpm, v = 20 mV s^{-1}), **(b)** RDE voltammetry curves for O_2 reduction on Au/AQ-10 electrode (ω = (*1*) 360, (*2*) 610, (*3*) 960, (*4*) 1900, (*5*) 3100 and (*6*) 4600 rpm, v = 20 mV s^{-1}) in O_2-saturated 0.1 M KOH. **(c)** Koutecky-Levich plots for ORR on Au/AQ-10 electrode. The inset presents the potential dependence of n [VI].

The blocking effect towards the ORR is similar in case of all Au/AQ electrodes suggesting that the Γ_{AQ} value does not affect the ORR performance on thick AQ film modified Au electrodes similarly as observed in case of thick AQ film modified GC electrodes (Section 7.1.6.2, Fig. 18e) [V].

The ORR polarisation curves on Au/AQ-10 electrode with the highest Γ_{AQ} value (21 nmol cm^{-2}, Table 8) at different rotation rates are presented in Fig. 32b. Despite the blocking effect of the thick AQ film on Au electrode the dependence on the ω is clearly observable. This electrochemical behaviour indicates that the electron tunnelling through AQ film takes place [236] or some of the Au catalytically active sites are accessible for O_2 molecules. These observations are also in accordance with the XPS and AFM results (Sections 7.2.4.1 and 7.2.4.3, respectively), where the photoelectron peaks of Au were registered (Fig. 24d) and pinholes in the AQ film were observed (Fig. 26b and c). The K–L plots derived from the RDE voltammetry curves shown in Fig. 32b are presented in Fig. 32c. The K–L analysis reveals that O_2 reduction is under the mixed kinetic-diffusion control in the studied potential range. In addition, the extrapolated K-L lines do not pass the origin and this refers to a substantial blocking of the active surface sites of Au by the thick AQ film [43]. The value of n was calculated according to the equation (10). The calculated value of n was between 2 and 3 (inset to Fig. 32c), which refers to the further partial reduction of HO_2^- to OH^-. The obtained value of n is lower than the one of bare Au [44]. This observation also refers to the inhibiting effect on the active sites of Au on the Au/AQ electrodes by thick AQ film [VI].

The O_2 reduction studies on Cu electrodes were performed in aqueous solution with pH = 7 as the electrochemical behaviour of Cu towards the ORR is well known in these conditions [49, 52, 54]. Firstly, the RDE voltammetry curves were registered at different ω values on bare Cu electrodes (Fig. 33a) and the K–L plots derived from the RDE polarisation curves are shown in Fig. 33b. K–L plots reveal that O_2 reduction is under the mixed kinetic-diffusion control at $E > -0.85$ V, but diffusion-limited from –0.85 V to –1 V. The latter phenomenon is shown by the extrapolated K-L lines passing the origin in the diffusion-controlled region. The value of n was close to 4 (inset to Fig. 33b) as expected [49, 52, 54]. It should be noted that for calculating the value of n, the equation (10) was used with a new value of diffusion coefficient of O_2 (D_{O2}= 1.8×10^{-5} cm^2 s^{-1} [52, 54]). The behaviour of the electrochemical O_2 reduction on Cu electrode is in agreement with the literature [52, 54].

In Figs. 33c and d, the RDE voltammetry curves for the Cu electrodes functionalised with AQ and NP films (Table 3), respectively, are presented. The *I-E* curve for bare Cu is shown for the comparison purposes. As in case of the bare polycrystalline Cu electrode, the value of n was also close to 4 for all aryl-film modified Cu electrodes. The blocking efficiency of NP and AQ films towards the ORR is noticeably lower than for $Fe(CN)_6^{3-}$ reduction (Fig. 31). Such phenomenon was also observed in case of AQ grafted Au (Figs. 30 and 32a) and has also been evidenced in previous studies by our workgroup [42, 43]. As an explanation, the hydrophobic aryl film could be more penetrable for

the small O_2 molecules in comparison with the bigger hydrophilic ferricyanide ions and therefore the reduction of O_2 could be less suppressed [195]. The blocking effect towards $Fe(CN)_6^{3-}$ reduction was very similar for Cu-NP-CV-1.2 and Cu-AQ-RDE-1.2 electrodes (Fig. 31 and Table 9).

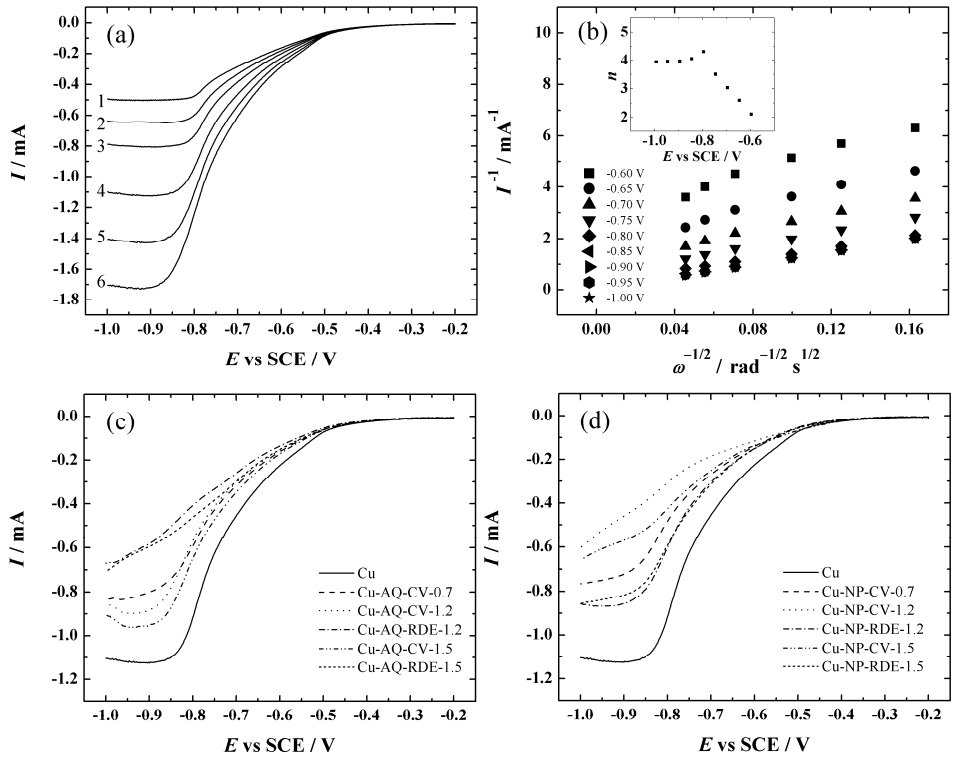

Fig. 33. (a) RDE voltammetry curves for oxygen reduction on a bare polycrystalline Cu electrode in O_2-saturated 0.1 M $NaClO_4$ and 0.1 M phosphate buffer solution (pH = 7) at different rotation rates: (1) 360, (2) 610, (3) 960, (4) 1900, (5) 3100 and (6) 4600 rpm (v = 20 mV s^{-1}). **(b)** Koutecky-Levich plots for O_2 reduction on bare polycrystalline Cu electrode. The inset of **(b)** presents the potential dependence of n. **(c, d)** Comparison of RDE voltammetry curves for oxygen reduction on **(c, d)** bare Cu and **(c)** AQ, **(d)** NP-modified Cu electrodes in the pH = 7 solution (ω = 1900 rpm, v = 20 mV s^{-1}) [VIII].

Surprisingly, the Cu-NP-CV-1.2 electrode exhibits better blocking efficiency than the Cu-AQ-RDE-1.2 electrode towards the ORR (Figs. 33c and d). This can be attributed to the higher surface concentration of NP groups referring to the higher film density compared to the AQ film on Cu (Table 8). Corresponding difference could have more effect on small O_2 molecule compared to bulkier $Fe(CN)_6^{3-}$ anion. In addition, at the negative values in the potential range used for ORR studies, the partial charging of the AQ groups could occur

resulting in the increase in the conductivity of the AQ films. The charging of NP groups occurs at more negative potentials and therefore, the conductivity of NP films would not be as much affected in the potential range corresponding to the ORR experiments. In addition to the inhibition of O_2 reduction observed herein, the AQ films are known to inhibit the electroreduction of CO_2 towards hydrocarbons on Cu nanowires [221].

The decrease of the blocking efficiency of the AQ and NP films on the aryl film modified Cu electrode due to cycling in ACN solution was also observed in case of the ORR studies similarly to ferricyanide reduction experiments (Section 7.2.5.3). Therefore, the surface blocking studies towards the ORR should be also carried out before performing the CV experiments in ACN solution [VIII].

7.3. Composite material coated GC electrodes

In the third part of the thesis several composite materials (SAN-MWCNT, SAN/PAN/CNT and PDC materials [IX–XI]) are studied as ORR electrocatalysts. Firstly, physical characterisation of the prepared materials by XPS and SEM was carried out [IX–XI]. The second section describes the ORR performance of the prepared catalysts in alkaline environment. Prior to this work, there was no information about the ORR catalysts based on SAN-MWCNT and SAN/PAN/CNT materials [IX, X]. The last paper [XI] is the first one proposing a new class of materials (SiOC based PDC) for being used as ORR electrocatalysts. The ORR on latter materials is also studied in neutral conditions [XI].

7.3.1. Physical characterisation of composite materials

7.3.1.1. SEM studies of the composite materials

The SEM micrographs (125 000× magnification) of MWCNT, SAN-MWCNT-700 and SAN-MWCNT-800 catalyst materials (Section 6.1.4) are presented in Figs. 34a–c. Both pyrolysed SAN-MWCNT catalysts consist mainly of MWCNTs according to the SEM images (Figs. 34b and c). Although, in the composition of SAN-MWCNT-700 catalyst more remaining material from SAN was observed compared to the SAN-MWCNT-800 catalyst material. This is in compliance with the reported decomposition of SAN during the pyrolysis [121]. Yang et al. have also carbonised SAN and MWCNTs based composite materials at 700 °C for 3 h using different precursor material ratios in the composite [237]. They reported that the pure SAN resin without any MWCNTs significantly shrank into a carbon block after the pyrolysis according to the SEM images [237]. Although, low content of MWCNTs (3 wt%) reduced the extent of shrinkage during carbonisation due to the clinging of the SAN-based carbons to the surface of MWCNTs [237]. In case of SAN-MWCNT-700 and SAN-MWCNT-800 catalysts containing 1 wt% of MWCNTs, also a considerable shrinkage of the material was observed due to the carbonisation [IX].

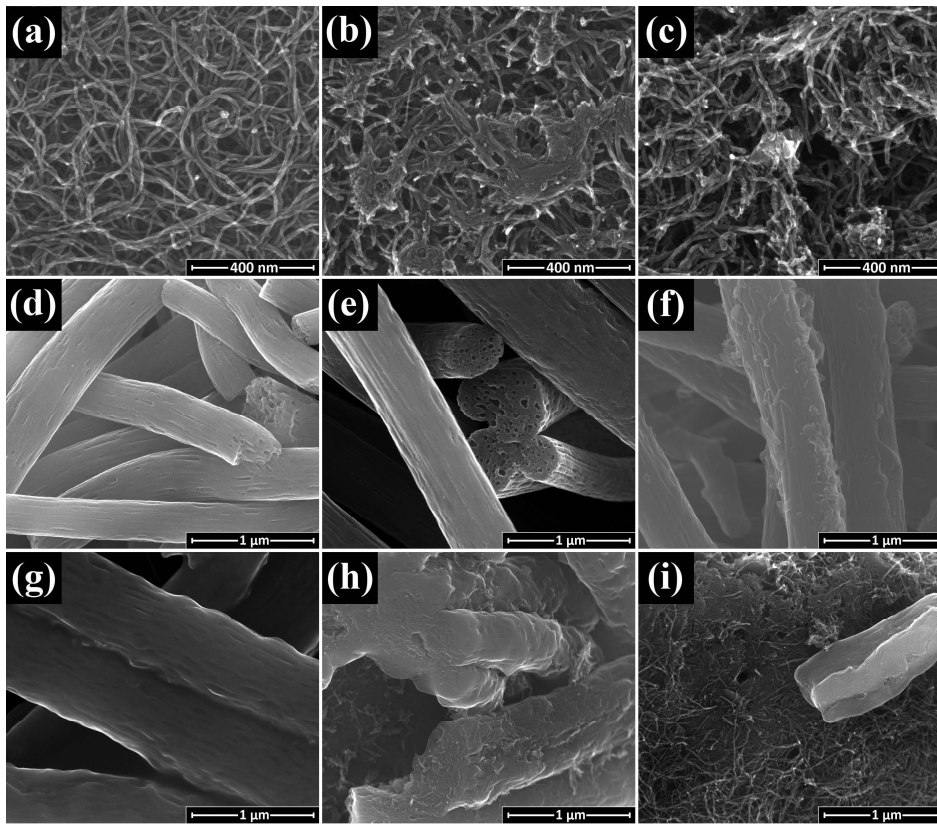

Fig. 34. SEM images of 125 000× magnification (scale bar: 400 nm): **(a)** MWCNT, **(b)** SAN-MWCNT-700, **(c)** SAN-MWCNT-800; 50 000× magnification (scale bar: 1 µm): **(d)** SAN/PAN-250/800, **(e)** SAN/PAN-250/1100, **(f)** SAN/PAN/CNT-250/800, **(g)** SAN/PAN/CNT-250/1100, **(h)** SAN/PAN/CNT-800, **(i)** SAN/PAN/CNT-1100 [IX, X].

In Figs. 34d–i, the SEM images (50 000× magnification) of different SAN/PAN and SAN/PAN/CNT based catalyst materials (Section 6.1.4) are presented. In case of all these materials, pyrolysed CNFs are observed with the diameter less than 1 µm. CNFs with a similar diameter have also been prepared in case of stabilised (250 °C) and pyrolysed (900 °C) electrospun PAN fibres with or without the addition of transition metal (Co) in the work by Kim et al. [238]. In Figs. 34d and e, the SEM micrographs of SAN/PAN-250/800 and SAN/PAN-250/1100 materials, respectively, are shown. One can see that the structure of the CNFs is not affected by the use of different pyrolysis temperatures. In the end cross-sections and the sides of CNFs pores are visible. The weight loss during the carbonisation of SAN is *ca* 96% according to the literature [239]. This explains the porous structure of CNFs, which is obtained during the decomposition and burning out of the SAN component. Similar results have been also obtained in previous studies by other workgroups [121, 122, 240]. In

Figs. 34f and g, the images of SAN/PAN/CNT based catalysts prepared at different pyrolysis temperatures and with prior stabilisation in the air are presented. Corresponding CNFs are very similar to the ones obtained in case of the carbon fibres without the addition of MWCNTs (Figs. 34d and e).

The SEM images of SAN/PAN/CNT based composite materials prepared without the prior stabilisation in air are presented in Figs. 34h and i. The CNFs that were not stabilised seemed to be somewhat fused together and more decomposed compared to the materials prepared with prior stabilisation (Figs. 34f and g). Also, due to the fusion, more bulky carbon chunks seemed to be present in the material. This was also supported by *ca* 20% difference in weight loss during thermal treatment between the materials carbonised with and without prior stabilisation (data presented in the Electronic supplementary material of the original article [X]). As a very important aspect, the MWCNTs were visible in case of the catalyst materials prepared without the prior stabilisation in the air (Figs. 34h and i) [X].

In Fig. 35, the SEM images (50 000× magnification) of the different PDC based catalyst materials (Section 6.1.5) are presented. The ball-milling was used to grind the ceramic material in order to reduce the particle size of the material [XI] and the SEM micrographs show that the ball-milling refined the SiOC ceramic material into powder with particle size less than 20 µm (Fig. 35a). The functionalisation of the materials with Ni, Co and N has no observable effect on the structure of the SiOC powder (Figs. 35b-f) as expected [XI].

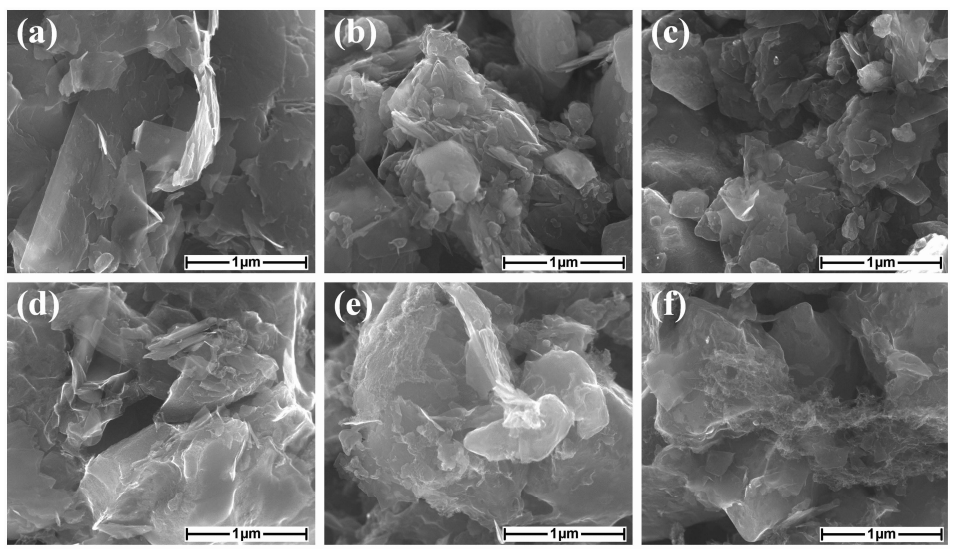

Fig. 35. SEM images (50 000× magnification, scale bar: 1 µm) of **(a)** PDC, **(b)** PDC-Ni, **(c)** PDC-Co, **(d)** PDC-N, **(e)** PDC-Ni-N, **(f)** PDC-Co-N catalysts [XI].

7.3.1.2. XPS characterisation of composite materials

In Figs. 36 and 37, the XPS survey spectra of different SAN-MWCNT and SAN/PAN(/CNT) based catalysts (Section 6.1.4), respectively, are presented. The calculated values (at%) of the elemental composition of these catalysts and pristine MWCNT material are presented in Table 10. All pyrolysed catalyst materials contain carbon (C1s peak at *ca* 284–285 eV, insets to Figs. 36a and b), nitrogen (N1s peak at *ca* 400 eV) and oxygen (O1s peak at *ca* 532 eV, insets to Figs. 36a and b) as expected. However, except the presence of N1s peak at 400 eV, the XPS survey spectra were similar with the one of MWCNTs (data not shown). Very close BE values corresponding to the specific C1s, N1s or O1s photoelectron peak have been reported for pyrolysed electrospun pristine PAN fibres [71] and porous PAN fibres prepared by burning out of SAN [121]. The content of oxygen (Table 10) for all catalysts prepared by pyrolysis is higher than 1.3 at% obtained for pristine MWCNTs herein. The latter value is in turn very similar to the one presented by White et al. for pristine MWCNTs [241].

The difference among the SAN-MWCNT based materials (Fig. 36) is *ca* 1 at% of N in the composition of the catalyst materials pyrolysed at 700 and 800 °C (Table 10, Figs. 36d and e) compared to the SAN-MWCNT-900 material with the N content of only 0.4 at% (Table 10, Figs. 36f). This may indicate that during carbonisation at lower temperatures more N moieties originating from the SAN could remain in the material. The deconvoluted N1s peaks (Table 10, Figs. 36d−f) reveal the notable trends in the ratios of different N species depending on the pyrolysis temperature. In case of using the higher pyrolysis temperature, the content of pyridinic-N (BE=398.1 eV) decreased while the content of pyrrolic-N (BE=400.6 eV) and graphitic-N (BE=402 eV) increased. This tendency for these three N species has previously been observed in case of carbonised PAN by Pels et al. [99]. The reasons behind these trends have been proposed to be that at higher temperatures (i) some of the pyridinic-N is converted to the graphitic-N and (ii) during the post-pyrolysis oxidation of the polymer char, part of the pyridinic-N is converted to pyridone-N. The latter one contributes to the XPS spectrum at very similar BE values (400.5 eV [99]) as pyrrolic-N [99]. Similar conversion of pyridinic-N to graphitic-N has been reported on N-doped carbon nanotubes in several papers together with the decrease in the content of pyridine-N-oxides (BE=405 eV) at elevated temperature [242, 243] as also observed herein. Furthermore, there was no detectable content of Co and Fe in the pyrolysed SAN-MWCNT based catalyst materials according to the XPS (inset to Fig. 36c) and SEM-EDX analysis (data not shown).

In case of SAN/PAN(/CNT) based materials (Fig. 37), the content of C, N and O for different pyrolysed materials (Table 10) seemed to be influenced by the carbonisation temperature rather than the application of stabilisation procedure or the fibre composition (Table 4). The content of C, N and O in case of catalysts pyrolysed at 800°C is very similar to the ones reported for different electrospun PAN based fibre materials carbonised at 800–900°C in several studies [69, 130].

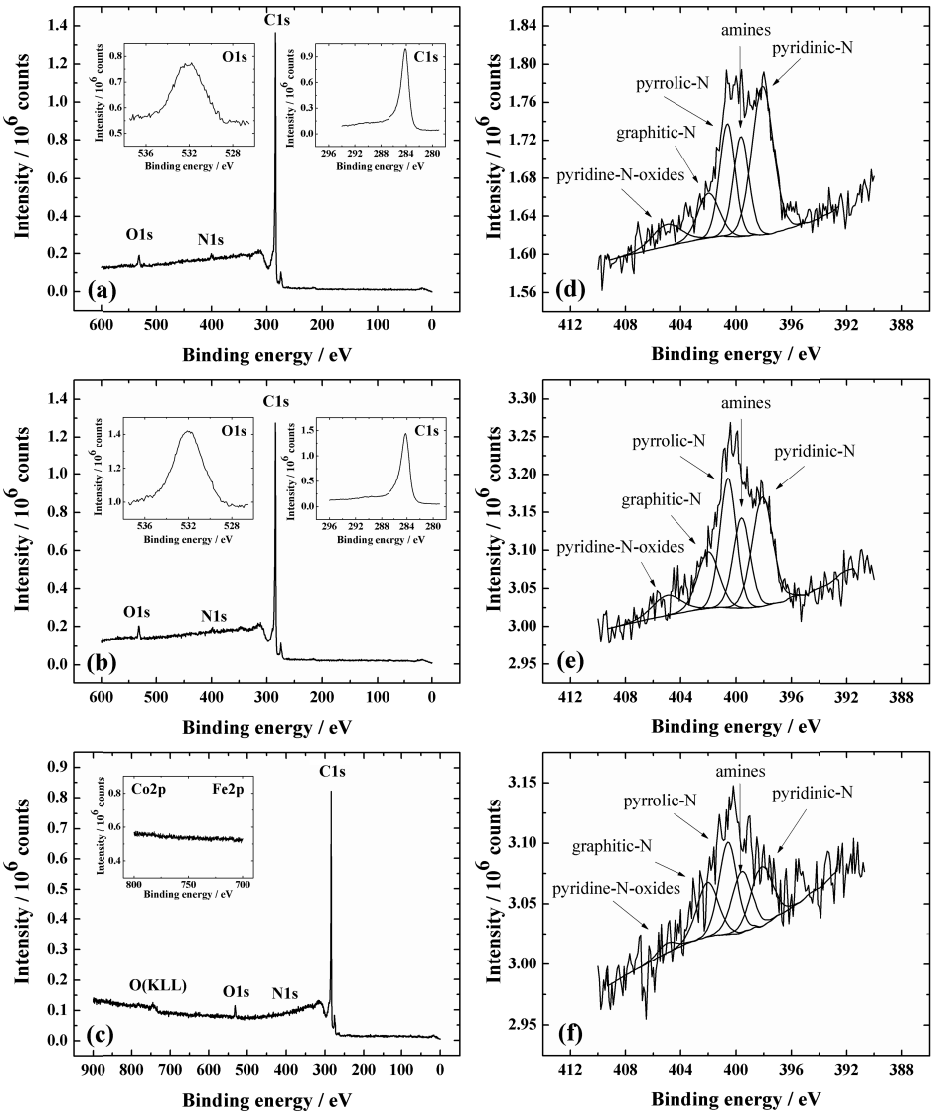

Fig. 36. (a−c) XPS survey spectra and **(d−f)** N1s spectra for SAN-MWCNT-700, SAN-MWCNT-800, and SAN-MWCNT-900 catalysts, respectively. The insets to Figs. a-c show high-resolution XPS spectra in the O1s, C1s, Fe2p and Co2p regions [IX].

The O content (*ca* 4 at%) is very similar among all the SAN/PAN(/CNT) based materials regardless of the used pyrolysis temperature (Table 10), while the C content is higher by *ca* 5 at% for the materials prepared at 1100 °C compared to the 800 °C ones. In compliance with the latter difference, the N content is *ca* 1.5 at% and 7 at% for the materials carbonised at 1100 °C and 800 °C, respectively.

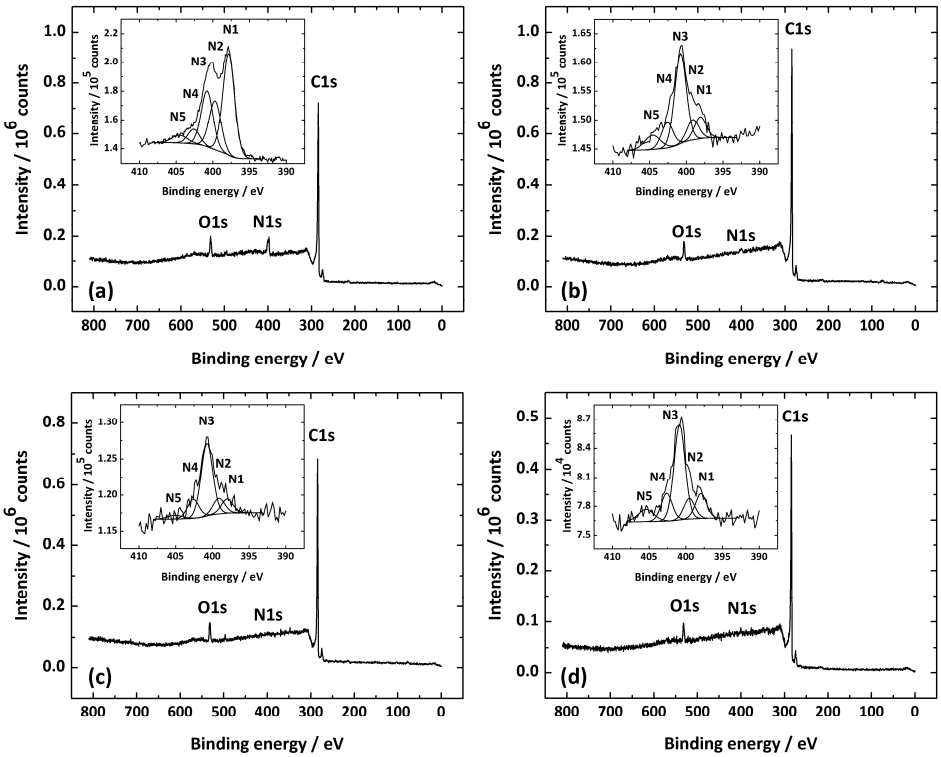

Fig. 37. XPS survey spectra of: **(a)** SAN/PAN/CNT-800, **(b)** SAN/PAN/CNT-1100, **(c)** SAN/PAN/CNT-250/1100 and **(d)** SAN/PAN-250/1100. The insets show high-resolution XPS spectra in the N1s region, which have been deconvoluted to different nitrogen species: **(N1)** pyridinic-N, **(N2)** amines, **(N3)** pyrrolic-N, **(N4)** graphitic-N and **(N5)** pyridine-N-oxides [X].

According to these observations, the increasing weight loss together with higher carbonisation temperatures (data presented in the Electronic supplementary material of the original paper [X]) could be due to the decomposition of N-containing functionalities. The N1s XPS spectra of SAN/PAN(/CNT) based catalyst materials (insets to Fig. 37) were also deconvoluted to 5 nitrogen species (Table 10). The N1s spectra with well distinguishable and intense pyridinic-N and pyrrolic-N peaks (N1 and N3, respectively, inset to Fig. 37a) are known to be inherent to CNFs prepared by carbonisation at 800–900°C from PAN electrospun fibres [71, 72, 117, 129, 130, 157, 238]. The outstanding difference among the SAN/PAN(/CNT) based catalysts is the noticeable decrease in pyridinic-N (N1) and amines (N2) for the materials pyrolysed at 1100 °C compared to the 800 °C ones (Table 10). Although, the amount of pyrrolic-N (N3) and graphitic-N (N4) is higher for the catalysts carbonised at higher temperature. Similar tendency was also observed in case of SAN-MWCNT based materials and the proposed explanations are probably also

applicable for SAN/PAN(/CNT) based catalyst materials. Furthermore, the XPS peak of amines (N2) could actually correspond to the cyano groups as they contribute at similar BE values [99, 134] and the existence of amines after high-temperature carbonisation is not likely [134].

Table 10. Elemental composition (at%) of different catalyst materials calculated from the XPS data. The relative content (%) of different nitrogen species has been determined from deconvoluted peaks of high-resolution N1s XPS spectra (the insets to Figs. 36 and 37): **(N1)** pyridinic-N, **(N2)** amines, **(N3)** pyrrolic-N, **(N4)** graphitic-N and **(N5)** pyridine-N-oxides [IX, X].

Catalyst material	C [at%]	O [at%]	N [at%]	N1 [%]	N2 [%]	N3 [%]	N4 [%]	N5 [%]
MWCNT	98.7	1.3	-	-	-	-	-	-
SAN-MWCNT-700	96.5	2.4	1.1	39	19	22	12	8
SAN-MWCNT-800	96.3	2.7	1.0	29	20	28	16	8
SAN-MWCNT-900	97.9	1.7	0.4	23	22	30	21	3
SAN/PAN/CNT-800	87.7	4.3	8.0	44.0	21.1	24.1	6.3	4.5
SAN/PAN/CNT-250/800	90.2	3.8	6.0	39.9	20.3	29.0	7.2	3.6
SAN/PAN-250/800	90.5	3.8	5.7	36.8	19.2	31.5	7.3	5.2
SAN/PAN/CNT-1100	95.0	3.6	1.4	12.4	11.5	51.1	14.2	10.8
SAN/PAN/CNT-250/1100	94.1	4.7	1.2	11.3	12.4	57.4	15.0	3.9
SAN/PAN-250/1100	94.6	3.6	1.8	13.5	11.1	51.0	15.0	9.4

The transition metal content in SAN/PAN(/CNT) based catalyst materials was verified by the SEM-EDX analysis. Contrary to SAN-MWCNT based materials, the low amounts of transition metals were found in case of the SAN/PAN/CNT based materials. The source of the metal impurities is most likely the MWCNT material as transition metals are used in the synthesis process of MWCNTs by CVD [241] and the MWCNTs are present in the catalyst materials (Table 4). In case of SAN/PAN/CNT-1100 catalyst, 0.02 at% of Co and 0.03 at% of Fe were detected [IX, X].

In Fig. 38, the XPS survey spectra of the studied PDC based materials are presented. The XPS spectra of the N-doped PDC materials (Figs. 38d–f) are otherwise similar to the ones of SAN-MWCNT and SAN/PAN(/CNT) based catalysts (Figs. 36 and 37, respectively), except the photoelectron peak of Si2p corresponding to Si was observed as expected for SiOC based PDC materials

[244]. The detection of nitrogen confirmed the successful N-doping of PDC based catalysts as was also observed in case of SAN-MWCNT based catalysts (Fig. 36). The content of different elements in the catalysts is presented in Table 11.

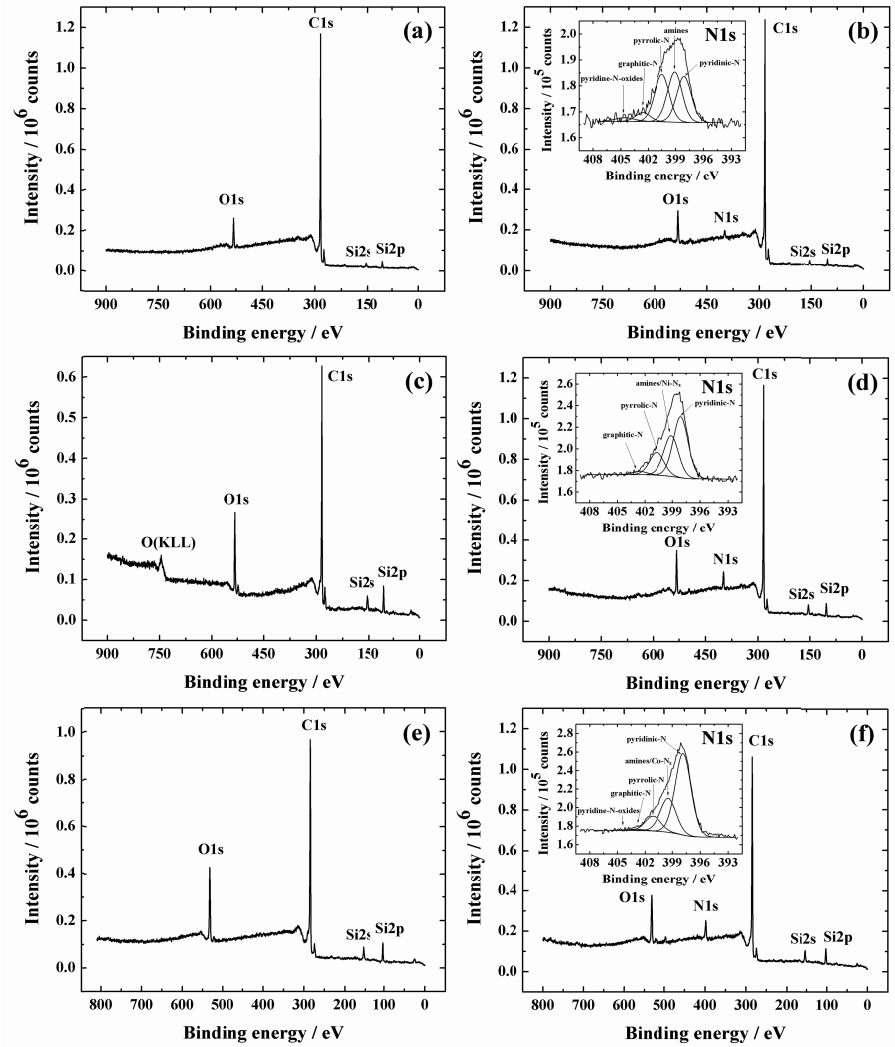

Fig. 38. XPS survey spectra of **(a)** PDC, **(b)** PDC-N, **(c)** PDC-Ni, **(d)** PDC-Ni-N, **(e)** PDC-Co, **(f)** PDC-Co-N catalysts. The insets to **(b, d, f)** show high-resolution XPS spectra in the N1s region [XI].

The intensity of the XPS photoelectron peaks for Co and Ni (Figs. 38c-f) is low and therefore rather difficult to distinguish from the background noise of the XPS spectra. This is a known phenomenon and has been also reported for carbon nanomaterial based ORR catalysts with low Co loading in several papers [128, 138, 147]. The presence of transition metals was additionally confirmed by the SEM-EDX and the content of corresponding transition metals (Ni or Co)

was found to be *ca* 0.3 at% in case of all transition metal modified catalysts similarly as in case of XPS (Table 11). The surface chemical composition of the PDC based catalysts is somewhat varying according to the XPS results: *ca* 3–9 at% Si, 7–13 at% O and 75–88 at% C. The presence of these elements is a result of the polysiloxanes conversion into ceramics and an additional use of carbon source.

Table 11. Elemental composition (at%) of catalyst materials calculated from the XPS data. Relative content (%) of different nitrogen species has been determined from deconvoluted peaks of high-resolution N1s XPS spectra (the insets to Figs. 38b, d and f): **(N1)** pyridinic-N, **(N2)** amines, **(N3)** pyrrolic-N, **(N4)** graphitic-N and **(N5)** pyridine-N-oxides [XI].

Catalyst material	C [at%]	O [at%]	N [at%]	Si [at%]	Ni [at%]	Co [at%]
PDC	88.6	8.1	-	3.3	-	-
PDC-Ni	79.3	11.2	-	9.3	0.2	-
PDC-Co	78.9	13.7	-	7.2	-	0.2
PDC-N	87.1	7.3	2.8	2.8	-	-
PDC-Ni-N	80.6	8.4	5.1	5.7	0.2	-
PDC-Co-N	75.7	10.2	7.0	6.9	-	0.2

Catalyst material	N1 [%]	N2 [%]	N3 [%]	N4 [%]	N5 [%]
PDC-N	29	32	30	6	3
PDC-Ni-N	48	32	18	3	-
PDC-Co-N	61	26	11	1	1

The majority of the C1s XPS peak of PDC-materials (Fig. 38) is attributed to the sp^2 carbon (284 eV) [244]. Low intensity C1s-signals from 286 to 289 eV most likely correspond to C–N or carbon oxygenated groups and the C1s XPS peak at 283 eV to the bonds of C–Si [244, 245]. In the O1s spectra a broad peak was registered at 533 eV indicating the existence of Si–O bonds and a smaller peak at 536 eV refers to the C-O bonds [246]. In the Si2p spectra, the XPS signals from 102 to 103 eV correspond to the Si–O–C bonds and Si–O bond [247]. These signals could be also masking the XPS signals of Si-C and Si-N bonds due to the high content of SiO_2 and SiOC in the Si2p XPS spectra. The high-resolution XPS spectra collected in the Co2p region for PDC-Co and PDC-Co-N catalysts are presented in Fig. 39. The outstanding difference between these two XPS spectra is the remarkably higher amount of Co registered at ca. 781 eV for PDC-Co-N catalyst compared to the PDC-Co material. The corresponding peak at ca. 781–782 eV is proposed to conform to the bonds in the Co-N_x center according to the literature [129, 143, 144, 147, 148]. This could refer to a considerable amount of Co coordinated to N in case of PDC-Co-N compared to the catalyst which was not doped with nitrogen (PDC-Co).

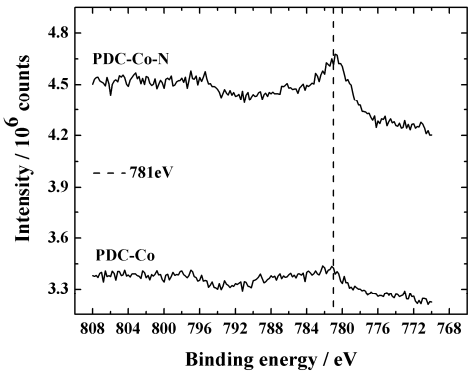

Fig. 39. XPS high resolution spectra in the Co2p region for PDC-Co and PDC-Co-N catalyst materials [XI].

The high resolution N1s XPS spectra of the N-doped PDC catalyst materials were also deconvoluted into different N species (the insets to Figs. 38b, d, f, Table 11). The content of pyridinic-N, amines and pyrrolic-N is very similar (*ca* 30%) in case of PDC-N material. Due to the possible disappearance of amine moieties during pyrolysis, the N1s peak of amines could be also assigned to the nitrile groups [134]. In addition, the N1s XPS peaks of pyridinic-N could also include the photoelectrons corresponding to the N-Si bond [248, 249]. The suppression of pyridine-N-oxide peak observed for transition metal (Co and Ni) and nitrogen codoped catalysts has been also previously noticed in our earlier study investigating carbon aerogel based catalysts [134]. If the PDC-N and PDC-Ni-N are compared, the higher amount of pyrrolic-N and lower amount of pyridinic-N is obtained for PDC-Ni-N. Analogous tendency has been previously observed in case of N-doped carbon and nickel nitride composite materials and this could be due to the conversion of the nitrogen species among each other during high temperature carbonisation [250]. The highest N content (7 at%) among the PDC materials is detected for PDC-Co-N catalyst (Table 11). This is in compliance with the literature as Co is proposed to act as a booster for increasing N content by creating more N groups that are electrocatalytically active towards the ORR [251]. Therefore, this could also explain the lower content of pyrrolic-N and higher content of pyridinic-N in PDC-Co-N compared to the PDC-Ni-N catalyst (Table 11). In the N1s region, the Co-N_x contributes to the XPS spectrum at very similar BE value (*ca* 399 eV) as pyridinic-N [148]. The presence of Co-N_x species [146, 148] was most likely also detected in the Co2p region (Fig. 39) [IX–XI].

7.3.2. ORR studies on composite material coated GC electrodes

7.3.2.1. ORR studies on SAN-MWCNT and SAN/PAN/CNT composite fibre based catalysts

The ORR on SAN-MWCNT and SAN/PAN/(CNT) based composite material coated GC electrodes was studied in O_2-saturated 0.1 M KOH. In Figs. 40a and b, comparative RDE voltammetry curves recorded at 1900 rpm for oxygen reduction on bare and different SAN-MWCNT catalyst coated GC electrodes are shown. The *I-E* curves presented in Fig. 40a correspond to the electrodes prepared with the catalyst ink made in 2-propanol (for MWCNTs it was DMF) and the ones in Fig. 40b correspond to the electrodes coated with the catalyst ink that contains 0.05% OH^- ionomer (Section 6.1.4). The values of E_{onset}, $E_{1/2}$ and the O_2 reduction current at −1.2 V derived from Figs. 40a and b are presented in Table 12. The electrode with the lowest ORR activity among the electrodes without the OH^- ionomer is GC/MWCNT (Fig. 40a). All pyrolysed SAN-MWCNT catalysts showed higher ORR performance (Fig. 40a and Table 12) in terms of E_{onset} values and O_2 reduction current than undoped MWCNTs. The highest ORR performance among the electrodes without the OH^- ionomer was registered in case of GC/SAN-MWCNT-800 electrode (Fig. 40a and Table 12). According to the obtained results, the functionalisation of MWCNTs with N during the carbonisation (Section 6.1.4 and 7.3.1.2) using SAN has positive effect on the ORR performance of the catalyst material.

In case of the OH^- ionomer containing catalyst coated electrodes, the SAN-MWCNT-700 possessed the lowest ORR activity (Fig. 40b and Table 12). The reduction current of the latter electrode was even lower than the one of pristine MWCNTs coated GC electrode (GC/MWCNT/I, Fig. 40b). The similar inhibiting effect in the presence of OH^- ionomer was also observed for the catalyst material carbonised at 800 °C (Fig. 40b). The ORR performance in case of catalysts pyrolysed at 900 and 1000 °C seems to be less influenced by the OH^- ionomer compared to the catalysts prepared at 700 and 800 °C. This could refer to the structure differences in the ORR active sites formed during pyrolysis at 900 °C or higher temperature. Furthermore, these sites formed at 900+ °C could be more susceptible for OH^- ionomer. Although, some decrease in the E_{onset}, $E_{1/2}$ and O_2 reduction current values was recorded also for 900 and 1000 °C materials most likely due to the diffusional resistance by the OH^- ionomer within the catalyst layer. Similar inhibition by the OH^- ionomer was also noticed and discussed in case of AQ-modified and unmodified nanomaterial coated GC electrodes in Section 7.1.6.1 (Fig. 14, Table 7). The GC/SAN-MWCNT-900/I electrode exhibits the highest ORR performance among the OH^- ionomer containing ink based electrodes with even lower E_{onset} and higher O_2 reduction current at −1.2 V than the best performing GC/MWCNT/AQ_S/I electrode from the Section 7.1.6.1 (Fig. 14, Table 7). This comparison is applicable as both of the catalyst materials contain the OH^- ionomer. The *n* values for different electrodes determined in the potential range from −0.4 to −1.2 V vs SCE are

presented in Figs. 40c and d. The *n* value is higher for all carbonised catalyst material compared to the MWCNT based electrodes. According to these results the SAN-MWCNT based catalysts are more suitable as ORR electrocatalysts for the fuel cell applications compared to the pristine MWCNTs.

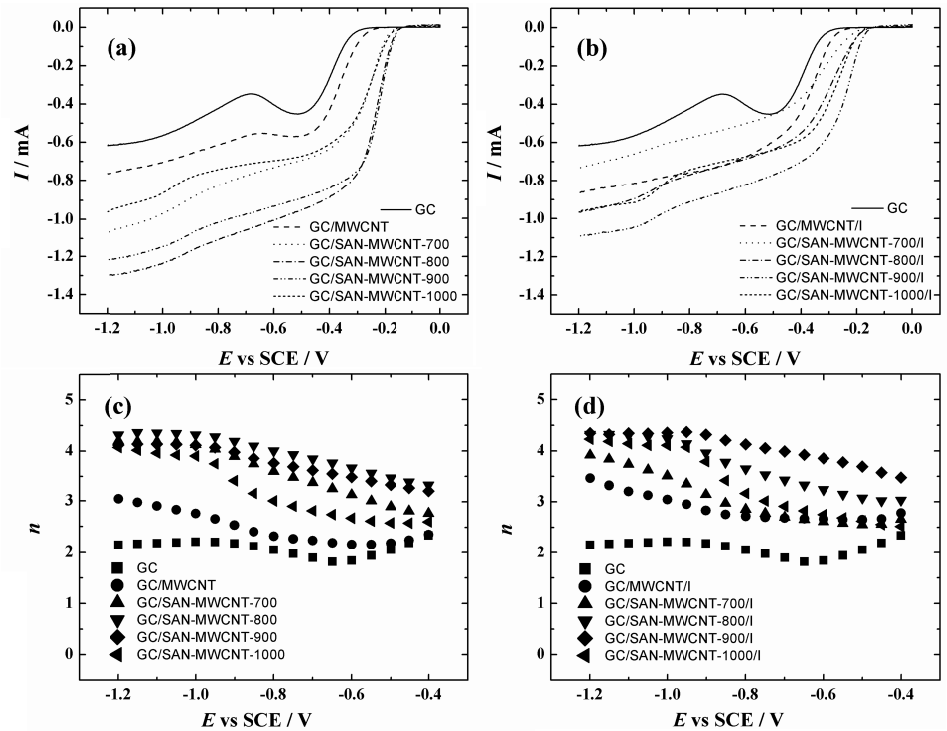

Fig. 40. (a, b) RDE voltammetry curves for oxygen reduction on bare and different catalyst material coated GC electrodes in O_2-saturated 0.1 M KOH (ω = 1900 rpm, v = 20 mV s^{-1}) and **(c, d)** the number of electrons transferred per O_2 molecule. The electrodes are coated with catalyst inks made in **(a, c)** 2-propanol and **(b, d)** 2-propanol containing 0.05% OH^- ionomer. The catalyst loading of 0.1 mg cm^{-2} was used [IX].

The comparative RDE voltammetry curves for oxygen reduction recorded at 1900 rpm on the non-stabilised SAN/PAN/CNT based catalyst coated GC electrodes are shown in Fig. 41a. The corresponding *I-E* curves for the stabilised SAN/PAN/CNT based catalysts showed a relatively similar tendency [X]. The values of E_{onset}, $E_{1/2}$ and the O_2 reduction current at −1.2 V derived from the RDE curves for all the studied electrodes are shown in Table 12. In case of stabilised and non-stabilised SAN/PAN/CNT based catalysts, the highest activity towards the ORR was observed for the catalysts prepared at 1100 °C (Figs. 41a, Table 12). In more specific, the SAN/PAN/CNT-1100 coated GC electrode showed higher ORR performance in terms of the E_{onset} of −0.13 V, $E_{1/2}$ of

−0.29 V and O_2 reduction current of −1 mA at −1.2 V. For the confirmation of the highest ORR activity compared to the other fibre materials (SAN/PAN and PAN/CNT, Table 4), the RDE voltammetry curves for SAN/PAN and PAN/CNT based catalysts carbonised at 1100 °C with or without prior stabilisation in air are shown in Fig. 41b (Table 12). In the literature, the preparation of the materials similar to PAN/CNT (CNFs carbonised from electrospun CNT and PAN composite fibres [114] and pyrolysed films made of PAN and CNT casted blends [252, 253]) have been reported and these materials have been studied for the application in supercapacitors [114, 252, 253].

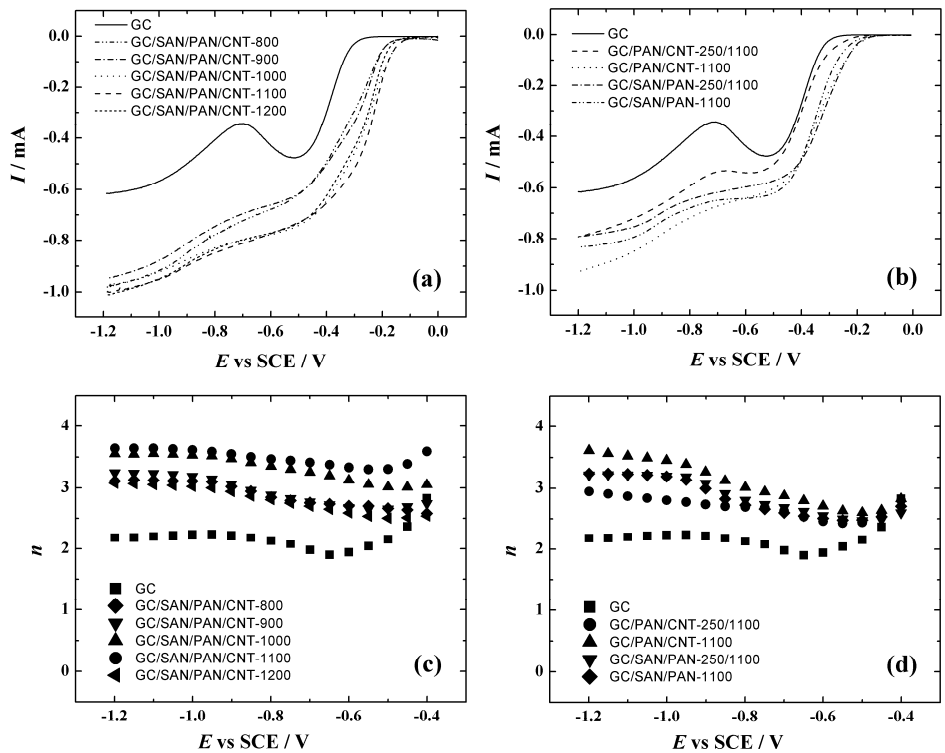

Fig. 41. (a, b) Rotating disc electrode voltammetry curves for O_2 reduction on bare and different catalyst material coated GC electrodes in O_2-saturated 0.1 M KOH (ω = 1900 rpm, v = 10 mV s^{-1}) and **(c, d)** electron transfer number (n) as a function of potential calculated from the K-L equation. The catalyst loading of 0.2 mg cm^{-2} was used [X].

No information was found regarding the use of corresponding materials as ORR electrocatalysts in the literature. Although, according to the results obtained herein, the electrocatalytic activity of SAN/PAN and PAN/CNT catalysts towards the ORR (Fig. 41b and Table 12) was lower than in case of SAN/PAN/CNT-1100 catalyst. These observations indicate the superiority of the latter

composite material for the application as an ORR electrocatalyst. The ORR on metal-free CNF (pyrolysed from PAN) catalysts is known to proceed via $2\times2e^-$ pathway involving the formation of HO_2^- as an intermediate according to the literature [71, 72]. Herein, the *n* values (Figs. 41c, d) between 2 and 4 were obtained for all the catalyst-coated GC electrodes supporting the proposed $2\times2e^-$ pathway. The obtained *n* values refer to the partial further reduction of HO_2^- to OH^-.

Table 12. The ORR onset potential (E_{onset}), half-wave potential ($E_{1/2}$) and O_2 reduction current at −1.2 V (*I*) for different electrodes in O_2-saturated in 0.1 M KOH. The data is derived from the RDE polarisation curves recorded at 1900 rpm and using v = 20 mV s^{-1} for SAN-MWCNT and MWCNT catalyst coated electrodes and v = 10 mV s^{-1} for all the other electrodes. All the potentials are given with respect to the SCE [IX, X].

Electrode designation	E_{onset} [V]	$E_{1/2}$ [V]	I [mA]
GC	−0.30	-	−0.61
GC/MWCNT	−0.28	−0.39	−0.76
GC/SAN-MWCNT-700	−0.20	−0.33	−1.07
GC/SAN-MWCNT-800	−0.17	−0.27	−1.30
GC/SAN-MWCNT-900	−0.17	−0.25	−1.22
GC/SAN-MWCNT-1000	−0.19	−0.31	−0.96
GC/MWCNT/I	−0.28	−0.40	−0.86
GC/SAN-MWCNT-700/I	−0.23	−0.40	−0.73
GC/SAN-MWCNT-800/I	−0.20	−0.36	−0.97
GC/SAN-MWCNT-900/I	**−0.18**	**−0.30**	**−1.09**
GC/SAN-MWCNT-1000/I	−0.20	−0.33	−0.96
GC/SAN/PAN-800	−0.26	−0.45	−0.95
GC/SAN/PAN-1100	−0.19	−0.37	−0.83
GC/SAN/PAN-250/800	−0.27	−0.43	−0.77
GC/SAN/PAN-250/1100	−0.17	−0.34	−0.79
GC/PAN/CNT-1100	−0.17	−0.38	−0.93
GC/PAN/CNT-250/1100	−0.23	−0.43	−0.79
GC/SAN/PAN/CNT-800	−0.16	−0.40	−0.98
GC/SAN/PAN/CNT-900	−0.17	−0.38	−0.95
GC/SAN/PAN/CNT-1000	−0.13	−0.32	−0.98
GC/SAN/PAN/CNT-1100	**−0.13**	**−0.29**	**−1.00**
GC/SAN/PAN/CNT-1200	−0.15	−0.34	−1.01
GC/SAN/PAN/CNT-250/800	−0.19	−0.43	−0.79
GC/SAN/PAN/CNT-250/900	−0.23	−0.44	−0.85
GC/SAN/PAN/CNT-250/1000	−0.20	−0.43	−0.88
GC/SAN/PAN/CNT-250/1100	−0.14	−0.31	−0.90
GC/SAN/PAN/CNT-250/1200	−0.16	−0.34	−0.90

The RDE polarisation curves at different rotation rates (ω=360−4600 rpm) for the most active catalyst coated GC electrodes (GC/SAN-MWCNT-900/I and GC/SAN/PAN/CNT-1100) prepared using the catalyst ink that contains binder (e.g. OH^- ionomer, Nafion®) are shown in Figs. 42a and b, respectively. It should be noted that different binders (OH^- ionomer vs Nafion®), potential sweep rates (20 vs 10 mV s^{-1}) and catalyst loadings (0.1 vs 0.2 mg cm^{-2}) were used in case of different electrodes. The lower E_{onset} was obtained in case of GC/SAN/PAN/CNT-1100 (Table 12), while the higher oxygen reduction currents were registered in case of GC/SAN-MWCNT-900/I up to 1900 rpm. The RDE voltammetry curves of both electrodes recorded at 3100 rpm exhibit very similar current values and when 4600 rpm is used, the GC/SAN/PAN/CNT-1100 shows better ORR performance than GC/SAN-MWCNT-900/I.

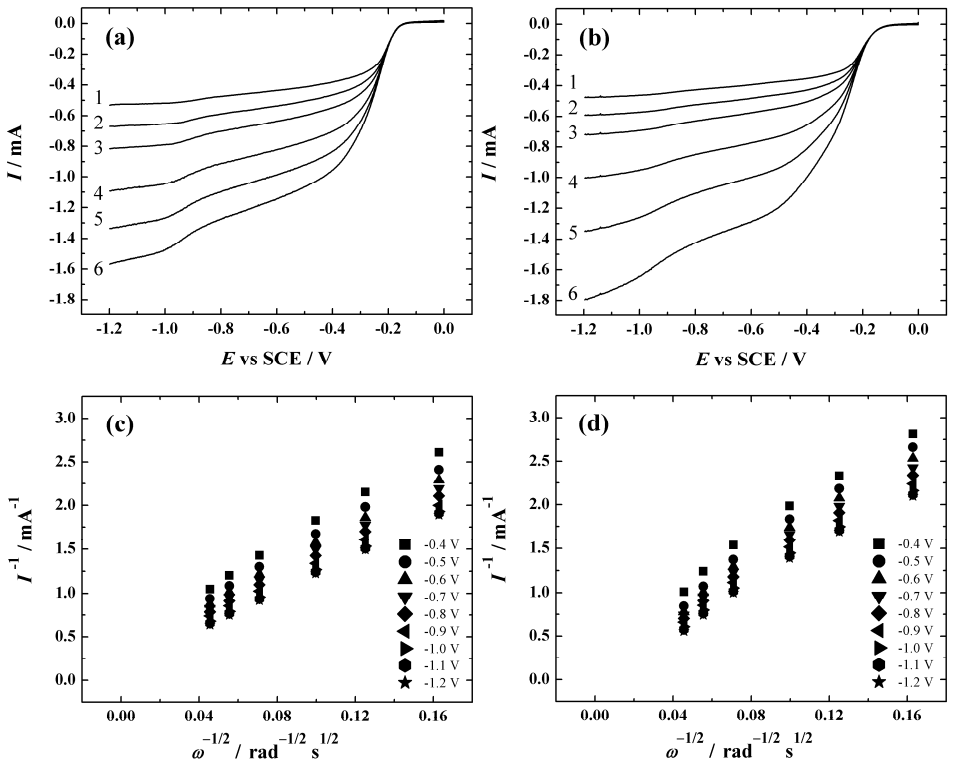

Fig. 42. RDE voltammetry curves for oxygen reduction on: **(a)** GC/SAN-MWCNT-900/I (v = 20 mV s^{-1}, catalyst loading 0.1 mg cm^{-2}) **(b)** GC/SAN/PAN/CNT-1100 (v = 10 mV s^{-1}, catalyst loading 0.2 mg cm^{-2}) recorded in O_2-saturated 0.1 M KOH at different rotation rates: (1) 360, (2) 610, (3) 960, (4) 1900, (5) 3100, (6) 4600 rpm. Koutecky-Levich plots for O_2 reduction: **(c)** GC/SAN-MWCNT-900/I and **(d)** GC/SAN/PAN/CNT-1100 derived from the RDE results of Figs. **(a)** and **(b)** [IX, X].

These differences could be explained by different binders, catalyst composition and catalyst loadings used. The K-L plots derived from the corresponding RDE polarisation data are presented in Figs. 42c and d. According to the intercepts on y-axis for the extrapolated K-L lines [24], the ORR process is under the mixed kinetic-diffusion control in the studied potential range in case of GC/SAN-MWCNT-900/I electrode as the extrapolated K-L lines pass the origin at positive values. At higher overpotentials (–1.1 to –1.2 V), the reduction of O_2 is diffusion-limited in case of GC/SAN/PAN/CNT-1100 electrode as indicated by the extrapolated K-L lines passing the origin [24].

In addition, the HO_2^- formation on the SAN-MWCNT based catalyst was studied in more detail by the RRDE method. The measurements were performed at 960 rpm with bare, SAN-MWCNT-800 and SAN-MWCNT-900 coated GC electrode. The recorded I_D and I_R are presented in Figs. 43a and b, respectively. The value of Φ was calculated using the equations (11) from Section 7.1.6.2 and the value of n was calculated according to the following equation:

$$n = \frac{4I_D}{I_D + I_R / N} \tag{14}$$

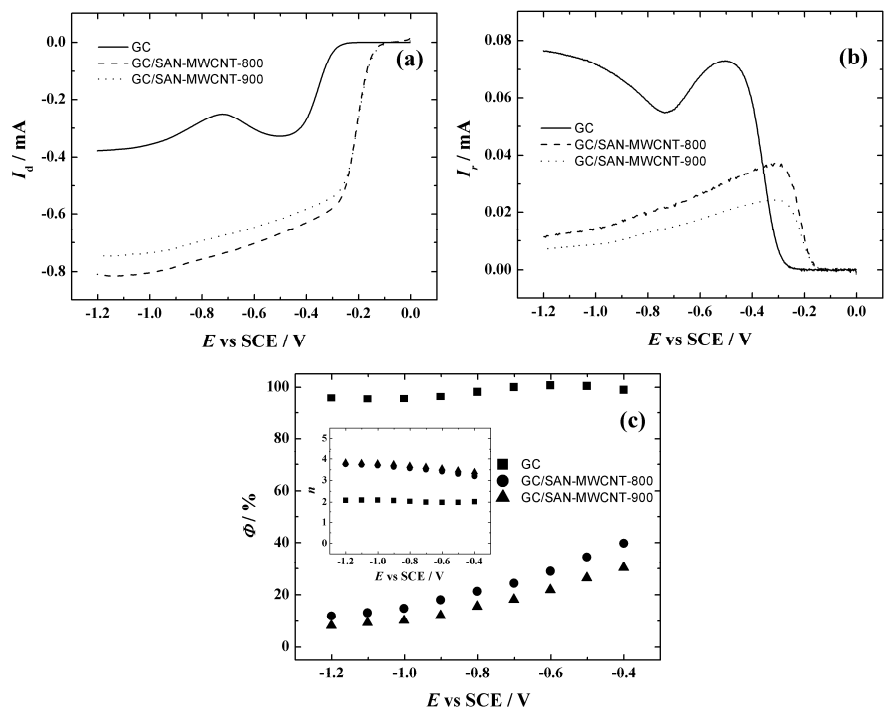

Fig. 43. (a) Disc current, **(b)** ring current and **(c)** dependence of the yield of peroxide formation (Φ) for oxygen reduction on bare, SAN-MWCNT-800 and SAN-MWCNT-900 catalyst coated GC disc and Pt ring electrode in O_2-saturated 0.1 M KOH (ω = 960 rpm, v = 20 mV s^{-1}). The inset to Fig. **(c)** presents the potential dependence of n [IX].

The dependences of Φ and n on the applied potential are shown in Fig. 43c and the inset to Fig. 43c, respectively. The ORR on bare GC proceeds via 2-electron pathway resulting in the production of HO_2^- in the studied potential range as also known from the literature [14, 254]. This result confirms the adequate detection of the HO_2^- on the Pt-ring. In case of the catalysts coated GC electrodes (SAN-MWCNT-800 or SAN-MWCNT-900), the value of Φ was around 10% at −1.2 V. This refers to the formation of a small amount of peroxide and the majority (*ca* 90%) of oxygen is reduced directly into water via four-electron pathway. The value of n (close to 4 at −1.2 V) is in accordance with the latter.

For a practical use of the catalyst material in a composition of the fuel cell cathode, the assessment of the stability of the catalyst is necessary. The stability testing was carried out with three most active ORR catalyst coated electrodes in O_2-saturated 0.1 M KOH according to the same procedure as used for GC/EG-AQ-1 electrode (Fig. 17a) in Section 7.1.6.1. The obtained results are presented in Fig. 44a, b and c for GC/SAN-MWCNT-800, GC/SAN-MWCNT-900 and GC/SAN/PAN/CNT-1100 electrode, respectively. After 1000th potential cycle, the E_{onset} value did not noticeably change, while the ORR current at −1.2 V decreased by 5–7 % compared to the initial value for all three electrodes. Similar behaviour during the stability testing was observed in case of AQ modified GR coated GC electrodes (Fig. 17, in Section 7.1.6.1) and N-doped carbide-derived carbon coated electrode in previous work by our workgroup [56]. The stability testing results reported for N-doped pyrolysed electrospun PAN based catalyst materials in the literature [67, 120] are very similar to the ones obtained with GC/SAN/PAN/CNT-1100 electrode (Fig. 44c).

Next, the reasons behind the ORR activity of the SAN/PAN/CNT-1100, SAN-MWCNT-800 and SAN-MWCNT-900 catalysts with the highest ORR performance will be discussed. The exact reason for the enhanced ORR activity of these catalysts is not known yet, but different properties and influence of the precursor materials have to be considered. One possible reason for the higher ORR performance of the catalysts could be the presence of the N species on the surface of the catalysts as detected by XPS (Section 7.3.1.2). This is supported by Borghei et al. study [110] in which a high ORR activity was observed for the few-walled carbon nanotubes (FWCNTs) containing as low as 0.56 at% of nitrogen. In case of SAN-MWCNT based catalysts, no clear correlation between the increased ORR electrocatalytic activity and relative concentration of specific N moieties was noticed (Tables 10 and 12). However, there is no agreement which specific N-functionality is responsible for the ORR activity. Mainly the pyridinic-N is considered to be advantageous for ORR applications [62, 112]. Although, several studies have found that the ORR performance is related to the amount of pyrrolic-N [60, 66, 73, 102, 104] or to the synergy of different N-species (e.g. co-existence of pyridinic-N and quaternary-N [56]) [67, 69, 103, 107, 118, 255]. Interestingly, in case of SAN/PAN/CNT-1100, pyrrolic-N (N3) and graphitic-N (N4) could be responsible for the enhanced ORR activity as a higher amount of these nitrogen species were detected by XPS (Tables 10 and

12). Also, for the high ORR activity of SAN/PAN/CNT-1100 catalyst, the porous structure (Fig. 34) and high number of defects in the carbon structure should be considered. The latter was evidenced by the I_D/I_G ratio of 2.93 from Raman spectroscopy results (presented in the original paper [X]). For comparison, the EG material with low amount of defects showed the I_D/I_G ratio of 0.1 (Section 7.1.4.1). According to the XPS data, the oxygen content was higher in all pyrolysed catalyst material coated electrodes compared to the pristine MWCNTs coated electrode (Table 10).

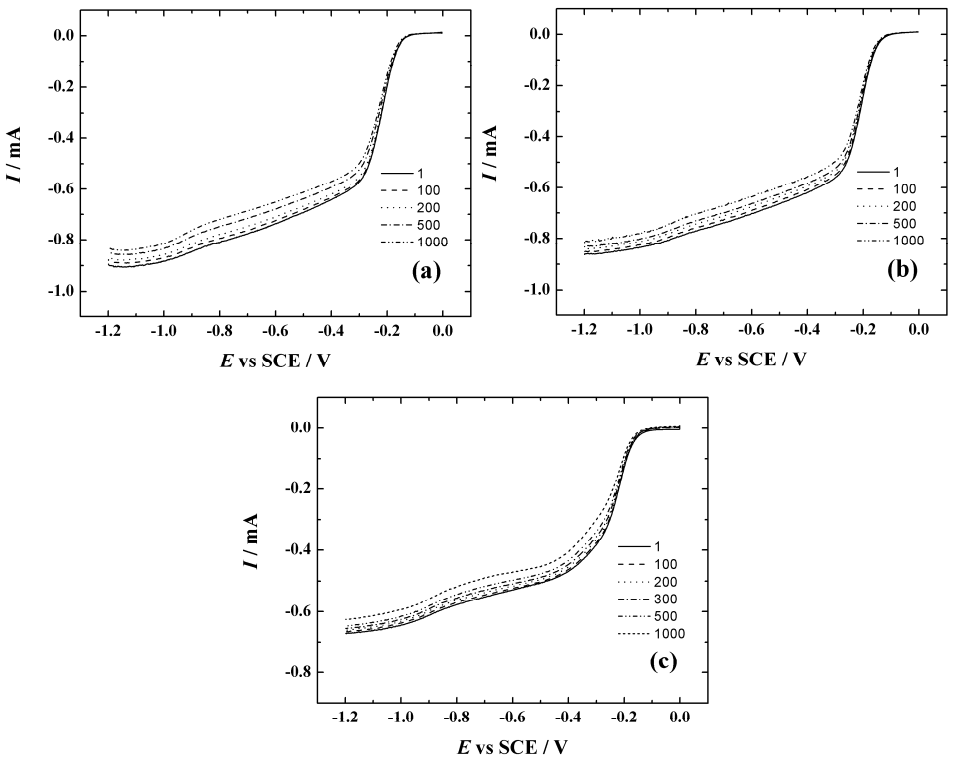

Fig. 44. Stability testing of: **(a)** GC/SAN-MWCNT-800 (v = 20 mV s^{-1}), **(b)** GC/SAN-MWCNT-900 (v = 20 mV s^{-1}) and **(c)** GC/SAN/PAN/CNT-1100 (v = 10 mV s^{-1}) electrodes in O_2-saturated 0.1 M KOH. The RDE voltammetry curves (ω = 960 rpm) were recorded after 1st, 100th, 200th, 300th, 500th and 1000th potential cycle [IX, X].

Therefore, the greater O1s signal in the XPS spectra could refer to the larger amount of quinone moieties in the catalyst material [I] [11, 207]. Quinones are known to catalyse the ORR process favouring the peroxide production (Section 4.1) [V] [60, 256]. Also, the incorporation of MWCNTs themselves into the composition of the catalyst material is known to be beneficial for the ORR performance according to our previous studies [57, 58, 138, 206]. The rise in

the ORR activity due to the very low amounts of transition metals originating from the MWCNTs (Section 7.3.1.2) could be rather excluded as the pristine MWCNTs coated electrodes exhibited relatively poor ORR performance compared to the pyrolysed catalyst materials (Table 12). In addition, the importance of the optimisation of the amount of binder (e.g. OH^- ionomer, Nafion®) in the catalyst ink is crucial in the aspect of higher ORR performance as it was experimentally investigated and ascertained [X]. In conclusion, the origin for the ORR activity of the catalysts in the present work could be linked to several different sources described in this section. All of them and their synergy could play an important role in the overall electrocatalytic activity towards the ORR of the catalyst materials presented herein [IX, X].

7.3.2.2. ORR studies on PDC catalyst materials

Prior to this work, there was no information about the application of SiOC based PDC materials as ORR electrocatalysts. Therefore, the ORR studies on the PDC-based catalysts were carried out in 0.1 M KOH (pH = 13) and 0.1 M PBS containing 0.1 M $NaClO_4$ (pH = 7) solution. The latter medium was used for the further possible application of the best performing PDC material as a cathode catalyst in the microbial fuel cell (MFC) [XI].

In Figs. 45a and b, the RDE polarisation curves for O_2 reduction on bare and different PDC catalyst coated GC electrodes recorded at 1900 rpm in solutions with different pH values (pH = 13 and 7, respectively) are presented. In addition, the RDE voltammetry curves obtained with commercial Pt/C catalyst are included for comparison purposes. The various parameters (E_{onset}, $E_{1/2}$ and O_2 reduction current density at −1.2 V) are presented in Table 13. According to the obtained results, the commercial Pt/C catalyst appears to be superior compared to all of the other catalysts studied herein. In contrast, the pristine PDC material exhibited the lowest activity towards the ORR, which could be explained by the absence of transition metal centres and/or nitrogen groups (Fig. 38a), which could provide high ORR activity. After the carbonisation of the material in the presence of nitrogen precursor (DCDA), the improvement in the value of E_{onset} and O_2 reduction current are observed (Fig. 45) due to the presence of N-containing groups (Fig. 38b). A similar tendency has been noticed in previous studies by our workgroup with different carbon-based catalysts after the pyrolysis with DCDA [55, 56, 257]. In case of both metal doped catalyst coated electrodes (GC/PDC-Ni and GC/PDC-Co), higher ORR activity is observed compared to the GC/PDC electrode referring to the known positive effect of the transition metal inclusion towards the ORR performance [258]. Furthermore, the PDC-Co catalyst shows better ORR activity than the PDC-Ni. Similar results have been reported by Abdelwahab et al. for Co- and Ni-doped carbon aerogels [259]. After carbonisation of PDC-Ni catalyst together with DCDA, the resulting material coated GC electrode (GC/PDC-Ni-N) exhibits similar ORR performance to that of GC/PDC-N electrode. Meanwhile, the ORR

activity of PDC-Ni-N is much lower compared to the PDC-Co-N catalyst. These observations indicate that the ORR activity of Ni-N_x present in the catalyst is lower than that of its Co-N_x counterpart or Ni does not form as many metal coordinated centres (Me-N_x) during high-temperature carbonisation. Similar information has been reported in the work by Liu et al. [260], where the influence of different metal dopants was evaluated in N-doped carbon xerogels. In the latter work, the value of E_{onset} in acidic solution for the Ni-doped and metal-free N-functionalised catalyst coated electrode was very similar, while the Co-doped counterpart showed significantly higher electrocatalytic activity towards the ORR [260]. The order of the ORR activity of the catalysts was similar in case of both studied solutions (pH = 13 and 7, Figs. 45a and b, respectively), although superior ORR performance was observed in alkaline media for all the catalysts. This could be attributed to the change in the ORR active sites and their interaction with O_2 molecule. This is supported by Wan et al. work [261], where the effect of pH was investigated on N-doped ordered mesoporous carbon.

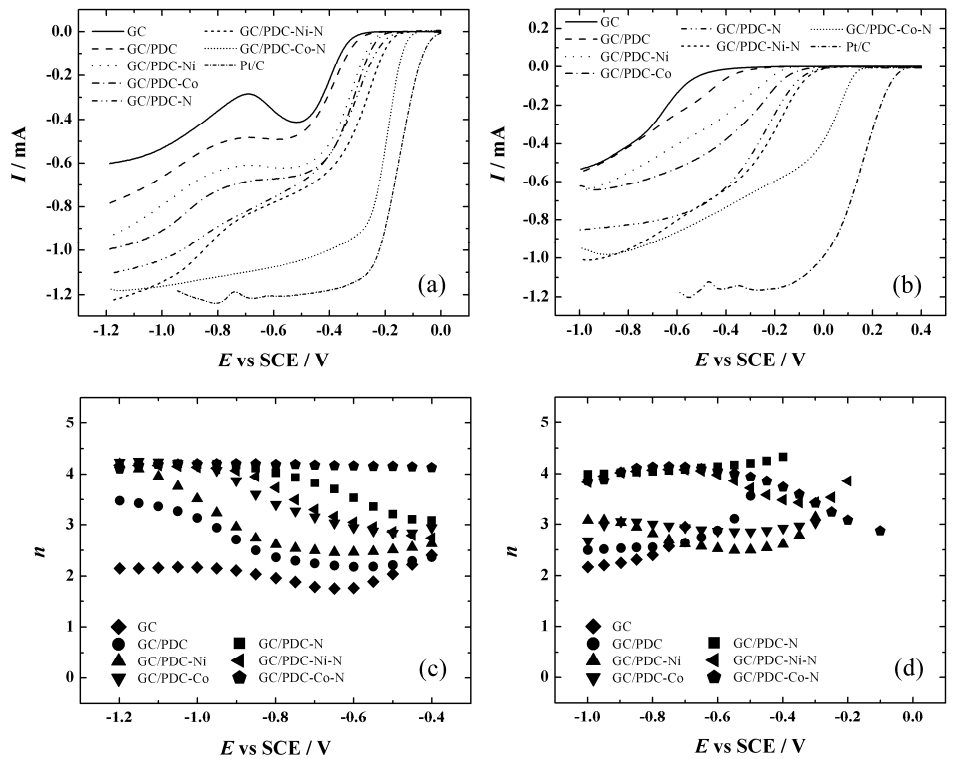

Fig. 45. RDE voltammetry curves for O_2 reduction on different electrodes in O_2-saturated **(a)** 0.1 M KOH and **(b)** 0.1 M PBS containing 0.1 M $NaClO_4$ (ω = 1900 rpm, v = 10 mV s^{-1}). **(c, d)** The potential dependence of n calculated using the K-L equation from the corresponding RDE data [XI].

Table 13. The ORR onset potential (E_{onset}), half-wave potential ($E_{1/2}$) and O_2 reduction current at −1.2 V (I) for different electrodes in O_2-saturated aqueous solutions. The data was derived from the RDE polarisation curves (ω = 1900 rpm and v = 10 mV s^{-1}) presented in Figs. 45a ([a]Data obtained in 0.1 M KOH) and b ([b]Data obtained in 0.1 M PBS containing 0.1 M $NaClO_4$) [XI].

Electrode designation	E_{onset}[a] [V]	$E_{1/2}$[a] [V]	I[a] [mA]	E_{onset}[b] [V]
GC	−0.30	-	−0.61	−0.43
GC/PDC	−0.28	−0.45	−0.78	−0.31
GC/PDC-Ni	−0.23	−0.38	−0.93	−0.17
GC/PDC-Co	−0.21	−0.37	−1.00	−0.10
GC/PDC-N	−0.18	−0.40	−1.11	−0.03
GC/PDC-Ni-N	−0.16	−0.39	−1.23	−0.02
GC/PDC-Co-N	**−0.11**	**−0.21**	**−1.17**	**0.14**
Pt/C	−0.02	−0.15	-	0.32

For the evaluation of the n value, the equation (10) from Section 7.1.6.1 was used and the results obtained in the solution of pH = 13 are presented in Fig. 45c. In case of pH = 7 solution, the equation (10) was used with a new value of O_2 diffusion coefficient (D_{O2}= 1.8×10^{-5} cm^2 s^{-1} [52, 54]) and the obtained results are shown in Fig. 45d. All the electrodes, except GC/PDC-Co-N show the value of n between 2 and 4 in the studied potential ranges indicating the partial production of peroxide. The GC/PDC-Co-N electrode showed the n value being 4 in the studied potential range in 0.1 M KOH. This is an expected result due to the presence of the Co–N_x centres (Section 7.3.1.2, Fig. 39), which is reported to be highly active for the 4-electron reduction of O_2 [146]. According to these results, the GC/PDC-Co-N is best performing ORR electrocatalyst among the PDC materials studied herein.

Since the GC/PDC-Co-N electrode showed the highest activity towards the ORR among all PDC based catalysts, the following discussion is mainly focused on the PDC-Co-N catalyst. In Fig. 46, the RDE voltammetry curves for O_2 reduction in 0.1 M KOH at different ω values and the K-L plots derived from the corresponding RDE data on the GC/PDC-Co-N electrode are presented. The diffusion limited O_2 reduction is obtained at relatively low overpotentials as the K-L lines coincide from ca. –0.6 V and the extrapolated K-L lines pass the origin. For the possible application of PDC-Co-N as a fuel cell cathode catalyst, the stability of the catalyst was tested as follows: the accelerated aging test was performed by CV method and the potential of the catalyst coated electrode was cycled for 10 000 times between –0.4 V and 0 V in Ar-saturated 0.1 M KOH. The experiment was performed with GC/PDC-Co-N and Pt/C electrodes and the RDE polarisation curves recorded in O_2-saturated 0.1 M KOH before and after 10 000 CV cycles are shown in Fig. 47. The $E_{1/2}$ was about 34 mV more negative and current value at –0.95 V decreased by 6% after the potential cycling in case of Pt/C electrode.

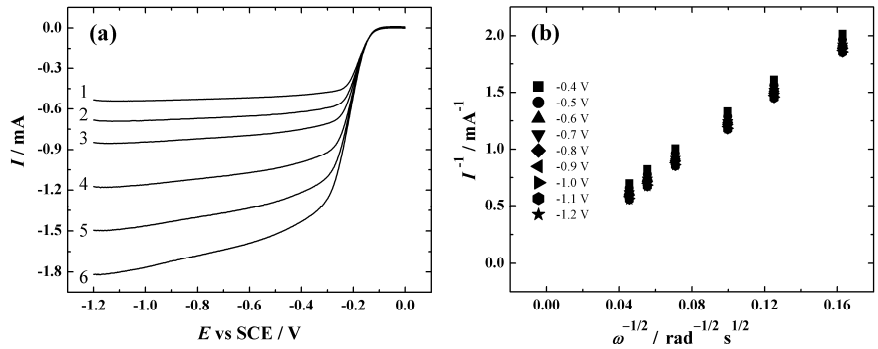

Fig. 46. (a) RDE voltammetry curves for oxygen reduction on a GC/PDC-Co-N electrode in O_2-saturated 0.1 M KOH (*ω*= *1*-360; *2*-610; *3*-960; *4*-1900; *5*-3100; *6*-4600 rpm, v = 10 mV s^{-1}), **(b)** Koutecky-Levich plots for O_2 reduction in 0.1 M KOH derived from the RDE data shown in Fig. 46a [XI].

In contrast, the corresponding values for GC/PDC-Co-N were 4 mV and less than 1%, respectively. The obtained results imply that the durability of the PDC-Co-N catalyst is higher compared to the commercial Pt/C catalyst.

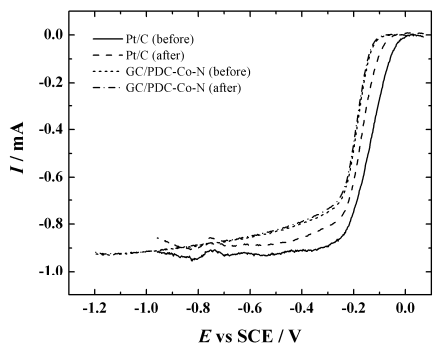

Fig. 47. RDE voltammetry curves for oxygen reduction on GC/PDC-Co-N and Pt/C catalysts in O_2-saturated 0.1 M KOH recorded before and after 10 000 cycles between –0.4 and 0 V vs SCE in Ar-saturated 0.1 M KOH. ω = 960 rpm, ν = 10 mV s^{-1} [XI].

Many papers have been reported about the ORR studies describing the Co-containing carbon-based catalysts doped with nitrogen via pyrolysis. Here only a brief comparison is given. More thorough comparison of the ORR performance with similar catalysts reported in the literature can be found in the Electronic supplementary information of the original article [XI]. In the present work, the E_{onset} of −0.11 V and $E_{1/2}$ of −0.21 V were determined for the GC/PDC-Co-N electrode in 0.1 M KOH at 1900 rpm (Table 13). These values are more positive than the ones obtained for GC/SAN-MWCNT-900/I and

GC/SAN/PAN/CNT-1100 electrodes (Table 12) in section 7.3.2.1 indicating the PDC-Co-N being the best performing NPM catalyst among the catalysts studied in the present thesis. For comparison, several more negative E_{onset} values have been reported for Co and N-containing catalysts in alkaline medium [126, 147]. However, very similar E_{onset} and $E_{1/2}$ values have been obtained in case of Co-containing nitrogen-doped carbon aerogels [134]. In addition, more positive E_{onset} values can be found in several studies [142, 144, 146, 148], and the highest value has been achieved for the cobalt nanocrystals grown through the N-doped graphene nanoparticles (0.05 V) [132]. In neutral conditions (pH = 7), the E_{onset} values of −0.07 V and −0.1 V have been obtained for NiCo-doped C-N nanocomposite in 0.5 M KNO_3 solution [107] and for square-like nano cobalt oxide anchored on N-doped graphene catalyst in PBS [131], respectively. It should be noted that the latter catalyst was further applied in the MFC [131]. In case of the GC/PDC-Co-N electrode, significantly more positive value of 0.14 V (Table 13, Figs. 45b) was obtained, which makes the PDC-Co-N catalyst attractive for the use in MFC conditions. For comparison, in section 7.2.5.4 the ORR was also studied on polycrystalline Cu electrode in the pH = 7 solution (E_{onset} = −0.38, Fig 33a). The ORR activity of GC/PDC-Co-N is also significantly higher compared to the polycrystalline Cu electrode.

The main reason behind the electrocatalytic activity of the PDC-Co-N catalyst is probably the presence of highly active Co-N_x functionalities [124, 134, 144, 146–148] which was confirmed by the XPS data (Section 7.3.1.2, Fig. 39). However, in the surface composition of the PDC-Co-N, a significantly higher amount of metal-free N functionalities compared to Co was detected according to the XPS studies (Table 11). In the literature describing the Co-containing carbon-based ORR catalysts functionalised with nitrogen via carbonisation with DCDA or other N precursors, one of the most active metal-free N species for oxygen reduction is reported to be pyridinic-N [131, 134, 146, 148, 251]. The reason behind the high ORR activity of the pyridinic-N is attributed to its N atom bonded with two C atoms that provides a basic lone electron pair of N atom. Due to a lone electron pair it is claimed that pyridinic-N can increase the electron-donating ability to promote ORR via 2×2e^- or direct 4e^- process [262–264]. In addition, the importance of pyridinic-N for promoting the ORR has also been emphasised regarding the application as MFC catalyst [131, 140, 265]. In case of PDC catalyst materials, the highest content of total nitrogen together with the highest relative content of the pyridinic-N (Table 11) was registered for PDC-Co-N. In addition to N, it is proposed that Si could improve the ORR activity due to changes in the charge distribution in the carbon lattice [266, 267]. Also, the high surface area confirmed by N_2 adsorption and CV experiments (the data is found in the original article [XI]) of the catalyst should be considered for enhanced ORR performance [140, 144]. Considering all these findings, the PDC-Co-N material is the most active ORR electrocatalyst reported among the NPM catalysts in the present thesis (Tables 7, 12, 13) and therefore should be further used in (microbial) fuel cell applications [XI].

8. SUMMARY

The first part of the thesis described the modification of carbon electrodes with different aryl films followed by physical and electrochemical characterisation of the prepared electrodes [I–VI]. The functionalisation of MWCNTs and graphene with AQ films were carried out spontaneously and via "normal" electrografting by the reduction of aryldiazonium salts method [I, II]. The GR prepared by CVD and GC electrodes were modified with NP and AQ films, respectively, using the RG method [III, V]. The CVD-grown GR was also derivatised using the "normal" electrografting method [III]. In addition, the GC electrodes were grafted with MAQ moieties using different electrografting procedure [IV]. Finally, the GC electrodes were electrografted with AQ by RG and RDE combined method [VI]. According to the XPS analysis, the presence of azo linkages within the electrografted multilayer aryl film was detected in case of several AQ and NP film modified electrodes [II, III, V]. The thickness of the electrografted NP films on the CVD-grown GR electrodes was measured to be from 5 to 30 nm depending on the electrografting procedure [III].

The amount of electroactive redox species in the aryl film-modified electrodes was determined electrochemically by CV. The highest Γ_{AQ} value of 35.1 nmol cm^{-2} for AQ modified nanomaterial based electrode was calculated in case of commercially available GR electrografted with AQ moieties (GC/GR/AQ_E,) [II]. The highest Γ_{AQ} value of 18 nmol cm^{-2} for electrografted GC electrode was obtained if the RG and RDE combined method was employed for electrochemical modification (GC/AQ-10) [VI]. Also, it was found that on the GC electrode the electrografted MAQ films were less than a monolayer compared to the multilayer AQ films obtained via reduction of aryldiazonium salts [IV–VI]. The surface blocking behaviour of the AQ films prepared by RG and RDE method on GC electrodes towards the $Fe(CN)_6^{3-/4-}$ redox probe was also studied. The response of the $Fe(CN)_6^{3-/4-}$ redox probe was strongly suppressed [VI].

The ORR was studied on AQ grafted and unmodified nanomaterial coated GC electrodes [I, II]. The highest electrocatalytic activity towards the ORR was observed in case of spontaneously modified MWCNTs and OH^- ionomer coated GC electrode (GC/MWCNT/AQ_S/I) [II]. The ORR was also investigated on GC electrodes electrografted with AQ and MAQ groups [IV, V]. The amount of electroactive redox species in the aryl film had no remarkable influence on the ORR performance in case of both, AQ and MAQ films [IV, V]. Stronger suppression of the oxygen reduction rate on the native GC surface sites was observed due to thicker AQ film compared to the thinner MAQ film [IV, V]. The inhibiting effect of OH^- ionomer on the ORR rate was observed when the RDE polarisation curves of the electrodes with and without OH^- ionomer were compared [I, II].

The second part of the thesis described the modification of Ni, Au and Cu electrodes with aryl films and characterisation of the prepared electrodes. The

modification of the electrodes was successful according to the XPS and AFM results verifying the presence of the aryl film on the electrodes. The aryl films of NP and AQ with the thickness up to 47 nm (Cu-NP-RDE-1.5) were prepared. The RG method was found to be beneficial for obtaining thicker NP film on Ni electrode compared to the "normal electrografting" [VII]. The RG and RDE combined method was more efficient for preparing thicker films on Cu and Au electrodes compared to the RG method [VI, VIII]. By using the latter method, the highest known Γ_{AQ} values of 12 nmol cm^{-2} and 21 nmol cm^{-2} for Cu-AQ-RDE-1.5 and Au/AQ-10 electrodes, respectively, were obtained [VI, VIII]. The surface blocking of Ni electrode towards the $Fe(CN)_6^{3-}$ reduction was more efficient in case of redox grafted NP film compared to the NP film prepared by "normal electrografting" [VII]. The $Fe(CN)_6^{3-}$ reduction on the Au electrode was most suppressed in case of the AQ film prepared by RG and RDE combined method (Au/AQ-10) [VI]. In case of Cu, the response of $Fe(CN)_6^{3-/4-}$ redox probe was completely suppressed in case of redox grafted NP film and the AQ film prepared by RG and RDE combined method [VIII]. The blocking of the ORR on the aryl film modified Au and Cu electrodes was not as sufficient as the blocking behaviour towards the ferricyanide reduction [VI, VIII]. In case of aryl film modified Cu electrodes, the suppression of ORR current did depend on the used electrografting conditions.

In the third part of the thesis the electrocatalysts prepared from the composite materials of SAN-MWCNT, SAN/PAN/CNT and PDC were studied towards the ORR [IX-XI]. In case of the SAN-MWCNT catalysts, the MWCNTs were successfully doped with N during the pyrolysis according to the XPS studies. The SAN-MWCNT carbonised at 800–900 °C appeared to be highly active catalyst material towards the ORR. The inhibiting effect of OH^- ionomer on the ORR current was also observed for SAN-MWCNT catalysts [IX]. In case of SAN/PAN/CNT materials, the CNF catalyst with highest ORR performance was obtained when the composite was pyrolysed at 1100 °C. The SAN/PAN/CNT catalysts also consisted of O, C and N as the SAN-MWCNT materials according to the XPS results [X]. Lastly, the transition metal containing and pristine PDC materials were studied as ORR catalysts. Different PDC materials were additionally functionalised with N via pyrolysis using the DCDA as nitrogen precursor at 800 °C. The catalyst with the highest activity towards the ORR was obtained in case of Co and N codoped PDC material exhibiting the E_{onset} of −0.11 V vs SCE and the ORR proceeded via 4-electron pathway. The PDC catalysts were also studied in neutral solution (pH = 7) for the possible further application of the best performing material as a cathode catalyst in MFC. In addition to N, O and C the PDC materials also contained Si according to the XPS studies [XI]. The high ORR performance of the Co and N codoped PDC catalyst was attributed to the introduction of N-functionalities and transition metal into the material during the pyrolysis [XI].

9. REFERENCES

[1] A. Berisha, M.M. Chehimi, J. Pinson, F.I. Podvorica, Electrode surface modification using diazonium salts, in: A.J. Bard, C.G. Zoski (Eds.), Electroanalytical Chemistry: A Series of Advances, Vol. 26, CRC Press, Boca Raton, 2015, pp. 115–223.

[2] M.M. Chehimi (Ed.), Aryl Diazonium Salts: New Coupling Agents and Surface Science, Wiley, Weinheim, 2012.

[3] M. Weissmann, O. Crosnier, T. Brousse, D. Bélanger, Electrochemical study of anthraquinone groups, grafted by the diazonium chemistry, in different aqueous media-relevance for the development of aqueous hybrid electrochemical capacitor, Electrochimica Acta 82 (2012) 250–256.

[4] J.J. Gooding, Advances in interfacial design sensors: Aryl diazonium salts for electrochemical biosensors and for modifying carbon and metal electrodes, Electroanalysis 20 (2008) 573–582.

[5] O. Lori, L. Elbaz, Advances in ceramic supports for polymer electrolyte fuel cells, Catalysts 5 (2015) 1445–1464.

[6] C. Song, J. Zhang, Electrocatalytic oxygen reduction reaction, in: J. Zhang (Ed.), PEM Fuel Cell Electrocatalysts and Catalyst Layers: Fundamentals and Applications, Springer, London, 2008, pp. 89–134.

[7] H. Liu, R. Ramnarayanan, B.E. Logan, Production of electricity during wastewater treatment using a single chamber microbial fuel cell, Environmental Science & Technology 38 (2004) 2281–2285.

[8] M. Rahimnejad, A. Adhami, S. Darvari, A. Zirepour, S.E. Oh, Microbial fuel cell as new technology for bioelectricity generation: A review, Alexandria Engineering Journal 54 (2015) 745–756.

[9] A. Sarapuu, E. Kibena-Põldsepp, M. Borghei, K. Tammeveski, Electrocatalysis of oxygen reduction on heteroatom-doped nanocarbons and transition metal-nitrogen-carbon catalysts for alkaline membrane fuel cells, Journal of Materials Chemistry A 6 (2018) 776–804.

[10] M.R. Tarasevich, A. Sadkowski, E. Yeager, Oxygen electrochemistry, in: B.E. Conway, J.O.M. Bockris, E. Yeager, S.U.M. Khan, R.E. White (Eds.), Comprehensive Treatise of Electrochemistry, Vol. 7, Plenum Press, New York, 1983, pp. 301–398.

[11] E. Kibena, M. Marandi, V. Sammelselg, K. Tammeveski, B.B.E. Jensen, A.B. Mortensen, M. Lillethorup, M. Kongsfelt, S.U. Pedersen, K. Daasbjerg, Electrochemical behaviour of HOPG and CVD-grown graphene electrodes modified with thick anthraquinone films by diazonium reduction, Electroanalysis 26 (2014) 2619–2630.

[12] A.T. Masheter, A. Poobalasingam, G.G. Wildgoose, W. Elicia, X. Lei, N.V. Rees, T. Robert, G.A. Attard, B. Ronan, C. Alison, J.-H. Jones, R.G. Compton, Investigating the reactive sites and the anomalously large changes in surface pKa values of chemically modified carbon nanotubes of different morphologies, Journal of Materials Chemistry 17 (2007) 2616–2626.

[13] G. Jürmann, D.J. Schiffrin, K. Tammeveski, The pH-dependence of oxygen reduction on quinone-modified glassy carbon electrodes, Electrochimica Acta 53 (2007) 390–399.

[14] K. Tammeveski, K. Kontturi, R.J. Nichols, R.J. Potter, D.J. Schiffrin, Surface redox catalysis for O_2 reduction on quinone-modified glassy carbon electrodes, Journal of Electroanalytical Chemistry 515 (2001) 101–112.
[15] Z. Gong, G.Q. Zhang, S. Wang, Electrochemical reduction of oxygen on anthraquinone/carbon nanotubes nanohybrid modified glassy carbon electrode in neutral medium, Journal of Chemistry (2013) 756307.
[16] M.S. Hossain, D. Tryk, E. Yeager, The electrochemistry of graphite and modified graphite surfaces: the reduction of O_2, Electrochimica Acta 34 (1989) 1733–1737.
[17] E. Lobyntseva, T. Kallio, N. Alexeyeva, K. Tammeveski, K. Kontturi, Electrochemical synthesis of hydrogen peroxide: rotating disk electrode and fuel cell studies, Electrochimica Acta 52 (2007) 7262–7269.
[18] Q. Li, C. Batchelor-McAuley, N.S. Lawrence, R.S. Hartshorne, R.G. Compton, Semiquinone intermediates in the two-electron reduction of quinones in aqueous media and their exceptionally high reactivity towards oxygen reduction, ChemPhysChem 12 (2011) 1255–1257.
[19] S. Fukuzumi, Y. Yamada, K.D. Karlin, Hydrogen peroxide as a sustainable energy carrier: electrocatalytic production of hydrogen peroxide and the fuel cell, Electrochimica Acta 82 (2012) 493–511.
[20] T.X.H. Le, M. Bechelany, S. Lacour, N. Oturan, M.A. Oturan, M. Cretin, High removal efficiency of dye pollutants by electron-Fenton process using a graphene based cathode, Carbon 94 (2015) 1003–1011.
[21] E. Mousset, Z.T. Ko, M. Syafiq, Z.X. Wang, O. Lefebvre, Electrocatalytic activity enhancement of a graphene ink-coated carbon cloth cathode for oxidative treatment, Electrochimica Acta 222 (2016) 1628–1641.
[22] K.S. Novoselov, D. Jiang, F. Schedin, T.J. Booth, V.V. Khotkevich, S.V. Morozov, A.K. Geim, Two-dimensional atomic crystals, Proceedings of the National Academy of Sciences of the United States of America 102 (2005) 10451–10453.
[23] S. Iijima, Helical microtubules of graphitic carbon, Nature 354 (1991) 56–58.
[24] A.J. Bard, L.R. Faulkner, Electrochemical Methods: Fundamentals and Applications, 2nd ed., Wiley, New York, 2001.
[25] I. Kruusenberg, M. Marandi, V. Sammelselg, K. Tammeveski, Hydrodynamic deposition of carbon nanotubes onto HOPG: the reduction of oxygen on CNT/HOPG electrodes in alkaline solution, Electrochemical and Solid State Letters 12 (2009) F31–F34.
[26] I. Kruusenberg, N. Alexeyeva, K. Tammeveski, The pH-dependence of oxygen reduction on multi-walled carbon nanotube modified glassy carbon electrodes, Carbon 47 (2009) 651–658.
[27] C.A. Dyke, J.M. Tour, Unbundled and highly functionalized carbon nanotubes from aqueous reactions, Nano Letters 3 (2003) 1215–1218.
[28] F. Mirkhalaf, K. Tammeveski, D.J. Schiffrin, Substituent effects on the electrocatalytic reduction of oxygen on quinone-modified glassy carbon electrodes, Physical Chemistry Chemical Physics 6 (2004) 1321–1327.
[29] A. Sarapuu, K. Vaik, D.J. Schiffrin, K. Tammeveski, Electrochemical reduction of oxygen on anthraquinone-modified glassy carbon electrodes in alkaline solution, Journal of Electroanalytical Chemistry 541 (2003) 23–29.
[30] K. Vaik, D.J. Schiffrin, K. Tammeveski, Electrochemical reduction of oxygen on anodically pre-treated and chemically grafted glassy carbon electrodes in alkaline solutions, Electrochemistry Communications 6 (2004) 1–5.

[31] K. Vaik, A. Sarapuu, K. Tammeveski, F. Mirkhalaf, D.J. Schiffrin, Oxygen reduction on phenanthrenequinone-modified glassy carbon electrodes in 0.1 M KOH, Journal of Electroanalytical Chemistry 564 (2004) 159–166.
[32] K. Vaik, U. Mäeorg, F.C. Maschion, G. Maia, D.J. Schiffrin, K. Tammeveski, Electrocatalytic oxygen reduction on glassy carbon grafted with anthraquinone by anodic oxidation of a carboxylate substituent, Electrochimica Acta 50 (2005) 5126–5131.
[33] G. Maia, F.C. Maschion, S.T. Tanimoto, K. Vaik, U. Mäeorg, K. Tammeveski, Attachment of anthraquinone derivatives to glassy carbon and the electrocatalytic behavior of the modified electrodes toward oxygen reduction, Journal of Solid State Electrochemistry 11 (2007) 1411–1420.
[34] J.-M. Seinberg, M. Kullapere, U. Mäeorg, F.C. Maschion, G. Maia, D.J. Schiffrin, K. Tammeveski, Spontaneous modification of glassy carbon surface with anthraquinone from the solutions of its diazonium derivative: an oxygen reduction study, Journal of Electroanalytical Chemistry 624 (2008) 151–160.
[35] M. Kullapere, J.-M. Seinberg, U. Mäeorg, G. Maia, D.J. Schiffrin, K. Tammeveski, Electroreduction of oxygen on glassy carbon electrodes modified with in situ generated anthraquinone diazonium cations, Electrochimica Acta 54 (2009) 1961–1969.
[36] M. Ceccato, A. Bousquet, M. Hinge, S.U. Pedersen, K. Daasbjerg, Using a mediating effect in the electroreduction of aryldiazonium salts to prepare conducting organic films of high thickness, Chemistry of Materials 23 (2011) 1551–1557.
[37] A. Bousquet, M. Ceccato, M. Hinge, S.U. Pedersen, K. Daasbjerg, Redox grafting of diazotated anthraquinone as a means of forming thick conducting organic films, Langmuir 28 (2012) 1267–1275.
[38] S. Chernyy, A. Bousquet, K. Torbensen, J. Iruthayaraj, M. Ceccato, S.U. Pedersen, K. Daasbjerg, Elucidation of the mechanism of redox grafting of diazotated anthraquinone, Langmuir 28 (2012) 9573–9582.
[39] V. Jouikov, J. Simonet, Efficient immobilization of 9,10-anthraquinonyl moiety at solid interfaces through 2-(bromomethyl)anthraquinone one-electron cleavage, Electrochemistry Communications 27 (2013) 180–183.
[40] G. Liu, T. Bocking, J.J. Gooding, Diazonium salts: stable monolayers on gold electrodes for sensing applications, Journal of Electroanalytical Chemistry 600 (2007) 335–344.
[41] M. Kullapere, J. Kozlova, L. Matisen, V. Sammelselg, H.A. Menezes, G. Maia, D.J. Schiffrin, K. Tammeveski, Electrochemical properties of aryl-modified gold electrodes, Journal of Electroanalytical Chemistry 641 (2010) 90–98.
[42] E. Kibena, M. Marandi, U. Mäeorg, L.B. Venarusso, G. Maia, L. Matisen, A. Kasikov, V. Sammelselg, K. Tammeveski, Electrochemical modification of gold electrodes with azobenzene derivatives by diazonium reduction, ChemPhysChem 14 (2013) 1043–1054.
[43] M. Kullapere, M. Marandi, L. Matisen, F. Mirkhalaf, A.E. Carvalho, G. Maia, V. Sammelselg, K. Tammeveski, Blocking properties of gold electrodes modified with 4-nitrophenyl and 4-decylphenyl groups, Journal of Solid State Electrochemistry 16 (2012) 569–578.
[44] A. Kuzume, E. Herrero, J.M. Feliu, E. Ahlberg, R.J. Nichols, D.J. Schiffrin, Electrochemical reactivity in nanoscale domains: O_2 reduction on a fullerene modified gold surface, Physical Chemistry Chemical Physics 7 (2005) 1293–1299.

[45] J. Zhang, J. Cai, M. Li, Grafting of PMMA brushes layer on Cu surface to create a stable superhydrophobic surface, Applied Surface Science 386 (2016) 309–318.
[46] M. Kendig, M. Hon, J. Sinko, Inhibition of oxygen reduction on copper in neutral sodium chloride, ECS Transactions 1 (2006) 119–129.
[47] B.L. Hurley, R.L. McCreery, Covalent bonding of organic molecules to Cu and Al alloy 2024 T3 surfaces via diazonium ion reduction, Journal of the Electrochemical Society 151 (2004) B252–B259.
[48] G. Kear, K. Brernhorst, S. Coles, S.H. Huang, Rates of mass transfer to patch electrodes in disturbed flows using oxygen reduction under limiting current conditions, Corrosion Science 50 (2008) 1789–1795.
[49] A.L. Colley, J.V. Macpherson, P.R. Unwin, Effect of high rates of mass transport on oxygen reduction at copper electrodes: implications for aluminium corrosion, Electrochemistry Communications 10 (2008) 1334–1336.
[50] I. Jiang, G.M. Brisard, Determination of the kinetic parameters of oxygen reduction on copper using a rotating ring single crystal disk assembly ($RRD_{Cu(h\ k\ l)}E$), Electrochimica Acta 52 (2007) 4487–4496.
[51] M.B. Vukmirovic, N. Vasiljevic, N. Dimitrov, K. Sieradzki, Diffusion-limited current density of oxygen reduction on copper, Journal of the Electrochemical Society 150 (2003) B10–B15.
[52] F. King, M.J. Quinn, C.D. Litke, Oxygen reduction on copper in neutral NaCl solution, Journal of Electroanalytical Chemistry 385 (1995) 45–55.
[53] M.V. Vazquez, S.R. Desanchez, E.J. Calvo, D.J. Schiffrin, The electrochemical reduction of oxygen on polycrystalline copper in borax buffer, Journal of Electroanalytical Chemistry 374 (1994) 189–197.
[54] F. King, C.D. Litke, Y. Tang, Effect of interfacial pH on the reduction of oxygen on copper in neutral $NaClO_4$ solution, Journal of Electroanalytical Chemistry 384 (1995) 105–113.
[55] R. Sibul, E. Kibena-Põldsepp, S. Ratso, M. Kook, M. Käärik, M. Merisalu, P. Paiste, J. Leis, V. Sammelselg, K. Tammeveski, Nitrogen-doped carbon-based electrocatalysts synthesised by ball-milling, Electrochemistry Communications 93 (2018) 39–43.
[56] S. Ratso, I. Kruusenberg, M. Käärik, M. Kook, R. Saar, M. Pärs, J. Leis, K. Tammeveski, Highly efficient nitrogen-doped carbide-derived carbon materials for oxygen reduction reaction in alkaline media, Carbon 113 (2017) 159–169.
[57] S. Ratso, I. Kruusenberg, U. Joost, R. Saar, K. Tammeveski, Enhanced oxygen reduction reaction activity of nitrogen-doped graphene/multi-walled carbon nanotube catalysts in alkaline media, International Journal of Hydrogen Energy 41 (2016) 22510–22519.
[58] I. Kruusenberg, S. Ratso, M. Vikkisk, P. Kanninen, T. Kallio, A.M. Kannan, K. Tammeveski, Highly active nitrogen-doped nanocarbon electrocatalysts for alkaline direct methanol fuel cell, Journal of Power Sources 281 (2015) 94–102.
[59] M. Vikkisk, I. Kruusenberg, S. Ratso, U. Joost, E. Shulga, I. Kink, P. Rauwel, K. Tammeveski, Enhanced electrocatalytic activity of nitrogen-doped multi-walled carbon nanotubes towards the oxygen reduction reaction in alkaline media, RSC Advances 5 (2015) 59495–59505.
[60] A.C. Ramirez-Perez, J. Quilez-Bermejo, J.M. Sieben, E. Morallon, D. Cazorla-Amoros, Effect of nitrogen-functional groups on the ORR activity of activated carbon fiber-polypyrrole-based electrodes, Electrocatalysis 9 (2018) 697–705.

[61] J. Masa, A. Zhao, W. Xia, M. Muhler, W. Schuhmann, Metal-free catalysts for oxygen reduction in alkaline electrolytes: influence of the presence of Co, Fe, Mn and Ni inclusions, Electrochimica Acta 128 (2014) 271–278.
[62] M. Rauf, J.W. Wang, P.X. Zhang, W. Iqbal, J.L. Qu, Y.L. Li, Non-precious nano-structured materials by electrospinning and their applications for oxygen reduction in polymer electrolyte membrane fuel cells, Journal of Power Sources 408 (2018) 17–27.
[63] D.K. Huang, Y.P. Luo, S.H. Li, B.Y. Zhang, Y. Shen, M.K. Wang, Active catalysts based on cobalt oxide@cobalt/N-C nanocomposites for oxygen reduction reaction in alkaline solutions, Nano Research 7 (2014) 1054–1064.
[64] J.J. Yan, H.Y. Lu, Y.P. Huang, J. Fu, S.Y. Mo, C. Wei, Y.E. Miao, T.X. Liu, Polydopamine-derived porous carbon fiber/cobalt composites for efficient oxygen reduction reactions, Journal of Materials Chemistry A 3 (2015) 23299–23306.
[65] L.W. Ji, Y.F. Yao, O. Toprakci, Z. Lin, Y.Z. Liang, Q. Shi, A.J. Medford, C.R. Millns, X.W. Zhang, Fabrication of carbon nanofiber-driven electrodes from electrospun polyacrylonitrile/polypyrrole bicomponents for high-performance rechargeable lithium-ion batteries, Journal of Power Sources 195 (2010) 2050–2056.
[66] C.Q. Shang, M.C. Li, Z.Y. Wang, S.F. Wu, Z.G. Lu, Electrospun nitrogen-doped carbon nanofibers encapsulating cobalt nanoparticles as efficient oxygen reduction reaction catalysts, ChemElectroChem 3 (2016) 1437–1445.
[67] J. Yin, Y.J. Qiu, J. Yu, X.S. Zhou, W.H. Wu, Enhancement of electrocatalytic activity for oxygen reduction reaction in alkaline and acid media from electrospun nitrogen-doped carbon nanofibers by surface modification, RSC Advances 3 (2013) 15655–15663.
[68] C. Liu, J. Wang, J.S. Li, J.Z. Liu, C.H. Wang, X.Y. Sun, J.Y. Shen, W.Q. Han, L.J. Wang, Electrospun ZIF-based hierarchical carbon fiber as an efficient electrocatalyst for the oxygen reduction reaction, Journal of Materials Chemistry A 5 (2017) 1211–1220.
[69] C. Alegre, E. Modica, A. Di Blasi, O. Di Blasi, C. Busacca, M. Ferraro, A.S. Arico, V. Antonucci, V. Baglio, NiCo-loaded carbon nanofibers obtained by electrospinning: bifunctional behavior as air electrodes, Renewable Energy 125 (2018) 250–259.
[70] C. Liu, J. Wang, J.S. Li, R. Luo, X.Y. Sun, J.Y. Shen, W.Q. Han, L.J. Wang, Fe/N decorated mulberry-like hollow mesoporous carbon fibers as efficient electrocatalysts for oxygen reduction reaction, Carbon 114 (2017) 706–716.
[71] S. Uhm, B. Jeong, J. Lee, A facile route for preparation of non-noble CNF cathode catalysts in alkaline ethanol fuel cells, Electrochimica Acta 56 (2011) 9186–9190.
[72] I.T. Kim, M.J. Song, S. Shin, M.W. Shin, Co- and defect-rich carbon nanofiber films as a highly efficient electrocatalyst for oxygen reduction, Applied Surface Science 435 (2018) 1159–1167.
[73] D. Liu, X.P. Zhang, Z.C. Sun, T.Y. You, Free-standing nitrogen-doped carbon nanofiber films as highly efficient electrocatalysts for oxygen reduction, Nanoscale 5 (2013) 9528–9531.
[74] Y.J. Qiu, J. Yu, W.H. Wu, J. Yin, X.D. Bai, Fe-N/C nanofiber electrocatalysts with improved activity and stability for oxygen reduction in alkaline and acid solutions, Journal of Solid State Electrochemistry 17 (2013) 565–573.
[75] M. Delamar, R. Hitmi, J. Pinson, J.M. Saveant, Covalent modification of carbon surfaces by grafting of functionalized aryl radicals produced from electrochemical

reduction of diazonium salts, Journal of the American Chemical Society 114 (1992) 5883–5884.
[76] J. Pinson, F. Podvorica, Attachment of organic layers to conductive or semiconductive surfaces by reduction of diazonium salts, Chemical Society Reviews 34 (2005) 429–439.
[77] A. Adenier, N. Barre, E. Cabet-Deliry, A. Chausse, S. Griveau, F. Mercier, J. Pinson, C. Vautrin-Ul, Study of the spontaneous formation of organic layers on carbon and metal surfaces from diazonium salts, Surface Science 600 (2006) 4801–4812.
[78] J.-M. Chretien, M.A. Ghanem, P.N. Bartlett, J.D. Kilburn, Covalent modification of glassy carbon surfaces by using electrochemical and solid-phase synthetic methodologies: application to bi- and trifunctionalisation with different redox centres, Chemistry: A European Journal 15 (2009) 11928–11936.
[79] X.Y. Lu, C. Zhao, Controlled electrochemical intercalation, exfoliation and in situ nitrogen doping of graphite in nitrate-based protic ionic liquids, Physical Chemistry Chemical Physics 15(2013) 20005–20009.
[80] A.M. Abdelkader, I.A. Kinloch, R.A.W. Dryfe, High-yield electro-oxidative preparation of graphene oxide, Chemical Communications 50 (2014) 8402–8404.
[81] R. Gondosiswanto, X.Y. Lu, C. Zhao, Preparation of metal-free nitrogen-doped graphene via direct electrochemical exfoliation of graphite in ammonium nitrate, Australian Journal of Chemistry 68 (2015) 830–835.
[82] F.L. Lou, M.E.M. Buan, N. Muthuswamy, J.C. Walmsley, M. Ronning, D. Chen, One-step electrochemical synthesis of tunable nitrogen-doped graphene, Journal of Materials Chemistry A 4 (2016) 1233–1243.
[83] O. Ustavytska, Y. Kurys, V. Koshechko, V. Pokhodenko, One-step electrochemical preparation of multilayer graphene functionalized with nitrogen, Nanoscale Research Letters 12 (2017) 175.
[84] T.H. Han, N. Parveen, S.A. Ansari, J.H. Shim, A.T.N. Nguyen, M.H. Cho, Electrochemically synthesized sulfur-doped graphene as a superior metal-free cathodic catalyst for oxygen reduction reaction in microbial fuel cells, RSC Advances 6 (2016) 103446–103454.
[85] B.D. Ossonon, D. Bélanger, Functionalization of graphene sheets by the diazonium chemistry during electrochemical exfoliation of graphite, Carbon 111 (2017) 83–93.
[86] M.C. Bernard, A. Chausse, E. Cabet-Deliry, M.M. Chehimi, J. Pinson, F. Podvorica, C. Vautrin-Ul, Organic layers bonded to industrial, coinage, and noble metals through electrochemical reduction of aryldiazonium salts, Chemistry of Materials 15 (2003) 3450–3462.
[87] D. Bélanger, J. Pinson, Electrografting: a powerful method for surface modification, Chemical Society Reviews 40 (2011) 3995–4048.
[88] G.G. Wildgoose, M. Pandurangappa, N.S. Lawrence, L. Jiang, T.G.J. Jones, R.G. Compton, Anthraquinone-derivatised carbon powder: reagentless voltammetric pH electrodes, Talanta 60 (2003) 887–893.
[89] B.D. Assresahegn, T. Brousse, D. Bélanger, Advances on the use of diazonium chemistry for functionalization of materials used in energy storage systems, Carbon 92 (2015) 362–381.
[90] Y.L. Liang, Y. Jing, S. Gheytani, K.Y. Lee, P. Liu, A. Facchetti, Y. Yao, Universal quinone electrodes for long cycle life aqueous rechargeable batteries, Nature Materials 16 (2017) 841–848.

[91] M. Shao, Q. Chang, J.P. Dodelet, R. Chenitz, Recent advances in electrocatalysts for oxygen reduction reaction, Chemical Reviews 116 (2016) 3594–3657.
[92] Z.Y. Wu, Z. Iqbal, X.Q. Wang, Metal-free, carbon-based catalysts for oxygen reduction reactions, Frontiers of Chemical Science and Engineering 9 (2015) 280–294.
[93] J. Yan, Z. Fan, L. Zhi, Functionalized carbon nanotubes and their enhanced polymers, in: M. Möller, K. Matyjaszewski (Eds.), Polymer Science: A Comprehensive Reference, Elsevier, Amsterdam, 2012, pp. 439–478.
[94] D.D.L. Chung, Carbon Composites: Composites with Carbon Fibers, Nanofibers, and Nanotubes, 2nd ed., Elsevier Science & Technology, Oxford, 2016, pp. 1–87.
[95] J. Lilloja, E. Kibena-Põldsepp, M. Merisalu, P. Rauwel, L. Matisen, A. Niilisk, E. Cardoso, G. Maia, V. Sammelselg, K. Tammeveski, An oxygen reduction study of graphene-based nanomaterials of different origin, Catalysts 6 (2016) 108.
[96] P. Trogadas, T.F. Fuller, P. Strasser, Carbon as catalyst and support for electrochemical energy conversion, Carbon 75 (2014) 5–42.
[97] D. Higgins, P. Zamani, A. Yu, Z. Chen, The application of graphene and its composites in oxygen reduction electrocatalysis: a perspective and review of recent progress, Energy & Environmental Science 9 (2016) 357–390.
[98] N. Daems, X. Sheng, I.F.J. Vankelecom, P.P. Pescarmona, Metal-free doped carbon materials as electrocatalysts for the oxygen reduction reaction, Journal of Materials Chemistry A 2 (2014) 4085–4110.
[99] J.R. Pels, F. Kapteijn, J.A. Moulijn, Q. Zhu, K.M. Thomas, Evolution of nitrogen functionalities in carbonaceous materials during pyrolysis, Carbon 33 (1995) 1641–1653.
[100] R. Silva, D. Voiry, M. Chhowalla, T. Asefa, Efficient metal-free electrocatalysts for oxygen reduction: polyaniline-derived N- and O-doped mesoporous carbons, Journal of the American Chemical Society 135 (2013) 7823–7826.
[101] J. Masa, A.Q. Zhao, W. Xia, Z.Y. Sun, B. Mei, M. Muhler, W. Schuhmann, Trace metal residues promote the activity of supposedly metal-free nitrogen-modified carbon catalysts for the oxygen reduction reaction, Electrochemistry Communications 34 (2013) 113–116.
[102] S.G. Wang, C.L. Dai, J.P. Li, L. Zhao, Z.H. Ren, Y.Q. Ren, Y.J. Qiu, J. Yu, The effect of different nitrogen sources on the electrocatalytic properties of nitrogen-doped electrospun carbon nanofibers for the oxygen reduction reaction, International Journal of Hydrogen Energy 40 (2015) 4673–4682.
[103] P. Zamani, D. Higgins, F. Hassan, G.P. Jiang, J. Wu, S. Abureden, Z.W. Chen, Electrospun iron-polyaniline-polyacrylonitrile derived nanofibers as non-precious oxygen reduction reaction catalysts for PEM fuel cells, Electrochimica Acta 139 (2014) 111–116.
[104] Y.J. Qiu, J. Yu, T.N. Shi, X.S. Zhou, X.D. Bai, J.Y. Huang, Nitrogen-doped ultrathin carbon nanofibers derived from electrospinning: large-scale production, unique structure, and application as electrocatalysts for oxygen reduction, Journal of Power Sources 196 (2011) 9862–9867.
[105] J. Yin, Y.J. Qiu, J. Yu, Porous nitrogen-doped carbon nanofibers as highly efficient metal-free electrocatalyst for oxygen reduction reaction, Journal of Electroanalytical Chemistry 702 (2013) 56–59.
[106] Y.J. Qiu, J. Yin, H.W. Hou, J. Yu, X.B. Zuo, Preparation of nitrogen-doped carbon submicrotubes by coaxial electrospinning and their electrocatalytic

activity for oxygen reduction reaction in acid media, Electrochimica Acta 96 (2013) 225–229.
[107] Z. Deng, Q. Yi, G. Li, Y. Chen, X. Yang, H. Nie, NiCo-doped C-N nano-composites for cathodic catalysts of Zn-air batteries in neutral media, Electrochimica Acta 279 (2018) 1–9.
[108] L.F. Lai, J.R. Potts, D. Zhan, L. Wang, C.K. Poh, C.H. Tang, H. Gong, Z.X. Shen, L.Y. Jianyi, R.S. Ruoff, Exploration of the active center structure of nitrogen-doped graphene-based catalysts for oxygen reduction reaction, Energy & Environmental Science 5 (2012) 7936–7942.
[109] S. Kabir, K. Artyushkova, A. Serov, B. Kiefer, P. Atanassov, Binding energy shifts for nitrogen-containing graphene-based electrocatalysts – experiments and DFT calculations, Surface and Interface Analysis 48 (2016) 293–300.
[110] M. Borghei, P. Kanninen, M. Lundahl, T. Susi, J. Sainio, I. Anoshkin, A. Nasibulin, T. Kalil, K. Tammeveski, E. Kauppinen, V. Ruiz, High oxygen reduction activity of few-walled carbon nanotubes with low nitrogen content, Applied Catalysis B: Environmental 158–159 (2014) 233–241.
[111] V. Gudkova, A. Krumme, T. Martson, M. Rikko, E. Tarasova, N. Savest, M. Viirsalu, 1-butyl-3-methylimidazolium chloride assisted electrospinning of SAN/MWCNTs conductive reinforced composite membranes, Journal of Electrostatics 78 (2015) 11–16.
[112] Q. Liu, J.H. Zhu, L.W. Zhang, Y.J. Qiu, Recent advances in energy materials by electrospinning, Renewable & Sustainable Energy Reviews 81 (2018) 1825–1858.
[113] F.J. Miao, C.L. Shao, X.H. Li, K.X. Wang, Y.C. Liu, Flexible solid-state supercapacitors based on freestanding nitrogen-doped porous carbon nanofibers derived from electrospun polyacrylonitrile@polyaniline nanofibers, Journal of Materials Chemistry A 4 (2016) 4180–4187.
[114] Y.W. Ju, G.R. Choi, H.R. Jung, W.J. Lee, Electrochemical properties of electrospun PAN/MWCNT carbon nanofibers electrodes coated with polypyrrole, Electrochimica Acta 53 (2008) 5796–5803.
[115] G.B. Xue, J. Zhong, Y.L. Cheng, B. Wang, Facile fabrication of cross-linked carbon nanofiber via directly carbonizing electrospun polyacrylonitrile nanofiber as high performance scaffold for supercapacitors, Electrochimica Acta 215 (2016) 29–35.
[116] Z.P. Zhou, X.F. Wu, H.Q. Hou, Electrospun carbon nanofibers surface-grown with carbon nanotubes and polyaniline for use as high-performance electrode materials of supercapacitors, RSC Advances 4 (2014) 23622–23629.
[117] X.X. Yan, K.X. Liu, T. Wang, Y. You, J.G. Liu, P. Wang, X.Q. Pan, G.F. Wang, J. Luo, J. Zhu, Atomic interpretation of high activity on transition metal and nitrogen-doped carbon nanofibers for catalyzing oxygen reduction, Journal of Materials Chemistry A 5 (2017) 3336–3345.
[118] Q. Liu, S. Cao, Y. Qiu, Effect of carbonization temperature on bimetallic FeCo-N/C nanofiber electrocatalysts for oxygen reduction reaction in sulfuric acid solution, International Journal of Hydrogen Energy 42 (2017) 29274–29282.
[119] J.X. Guo, Q.J. Niu, Y.C. Yuan, I. Maitlo, J. Nie, G.P. Ma, Electrospun core-shell nanofibers derived Fe-S/N doped carbon material for oxygen reduction reaction, Applied Surface Science 416 (2017) 118–123.
[120] J.Y. Guo, J.Q. Liu, H.H. Dai, R. Zhou, T.Y. Wang, C.C. Zhang, S. Ding, H.G. Wang, Nitrogen doped carbon nanofiber derived from polypyrrole functionalized

polyacrylonitrile for applications in lithium-ion batteries and oxygen reduction reaction, Journal of Colloid and Interface Science 507 (2017) 154–161.
[121] B.S. Lee, S.B. Son, K.M. Park, G. Lee, K.H. Oh, S.H. Lee, W.R. Yu, Effect of pores in hollow carbon nanofibers on their negative electrode properties for a lithium rechargeable battery, ACS Applied Materials & Interfaces 4 (2012) 6701–6709.
[122] C.F. Zhou, T. Liu, T. Wang, S. Kumar, PAN/SAN/SWNT ternary composite: pore size control and electrochemical supercapacitor behavior, Polymer 47 (2006) 5831–5837.
[123] R. Li, X.Z. Wang, Y.F. Dong, X. Pan, X.G. Liu, Z.B. Zhao, J.S. Qiu, Nitrogen-doped carbon nanotubes decorated with cobalt nanoparticles derived from zeolitic imidazolate framework-67 for highly efficient oxygen reduction reaction electrocatalysis, Carbon 132 (2018) 580–588.
[124] S. Ratso, I. Kruusenberg, A. Sarapuu, M. Kook, P. Rauwel, R. Saar, J. Aruväli, K. Tammeveski, Electrocatalysis of oxygen reduction on iron- and cobalt-containing nitrogen-doped carbon nanotubes in acid media, Electrochimica Acta 218 (2016) 303–310.
[125] Z.L. Wang, S. Xiao, Z.L. Zhu, X. Long, X.L. Zheng, X.H. Lu, S.H. Yang, Cobalt-embedded nitrogen doped carbon nanotubes: a bifunctional catalyst for oxygen electrode reactions in a wide pH range, ACS Applied Materials & Interfaces 7 (2015) 4048–4055.
[126] Y.C. Hao, Z.Y. Lu, G.X. Zhang, Z. Chang, L. Luo, X.M. Sun, Cobalt-embedded nitrogen-doped carbon nanotubes as high-performance bifunctional oxygen catalysts, Energy Technology 5 (2017) 1265–1271.
[127] I. Kruusenberg, D. Ramani, S. Ratso, U. Joost, R. Saar, P. Rauwel, A. Kannan, K. Tammeveski, Cobalt-nitrogen co-doped carbon nanotube cathode catalyst for alkaline membrane fuel cells, ChemElectroChem 3 (2016) 1455–1465.
[128] Q.Q. Cheng, L.J. Yang, L.L. Zou, Z.Q. Zou, C. Chen, Z. Hu, H. Yang, Single cobalt atom and N codoped carbon nanofibers as highly durable electrocatalyst for oxygen reduction reaction, ACS Catalysis 7 (2017) 6864–6871.
[129] K.X. Liu, S. Kattel, V. Mao, G.F. Wang, Electrochemical and computational study of oxygen reduction reaction on nonprecious transition metal/nitrogen doped carbon nanofibers in acid medium, Journal of Physical Chemistry C 120 (2016) 1586–1596.
[130] J.P. McClure, R.Z. Jiang, D. Chu, P.S. Fedkiw, Oxygen electroreduction on Fe- or Co-containing carbon fibers, Carbon 79 (2014) 457–469.
[131] C. Cao, L.L. Wei, M. Su, G. Wang, J.Q. Shen, Enhanced power generation using nano cobalt oxide anchored nitrogen-decorated reduced graphene oxide as a high-performance air-cathode electrocatalyst in biofuel cells, RSC Advances 6 (2016) 52556–52563.
[132] L.B. Lv, T.N. Ye, L.H. Gong, K.X. Wang, J. Su, X.H. Li, J.S. Chen, Anchoring cobalt nanocrystals through the plane of graphene: highly integrated electrocatalyst for oxygen reduction reaction, Chemistry of Materials 27 (2015) 544–549.
[133] K. Kreek, A. Sarapuu, L. Samolberg, U. Joost, V. Mikli, M. Koel, K. Tammeveski, Cobalt-containing nitrogen-doped carbon aerogels as efficient electrocatalysts for the oxygen reduction reaction, ChemElectroChem 2 (2015) 2079–2088.
[134] A. Sarapuu, L. Samolberg, K. Kreek, M. Koel, L. Matisen, K. Tammeveski, Cobalt- and iron-containing nitrogen-doped carbon aerogels as non-precious

metal catalysts for electrochemical reduction of oxygen, Journal of Electro-analytical Chemistry 746 (2015) 9–17.
[135] K. Kisand, A. Sarapuu, A. Peikolainen, H. Seemen, M. Kook, M. Kaarik, J. Leis, V. Sammelselg, K. Tammeveski, Oxygen reduction on Fe- and Co-containing nitrogen-doped nanocarbons, ChemElectroChem 5 (2018) 2002–2009.
[136] X. Wan, H.J. Wang, H. Yu, F. Peng, Highly uniform and monodisperse carbon nanospheres enriched with cobalt-nitrogen active sites as a potential oxygen reduction electrocatalyst, Journal of Power Sources 346 (2017) 80–88.
[137] Q.J. Mo, N.N. Chen, M.D. Deng, L.C. Yang, Q.S. Gao, Metallic cobalt@nitrogen-doped carbon nanocomposites: carbon-shell regulation toward efficient bi-functional electrocatalysis, ACS Applied Materials & Interfaces 9 (2017) 37721–37730.
[138] K.K. Türk, I. Kruusenberg, J. Mondal, P. Rauwel, J. Kozlova, L. Matisen, V. Sammelselg, K. Tammeveski, Oxygen electroreduction on MN_4-macrocycle modified graphene/multi-walled carbon nanotube composites, Journal of Electroanalytical Chemistry 756 (2015) 69–76.
[139] F. Guo, H. Yang, B. Aguila, A.M. Al-Enizi, A. Nafady, M. Singh, V. Bansal, S.Q. Ma, Cobalt nanoparticles incorporated into hollow doped porous carbon capsules as a highly efficient oxygen reduction electrocatalyst, Catalysis Science & Technology 8 (2018) 5244–5250.
[140] X.H. Tang, H.Y. Ng, Cobalt and nitrogen-doped carbon catalysts for enhanced oxygen reduction and power production in microbial fuel cells, Electrochimica Acta 247 (2017) 193–199.
[141] G.M. Kim, S. Baik, J.W. Lee, Enhanced oxygen reduction from the insertion of cobalt into nitrogen-doped porous carbons, RSC Advances 5 (2015) 87971–87980.
[142] S. Ratso, I. Kruusenberg, M. Käärik, M. Kook, L. Puust, R. Saar, J. Leis, K. Tammeveski, Highly efficient transition metal and nitrogen co-doped carbide-derived carbon electrocatalysts for anion exchange membrane fuel cells, Journal of Power Sources 375 (2018) 233–243.
[143] A.Q. Zhu, P.F. Tan, L. Qiao, Y.J. Liu, Y. Ma, X. Xiong, J. Pan, Multiple active components, synergistically driven cobalt and nitrogen Co-doped porous carbon as high-performance oxygen reduction electrocatalyst, Inorganic Chemistry Frontiers 4 (2017) 1748–1756.
[144] T.T. Sun, L.B. Xu, S.Y. Li, W.X. Chai, Y. Huang, Y.S. Yan, J.F. Chen, Cobalt-nitrogen-doped ordered macro-/mesoporous carbon for highly efficient oxygen reduction reaction, Applied Catalysis B: Environmental 193 (2016) 1–8.
[145] S. Bhattacharyya, B. Konkena, K. Jayaramulu, W. Schuhmann, T.K. Maji, Synthesis of nano-porous carbon and nitrogen doped carbon dots from an anionic MOF: a trace cobalt metal residue in carbon dots promotes electrocatalytic ORR activity, Journal of Materials Chemistry A 5 (2017) 13573–13580.
[146] R. Zhang, L. Liu, J. Zhang, W.Y. Wang, F. Ma, R.F. Li, L.Z. Gao, Fabrication of the pyrolyzing carbon-supported cobalt-dicyandiamide electrocatalysts and study on the active sites and mechanism for oxygen reduction in alkaline electrolyte, Journal of Solid State Electrochemistry 19 (2015) 1695–1707.
[147] Y.D. Qian, Z. Liu, H. Zhang, P. Wu, C.X. Cai, Active site structures in nitrogen-doped carbon-supported cobalt catalysts for the oxygen reduction reaction, ACS Applied Materials & Interfaces 8 (2016) 32875–32886.

[148] Q.P. Zhao, Q. Ma, F.P. Pan, J.H. Guo, J.Y. Zhang, Facile synthesis of N-doped carbon nanosheet-encased cobalt nanoparticles as efficient oxygen reduction catalysts in alkaline and acidic media, Ionics 22 (2016) 2203–2212.
[149] R.L. McCreery, Advanced carbon electrode materials for molecular electrochemistry, Chemical Reviews 108 (2008) 2646–2687.
[150] R. Borup, J. Meyers, B. Pivovar, Y.S. Kim, R. Mukundan, N. Garland, D. Myers, M. Wilson, F. Garzon, D. Wood, P. Zelenay, K. More, K. Stroh, T. Zawodzinski, J. Boncella, J.E. McGrath, M. Inaba, K. Miyatake, M. Hori, K. Ota, Z. Ogumi, S. Miyata, A. Nishikata, Z. Siroma, Y. Uchimoto, K. Yasuda, K.I. Kimijima, N. Iwashita, Scientific aspects of polymer electrolyte fuel cell durability and degradation, Chemical Reviews 107 (2007) 3904–3951.
[151] L. David, R. Bhandavat, U. Barrera, G. Singh, Silicon oxycarbide glass-graphene composite paper electrode for long-cycle lithium-ion batteries, Nature Communications 7 (2016) 10998.
[152] M.S. Kolathodi, L. David, M.A. Abass, G. Singh, Polysiloxane-functionalized graphene oxide paper: pyrolysis and performance as a Li-ion battery and supercapacitor electrode, RSC Advances 6 (2016) 74323–74331.
[153] G. Chamoulaud, D. Bélanger, Spontaneous derivatization of a copper electrode with in situ generated diazonium cations in aprotic and aqueous media, The Journal of Physical Chemistry C 111 (2007) 7501–7507.
[154] G. Shul, R. Parent, H.A. Mosqueda, D. Bélanger, Localized in situ generation of diazonium cations by electrocatalytic formation of a diazotization reagent, ACS Applied Materials & Interfaces 5 (2013) 1468–1473.
[155] E. Kibena, M. Mooste, J. Kozlova, M. Marandi, V. Sammelselg, K. Tammeveski, Surface and electrochemical characterisation of CVD grown graphene sheets, Electrochemistry Communications 35 (2013) 26–29.
[156] A. Le Comte, T. Brousse, D. Bélanger, Simpler and greener grafting method for improving the stability of anthraquinone-modified carbon electrode in alkaline media, Electrochimica Acta 137 (2014) 447–453.
[157] J.P. McClure, C.K. Devine, R.Z. Jiang, D. Chu, J.J. Cuomo, G.N. Parsons, P.S. Fedkiw, Oxygen electroreduction on Ti- and Fe-containing carbon fibers, Journal of the Electrochemical Society 160 (2013) F769–F778.
[158] J.F. Drillet, M. Adam, S. Barg, A. Herter, D. Koch, V.M. Schmidt, M. Wilhelm, Development of a novel zinc/air fuel cell with a Zn foam anode, a PVA/KOH membrane and a MnO_2/SiOC-based air cathode, ECS Transactions 28 (2010) 13–24.
[159] F. Schluter, J. Meyer, M. Wilhelm, K. Rezwan, Hierarchical emulsion based hybrid ceramics synthesized with different siloxane precursor and with embedded nickel nanoparticles, Colloid Surface A 492 (2016) 160–169.
[160] W.J. Albery, M.L. Hitchman, Ring-disc electrodes, Clarendon Press, Oxford, 1971, p. 175.
[161] A. Salimi, C.E. Banks, R.G. Compton, Ultrasonic effects on the electro-reduction of oxygen at a glassy carbon anthraquinone-modified electrode. The Koutecky-Levich equation applied to insonated electro-catalytic reactions, Physical Chemistry Chemical Physics 5 (2003) 3988–3993.
[162] Y. Zhou, G. Zhang, J. Chen, G.e. Yuan, L. Xu, L. Liu, F. Yang, A facile two-step electroreductive synthesis of anthraquinone/graphene nanocomposites as efficient electrocatalyst for O_2 reduction in neutral medium, Electrochemistry Communications 22 (2012) 69–72.

[163] K. Tanaka, S. Iijima, Carbon Nanotubes and Graphene, 2nd ed., Elsevier, Amsterdam, 2014.
[164] P. Allongue, M. Delamar, B. Desbat, O. Fagebaume, R. Hitmi, J. Pinson, J.M. Saveant, Covalent modification of carbon surfaces by aryl radicals generated from the electrochemical reduction of diazonium salts, Journal of the American Chemical Society 119 (1997) 201–207.
[165] J. Pinson, Attachment of organic layers to materials surfaces by reduction of diazonium salts, in: M.M. Chehimi (Ed.), Aryl diazonium salts: New coupling agents in polymer and surface science, Wiley-VCH, Weinheim, 2012, pp. 1–35.
[166] M.W. Lehmann, D.H. Evans, Anomalous behavior in the two-step reduction of quinones in acetonitrile, Journal of Electroanalytical Chemistry 500 (2001) 12–20.
[167] F.C. de Abreu, A.C.O. Lopes, M.O.F. Goulart, Influence of the leaving group and of the annelation in the electroreduction of 2-methyl-substituted quinones, Journal of Electroanalytical Chemistry 562 (2004) 53–59.
[168] D. Ajloo, B. Yoonesi, A. Soleymanpour, Solvent effect on the reduction potential of anthraquinones derivatives. The experimental and computational studies, International Journal of Electrochemical Science 5 (2010) 459–477.
[169] Y. Zhang, L.Q. Ren, S.R. Wang, A. Marathe, J. Chaudhuri, G.G. Li, Functionalization of graphene sheets through fullerene attachment, Journal of Materials Chemistry 21 (2011) 5386–5391.
[170] P.P. Chen, G.Q. Deng, D.H. Hu, Y. Wang, Z. Meng, W.W. Hua, K. Xi, Enhanced mechanical properties and thermal stability of PSMA by functionalized graphene nanosheets, RSC Advances 6 (2016) 68748–68753.
[171] X.Q. Ji, Y.H. Xu, W.L. Zhang, L. Cui, J.Q. Liu, Review of functionalization, structure and properties of graphene/polymer composite fibers, Composites Part A: Applied Science and Manufacturing 87 (2016) 29–45.
[172] H.H. Liu, L.C. Hou, W.W. Peng, Q. Zhang, X.X. Zhang, Fabrication and characterization of polyamide 6-functionalized graphene nanocomposite fiber, Journal of Materials Science 47 (2012) 8052–8060.
[173] L.M. Malard, M.A. Pimenta, G. Dresselhaus, M.S. Dresselhaus, Raman spectroscopy in graphene, Physics Reports 473 (2009) 51–87.
[174] A. Ambrosi, C.K. Chua, A. Bonanni, M. Pumera, Electrochemistry of graphene and related materials, Chemical Reviews 114 (2014) 7150–7188.
[175] H. Wang, Y.F. Wang, X.W. Cao, M. Feng, G.X. Lan, Vibrational properties of graphene and graphene layers, Journal of Raman Spectroscopy 40 (2009) 1791–1796.
[176] K. Parvez, R.J. Li, S.R. Puniredd, Y. Hernandez, F. Hinkel, S.H. Wang, X.L. Feng, K. Mullen, Electrochemically exfoliated graphene as solution-processable, highly conductive electrodes for organic electronics, ACS Nano 7 (2013) 3598–3606.
[177] A. Guermoune, T. Chari, F. Popescu, S.S. Sabri, J. Guillemette, H.S. Skulason, T. Szkopek, M. Siaj, Chemical vapor deposition synthesis of graphene on copper with methanol, ethanol, and propanol precursors, Carbon 49 (2011) 4204–4210.
[178] S. Eissa, G.C. Jimenez, F. Mahvash, A. Guermoune, C. Tlili, T. Szkopek, M. Zourob, M. Siaj, Functionalized CVD monolayer graphene for label-free impedimetric biosensing, Nano Research 8 (2015) 1698–1709.

[179] G.K. Ramesha, S. Sampath, Electrochemical reduction of oriented graphene oxide films: an in situ raman spectroelectrochemical study, Journal of Physical Chemistry C 113 (2009) 7985–7989.
[180] H. Lim, J.S. Lee, H.-J. Shin, H.S. Shin, H.C. Choi, Spatially resolved spontaneous reactivity of diazonium salt on edge and basal plane of graphene without surfactant and its doping effect, Langmuir 26 (2010) 12278–12284.
[181] J. Guan, X. Chen, T. Wei, F.P. Liu, S. Wang, Q. Yang, Y.L. Lu, S.F. Yang, Directly bonded hybrid of graphene nanoplatelets and fullerene: facile solid-state mechanochemical synthesis and application as carbon-based electrocatalyst for oxygen reduction reaction, Journal of Materials Chemistry A 3 (2015) 4139–4146.
[182] M. Pandurangappa, T. Ramakrishnappa, Spectroscopic and thermal characterization of carbon nanotubes functionalized through diazonium salt reduction, Materials Chemistry and Physics 122 (2010) 567–573.
[183] Z. Salmi, S. Gam-Derouich, S. Mahouche-Chergui, M. Turmine, M.M. Chehimi, On the interfacial chemistry of aryl diazonium compounds in polymer science, Chemical Papers 66 (2012) 369–391.
[184] P. Doppelt, G. Hallais, J. Pinson, F. Podvorica, S. Verneyre, Surface modification of conducting substrates. Existence of azo bonds in the structure of organic layers obtained from diazonium salts, Chemistry of Materials 19 (2007) 4570–4575.
[185] A. Laforgue, T. Addou, D. Bélanger, Characterization of the deposition of organic molecules at the surface of gold by the electrochemical reduction of aryldiazonium cations, Langmuir 21 (2005) 6855–6865.
[186] A.M. Ricci, L.P. Mendez De Leo, F.J. Williams, E.J. Calvo, Some evidence for the formation of an azo bond during the electroreduction of diazonium salts on Au substrates, ChemPhysChem 13 (2012) 2119–2127.
[187] E. Pembroke, G. Ruan, A. Sinitskii, D.A. Corley, Z. Yan, Z. Sun, J.M. Tour, Effect of anchor and functional groups in functionalized graphene devices, Nano Research 6 (2013) 138–148.
[188] P. Mendes, M. Belloni, M. Ashworth, C. Hardy, K. Nikitin, D. Fitzmaurice, K. Critchley, S. Evans, J. Preece, A novel example of X-ray-radiation-induced chemical reduction of an aromatic nitro-group-containing thin film on SiO_2 to an aromatic amine film, ChemPhysChem 4 (2003) 884–889.
[189] A. Adenier, E. Cabet-Deliry, A. Chausse, S. Griveau, F. Mercier, J. Pinson, C. Vautrin-Ul, Grafting of nitrophenyl groups on carbon and metallic surfaces without electrochemical induction, Chemistry of Materials 17 (2005) 491–501.
[190] N. Lalaoui, A. Le Goff, M. Holzinger, M. Mermoux, S. Cosnier, Wiring laccase on covalently modified graphene: carbon nanotube assemblies for the direct bioelectrocatalytic reduction of oxygen, Chemistry: A European Journal 21 (2015) 3198–3201.
[191] A.S. Kumar, P. Swetha, Simple adsorption of anthraquinone on carbon nanotube modified electrode and its efficient electrochemical behaviors, Colloids and Surfaces A: Physicochemical and Engineering Aspects 384 (2011) 597–604.
[192] P.A. Brooksby, A.J. Downard, Electrochemical and atomic force microscopy study of carbon surface modification via diazonium reduction in aqueous and acetonitrile solutions, Langmuir 20 (2004) 5038–5045.
[193] S. Ernst, L. Aldous, R.G. Compton, The voltammetry of surface bound 2-anthraquinonyl groups in room temperature ionic liquids: cation size effects, Chemical Physics Letters 511 (2011) 461–465.

[194] A. Sarapuu, K. Helstein, D.J. Schiffrin, K. Tammeveski, Kinetics of oxygen reduction on quinone-modified HOPG and BDD electrodes in alkaline solution, Electrochemical and Solid State Letters 8 (2005) E30–E33.
[195] M. Kullapere, G. Jürmann, T.T. Tenno, J.J. Paprotny, F. Mirkhalaf, K. Tammeveski, Oxygen electroreduction on chemically modified glassy carbon electrodes in alkaline solution, Journal of Electroanalytical Chemistry 599 (2007) 183–193.
[196] J. Haccoun, C. Vautrin-Ul, A. Chausse, A. Adenier, Electrochemical grafting of organic coating onto gold surfaces: influence of the electrochemical conditions on the grafting of nitrobenzene diazonium salt, Progress in Organic Coatings 63 (2008) 18–24.
[197] T. Fluteau, C. Bessis, C. Barraud, M.L. Della Rocca, P. Martin, J.C. Lacroix, P. Lafarge, Tuning the thickness of electrochemically grafted layers in large area molecular junctions, Journal of Applied Physics 116 (2014) 114509.
[198] G.Z. Liu, J.Q. Liu, T. Bocking, P.K. Eggers, J.J. Gooding, The modification of glassy carbon and gold electrodes with aryl diazonium salt: the impact of the electrode materials on the rate of heterogeneous electron transfer, Chemical Physics 319 (2005) 136–146.
[199] J.J. Wu, D. Zhang, Y. Wang, Y. Wan, B.R. Hou, Catalytic activity of graphene-cobalt hydroxide composite for oxygen reduction reaction in alkaline media, Journal of Power Sources 198 (2012) 122–126.
[200] C.E. Banks, G.G. Wildgoose, C.G.R. Heald, R.G. Compton, Oxygen reduction catalysis at anthraquinone centres molecularly wired via carbon nanotubes, Journal of the Iranian Chemical Society 2 (2005) 60–64.
[201] S. Zhao, G.Q. Zhang, L. Fu, L.F. Liu, X.H. Fang, F.L. Yang, Enhanced electrocatalytic performance of anthraquinonemonosulfonate-doped polypyrrole composite: electroanalysis for the specific roles of anthraquinone derivative and polypyrrole layer on oxygen reduction reaction, Electroanalysis 23 (2011) 355–363.
[202] P. Manisankar, A. Gomathi, Electrocatalysis of oxygen reduction at polypyrrole modified glassy carbon electrode in anthraquinone solutions, Journal of Molecular Catalysis A: Chemical 232 (2005) 45–52.
[203] S. Valarselvan, P. Manisankar, Electrocatalytic reduction of oxygen at glassy carbon electrode modified by polypyrrole/anthraquinones composite film in various pH media, Electrochimica Acta 56 (2011) 6945–6953.
[204] R.E. Davis, G.L. Horvath, C.W. Tobias, The solubility and diffusion coefficient of oxygen in potassium hydroxide solutions, Electrochimica Acta 12 (1967) 287–297.
[205] D.R. Lide (Ed.), CRC Handbook of Chemistry and Physics, 82nd ed., CRC Press, Boca Raton, 2001, p. 2664.
[206] S. Ratso, I. Kruusenberg, M. Vikkisk, U. Joost, E. Shulga, I. Kink, T. Kallio, K. Tammeveski, Highly active nitrogen-doped few-layer graphene/carbon nanotube composite electrocatalyst for oxygen reduction reaction in alkaline media, Carbon 73 (2014) 361–370.
[207] A. Sarapuu, K. Helstein, K. Vaik, D.J. Schiffrin, K. Tammeveski, Electrocatalysis of oxygen reduction by quinones adsorbed on highly oriented pyrolytic graphite electrodes, Electrochimica Acta 55 (2010) 6376–6382.
[208] M. Kullapere, L. Matisen, A. Saar, V. Sammelselg, K. Tammeveski, Electrochemical behaviour of nickel electrodes modified with nitrophenyl groups, Electrochemistry Communications 9 (2007) 2412–2417.

[209] M. Kullapere, M. Marandi, V. Sammelselg, H.A. Menezes, G. Maia, K. Tammeveski, Surface modification of gold electrodes with anthraquinone diazonium cations, Electrochemistry Communications 11 (2009) 405–408.
[210] L. Lee, P.A. Brooksby, P. Hapiot, A.J. Downard, Electrografting of 4-nitrobenzenediazonium ion at carbon electrodes: catalyzed and uncatalyzed reduction processes, Langmuir 32 (2016) 468–76.
[211] E.P. Koval'chuk, O.V. Reshetnyak, O.B. Pereviznyk, I.E. Marchuk, V.Y. Smetanets'kyj, J. Blazejowski, Reaction of metals with benzenediazonium tetrafluoroborate in aprotic solvents, Central European Journal of Chemistry 8 (2010) 652–661.
[212] J. Greenwood, P. Thanh Hai, Y. Fujita, Z. Li, O. Lvasenko, W. Vanderlinden, H. Van Gorp, W. Frederickx, G. Lu, K. Tahara, Y. Tobe, H. Uji-i, S.F.L. Mertens, S. De Feyter, Covalent modification of graphene and graphite using diazonium chemistry: tunable grafting and nanomanipulation, ACS Nano 9 (2015) 5520–5535.
[213] A. Adenier, C. Combellas, F. Kanoufi, J. Pinson, F.I. Podvorica, Formation of polyphenylene films on metal electrodes by electrochemical reduction of benzenediazonium salts, Chemistry of Materials 18 (2006) 2021–2029.
[214] S.F.L. Mertens, A. Butikofer, L. Siffert, T. Wandlowski, Covalent versus electrostatic strategies for nanoparticle immobilisation, Electroanalysis 22 (2010) 2940–2946.
[215] I. Tabakovic, S. Riemer, M. Sun, Self-assembled monolayer of 3-N,N-Dimethylaminodithiocarbamoyl-1-propanesulfonic acid (DPS) used in electrodeposition of copper, Journal of the Electrochemical Society 160 (2013) D3197–D3205.
[216] C. Combellas, D.E. Jiang, F. Kanoufi, J. Pinson, F.I. Podvorica, Steric effects in the reaction of aryl radicals on surfaces, Langmuir 25 (2009) 286–293.
[217] J. Lyskawa, D. Bélanger, Direct modification of a gold electrode with aminophenyl groups by electrochemical reduction of in situ generated aminophenyl monodiazonium cations, Chemistry of Materials 18 (2006) 4755–4763.
[218] I. Bakas, Z. Salmi, S. Gam-Derouich, M. Jouini, S. Lepinay, B. Carbonnier, A. Khlifi, R. Kalfat, F. Geneste, Y. Yagci, M.M. Chehimi, Molecularly imprinted polymeric sensings layers grafted from aryl diazonium-modified surfaces for electroanalytical applications. A mini review, Surface and Interface Analysis 46 (2014) 1014–1020.
[219] C.L. Chevalier, E.C. Landis, Electrochemical attachment of diazonium-generated films on nanoporous gold, Langmuir 31 (2015) 8633–8641.
[220] I. Gallardo, J. Pinson, N. Vila, Spontaneous attachment of amines to carbon and metallic surfaces, Journal of Physical Chemistry B 110 (2006) 19521–19529.
[221] M.S. Xie, B.Y. Xia, Y. Li, Y. Yan, Y. Yang, Q. Sun, S.H. Chan, A. Fisher, X. Wang, Amino acid modified copper electrodes for the enhanced selective electroreduction of carbon dioxide towards hydrocarbons, Energy & Environmental Science 9 (2016) 1687–1695.
[222] M. Grden, Interfacial capacitance of an oxidised copper electrode, Journal of Electroanalytical Chemistry 713 (2014) 47–57.
[223] C. Combellas, F. Kanoufi, J. Pinson, F.I. Podvorica, Sterically hindered diazonium salts for the grafting of a monolayer on metals, Journal of the American Chemical Society 130 (2008) 8576–8577.
[224] T. Takahagi, I. Shimada, M. Fukuhara, K. Morita, A. Ishitani, XPS Studies on the chemical-structure of the stabilized polyacrylonitrile fiber in the carbon-fiber

production process, Journal of Polymer Science Part A: Polymer Chemistry 24 (1986) 3101–3107.
[225] M. D'Amours, D. Bélanger, Stability of substituted phenyl groups electrochemically grafted at carbon electrode surface, Journal of Physical Chemistry B 107 (2003) 4811–4817.
[226] K. Shimizu, K. Malmos, S.A. Spiegelhauer, J. Hinke, A.H. Holm, S.U. Pedersen, K. Daasbjerg, M. Hinge, Durability of PEEK adhesive to stainless steel modified with aryldiazonium salts, International Journal of Adhesion and Adhesives 51 (2014) 1–12.
[227] P.A. Brooksby, J.D. Shields, A.K. Farquhar, A.J. Downard, Reduction of nitrophenyl films in aqueous solutions: how many electrons?, ChemElectroChem 3 (2016) 2021–2026.
[228] M. Ceccato, L.T. Nielsen, J. Iruthayaraj, M. Hinge, S.U. Pedersen, K. Daasbjerg, Nitrophenyl groups in diazonium-generated multilayered films: which are electrochemically responsive?, Langmuir 26 (2010) 10812–10821.
[229] A. Mesnage, X. Lefevre, P. Jegou, G. Deniau, S. Palacin, Spontaneous grafting of diazonium salts: chemical mechanism on metallic surfaces, Langmuir 28 (2012) 11776–11787.
[230] J. Heyrovský, J. Kúta, Principles of Polarography, Academic Press, New York, 1966.
[231] M.G. Paulik, P.A. Brooksby, A.D. Abell, A.J. Downard, Grafting aryl diazonium cations to polycrystalline gold: insights into film structure using gold oxide reduction, redox probe electrochemistry, and contact angle behavior, Journal of Physical Chemistry C 111 (2007) 7808–7815.
[232] S. Baranton, D. Bélanger, Electrochemical derivatization of carbon surface by reduction of in situ generated diazonium cations, Journal of Physical Chemistry B 109 (2005) 24401–24410.
[233] J. Mason, C. Batchelor-McAuley, R.G. Compton, Surface modification imparts selectivity, facilitating redox catalytic studies: quinone mediated oxygen reduction, Physical Chemistry Chemical Physics 15 (2013) 8362–8366.
[234] A. Sarapuu, M. Nurmik, H. Mändar, A. Rosental, T. Laaksonen, K. Kontturi, D.J. Schiffrin, K. Tammeveski, Electrochemical reduction of oxygen on nanostructured gold electrodes, Journal of Electroanalytical Chemistry 612 (2008) 78–86.
[235] H. Erikson, G. Jürmann, A. Sarapuu, R.J. Potter, K. Tammeveski, Electroreduction of oxygen on carbon-supported gold catalysts, Electrochimica Acta 54 (2009) 7483–7489.
[236] H.H. Yang, R.L. McCreery, Elucidation of the mechanism of dioxygen reduction on metal-free carbon electrodes, Journal of the Electrochemical Society 147 (2000) 3420–3428.
[237] X.Q. Yang, D.C. Wu, R.W. Fu, Nanoporous carbon produced from a styrene-acrylonitrile random copolymer/carbon nanotube composite, Micro & Nano Letters 5 (2010) 105–109.
[238] M. Kim, D.H. Nam, H.Y. Park, C. Kwon, K. Eom, S. Yoo, J. Jang, H.J. Kim, E. Cho, H. Kwon, Cobalt-carbon nanofibers as an efficient support-free catalyst for oxygen reduction reaction with a systematic study of active site formation, Journal of Materials Chemistry A 3 (2015) 14284–14290.
[239] S. Igarashi, H. Kambe, Thermogravimetric analysis of styrene-acrylonitrile copolymer, Macromolecular Chemistry and Physics 79 (1964) 180–188.

[240] B.A. Zhang, F.Y. Kang, J.M. Tarascon, J.K. Kim, Recent advances in electrospun carbon nanofibers and their application in electrochemical energy storage, Progress in Materials Science 76 (2016) 319–380.
[241] C.M. White, R. Banks, I. Hamerton, J.F. Watts, Characterisation of commercially CVD grown multi-walled carbon nanotubes for paint applications, Progress in Organic Coatings 90 (2016) 44–53.
[242] T. Sharifi, G. Hu, X.E. Jia, T. Wagberg, Formation of active sites for oxygen reduction reactions by transformation of nitrogen functionalities in nitrogen-doped carbon nanotubes, ACS Nano 6 (2012) 8904–8912.
[243] R. Arrigo, M. Havecker, R. Schlogl, D.S. Su, Dynamic surface rearrangement and thermal stability of nitrogen functional groups on carbon nanotubes, Chemical Communications 40 (2008) 4891–4893.
[244] X.D. Zhang, X.X. Huang, G.W. Wen, X. Geng, J.D. Zhu, T. Zhang, H.W. Bai, Novel SiOC nanocomposites for high-yield preparation of ultra-large-scale SiC nanowires, Nanotechnology 21 (2010) 385601.
[245] Z.Q. Luo, S.H. Lim, Z.Q. Tian, J.Z. Shang, L.F. Lai, B. MacDonald, C. Fu, Z.X. Shen, T. Yu, J.Y. Lin, Pyridinic N doped graphene: synthesis, electronic structure, and electrocatalytic property, Journal of Materials Chemistry 21 (2011) 8038–8044.
[246] D.M.K. Abro, P. Dablé, F. Cortés-Salazar, V. Amstutz, H. Girault, Characterization of surface state of inert particles: case of Si and SiC, Journal of Minerals and Materials Characterization and Engineering 4 (2916) 62–72.
[247] S. Roualdes, R. Berjoan, J. Durand, ^{29}Si NMR and Si2p XPS correlation in polysiloxane membranes prepared by plasma enhanced chemical vapor deposition, Separation and Purification Technology 25 (2001) 391–397.
[248] V.L. Nguyen, N.B. Laidani, G.D. Soraru, N-doped polymer-derived Si(N)OC: the role of the N-containing precursor, Journal of Materials Research 30 (2015) 770–781.
[249] K. Yamamoto, Y. Koga, S. Fujiwara, XPS studies of amorphous SiCN thin films prepared by nitrogen ion-assisted pulsed-laser deposition of SiC target, Diamond and Related Materials 10 (2001) 1921–1926.
[250] S.H. Gage, D.A. Ruddy, S. Pylypenko, R.M. Richards, Deep eutectic solvent approach towards nickel/nickel nitride nanocomposites, Catalysis Today 306 (2018) 9–15.
[251] H.S. Oh, H. Kim, The role of transition metals in non-precious nitrogen-modified carbon-based electrocatalysts for oxygen reduction reaction, Journal of Power Sources 212 (2012) 220–225.
[252] F. Beguin, K. Szostak, G. Lota, E. Frackowiak, A self-supporting electrode for supercapacitors prepared by one-step pyrolysis of carbon nanotube/polyacrylonitrile blends, Advanced Materials 17 (2005) 2380–2384.
[253] S. Jagannathan, T. Liu, S. Kumar, Pore size control and electrochemical capacitor behavior of chemically activated polyacrylonitrile – carbon nanotube composite films, Composites Science and Technology 70 (2010) 593–598.
[254] R.J. Taylor, A.A. Humffray, Electrochemical studies on glassy carbon electrodes: II. Oxygen reduction in solutions of high pH (pH>10), Journal of Electroanalytical Chemistry and Interfacial Electrochemistry 64 (1975) 63–84.
[255] Q. Liu, S. Cao, Y. Fu, Y. Guo, Y. Qiu, Trimetallic FeCoNi-N/C nanofibers with high electrocatalytic activity for oxygen reduction reaction in sulfuric acid solution, Journal of Electroanalytical Chemistry 813 (2018) 52–57.

[256] M. Vikkisk, I. Kruusenberg, U. Joost, E. Shulga, K. Tammeveski, Electrocatalysis of oxygen reduction on nitrogen-containing multi-walled carbon nanotube modified glassy carbon electrodes, Electrochimica Acta 87 (2013) 709–716.
[257] M. Vikkisk, I. Kruusenberg, U. Joost, E. Shulga, I. Kink, K. Tammeveski, Electrocatalytic oxygen reduction on nitrogen-doped graphene in alkaline media, Applied Catalysis B: Environmental 147 (2014) 369–376.
[258] N. Gavrilov, M. Momcilovic, A.S. Dobrota, D.M. Stankovic, B. Jokic, B. Babic, N.V. Skorodumova, S.V. Mentus, I.A. Pasti, A study of ordered mesoporous carbon doped with Co and Ni as a catalyst of oxygen reduction reaction in both alkaline and acidic media, Surface & Coatings Technology 349 (2018) 511–521.
[259] A. Abdelwahab, J. Castelo-Quibén, J. Vivo-Vilches, M. Pérez-Cadenas, F. Maldonado-Hódar, F. Carrasco-Marín, A. Pérez-Cadenas, Electrodes based on carbon aerogels partially graphitized by doping with transition metals for oxygen reduction reaction, Nanomaterials 8 (2018) 266.
[260] S.S. Liu, C.W. Deng, L. Yao, H.X. Zhong, H.M. Zhang, The key role of metal dopants in nitrogen-doped carbon xerogel for oxygen reduction reaction, Journal of Power Sources 269 (2014) 225–235.
[261] K. Wan, Z.P. Yu, X.H. Li, M.Y. Liu, G. Yang, J.H. Piao, Z.X. Liang, pH effect on electrochemistry of nitrogen-doped carbon catalyst for oxygen reduction reaction, ACS Catalysis 5 (2015) 4325–4332.
[262] G. Liu, X.G. Li, P. Ganesan, B.N. Popov, Development of non-precious metal oxygen-reduction catalysts for PEM fuel cells based on N-doped ordered porous carbon, Applied Catalysis B: Environmental 93(1–2) (2009) 156–165.
[263] J.Y. Chen, X. Wang, X.Q. Cui, G.M. Yang, W.T. Zheng, Amorphous carbon enriched with pyridinic nitrogen as an efficient metal-free electrocatalyst for oxygen reduction reaction, Chemical Communications 50 (2014) 557–559.
[264] S.K. Singh, K. Takeyasu, J. Nakamura, Active sites and mechanism of oxygen reduction reaction electrocatalysis on nitrogen-doped carbon materials, Advanced Materials 31 (2019) 1804297.
[265] K.K. Türk, I. Kruusenberg, E. Kibena-Põldsepp, G.D. Bhowmick, M. Kook, K. Tammeveski, L. Matisen, M. Merisalu, V. Sammelselg, M.M. Ghangrekar, A. Mitra, R. Banerjee, Novel multi walled carbon nanotube based nitrogen impregnated Co and Fe cathode catalysts for improved microbial fuel cell performance, International Journal of Hydrogen Energy 43 (2018) 23027–23035.
[266] Z. Liu, X. Fu, M. Li, F. Wang, Q. Wang, G. Kang, F. Peng, Novel silicon-doped, silicon and nitrogen-codoped carbon nanomaterials with high activity for the oxygen reduction reaction in alkaline medium, Journal of Materials Chemistry A 3 (2015) 3289–3293.
[267] S.C. Abbas, K. Ding, Q. Liu, Y. Huang, Y. Bu, J. Wu, J. Lv, M.A. Ghausi, Y. Wang, Si–C–F decorated porous carbon materials: a new class of electrocatalysts for the oxygen reduction reaction, Journal of Materials Chemistry A 4(20) (2016) 7924–7929.

10. SUMMARY IN ESTONIAN

Arüülkilede ja nanokomposiitmaterjalidega modifitseeritud süsinik- ja metallelektroodide pinna ja elektrokeemiliste omaduste karakteriseerimine

Käesoleva doktoritöö eesmärk oli valmistada ja uurida arüülkiledega modifitseeritud süsinik- ja metallelektroodide ning mitteväärismetallidel põhinevate katalüsaatormaterjalide pinna- ja elektrokeemilisi omadusi. Sellest lähtuvalt on käesolev doktoritöö jagatud kolmeks osaks.

Doktoritöö esimene osa kirjeldab süsinikelektroodide modifitseerimist erinevate arüülkiledega ning valmistatud elektroodide füüsikalist ja elektrokeemilist karakteriseerimist [I–VI]. Mitmeseinaliste süsiniknanotorude (MWCNT) ja grafeeni funktsionaliseerimine 9,10-antrakinooni (AQ) rühmadega viidi läbi diasooniumisoolade redutseerumise meetodil nii spontaanselt kui ka „tavalisel" elektrokeemilisel meetodil [I, II]. Keemilisel aurufaasist sadestamise meetodil valmistatud grafeeni (CVD-GR) ja klaassüsinik elektroodidel (GC) valmistati lisaks paksusid AQ ja 4-nitrofenüülrühmade (NP) kilesid redokspookimise meetodil [III, V]. Redokspookimise meetodil valmistatud NP kile paksus CVD-GR elektroodil oli 30 nm [III]. GC elektroodidel valmistati lisaks ka metüülantrakinooni (MAQ) kilesid. Valmistatud MAQ kiled olid vähem kui monokihi paksused võrreldes mitmekihiliste AQ kiledega GC elektroodide korral [IV, V]. Viimasena valmistati paksusid AQ kilesid GC elektroodidel teadaolevalt esmakordselt redokspookimise ja pöörleva ketaselektroodi (RDE) kombineeritud meetodil [VI]. Sellisel viisil valmistatud AQ kiles määrati ka suurim teadaolev AQ elektroaktiivsete rühmade hulk (Γ_{AQ}) GC elektroodil (18 nmol cm^{-2}) [VI].

Hapniku redutseerumise uuringud aluselises keskkonnas viidi läbi AQ kiledega modifitseeritud süsinikmaterjalidega ja (M)AQ kiledega kaetud GC elektroodidel [I, II, IV–V]. Kõige aktiivsem katalüsaatormaterjal hapniku redutseerumisel oli AQ rühmadega spontaanselt modifitseeritud MWCNT [II]. Erinev elektroaktiivsete MAQ ja AQ rühmade hulk arüülkiles GC elektroodidel ei mõjutanud hapniku redutseerumise elektrokatalüüsi efektiivsust. Küll aga oli märgata rohkem hapniku redutseerumise inhibeerimist GC enda tsentritel paksemate AQ kilede korral võrreldes õhemate MAQ kiledega [IV, V]. Anioonvahetus polümeeri (OH^- ionomeer) kasutamise puhul katalüsaatormaterjali koostises oli märgata voolu mõningat inhibeerimist OH^- ionomeeri kasutamise tõttu [I, II]. Lisaks viidi läbi ka pinna blokeerumise uuringud redokspookimise ja RDE kombineeritud meetodil valmistatud AQ kiledega GC elektroodidel. Vastavate AQ kilede tõttu oli $Fe(CN)_6^{3-/4-}$ redokspaari vool elektroodidel tugevalt maha surutud võrreldes puhta GC elektroodiga [VI].

Doktoritöö teises osas uuriti NP ja AQ arüülkilede valmistamist ja kilede füüsikalisi ning elektrokeemilisi omadusi metallelektroodidel (Au, Ni, Cu) [VI–VIII]. Arüülkilede olemasolule modifitseeritud elektroodidel saadi kinnitust röntgenfotoelektronspektroskoopia (XPS) ja aatomjõumikroskoopia (AFM)

eksperimentidest. Kõige paksem arüülkile käesolevas doktoritöös (47 nm) mõõdeti NP kilega Cu elektroodil, mis oli valmistatud redokspookimise ja RDE kombineeritud meetodil (Cu-NP-RDE-1.5) [VIII]. Redokspookimise meetodil valmistatud NP kile Ni elektroodil oli paksem võrreldes „tavalise" elektrokeemilise meetodiga valmistatud NP kilega [VII]. Redokspookimise ja RDE kombineeritud meetod osutus efektiivsemaks paksemate arüülkilede valmistamiseks Au ja Cu elektroodidel võrreldes ainult redokspookimise meetodiga [VI, VIII]. Kasutades redokspookimise ja RDE kombineeritud meetodit valmistati suurima teadaoleva Γ_{AQ} väärtusega AQ kiled vask- (12 nmol cm^{-2}, Cu-AQ-RDE-1.5) ja kuldelektroodidel (21 nmol cm^{-2}, Au/AQ-10) [VI, VIII]. Pinna blokeerimine $Fe(CN)_6^{3-/4-}$ redokspaari suhtes oli efektiivsem NP kilega kaetud Ni elektroodi puhul, mis oli valmistatud redokspookimise meetodil [VII]. AQ kiledega kaetud Au elektroodide puhul oli kõige efektiivsem pinna blokeerimine $Fe(CN)_6^{3-/4}$ redokspaari suhtes redokspookimise ja RDE kombineeritud meetodil valmistatud kile korral (Au/AQ-10) [VI]. Cu elektroodide korral oli elektroodi pind $Fe(CN)_6^{3-/4}$ redokspaari jaoks kõige efektiivsemalt blokeeritud redokspookimise meetodil tehtud NP kile ja redokspookimise ning RDE kombineeritud meetodil tehtud AQ kile korral [VIII]. Hapniku redutseerumise blokeerimine arüülkiledega modifitseeritud Au ja Cu elektroodidel ei olnud niivõrd efektiivne kui $Fe(CN)_6^{3-/4}$ redokspaari korral. Arüülkiledega modifitseeritud Cu elektroodide puhul olenes arüülkile blokeerimise mõju hapniku redutseerumisele kasutatud modifitseerimisprotseduurist [VIII].

Doktoritöö viimases osas uuriti elektrokedratud polümeeridel põhinevaid süsiniknanotorusid sisaldavaid materjale (SAN-MWCNT, SAN/PAN/CNT) ja ränioksükarbiidil põhinevaid materjale eesmärgiga kasutada neid mitte-väärismetallkatalüsaatorina hapniku redutseerumisreaktsiooni jaoks [IX–XI]. Kõige efektiivsem SAN-MWCNT materjalil põhinev hapniku redutseerumise katalüsaator valmistati pürolüüsil 800–900 °C juures ning lisaks oli elektrokeemiliste katsete käigus märgata ka OH^- ionomeeri inhibeerivat mõju hapniku redutseerumisele [IX]. SAN/PAN/CNT materjali korral õnnestus valmistada kõige efektiivsem hapniku redutseerumise katalüsaator 1100 °C juures [X]. XPS analüüsi põhjal sisaldasid mõlemad polümeeridel põhinevad ja süsiniknanotorusid sisaldavad katalüsaatormaterjalid elemente O, N ja C. Ränioksükarbiidil põhinevate materjalide korral osutus kõige aktiivsemaks katalüsaatoriks siirdemetalli (Co) sisaldav materjal, mida oli dopeeritud lämmastikuga pürolüüsil 800 °C juures kasutades lämmastikuallikana ditsüaandiamiidi. Antud materjalil toimus 4-elektroniline hapniku redutseerumine ning veel täheldati, et vastav reaktsioon algas suhteliselt madalal ülepingel [XI]. Lisaks testiti seda materjali ka neutraalses keskkonnas eesmärgiga kasutada valmistatud katalüsaatormaterjali mikroobse kütuselemendi katoodil. Antud katalüsaatormaterjali hapniku redutseerumise aktiivsuse olulisimaks põhjuseks leiti olevat materjali struktuuri pürolüüsi käigus viidud aktiivsed lämmastikurühmad ja siirdemetall [XI].

11. ACKNOWLEDGEMENTS

First I would like to thank my supervisors Dr. Elo Kibena-Põldsepp and Assoc. Prof. Kaido Tammeveski for continuous support, patience and contribution to my work during my academic studies in the University of Tartu.

Also, I would like to thank all the co-authors and contributors of the scientific publications that present PhD thesis is based on: Dr. Jaan Aruväli, Prof. Daniel Bélanger, Thamires Canuto de Almeida e Silva, Dr. Vambola Kisand, Mati Kook, Jekaterina Kozlova, Prof. Andres Krumme, Prof. Gilberto Maia, Dr. Margus Marandi, Dr. Leonard Matisen, Maido Merisalu, Dr. Uno Mäeorg, Dr. Ahti Niilisk, Dr. Benjamin Diby Ossonon, Prof. Fetah I. Podvorica, Prof. Väino Sammelselg, Dr. Ave Sarapuu, Prof. Kurosch Rezwan, Dr. Alexey Treshchalov, Dr. Mai Uibu, Dr. Viktoria Vassiljeva, Dr. Michaela Wilhelm. Additionally, I would like to thank all the present and former colleagues from the Institute of Chemistry for their support and advice.

Additionally, I would like to thank my friends and family, especially my parents, Kersti Mooste and Mart Mooste, for their support and guidance throughout my studies in the University of Tartu. Special gratitude goes to Triinu Loorents for her patience and support throughout the PhD studies. Also, I am very grateful for Mare Kekkonen from Pärnu Old Town Elementary School and Evelin Saks from Pärnu Co-educational Gymnasium for generating and maintaining the interest in Chemistry prior to my studies in the University of Tartu.

This work has been financially supported by the European Union through the European Regional Development Fund (TK141 “Advanced materials and high-technology devices for energy recuperation systems” and Smart specialisation scholarship for Marek Mooste). This work was also financially supported by Estonian Ministry of Education and Research (IUT20-16 and IUT02-24), Estonian Research Council (Grant No. 9323, TK117 and INNO INDIGO project), Education Agency Archimedes (Kristjan Jaak Scholarships for Marek Mooste) and Graduate School of Functional materials and technologies receiving funding from the European Regional Development Fund in University of Tartu, Estonia.

12. PUBLICATIONS

CURRICULUM VITAE

Name: Marek Mooste
Date of birth: July 24, 1990
Citizenship: Estonian
Address: Ravila 14a, 50411 Tartu, Estonia
Phone: +372 5348 4229
E-mail: marek.mooste@ut.ee

Education:

2015–	University of Tartu, PhD student, Chemistry
2012–2014	University of Tartu, MSc, Materials Science
2009–2012	University of Tartu, BSc, Chemistry

Professional employment:

2012–	University of Tartu, Institute of Chemistry, chemist

Major scientific publications:

1. M. Mooste, E. Kibena, A. Sarapuu, L. Matisen, K. Tammeveski, Oxygen reduction on thick anthraquinone films electrografted to glassy carbon, *Journal of Electroanalytical Chemistry* 702 (2013) 8–14.
2. E. Kibena, M. Mooste, J. Kozlova, M. Marandi, V. Sammelselg, K. Tammeveski, Surface and electrochemical characterisation of CVD grown graphene sheets, *Electrochemistry Communications* 35 (2013) 26–29.
3. M. Mooste, E. Kibena, A. Sarapuu, U. Mäeorg, G. Maia, K. Tammeveski, Electrocatalysis of oxygen reduction on glassy carbon electrodes modified with anthraquinone moieties, *Journal of Solid State Electrochemistry* 18 (2014) 1725–1733.
4. M. Mooste, E. Kibena, J. Kozlova, M. Marandi, L. Matisen, A. Niilisk, V. Sammelselg, K. Tammeveski, Electrografting and morphological studies of chemical vapour deposition grown graphene sheets modified by electro-reduction of aryldiazonium salts, *Electrochimica Acta* 161 (2015) 195–204.
5. M. Mooste, E. Kibena, L. Matisen, K. Tammeveski, Blocking properties of nickel electrodes modified with aryldiazonium compounds, *International Journal of Electrochemical Science* 10 (2015) 3803–3819.
6. M. Mooste, E. Kibena-Põldsepp, M. Marandi, L. Matisen, V. Sammelselg, K. Tammeveski, Electrochemical properties of gold and glassy carbon electrodes electrografted with an anthraquinone diazonium compound using the rotating disc electrode method, *RSC Advances* 6 (2016) 40982–40990.
7. M. Mooste, E. Kibena-Põldsepp, L. Matisen, K. Tammeveski, Oxygen reduction on anthraquinone diazonium compound derivatised multi-walled

carbon nanotube and graphene based electrodes, *Electroanalysis* 29 (2017) 548–558.
8. M. Mooste, E. Kibena-Põldsepp, B.D. Ossonon, D. Bélanger, K. Tammeveski, Oxygen reduction on graphene sheets functionalised by anthraquinone diazonium compound during electrochemical exfoliation of graphite, *Electrochimica Acta* 267 (2018) 246–254.
9. M. Mooste, E. Kibena-Põldsepp, M. Marandi, L. Matisen, V. Sammelselg, F.I. Podvorica, K. Tammeveski, Surface and electrochemical characterization of aryl films grafted on polycrystalline copper from the diazonium compounds using the rotating disk electrode method, *Journal of Electroanalytical Chemistry* 817 (2018) 89–100.
10. M. Mooste, E. Kibena-Põldsepp, L. Matisen, M. Merisalu, M. Kook, V. Kisand, V. Vassiljeva, A. Krumme, V. Sammelselg, K. Tammeveski, Oxygen reduction on catalysts prepared by pyrolysis of electrospun styrene-acrylonitrile copolymer and multi-walled carbon nanotube composite fibres, *Catalysis Letters* 148 (2018) 1815–1826.
11. J. Metsik, M. Timusk, A. Sutka, M. Mooste, K. Tammeveski, U. Mäeorg, In situ investigation of poly(3,4-ethylenedioxythiophene) film growth during liquid phase deposition polymerization, *Thin Solid Films* 653 (2018) 274–283.
12. T. Canuto de Almeida e Silva, M. Mooste, E. Kibena-Põldsepp, L. Matisen, M. Merisalu, M. Kook, V. Sammelselg, K. Tammeveski, M. Wilhelm, K. Rezwan, Polymer-derived Co/Ni–SiOC(N) ceramic electrocatalysts for oxygen reduction reaction in fuel cells, *Catalysis Science & Technology* 9 (2019) 854–866.
13. M. Mooste, E. Kibena-Põldsepp, V. Vassiljeva, M. Merisalu, M. Kook, A. Treshchalov, V. Kisand, M. Uibu, A. Krumme, V. Sammelselg, K. Tammeveski, Electrocatalysts for oxygen reduction reaction based on electrospun polyacrylonitrile, styrene-acrylonitrile copolymer and carbon nanotube composite fibres, *Journal of Materials Science* 54 (2019), 11618–11634.

ELULOOKIRJELDUS

Nimi: Marek Mooste
Sünniaeg: 24. juuli 1990
Kodakondsus: Eesti
Aadress: Ravila 14a, 50411 Tartu, Eesti
Telefon: +372 5348 4229
E-post: marek.mooste@ut.ee

Haridus:

2015–	Tartu Ülikool, Doktorant, Keemia eriala
2012–2014	Tartu Ülikool, MSc, Materjaliteaduse eriala
2009–2012	Tartu Ülikool, BSc, Keemia eriala

Teenistuskäik:

2012–	Tartu Ülikool, Keemia Instituut, keemik

Olulisemad publikatsioonid:

1. M. Mooste, E. Kibena, A. Sarapuu, L. Matisen, K. Tammeveski, Oxygen reduction on thick anthraquinone films electrografted to glassy carbon, *Journal of Electroanalytical Chemistry* 702 (2013) 8–14.
2. E. Kibena, M. Mooste, J. Kozlova, M. Marandi, V. Sammelselg, K. Tammeveski, Surface and electrochemical characterisation of CVD grown graphene sheets, *Electrochemistry Communications* 35 (2013) 26–29.
3. M. Mooste, E. Kibena, A. Sarapuu, U. Mäeorg, G. Maia, K. Tammeveski, Electrocatalysis of oxygen reduction on glassy carbon electrodes modified with anthraquinone moieties, *Journal of Solid State Electrochemistry* 18 (2014) 1725–1733.
4. M. Mooste, E. Kibena, J. Kozlova, M. Marandi, L. Matisen, A. Niilisk, V. Sammelselg, K. Tammeveski, Electrografting and morphological studies of chemical vapour deposition grown graphene sheets modified by electro-reduction of aryldiazonium salts, *Electrochimica Acta* 161 (2015) 195–204.
5. M. Mooste, E. Kibena, L. Matisen, K. Tammeveski, Blocking properties of nickel electrodes modified with aryldiazonium compounds, *International Journal of Electrochemical Science* 10 (2015) 3803–3819.
6. M. Mooste, E. Kibena-Põldsepp, M. Marandi, L. Matisen, V. Sammelselg, K. Tammeveski, Electrochemical properties of gold and glassy carbon electrodes electrografted with an anthraquinone diazonium compound using the rotating disc electrode method, *RSC Advances* 6 (2016) 40982–40990.
7. M. Mooste, E. Kibena-Põldsepp, L. Matisen, K. Tammeveski, Oxygen reduction on anthraquinone diazonium compound derivatised multi-walled carbon nanotube and graphene based electrodes, *Electroanalysis* 29 (2017) 548–558.

8. M. Mooste, E. Kibena-Põldsepp, B.D. Ossonon, D. Bélanger, K. Tammeveski, Oxygen reduction on graphene sheets functionalised by anthraquinone diazonium compound during electrochemical exfoliation of graphite, *Electrochimica Acta* 267 (2018) 246–254.
9. M. Mooste, E. Kibena-Põldsepp, M. Marandi, L. Matisen, V. Sammelselg, F.I. Podvorica, K. Tammeveski, Surface and electrochemical characterization of aryl films grafted on polycrystalline copper from the diazonium compounds using the rotating disk electrode method, *Journal of Electroanalytical Chemistry* 817 (2018) 89–100.
10. M. Mooste, E. Kibena-Põldsepp, L. Matisen, M. Merisalu, M. Kook, V. Kisand, V. Vassiljeva, A. Krumme, V. Sammelselg, K. Tammeveski, oxygen reduction on catalysts prepared by pyrolysis of electrospun styrene-acrylonitrile copolymer and multi-walled carbon nanotube composite fibres, *Catalysis Letters* 148 (2018) 1815–1826.
11. J. Metsik, M. Timusk, A. Sutka, M. Mooste, K. Tammeveski, U. Mäeorg, In situ investigation of poly(3,4-ethylenedioxythiophene) film growth during liquid phase deposition polymerization, *Thin Solid Films* 653 (2018) 274–283.
12. T. Canuto de Almeida e Silva, M. Mooste, E. Kibena-Põldsepp, L. Matisen, M. Merisalu, M. Kook, V. Sammelselg, K. Tammeveski, M. Wilhelm, K. Rezwan, Polymer-derived Co/Ni–SiOC(N) ceramic electrocatalysts for oxygen reduction reaction in fuel cells, *Catalysis Science & Technology* 9 (2019) 854–866.
13. M. Mooste, E. Kibena-Põldsepp, V. Vassiljeva, M. Merisalu, M. Kook, A. Treshchalov, V. Kisand, M. Uibu, A. Krumme, V. Sammelselg, K. Tammeveski, Electrocatalysts for oxygen reduction reaction based on electrospun polyacrylonitrile, styrene-acrylonitrile copolymer and carbon nanotube composite fibres, *Journal of Materials Science* 54 (2019), 11618–11634.

DISSERTATIONES CHIMICAE UNIVERSITATIS TARTUENSIS

1. **Toomas Tamm.** Quantum-chemical simulation of solvent effects. Tartu, 1993, 110 p.
2. **Peeter Burk.** Theoretical study of gas-phase acid-base equilibria. Tartu, 1994, 96 p.
3. **Victor Lobanov.** Quantitative structure-property relationships in large descriptor spaces. Tartu, 1995, 135 p.
4. **Vahur Mäemets.** The ^{17}O and ^{1}H nuclear magnetic resonance study of H_2O in individual solvents and its charged clusters in aqueous solutions of electrolytes. Tartu, 1997, 140 p.
5. **Andrus Metsala.** Microcanonical rate constant in nonequilibrium distribution of vibrational energy and in restricted intramolecular vibrational energy redistribution on the basis of slater's theory of unimolecular reactions. Tartu, 1997, 150 p.
6. **Uko Maran.** Quantum-mechanical study of potential energy surfaces in different environments. Tartu, 1997, 137 p.
7. **Alar Jänes.** Adsorption of organic compounds on antimony, bismuth and cadmium electrodes. Tartu, 1998, 219 p.
8. **Kaido Tammeveski.** Oxygen electroreduction on thin platinum films and the electrochemical detection of superoxide anion. Tartu, 1998, 139 p.
9. **Ivo Leito.** Studies of Brønsted acid-base equilibria in water and non-aqueous media. Tartu, 1998, 101 p.
10. **Jaan Leis.** Conformational dynamics and equilibria in amides. Tartu, 1998, 131 p.
11. **Toonika Rinken.** The modelling of amperometric biosensors based on oxidoreductases. Tartu, 2000, 108 p.
12. **Dmitri Panov.** Partially solvated Grignard reagents. Tartu, 2000, 64 p.
13. **Kaja Orupõld.** Treatment and analysis of phenolic wastewater with microorganisms. Tartu, 2000, 123 p.
14. **Jüri Ivask.** Ion Chromatographic determination of major anions and cations in polar ice core. Tartu, 2000, 85 p.
15. **Lauri Vares.** Stereoselective Synthesis of Tetrahydrofuran and Tetrahydropyran Derivatives by Use of Asymmetric Horner-Wadsworth-Emmons and Ring Closure Reactions. Tartu, 2000, 184 p.
16. **Martin Lepiku.** Kinetic aspects of dopamine D_2 receptor interactions with specific ligands. Tartu, 2000, 81 p.
17. **Katrin Sak.** Some aspects of ligand specificity of P2Y receptors. Tartu, 2000, 106 p.
18. **Vello Pällin.** The role of solvation in the formation of iotsitch complexes. Tartu, 2001, 95 p.
19. **Katrin Kollist.** Interactions between polycyclic aromatic compounds and humic substances. Tartu, 2001, 93 p.

20. **Ivar Koppel.** Quantum chemical study of acidity of strong and superstrong Brønsted acids. Tartu, 2001, 104 p.
21. **Viljar Pihl.** The study of the substituent and solvent effects on the acidity of OH and CH acids. Tartu, 2001, 132 p.
22. **Natalia Palm.** Specification of the minimum, sufficient and significant set of descriptors for general description of solvent effects. Tartu, 2001, 134 p.
23. **Sulev Sild.** QSPR/QSAR approaches for complex molecular systems. Tartu, 2001, 134 p.
24. **Ruslan Petrukhin.** Industrial applications of the quantitative structure-property relationships. Tartu, 2001, 162 p.
25. **Boris V. Rogovoy.** Synthesis of (benzotriazolyl)carboximidamides and their application in relations with *N*- and *S*-nucleophyles. Tartu, 2002, 84 p.
26. **Koit Herodes.** Solvent effects on UV-vis absorption spectra of some solvatochromic substances in binary solvent mixtures: the preferential solvation model. Tartu, 2002, 102 p.
27. **Anti Perkson.** Synthesis and characterisation of nanostructured carbon. Tartu, 2002, 152 p.
28. **Ivari Kaljurand.** Self-consistent acidity scales of neutral and cationic Brønsted acids in acetonitrile and tetrahydrofuran. Tartu, 2003, 108 p.
29. **Karmen Lust.** Adsorption of anions on bismuth single crystal electrodes. Tartu, 2003, 128 p.
30. **Mare Piirsalu.** Substituent, temperature and solvent effects on the alkaline hydrolysis of substituted phenyl and alkyl esters of benzoic acid. Tartu, 2003, 156 p.
31. **Meeri Sassian.** Reactions of partially solvated Grignard reagents. Tartu, 2003, 78 p.
32. **Tarmo Tamm.** Quantum chemical modelling of polypyrrole. Tartu, 2003. 100 p.
33. **Erik Teinemaa.** The environmental fate of the particulate matter and organic pollutants from an oil shale power plant. Tartu, 2003. 102 p.
34. **Jaana Tammiku-Taul.** Quantum chemical study of the properties of Grignard reagents. Tartu, 2003. 120 p.
35. **Andre Lomaka.** Biomedical applications of predictive computational chemistry. Tartu, 2003. 132 p.
36. **Kostyantyn Kirichenko.** Benzotriazole – Mediated Carbon–Carbon Bond Formation. Tartu, 2003. 132 p.
37. **Gunnar Nurk.** Adsorption kinetics of some organic compounds on bismuth single crystal electrodes. Tartu, 2003, 170 p.
38. **Mati Arulepp.** Electrochemical characteristics of porous carbon materials and electrical double layer capacitors. Tartu, 2003, 196 p.
39. **Dan Cornel Fara.** QSPR modeling of complexation and distribution of organic compounds. Tartu, 2004, 126 p.
40. **Riina Mahlapuu.** Signalling of galanin and amyloid precursor protein through adenylate cyclase. Tartu, 2004, 124 p.

41. **Mihkel Kerikmäe.** Some luminescent materials for dosimetric applications and physical research. Tartu, 2004, 143 p.
42. **Jaanus Kruusma.** Determination of some important trace metal ions in human blood. Tartu, 2004, 115 p.
43. **Urmas Johanson.** Investigations of the electrochemical properties of polypyrrole modified electrodes. Tartu, 2004, 91 p.
44. **Kaido Sillar.** Computational study of the acid sites in zeolite ZSM-5. Tartu, 2004, 80 p.
45. **Aldo Oras.** Kinetic aspects of dATPαS interaction with $P2Y_1$ receptor. Tartu, 2004, 75 p.
46. **Erik Mölder.** Measurement of the oxygen mass transfer through the air-water interface. Tartu, 2005, 73 p.
47. **Thomas Thomberg.** The kinetics of electroreduction of peroxodisulfate anion on cadmium (0001) single crystal electrode. Tartu, 2005, 95 p.
48. **Olavi Loog.** Aspects of condensations of carbonyl compounds and their imine analogues. Tartu, 2005, 83 p.
49. **Siim Salmar.** Effect of ultrasound on ester hydrolysis in aqueous ethanol. Tartu, 2006, 73 p.
50. **Ain Uustare.** Modulation of signal transduction of heptahelical receptors by other receptors and G proteins. Tartu, 2006, 121 p.
51. **Sergei Yurchenko.** Determination of some carcinogenic contaminants in food. Tartu, 2006, 143 p.
52. **Kaido Tämm.** QSPR modeling of some properties of organic compounds. Tartu, 2006, 67 p.
53. **Olga Tšubrik.** New methods in the synthesis of multisubstituted hydrazines. Tartu. 2006, 183 p.
54. **Lilli Sooväli.** Spectrophotometric measurements and their uncertainty in chemical analysis and dissociation constant measurements. Tartu, 2006, 125 p.
55. **Eve Koort.** Uncertainty estimation of potentiometrically measured ph and pK_a values. Tartu, 2006, 139 p.
56. **Sergei Kopanchuk.** Regulation of ligand binding to melanocortin receptor subtypes. Tartu, 2006, 119 p.
57. **Silvar Kallip.** Surface structure of some bismuth and antimony single crystal electrodes. Tartu, 2006, 107 p.
58. **Kristjan Saal.** Surface silanization and its application in biomolecule coupling. Tartu, 2006, 77 p.
59. **Tanel Tätte.** High viscosity $Sn(OBu)_4$ oligomeric concentrates and their applications in technology. Tartu, 2006, 91 p.
60. **Dimitar Atanasov Dobchev**. Robust QSAR methods for the prediction of properties from molecular structure. Tartu, 2006, 118 p.
61. **Hannes Hagu**. Impact of ultrasound on hydrophobic interactions in solutions. Tartu, 2007, 81 p.
62. **Rutha Jäger.** Electroreduction of peroxodisulfate anion on bismuth electrodes. Tartu, 2007, 142 p.

63. **Kaido Viht.** Immobilizable bisubstrate-analogue inhibitors of basophilic protein kinases: development and application in biosensors. Tartu, 2007, 88 p.
64. **Eva-Ingrid Rõõm.** Acid-base equilibria in nonpolar media. Tartu, 2007, 156 p.
65. **Sven Tamp.** DFT study of the cesium cation containing complexes relevant to the cesium cation binding by the humic acids. Tartu, 2007, 102 p.
66. **Jaak Nerut.** Electroreduction of hexacyanoferrate(III) anion on Cadmium (0001) single crystal electrode. Tartu, 2007, 180 p.
67. **Lauri Jalukse.** Measurement uncertainty estimation in amperometric dissolved oxygen concentration measurement. Tartu, 2007, 112 p.
68. **Aime Lust.** Charge state of dopants and ordered clusters formation in CaF_2:Mn and CaF_2:Eu luminophors. Tartu, 2007, 100 p.
69. **Iiris Kahn**. Quantitative Structure-Activity Relationships of environmentally relevant properties. Tartu, 2007, 98 p.
70. **Mari Reinik.** Nitrates, nitrites, N-nitrosamines and polycyclic aromatic hydrocarbons in food: analytical methods, occurrence and dietary intake. Tartu, 2007, 172 p.
71. **Heili Kasuk.** Thermodynamic parameters and adsorption kinetics of organic compounds forming the compact adsorption layer at Bi single crystal electrodes. Tartu, 2007, 212 p.
72. **Erki Enkvist.** Synthesis of adenosine-peptide conjugates for biological applications. Tartu, 2007, 114 p.
73. **Svetoslav Hristov Slavov**. Biomedical applications of the QSAR approach. Tartu, 2007, 146 p.
74. **Eneli Härk.** Electroreduction of complex cations on electrochemically polished Bi(*hkl*) single crystal electrodes. Tartu, 2008, 158 p.
75. **Priit Möller.** Electrochemical characteristics of some cathodes for medium temperature solid oxide fuel cells, synthesized by solid state reaction technique. Tartu, 2008, 90 p.
76. **Signe Viggor.** Impact of biochemical parameters of genetically different pseudomonads at the degradation of phenolic compounds. Tartu, 2008, 122 p.
77. **Ave Sarapuu.** Electrochemical reduction of oxygen on quinone-modified carbon electrodes and on thin films of platinum and gold. Tartu, 2008, 134 p.
78. **Agnes Kütt.** Studies of acid-base equilibria in non-aqueous media. Tartu, 2008, 198 p.
79. **Rouvim Kadis.** Evaluation of measurement uncertainty in analytical chemistry: related concepts and some points of misinterpretation. Tartu, 2008, 118 p.
80. **Valter Reedo.** Elaboration of IVB group metal oxide structures and their possible applications. Tartu, 2008, 98 p.
81. **Aleksei Kuznetsov.** Allosteric effects in reactions catalyzed by the cAMP-dependent protein kinase catalytic subunit. Tartu, 2009, 133 p.

82. **Aleksei Bredihhin.** Use of mono- and polyanions in the synthesis of multisubstituted hydrazine derivatives. Tartu, 2009, 105 p.
83. **Anu Ploom.** Quantitative structure-reactivity analysis in organosilicon chemistry. Tartu, 2009, 99 p.
84. **Argo Vonk.** Determination of adenosine A_{2A}- and dopamine D_1 receptor-specific modulation of adenylate cyclase activity in rat striatum. Tartu, 2009, 129 p.
85. **Indrek Kivi.** Synthesis and electrochemical characterization of porous cathode materials for intermediate temperature solid oxide fuel cells. Tartu, 2009, 177 p.
86. **Jaanus Eskusson.** Synthesis and characterisation of diamond-like carbon thin films prepared by pulsed laser deposition method. Tartu, 2009, 117 p.
87. **Marko Lätt.** Carbide derived microporous carbon and electrical double layer capacitors. Tartu, 2009, 107 p.
88. **Vladimir Stepanov.** Slow conformational changes in dopamine transporter interaction with its ligands. Tartu, 2009, 103 p.
89. **Aleksander Trummal.** Computational Study of Structural and Solvent Effects on Acidities of Some Brønsted Acids. Tartu, 2009, 103 p.
90. **Eerold Vellemäe.** Applications of mischmetal in organic synthesis. Tartu, 2009, 93 p.
91. **Sven Parkel.** Ligand binding to 5-HT_{1A} receptors and its regulation by Mg^{2+} and Mn^{2+}. Tartu, 2010, 99 p.
92. **Signe Vahur.** Expanding the possibilities of ATR-FT-IR spectroscopy in determination of inorganic pigments. Tartu, 2010, 184 p.
93. **Tavo Romann**. Preparation and surface modification of bismuth thin film, porous, and microelectrodes. Tartu, 2010, 155 p.
94. **Nadežda Aleksejeva.** Electrocatalytic reduction of oxygen on carbon nanotube-based nanocomposite materials. Tartu, 2010, 147 p.
95. **Marko Kullapere.** Electrochemical properties of glassy carbon, nickel and gold electrodes modified with aryl groups. Tartu, 2010, 233 p.
96. **Liis Siinor.** Adsorption kinetics of ions at Bi single crystal planes from aqueous electrolyte solutions and room-temperature ionic liquids. Tartu, 2010, 101 p.
97. **Angela Vaasa.** Development of fluorescence-based kinetic and binding assays for characterization of protein kinases and their inhibitors. Tartu 2010, 101 p.
98. **Indrek Tulp.** Multivariate analysis of chemical and biological properties. Tartu 2010, 105 p.
99. **Aare Selberg.** Evaluation of environmental quality in Northern Estonia by the analysis of leachate. Tartu 2010, 117 p.
100. **Darja Lavõgina.** Development of protein kinase inhibitors based on adenosine analogue-oligoarginine conjugates. Tartu 2010, 248 p.
101. **Laura Herm.** Biochemistry of dopamine D_2 receptors and its association with motivated behaviour. Tartu 2010, 156 p.

102. **Terje Raudsepp.** Influence of dopant anions on the electrochemical properties of polypyrrole films. Tartu 2010, 112 p.
103. **Margus Marandi.** Electroformation of Polypyrrole Films: *In-situ* AFM and STM Study. Tartu 2011, 116 p.
104. **Kairi Kivirand.** Diamine oxidase-based biosensors: construction and working principles. Tartu, 2011, 140 p.
105. **Anneli Kruve.** Matrix effects in liquid-chromatography electrospray mass-spectrometry. Tartu, 2011, 156 p.
106. **Gary Urb.** Assessment of environmental impact of oil shale fly ash from PF and CFB combustion. Tartu, 2011, 108 p.
107. **Nikita Oskolkov.** A novel strategy for peptide-mediated cellular delivery and induction of endosomal escape. Tartu, 2011, 106 p.
108. **Dana Martin.** The QSPR/QSAR approach for the prediction of properties of fullerene derivatives. Tartu, 2011, 98 p.
109. **Säde Viirlaid.** Novel glutathione analogues and their antioxidant activity. Tartu, 2011, 106 p.
110. **Ülis Sõukand.** Simultaneous adsorption of Cd^{2+}, Ni^{2+}, and Pb^{2+} on peat. Tartu, 2011, 124 p.
111. **Lauri Lipping.** The acidity of strong and superstrong Brønsted acids, an outreach for the "limits of growth": a quantum chemical study. Tartu, 2011, 124 p.
112. **Heisi Kurig.** Electrical double-layer capacitors based on ionic liquids as electrolytes. Tartu, 2011, 146 p.
113. **Marje Kasari.** Bisubstrate luminescent probes, optical sensors and affinity adsorbents for measurement of active protein kinases in biological samples. Tartu, 2012, 126 p.
114. **Kalev Takkis.** Virtual screening of chemical databases for bioactive molecules. Tartu, 2012, 122 p.
115. **Ksenija Kisseljova**. Synthesis of aza-β^3-amino acid containing peptides and kinetic study of their phosphorylation by protein kinase A. Tartu, 2012, 104 p.
116. **Riin Rebane.** Advanced method development strategy for derivatization LC/ESI/MS. Tartu, 2012, 184 p.
117. **Vladislav Ivaništšev.** Double layer structure and adsorption kinetics of ions at metal electrodes in room temperature ionic liquids. Tartu, 2012, 128 p.
118. **Irja Helm.** High accuracy gravimetric Winkler method for determination of dissolved oxygen. Tartu, 2012, 139 p.
119. **Karin Kipper.** Fluoroalcohols as Components of LC-ESI-MS Eluents: Usage and Applications. Tartu, 2012, 164 p.
120. **Arno Ratas.** Energy storage and transfer in dosimetric luminescent materials. Tartu, 2012, 163 p.
121. **Reet Reinart-Okugbeni**. Assay systems for characterisation of subtype-selective binding and functional activity of ligands on dopamine receptors. Tartu, 2012, 159 p.

122. **Lauri Sikk.** Computational study of the Sonogashira cross-coupling reaction. Tartu, 2012, 81 p.
123. **Karita Raudkivi.** Neurochemical studies on inter-individual differences in affect-related behaviour of the laboratory rat. Tartu, 2012, 161 p.
124. **Indrek Saar.** Design of GalR2 subtype specific ligands: their role in depression-like behavior and feeding regulation. Tartu, 2013, 126 p.
125. **Ann Laheäär.** Electrochemical characterization of alkali metal salt based non-aqueous electrolytes for supercapacitors. Tartu, 2013, 127 p.
126. **Kerli Tõnurist.** Influence of electrospun separator materials properties on electrochemical performance of electrical double-layer capacitors. Tartu, 2013, 147 p.
127. **Kaija Põhako-Esko.** Novel organic and inorganic ionogels: preparation and characterization. Tartu, 2013, 124 p.
128. **Ivar Kruusenberg.** Electroreduction of oxygen on carbon nanomaterial-based catalysts. Tartu, 2013, 191 p.
129. **Sander Piiskop.** Kinetic effects of ultrasound in aqueous acetonitrile solutions. Tartu, 2013, 95 p.
130. **Ilona Faustova**. Regulatory role of L-type pyruvate kinase N-terminal domain. Tartu, 2013, 109 p.
131. **Kadi Tamm.** Synthesis and characterization of the micro-mesoporous anode materials and testing of the medium temperature solid oxide fuel cell single cells. Tartu, 2013, 138 p.
132. **Iva Bozhidarova Stoyanova-Slavova.** Validation of QSAR/QSPR for regulatory purposes. Tartu, 2013, 109 p.
133. **Vitali Grozovski**. Adsorption of organic molecules at single crystal electrodes studied by *in situ* STM method. Tartu, 2014, 146 p.
134. **Santa Veikšina**. Development of assay systems for characterisation of ligand binding properties to melanocortin 4 receptors. Tartu, 2014, 151 p.
135. **Jüri Liiv.** PVDF (polyvinylidene difluoride) as material for active element of twisting-ball displays. Tartu, 2014, 111 p.
136. **Kersti Vaarmets.** Electrochemical and physical characterization of pristine and activated molybdenum carbide-derived carbon electrodes for the oxygen electroreduction reaction. Tartu, 2014, 131 p.
137. **Lauri Tõntson**. Regulation of G-protein subtypes by receptors, guanine nucleotides and Mn^{2+}. Tartu, 2014, 105 p.
138. **Aiko Adamson.** Properties of amine-boranes and phosphorus analogues in the gas phase. Tartu, 2014, 78 p.
139. **Elo Kibena**. Electrochemical grafting of glassy carbon, gold, highly oriented pyrolytic graphite and chemical vapour deposition-grown graphene electrodes by diazonium reduction method. Tartu, 2014, 184 p.
140. **Teemu Näykki.** Novel Tools for Water Quality Monitoring – From Field to Laboratory. Tartu, 2014, 202 p.
141. **Karl Kaupmees.** Acidity and basicity in non-aqueous media: importance of solvent properties and purity. Tartu, 2014, 128 p.

142. **Oleg Lebedev**. Hydrazine polyanions: different strategies in the synthesis of heterocycles. Tartu, 2015, 118 p.
143. **Geven Piir.** Environmental risk assessment of chemicals using QSAR methods. Tartu, 2015, 123 p.
144. **Olga Mazina.** Development and application of the biosensor assay for measurements of cyclic adenosine monophosphate in studies of G protein-coupled receptor signalinga. Tartu, 2015, 116 p.
145. **Sandip Ashokrao Kadam.** Anion receptors: synthesis and accurate binding measurements. Tartu, 2015, 116 p.
146. **Indrek Tallo.** Synthesis and characterization of new micro-mesoporous carbide derived carbon materials for high energy and power density electrical double layer capacitors. Tartu, 2015, 148 p.
147. **Heiki Erikson.** Electrochemical reduction of oxygen on nanostructured palladium and gold catalysts. Tartu, 2015, 204 p.
148. **Erik Anderson.** *In situ* Scanning Tunnelling Microscopy studies of the interfacial structure between Bi(111) electrode and a room temperature ionic liquid. Tartu, 2015, 118 p.
149. **Girinath G. Pillai.** Computational Modelling of Diverse Chemical, Biochemical and Biomedical Properties. Tartu, 2015, 140 p.
150. **Piret Pikma.** Interfacial structure and adsorption of organic compounds at Cd(0001) and Sb(111) electrodes from ionic liquid and aqueous electrolytes: an *in situ* STM study. Tartu, 2015, 126 p.
151. **Ganesh babu Manoharan.** Combining chemical and genetic approaches for photoluminescence assays of protein kinases. Tartu, 2016, 126 p.
152. **Carolin Siimenson**. Electrochemical characterization of halide ion adsorption from liquid mixtures at Bi(111) and pyrolytic graphite electrode surface. Tartu, 2016, 110 p.
153. **Asko Laaniste.** Comparison and optimisation of novel mass spectrometry ionisation sources. Tartu, 2016, 156 p.
154. **Hanno Evard.** Estimating limit of detection for mass spectrometric analysis methods. Tartu, 2016, 224 p.
155. **Kadri Ligi.** Characterization and application of protein kinase-responsive organic probes with triplet-singlet energy transfer. Tartu, 2016, 122 p.
156. **Margarita Kagan.** Biosensing penicillins' residues in milk flows. Tartu, 2016, 130 p.
157. **Marie Kriisa.** Development of protein kinase-responsive photoluminescent probes and cellular regulators of protein phosphorylation. Tartu, 2016, 106 p.
158. **Mihkel Vestli.** Ultrasonic spray pyrolysis deposited electrolyte layers for intermediate temperature solid oxide fuel cells. Tartu, 2016, 156 p.
159. **Silver Sepp**. Influence of porosity of the carbide-derived carbon on the properties of the composite electrocatalysts and characteristics of polymer electrolyte fuel cells. Tartu, 2016, 137 p.
160. **Kristjan Haav**. Quantitative relative equilibrium constant measurements in supramolecular chemistry. Tartu, 2017, 158 p.

161. **Anu Teearu**. Development of MALDI-FT-ICR-MS methodology for the analysis of resinous materials. Tartu, 2017, 205 p.
162. **Taavi Ivan**. Bifunctional inhibitors and photoluminescent probes for studies on protein complexes. Tartu, 2017, 140 p.
163. **Maarja-Liisa Oldekop**. Characterization of amino acid derivatization reagents for LC-MS analysis. Tartu, 2017, 147 p.
164. **Kristel Jukk**. Electrochemical reduction of oxygen on platinum- and palladium-based nanocatalysts. Tartu, 2017, 250 p.
165. **Siim Kukk**. Kinetic aspects of interaction between dopamine transporter and *N*-substituted nortropane derivatives. Tartu, 2017, 107 p.
166. **Birgit Viira**. Design and modelling in early drug development in targeting HIV-1 reverse transcriptase and Malaria. Tartu, 2017, 172 p.
167. **Rait Kivi**. Allostery in cAMP dependent protein kinase catalytic subunit. Tartu, 2017, 115 p.
168. **Agnes Heering**. Experimental realization and applications of the unified acidity scale. Tartu, 2017, 123 p.
169. **Delia Juronen**. Biosensing system for the rapid multiplex detection of mastitis-causing pathogens in milk. Tartu, 2018, 85 p.
170. **Hedi Rahnel.** ARC-inhibitors: from reliable biochemical assays to regulators of physiology of cells. Tartu, 2018, 176 p.
171. **Anton Ruzanov.** Computational investigation of the electrical double layer at metal–aqueous solution and metal–ionic liquid interfaces. Tartu, 2018, 129 p.
172. **Katrin Kestav.** Crystal Structure-Guided Development of Bisubstrate-Analogue Inhibitors of Mitotic Protein Kinase Haspin. Tartu, 2018, 166 p.
173. **Mihkel Ilisson.** Synthesis of novel heterocyclic hydrazine derivatives and their conjugates. Tartu, 2018, 101 p.
174. **Anni Allikalt.** Development of assay systems for studying ligand binding to dopamine receptors. Tartu, 2018, 160 p.
175. **Ove Oll.** Electrical double layer structure and energy storage characteristics of ionic liquid based capacitors. Tartu, 2018, 187 p.
176. **Rasmus Palm.** Carbon materials for energy storage applications. Tartu, 2018, 114 p.
177. **Jörgen Metsik.** Preparation and stability of poly(3,4-ethylenedioxythiophene) thin films for transparent electrode applications. Tartu, 2018, 111 p.
178. **Sofja Tšepelevitš.** Experimental studies and modeling of solute-solvent interactions. Tartu, 2018, 109 p.
179. **Märt Lõkov.** Basicity of some nitrogen, phosphorus and carbon bases in acetonitrile. Tartu, 2018, 104 p.
180. **Anton Mastitski**. Preparation of α-aza-amino acid precursors and related compounds by novel methods of reductive one-pot alkylation and direct alkylation. Tartu, 2018, 155 p.
181. **Jürgen Vahter**. Development of bisubstrate inhibitors for protein kinase CK2. Tartu, 2019, 186 p.

182. **Piia Liigand.** Expanding and improving methodology and applications of ionization efficiency measurements. Tartu, 2019, 189 p.
183. **Sigrid Selberg.** Synthesis and properties of lipophilic phosphazene-based indicator molecules. Tartu, 2019, 74 p.
184. **Jaanus Liigand.** Standard substance free quantification for LC/ESI/MS analysis based on the predicted ionization efficiencies. Tartu, 2019, 254 p.